

## AN ABSTRACT OF THE THESIS OF

Katherine Jane Howard for the degree of Master of Science  
in Oceanography presented on January 31, 1989

Title: Hydrothermal Vents of the Gorda Ridge, NE Pacific:  
Mineralogy and Chemistry of Sulfide Chimneys,  
Precipitates and Alteration Products

Redacted for privacy

Abstract approved

Dr. Martin R. Fisk

Hydrothermal activity on the Gorda Ridge produced three types of deposits addressed in this study: (1) Mineral encrustations removed from dredged basalts in the vicinity of the SEA CLIFF Hydrothermal Field on the east wall of the northern Gorda Ridge are dominantly mixtures of Fe-oxyhydroxides, Mn oxides and clays similar to hydrothermal deposits observed at other hydrothermal fields such as TAG and Transform Fault "A" on the Mid-Atlantic Ridge and the Galapagos Mounds. Mineralogical and chemical analyses of these precipitates demonstrate their use for hydrothermal vent prospecting. The thickness of the deposits, diversity in mineralogy and chemistry and high metal/Mn ratios noted in samples from two dredges on the eastern flank of the Gorda Ridge axial valley make these likely targets for hydrothermal activity.

(2) Hydrothermal alteration of basalt on the northern Gorda Ridge produced an alteration crust up to 1 mm thick that can be divided into two layers based on mineralogy. An inner layer next to the basalt surface is an Al-rich interlayered smectite/chlorite similar to high temperature Al-rich clays recovered from the East Pacific Rise, 21°N with minor quartz, zeolite (phillipsite ?) and relict plagioclase. An exterior layer of boehmite, AlO(OH) and minor anatase results from severe leaching of the underlying clays. The alteration crust is progressively enriched in Al, Ti, V, and Cr from interior to exterior by residual weathering. The presence of boehmite and absence of a silica-rich phase in the exterior of the crust indicates the hydrothermal fluids were silica undersaturated or silica was maintained in solution by extremely acidic fluids. This constitutes the first reporting of boehmite as a major alteration mineral in a mid-ocean ridge hydrothermal environment.

(3) Mineralogical and chemical analysis of highly weathered sulfide chimneys recovered during SEA CLIFF dives in the Escanaba Trough, southern Gorda Ridge indicate that primary mineralogy (pyrrhotite, isocubanite and sphalerite) weathers to elemental sulfur, atacamite and Fe-oxyhydroxide. Weathered rinds of chimneys are enriched in elements associated with clays (Al, Si, K) and Co, As, Pb, Zn and Cd are enriched in chimney exteriors relative to fresher chimney interiors by either differential precipitation or weathering processes. Chemical analyses of individual chimneys show that maximum concentrations of minor elements Pb and Cu are up to 3 wt%, As is up to 1.9 wt %, and Co is up to 1750 ppm. Small amounts of minerals previously unidentified in mid-ocean ridge hydrothermal environments include cassiterite, bismuth telluride, a Cu-Zn-Ni sulfide and cinnabar. Arsenopyrite identified in Escanaba Trough samples is not commonly reported in mid-ocean ridge hydrothermal deposits. The high combined metal content and unusual trace mineralogy of Escanaba Trough deposits compared to hydrothermal deposits at other sedimented spreading ocean ridges may reflect differences in the degree of interaction between sediments and hydrothermal fluids or differences in sediment composition.

Hydrothermal Vents of the Gorda Ridge, NE Pacific:  
Mineralogy and Chemistry of Sulfide Chimneys,  
Precipitates and Alteration Products

by

Katherine Jane Howard

A THESIS

submitted to

Oregon State University

in partial fulfillment of  
the requirements for  
the degree of

Master of Science

Completed January 31, 1989

Commencement June 1989

APPROVED:

Redacted for privacy

\_\_\_\_\_  
Professor of Oceanography in charge of major

Redacted for privacy

\_\_\_\_\_  
Dean of College of Oceanography

Redacted for privacy

\_\_\_\_\_  
Dean of Graduate School

Date thesis is presented \_\_\_\_\_ January 31, 1989

Typed by Katie Howard

## Acknowledgements

I wish to express my gratitude to Dr. Martin R. Fisk whose patient guidance and attentive ears during the rather lengthy research made this thesis possible. I most appreciated his encouragement for my future continuance of related research and his desire to tackle anything new. I thank my other committee members Drs. Cyrus Field, Mitch Lyle and Muhammed Aliniaze for their assistance. My appreciation goes to Dr. Cyrus Field for his assistance with petrographic analysis of sulfide chimneys and painstaking preparation of sulfides and barite for sulfur isotope analyses. Dr. Mitch Lyle initiated the research in Chapter III. His scientific expertise and encouragement contributed greatly to its completion.

The U.S. Geological Survey contributed shiptime, dredge samples and SEA CLIFF dive samples for this study. Many thanks to the chief scientists (Dave Clague, Andy Stevenson and Randy Koski) captain, crew and scientific party of L5-85-NC and chief scientists (Dave Clague and Peter Rona), captain, crew and scientific party of L3-86-NC for their technical support and hospitality. Randy Koski and Rob Zierenberg of the U.S.G.S. were valued scientific resources and discussions with them contributed significantly to the interpretations in Chapter IV of this study. Randy Koski of the U.S.G.S. arranged for my use of the SEM facility at Menlo Park and Bob Oscarson is thanked for technical support. Jim Robbins provided the atomic absorption analyses and assistance with understanding them. Greg Campi facilitated my use of the SCINTAG and Mike Shaffer and University of Oregon are thanked for microprobe time. Sulfur isotopes were determined at Global Geochemistry under the supervision of I.R. Kaplan. Laura Suskin at University of Oregon is thanked for polished thin sections used in Chapter III. Discussions with Curt Peterson contributed significantly to the interpretations in Chapter III. Drs. Mitch Lyle and Hrefna Kristmannsdottir kindly critically read an early draft of Chapter III and official reviews by Gary McMurtry and an anonymous reviewer improved the quality of the manuscript. This research was supported by a grant from Minerals Management Service administered by Oregon Department of Geology and Mineral Industries under Grant #63-630-8509.

I thank Devon Thor, Robert Bostrom and Bernard Evans for early support of my scientific endeavors. Once I arrived at OSU, I was greatly influenced by Dallas Abbott who continues to be a source of inspiration. Ross Heath initially paid my bills and fellow students Myung Han, Sarah Hoffman, Marijke Van Heesjwik Bruce Finney and Emily Verplank provided greatly varied input. I am still learning from your examples. I owe a special debt of thanks to Bryndis Brandsdottir who introduced me to Iceland, Hrefna

Kristmannsdottir, and a much needed change of perspective. I especially thank Jon Orn Bjarnasson for all his time as a tour guide and encouragement to continue with my research and to try a little thermodynamics sometime.

Alan Mix, Steven Neshyba and Martin Fisk/Dave Carlson offered me the chance to teach a variety of Oceanography courses. I am grateful for the experience and thank the students that taught me so much about what I thought I knew but didn't. I much enjoyed my final cruise to my thesis area with Laney Chouest, Navy personnel and SEA CLIFF, chief scientist Peter Rona, Greg McMurray and the rest of Gorda Ridge Technical Working Group B that was made possible by Dr. Martin Fisk.

Thanks to Ahmed Rushdi for teaching me some chemistry, Randy Keller for teaching me developing, Dana Desonie for not giving up, Roger Hart for late night conversations on assertiveness, Doug Pyle for telling me how and why I could do this, John O'Connor for a good word now and then, Tom Lippman for being a tease, Margaret Mumford for a ready smile, Leigh Welling and Laurel Muelhausen for your refreshing attitudes and Sharon Roth for noticing Jim wasn't around. Jackie Poppleton and Sue Pullen were helpful without exception. Comraderie with geologists Reed and Karen, Shahid, Polly, Jill, Maya, Heidi, Susan and Sheri Lee brought relief at various stages of this thesis.

Scott Hughes, Vivian Golightly, Anita Grunder, and John Dilles gave more than I could ever return in time and love. I hope the future brings me the opportunity to do so. I also especially thank Myung, Inyang, Joyce and Julie Han for their friendship. I am ever grateful for the love and support of my family, GMH, Andy and Mary Howard Rhonda Kranz, Linda Harms and the McDougalls (Doris, Bill and Bob). I could never have finished this thesis without the love and inspiration provided by Jim McDougall.

## Table of Contents

CHAPTER I	GENERAL INTRODUCTION	2
CHAPTER II	HYDROTHERMAL PRECIPITATES FROM BASALTS ON THE GORDA RIDGE AND PRESIDENT JACKSON SEAMOUNTS	4
	Abstract	5
	Introduction	6
	Mineralogical and Chemical Zonation	7
	Hydrogenous Versus Hydrothermal	9
	Methods	10
	Samples	10
	Techniques	10
	Results	12
	Mineralogy	12
	Chemistry	13
	Inter-Element Correlations	14
	Discussion	17
	Mineralogy	17
	Chemistry	18
	Nickel Enrichment	20
	Conclusions	23
	Tables	24
	Figures	32
	References	50
CHAPTER III	HYDROTHERMAL ALUMINA-RICH CLAYS AND BOEHMITE ON THE GORDA RIDGE	57
	Abstract	58
	Introduction	59
	Tectonic Setting	60
	Sample Location and Description	61
	Petrography	62
	Analytical Techniques	63
	Results	64

(A) <i>Mineralogy</i>	64
Inner Layer	64
Outer Layer	65
(B) <i>Chemical Compositions of Crusts</i>	66
(C) <i>Scanning Electron Microscopy (SEM)</i>	67
Discussion	68
<i>Formation of Al-rich Clays</i>	68
<i>Residual Enrichment</i>	69
<i>Proximity to Hydrothermal Vents</i>	69
<i>Occurrence of Boehmite</i>	70
<i>Stages of Alteration</i>	71
Conclusions	73
Tables	75
Figures	79
References	91
CHAPTER IV WEATHERED SULFIDE CHIMNEYS FROM THE ESCANABA TROUGH, GORDA RIDGE	96
Abstract	97
Introduction	98
Tectonic Setting	100
<i>Sample Location</i>	100
Methods	102
<i>Subsampling</i>	102
<i>X-ray Diffraction</i>	102
<i>Atomic Absorption</i>	102
<i>Electron Microprobe and SEM</i>	103
<i>Sulfur Isotopes</i>	103
Results	104
(A) <i>Mineralogy</i>	104
(a) Interiors	104
(b) Exteriors	104
Petrography	105
Scanning Electron Microscopy (SEM)	105
(a) Trace Minerals	105
(b) Replacement Minerals	106
(c) Alteration Minerals	106
(B) Mineral Chemistry	106
(C) Bulk Chemistry	107
(D) Sulfur Isotopes	108
Discussion	110
(A) Chimney Chemistry	110



<i>Comparison With Basalt</i>	110
<i>Inter-Element Correlations</i>	111
(a) Interiors	111
(b) Exteriors	111
<i>Chemical Fluxes</i>	112
(B) Comparison to Other Ridge-Crest Sulfide Deposits	113
<i>Mineralogy and Sulfide Paragenesis</i>	113
<i>Weathering and Aging of Chimneys</i>	115
<i>Deciphering Sediment Effects</i>	116
(C) Sulfur Isotopes	117
<i>Geothermometry</i>	118
<i>Sources of Sulfur</i>	119
Conclusions	121
Tables	122
Figures	130
References	152
BIBLIOGRAPHY	158
APPENDICES	
I. Correlation Matrices	171
II-1. Description of Weathered Sulfide Chimneys from the Escanaba Trough, Gorda Ridge	178
2. Selected X-Ray Diffractograms.	188
3. Description of SEM Results.	191
III. Experimental Study of the Formation of FETI Basalts	192

## List of Figures

### Chapter II

<u>Figure</u>	<u>Page</u>
II-1 Detailed bathymetric maps showing sample locations after NOAA SEABEAM for the (a) GR-14 area and (b) President Jackson Seamounts.	32
II-2 (a) X-ray diffractogram of sample L5-85-NC-4D-1B showing two major peaks for todorokite. (b) X-ray diffractogram of sample W7605B-5D-55 showing major peaks for clinocllore. (c) X-ray diffractogram of sample W7605B-4D-14 showing the major peaks for talc.	34
II-3 Bathymetric maps with location of major minerals identified in hydrothermal precipitates from (a) GR-14 and (b) President Jackson Seamounts.	36
II-4 Ternary plot with apices Al, Fe and Mn.	38
II-5 Elements versus Mn plots for Gorda Ridge axis, off axis and President Jackson Seamount samples.	40
II-6 Ternary plot with apices Co, Cu and Ni showing relative enrichment of all samples in Ni and enrichment in President Jackson Seamount samples in Co relative to Gorda Ridge Samples.	46
II-7 Co/Zn versus Co + Ni + Cu.	48
II-8 Ternary plot with apices Fe, Mn and (Cu + Ni + Co)x10 .	49

### Chapter III

<u>Figure</u>	<u>Page</u>
III-1 Location of the Gorda Ridge off the coast of Oregon and California.	79
III-2 Bathymetric map of the northern Gorda Ridge from NOAA SEABEAM with locations of L3-86-NC and L5-85-NC dredges on the USGS R/V S.P. Lee.	80
III-3 Drawing of basalt and alteration crust with mineralogy and textures observed in thin section.	81
III-4 X-ray diffractogram of the inner layer of sample L3-86-NC-11D (0° to 30° 2θ) showing the presence of smectite/chlorite interlayered clays. (a) random mount, (b) oriented mount, (c) oriented mount (ethylene glycolated) and (d) oriented mount heated to 350°C.	82

III-5	X-ray diffractogram of outer layer of sample L3-86-NC-15D from the northern Gorda Ridge showing the presence of boehmite, $\text{AlO}(\text{OH})$ and anatase.	84
III-6	Major element oxides from microprobe analyses versus distance from the basalt/crust interface (inner) to the exterior (outer) of sample 15D.	85
III-7	SEM electron backscattering images of Gorda Ridge hydrothermal alteration crusts. (a) Quartz grains, (b) Anatase crystals.	87
III-8	Phase relations in the system $\text{Al}_2\text{O}_3\text{-SiO}_2\text{-H}_2\text{O}$ at 1kb from Hemley et al., 1980.	90

#### Chapter IV

<u>Figure</u>	<u>Page</u>	
IV-1	Bathymetric map of the Escanaba Trough after Wilde et al., 1979 showing the locations of six major volcanic edifices.	130
IV-2	Detailed bathymetry of the (a) NESCA site (Dome D) and (b) SESCA site (Dome B) in the Escanaba Trough, southern Gorda Ridge from NOAA SEABEAM.	131
IV-3	Photomicrograph of a polished thin section of sample 659-2 showing large boxwork pyrrhotite in chimney flow channels and abrupt change in crystal size at channel margins.	134
IV-4	SEM backscattering image of an As-rich mineral intergrown with isocubanite with Zn-rich rim from chimney sample 7 (659-3).	136
IV-5	SEM backscattering image of barite chimney showing fine scale zonation from variable Sr content (light and dark bands) and small cinnabar crystal.	138
IV-6	SEM backscattering image of fractured pyrrhotite crystal showing oxidation to marcasite and corresponding SEM spectra.	140
IV-7	SEM backscattering image of goethite and lepidocrosite (FeOOH) from weathering of pyrrhotite.	143
IV-8	Histogram of mole% FeS in sphalerite from the Escanaba Trough compared to Guaymas Basin and Type A sphalerite from the southern Juan de Fuca Ridge.	145
IV-9	Composition of isocubanite from the Escanaba Trough compared to southern Juan de Fuca Ridge.	146
IV-10	Ternary diagram with apices Pb-Cu-Zn comparing the chemistry of Escanaba Trough sulfide deposits to other mid-ocean ridge sulfide deposits and deposits from the Troodos ophiolite, Cyprus.	147

- IV-11 Plots of enrichment factors calculated for chimney samples designated 2, 4, 6 and 11 in Table IV-3 for selected elements. 149
- IV-12 Phase relations in the system Cu-Fe-S-O at 300°C and 20MPa from Koski et al., 1985 with approximate  $fs_2$  for sphalerite with mole% FeS contents equal to those measured in Escanaba Trough sulfides. 151

## List of Tables

### Chapter II

<u>Table</u>	<u>Page</u>
II-1 Minerals associated with hydrothermal deposits.	24
II-2 Location and depth of dredge stations.	25
II-3 Mineralogy of Gorda Ridge axis precipitates from OSU cruise W7605B.	26
II-4 Mineralogy of Gorda Ridge axis precipitates from cruise L5-85-NC.	27
II-5 Mineralogy of Gorda Ridge off-axis precipitates from L5-85-NC.	28
II-6 Mineralogy of President Jackson Seamounts precipitates from cruise L5-85-NC.	30
II-7 Atomic absorption analyses of hydrothermal precipitates from the Gorda Ridge and President Jackson Seamounts.	31

### Chapter III

<u>Table</u>	<u>Page</u>
III-I Average of three atomic absorption analyses (this study) of U.S. Geological Survey standard rocks, G-2, GSP-1 and BCR-3 compared with consensus values (Gladney and Burns, 1983).	75
III-2 Comparison of basal reflections for Gorda Ridge (GR-14) Al-rich chlorite/smectite and East Pacific Rise, 21°N Al-rich chlorite/smectite.	76
III-3 Atomic absorption analyses of alteration crusts from Gorda Ridge, GR-14.	77
III-4 Microprobe analyses from samples L3-86-NC-11D and L3-86-NC-15D, Gorda Ridge, GR-14.	78

### Chapter IV

<u>Table</u>	<u>Page</u>
IV-1 Mineralogy of weathered sulfide chimneys from NESCA and SESCOA sites, Escanaba Trough, Gorda Ridge.	122
IV-2 (a) Electron microprobe analyses of (a) iron sulfides, (b) sphalerite	123 124

	(c) isocubanite from sample 658-R3-A,	124
	(d) barite.	125
IV-3	Atomic absorption analyses of sulfide chimneys from the Escanaba Trough, Gorda Ridge.	126
IV-4	Atomic absorption analyses recalculated as major oxides, sulfides and sulfates.	126a
IV-5	Sulfur isotope determinations.	127
IV-6	Correlation matrix for analytical data in Table IV-3.	128
IV-7	Comparative $\delta^{34}\text{S}$ of mid-ocean ridge hydrothermal vents.	129

## General Introduction

Hydrothermal activity at mid-ocean ridges makes a significant contribution to the chemistry of seawater (Hart, 1973, Bischoff and Dickson, 1975, Edmond et al., 1979). Seawater penetrates deep into the ocean crust, becomes heated and exits at the seafloor chemically and isotopically changed by interaction with the crust. When the heated water mixes with cold, bottom water or pore fluids, several chemical compounds reach saturation and precipitate. The precipitation of mineral deposits form mounds and chimneys where hydrothermal fluids vent on the sea floor. Some of the more spectacular results are sulfide chimneys that grow into spires as high as five-story buildings. Some minerals precipitate within the oceanic crust or in sediments before the fluid reaches the ocean floor and some minerals (either dissolved or particulate) are carried as much as several kilometers away from the vent site in hydrothermal plumes. Precipitates dispersed in plumes from a hydrothermal vent site create thin coatings on surrounding seafloor basalts. Near the vent site, high temperature acidic vent fluids can rapidly alter basalts.

This thesis is a study of the mineralogy and chemistry of material created when seawater interacts with basalt and vents on the seafloor. It is divided into three chapters. Chapters II and III deal with material recovered during dredging operations on a portion of the northern Gorda Ridge and on the President Jackson Seamounts (Figure III-1). Chapter II is devoted to hydrothermal precipitates which create a thin coating on dredged basalts. The mineralogy and chemistry of these deposits was used to assist in locating regions of potential high temperature venting. A hydrothermal vent field has since been discovered near one of the sites targeted by this study. Some of the findings of Chapter II have been published in an Oregon Department of Geology and Mineral Industries (DOGAMI) Open-file report (Howard and Fisk, 1986a) and an AGU abstract (Howard and Fisk, 1986b) which have been combined and presented here.

Chapter III is devoted to some unique basalt alteration recovered during dredging in the vicinity of a region determined to be a site of high temperature hydrothermal activity partially based on findings presented in Chapter II. This chapter has been published in *Geochimica et Cosmochimica Acta* with M.R. Fisk as a coauthor.

Chapter IV is devoted to sulfide chimneys recovered during the submersible SEA CLIFF dives on the Escanaba Trough, the sedimented portion of the southern Gorda Ridge. Their mineralogy and chemistry is studied with special emphasis placed on weathering processes and comparison to other sedimented hydrothermal systems. These

results are in tandem with concurrent studies by the USGS and it is anticipated that changes in interpretation may take place to accommodate the USGS studies.

Three appendices are included. Appendix I contains correlation matrices calculated for elements analyzed in hydrothermal precipitates studied in Chapter II. Appendix II contains data collected in connection with Chapter IV that was not included in the shortened manuscript format. Appendix III is a short summary of the authors findings from an experimental study of the formation of FeTi basalts. Part of these results were presented in an abstract at the American Geophysical Union meeting (Howard and Fisk, 1985).



## CHAPTER II

### HYDROTHERMAL PRECIPITATES FROM BASALTS ON THE GORDA RIDGE AND THE PRESIDENT JACKSON SEAMOUNTS

### Abstract

Mineral encrustations removed from dredged basalts in the vicinity of the recently discovered Sea Cliff Hydrothermal Field on the Gorda Ridge, are dominantly mixtures of Fe oxyhydroxides, Mn oxides and clays similar to hydrothermal deposits observed at other off-axis hydrothermal fields at TAG, and Transform Fault "A" on the Mid-Atlantic Ridge and the Galapagos Mounds. Temperatures of formation up to 300°C are suggested by the presence of one or more of the following minerals in some samples: pyrrhotite, talc, albite and chlorite. Mineralogical and chemical analyses of these precipitates demonstrate their use for hydrothermal vent prospecting. The thickness of the deposits, diversity in mineralogy and chemistry, and high metal/Mn ratios noted in samples from two dredges on the eastern flank of the Gorda Ridge axial valley make these likely targets for hydrothermal activity. Seismic activity up to 20 km deep, coupled with elevated Ni concentrations and tentative identification of sepiolite in one of these samples allow speculation that deeply circulating hydrothermal fluids are chemically modified by interaction with deep-seated, primitive rocks. Hydrothermal precipitates from the nearby President Jackson Seamounts are chemically and mineralogically distinct from Gorda Ridge deposits. The increased abundance of zeolites and higher Co/Zn ratios in President Jackson Seamount precipitates reflect modification by low temperature weathering and seawater scavenging characteristic of aging hydrothermal deposits.

## Introduction

Hydrothermal activity on the flanks of spreading ocean ridges was first discovered on the south flank of the Galapagos Rift where low temperature ( $13^{\circ}\text{C}$ ) waters discharge and form mounds of hydrothermal deposits up to 20m high (Corliss et al., 1978, Williams et al., 1979). The mounds form on top of sediments believed to overlie buried faults (Lonsdale, 1977, Williams et al., 1979). At Transform Fault "A" in the FAMOUS area ( $37^{\circ}\text{N}$  on the Mid-Atlantic Ridge), relict deposits similar to those seen in the Galapagos are found at the top of fracture zone walls (Arcyana, 1975, Hoffert et al., 1978) and samples taken in the Trans-Atlantic Geotraverse (TAG) hydrothermal field at  $26^{\circ}\text{N}$  on the east wall of the Mid-Atlantic Ridge are similar to the Galapagos Mounds (Rona et al., 1984, Thompson et al., 1985). The chemistry and mineralogy of these deposits now characterize both hydrothermal fields with low-temperature diffuse flow and deposits proximal to high-temperature black smoker vent fields. Hydrothermal activity in each of these areas is associated with rift-bounding faults and may characterize hydrothermal systems fundamentally different from hydrothermal systems discharging on the axis of spreading ocean ridges, such as the Juan de Fuca Ridge and East Pacific Rise at  $21^{\circ}\text{N}$ .

Hydrothermal activity on the flanks of the northern Gorda Ridge was first postulated after the discovery of thermal anomalies, dissolved species and particulate matter indicative of hydrothermal activity in the water (Collier et al., 1986). On the east wall of the rift valley, two locations, designated GR-14 and GR-15 appeared the most promising from the water column surveys. The hypothesized off-axis hydrothermal activity was assumed to be associated with rift-bounding faults with a hydrothermal system comparable to the TAG hydrothermal field on the Mid-Atlantic Ridge and the Galapagos Mounds.

The discovery by Collier et al. (1986) prompted vigorous investigations by a team of scientists from Oregon State University, U.S. Geological Survey and Minerals Management Service administrated through Oregon Department of Geology and Mineral Industries (DOGAMI) involving dredging and camera tows during a cruise aboard the R/V S.P. Lee in 1985. The GR-14 area was chosen for the 1985 program (cruise L5-85-NC) because it had the highest thermal anomalies. During this program, no active vents were photographed or dredged but to assist in the continuing search for hydrothermal vents, hydrothermal precipitates on basalts dredged in the GR-14 area were analyzed. During this cruise, samples were also obtained from the President Jackson Seamounts. Additional samples from the Gorda Ridge axis were selected from the most hydrothermally-altered samples from three dredges collected during Oregon State

University (OSU) cruise W7605B. The mineralogy and chemistry of the OSU basalts from these dredges are described by Wakeham (1978). Petrochemical analysis of basalts collected from the GR-14 area during the L5-85-NC cruise is being completed by Davis and Clague (1989, in prep).

This report describes the chemistry and mineralogy of deposits on the basalts and evaluates their use as a prospecting tool for locating high-temperature vent fields. Subsequent discovery of the Sea Cliff Hydrothermal Field in September, 1988 on a fault bounding scarp in the GR-14 area (Rona et al., 1988) confirmed speculation regarding hydrothermal activity on the east wall of the Gorda Ridge axial valley.

### Mineralogical and Chemical Zonation

Mineralogical and chemical zonations have long been used for ore prospecting on land (cf. review by Blain and Andrews, 1977) and have been described near submarine hydrothermal vent fields (Hoffert et al., 1978). In hydrothermal systems, zonations are created in response to changes in temperature, pressure, and composition. When acidic, reducing hydrothermal fluid ascends from deep in the crust to react with cold, oxygenated seawater, adiabatic expansion and cooling causes mineral precipitation and the minerals that form are determined primarily by the composition, temperature, pressure, pH and oxidation state of the mixed sea water and hydrothermal fluid (Bischoff, 1980). Among the first minerals to precipitate are polymetallic sulfides and sulfates such as those observed in hydrothermal chimney deposits (Spiess et al., 1979, Haymon, 1983, Oudin, 1983). Sulfides and sulfates precipitate in response to changes in pressure and temperature within the upper few hundred meters of the seafloor and on the seafloor itself (Bischoff, 1980). Sulfides and sulfates are relatively unstable in an oxidizing environment and quickly alter to oxides and oxyhydroxides (Blain and Andrews, 1977), which potentially recombine with opal in silica saturated fluids to form clays (Harder, 1976, Lyle et al., 1977, Haymon and Kastner, 1981). Close to the vent site these weathering products may be temporarily enriched in metals by analogy to trace metal enriched gossans overlying ophiolitic massive sulfides (Robertson and Boyle, 1983).

The removal of  $Mg^{2+}$  from seawater by the precipitation of  $Mg(OH)_2$  in secondary silicates results in rapid generation of  $H^+$  (Mottl, 1983) and thus end member hydrothermal fluids are highly acidic. When the end member fluid mixes with seawater of about pH 8, a range of pH values from acidic to slightly basic is created and thus a range of mineral stability fields may be intersected. Under very acidic conditions (i.e. pH < 4) the nucleation of quartz is inhibited and this can cause localized fractionation of quartz from hydrothermal fluids mixing with seawater and favors precipitation of

amorphous silica from hydrothermal fluids (Seyfried and Mottl, 1982, Herzig et al., 1988). Low pH is required to stabilize  $\text{SO}_4$  relative to  $\text{CO}_3$  with the result that anhydrite ( $\text{CaSO}_4$ ) rather than calcite ( $\text{CaCO}_3$ ) is the initially favored sink for calcium in hydrothermal precipitates (Stumm and Morgan, 1981). Retrograde solubility of anhydrite in seawater accounts for its scarcity in hydrothermal precipitates (Tivey and Delaney, 1987). Acidity at the site of deposition can be maintained by the production of  $\text{H}_2\text{SO}_4$  during oxidation of sulfides. This in turn further accelerates the weathering of sulfides (Blain and Andrews, 1977).

Changes in redox conditions in hydrothermal systems creates a fractionation between Mn and Fe (Krauskopf, 1957). Iron precipitates more rapidly under slightly reducing conditions, before the precipitation of Mn (Harder, 1976, Corliss et al., 1978, Lyle, 1981). Harder (1976) has shown that synthesis of nontronite (an Fe-rich smectite) is critically controlled by the local Eh and concentration of  $\text{Fe}^{2+}$  and Si in the solutions. These studies show that a high proportion of Fe oxyhydroxides and Fe-rich clays should precipitate closer to the vent source than Mn oxides. This mineralogical zonation can also be expressed as a chemical zonation of increasing Fe/Mn ratio in deposits toward the vent site.

Mineralogical and chemical zonation are reflected in the color of deposits. At the Galapagos mounds and the TAG hydrothermal field on the Mid-Atlantic Ridge, color variations reflect distinct changes in mineralogy and chemistry (Corliss et al., 1978, Thompson et al., 1985, Rona et al., 1984). Earthy red deposits are rich in Fe-oxyhydroxides. Mn oxides are brown to black and hydrothermal clays are typically green if formed under reducing conditions and yellow if formed under oxidizing conditions. Thus, color banding on rock surfaces can result from changes in chemistry or oxidation state of the hydrothermal fluids. In addition, colors observed on samples can reflect secondary oxidation and changes due to differences in temperature and possibly pressure after sample collection.

Rapid changes of pressure, temperature, pH and Eh affecting hydrothermal solutions exiting from seafloor vents, coupled with the large variety of contained metals, results in the precipitation of many different minerals. Minerals previously identified in mid-ocean ridge hydrothermal deposits are listed in Table II-1. Stability of these minerals following changes in the conditions of precipitation is in many cases only qualitatively known. Some alter to new minerals (eg oxidation of sulfides to other sulfides and sulfates and finally, oxides and oxyhydroxides) (Blain and Andrews, 1977, Haymon and Kastner, 1986b), some redissolve in seawater (Feely et al., 1987), some act as sites of nucleation

for more minerals of the same type (Koski, 1985) or they may be modified by bacterial scavenging (eg by S,  $Mn^{2+}$  or  $Fe^{2+}$  -oxidizing bacteria) (Jannash, 1983).

### Hydrogenous Versus Hydrothermal

Since hydrogenous and hydrothermal deposits form a continuum (Fleet, 1983), there is no clear way of distinguishing them. Hydrothermal deposits frequently contain elements scavenged from seawater and hydrogenous accumulations can have a distal hydrothermal source. However, hydrogenous accumulations imply that conditions of precipitation are relatively constant compared with the variable conditions associated with hydrothermal interactions with seawater that produces rapid changes over a short distance. Samples with several color/mineral bands reflect these rapidly changing conditions, in contrast to long term accumulations in which environmental changes may be discernable but their effects less dramatic in ferromanganese crusts. Toth (1980) used low Co/Zn ratios, low REE and Th and high  $^{234}U/^{238}U$  to distinguish hydrothermally derived crusts from dominantly hydrogenous crusts. Ingram-DePaolo and Hein (1988) used  $^{87}Sr/^{86}Sr$  ratios to determine the extent of hydrothermal input to Fe-Mn crusts. The chemistry of deposits described in this study supports the assertion that they are mixtures of hydrothermal and hydrogenous material, but also indicates that a hydrothermal source is a significant component in most of the samples.

## Methods

### Samples

The samples described in this study are from the Oregon State University (OSU) collection and from samples dredged from the Gorda Ridge and the President Jackson Seamounts during the USGS cruise L5-85-NC. Twenty-one samples from the OSU collection and twenty-nine samples from the USGS collection were analyzed by X-ray diffraction. In addition, thirty of these samples were analyzed by atomic absorption. The sample locations are indicated in Figures II-1a and b and Table II-2. A slight error in SEABEAM navigation required readjustment of latitudes and longitudes. The correction made by Rona and Clague (1989, in prep) as shown in Figure II-1a is dominantly in latitude.

Material for analysis was removed from the exterior of the basalts and caution was taken to prevent the cross contamination of individual layers on a single rock. In some instances it was not possible to separate individual colored bands because of their small size relative to 1 mg of material needed for X-ray diffraction analysis. Under these circumstances it was necessary to combine the mixed precipitate into a bulk sample.

Thick brown powdery ferromanganese crusts on seamount samples probably represent predominantly hydrogenous accumulations. For this reason, sampling was made of what appeared to be dominantly hydrothermal material beneath crusts. This material, dominantly colored yellow to red, appeared richer in Fe oxyhydroxides. Mixing of some proportion of this lower crust with upper hydrogenous crustal material was unavoidable.

### Techniques

X-ray diffraction patterns were obtained using an automated Scintag PAD-V X-ray diffractometer. The sample was mounted on a glass disk and rotated while the detector scanned continuously at  $1^\circ 2\theta$  per minute over  $2^\circ$ - $75^\circ 2\theta$ . Background signals were removed from the spectrum and peaks selected by a standard computer program. Computer programs that edit selected peaks and compare them with the inorganic mineral file of JCPDS allowed computer assisted mineral identification. In some cases (especially when only one peak of a mineral was recorded), it was necessary to perform this last step by hand. Identification of clay minerals required glycolation to determine expansions of the 001 basal reflections and in some cases heat treatments at  $150^\circ\text{C}$  and  $350^\circ\text{C}$  for further refinement. These techniques are described in Brindley and Brown (1980) and in Starkey et al., 1984).

Atomic absorption analyses were completed using standard techniques on a Perkin-Elmer 5000 atomic absorption spectrophotometer (Perkin-Elmer, 1982). The samples were analyzed for Al, Ba, Ca, Co, Cu, Fe, K, Li, Mg, Mn, Na, Ni, Rb, Si, Sr, Ti, V, and Zn. The precision of the analyses is within  $\pm 2\%$  for most elements but is within  $\pm 4\%$  for silicon, iron and barium and within  $\pm 11\%$  for titanium based on the standard deviation of three analyses of a standard manganese nodule. Table III-1 shows the precision and accuracy of the analyses.



## Results

### Mineralogy

The mineralogy of hydrothermal precipitates scraped from basalts is shown in four Tables: Table II-3 for OSU cruise W7605B dredge collection; Table II-4 for cruise L5-85-NC ridge axis samples; Table II-5 for cruise L5-85-NC off axis samples; and Table II-6 for cruise L5-85-NC President Jackson Seamount samples. The samples are dominantly mixtures of iron oxyhydroxides, manganese oxides, albite and clays. Minor mineralogy includes talc, boehmite ( $\text{AlOOH}$ ), gypsum, zeolites and tentative identifications of pyrite, calcite and natrojarosite. Most samples display albite peaks in their X-ray diffractograms in agreement with previous studies of hydrothermal precipitates from the Gorda Ridge (Clague et al., 1984) and many contain one or more clay minerals. Peaks identified as kaolinite may also represent the presence of amesite or lizardite, serpentine minerals with similar diffraction patterns (Brindley and Brown, 1980, Haymon and Kastner, 1986b). However, the presence of kaolinite is favored based on the association of boehmite (Peterson, 1971, Valetton, 1972, Norton, 1973). The presence of boehmite suggests that some of the material scraped from the basalts results from alteration of the underlying basalt rather than direct precipitation from a hydrothermal fluid (Howard and Fisk, 1988).

Hydrothermal clays identified as smectite (nontronite or saponite) had a  $14\text{\AA}$  001 reflection which expanded upon glycolation. Sepiolite was tentatively identified in sample 4D-1A based on a nonexpandable  $12\text{\AA}$  001 reflection (Starkey et al., 1984). The identification of sepiolite in subsample 4D-1 was inferred based on the presence of a  $12\text{\AA}$  reflection although this sample was not glycolated. Further examination of the 060 d-spacing required for distinction between dioctahedral and trioctahedral clays was used when possible. Gypsum was tentatively identified in several samples based on the presence of reflections at  $7.5\text{-}7.6\text{\AA}$  and  $3.06\text{\AA}$ . Mn oxides were inferred in some poorly crystalline samples with brown color and significant chemically determined Mn content ( $>5\text{wt}\%$ ). Otherwise,  $\delta\text{-MnO}_2$  (vernadite) was identified by reflections at  $2.4\text{\AA}$  and  $1.42\text{\AA}$  and todorokite was identified by a reflection at  $9.8\text{\AA}$ .  $\delta\text{-MnO}_2$  was identified in only two samples. The high Fe content of these samples may restrict the growth of a discrete  $\delta\text{-MnO}_2$  phase since  $\delta\text{-MnO}_2$  forms intergrowths with X-ray amorphous iron ( $\text{FeOOH} \cdot x\text{H}_2\text{O}$ ) (Burns, 1976, Craig et al., 1982). Birnessite could not be reliably identified by its  $7\text{\AA}$  peak because of overlap with the 002 reflection of ubiquitous clay minerals. In these circumstances, the  $3.6\text{\AA}$  peak of birnessite was used for more positive

identification. Birnessite was identified in one off-axis sample (4D-1B) and one seamount sample (34D-3).

Examples of X-ray diffraction patterns for three types of material collected from the hydrothermal deposits are shown in Figure II-2. In Figure II-2a, two peaks of the manganese oxide, todorokite, can be distinguished. Figure II-2b shows the major peaks for clinocllore, a Mg-rich chlorite that forms at moderately high temperatures ( $> 230^{\circ}\text{C}$ ) (Tomasson and Kristmannsdottir, 1972) and Figure II-2c is the diffractogram of a sample composed predominantly of talc.

Figure II-3 shows the detailed bathymetry from Figure II-1 with the location of minerals identified in mineral encrustations from the GR-14 area. Three on-axis dredges (42D, 43D and 45D) collected basalt essentially without mineral encrustations. One dredge lies to the north and two dredges lie to the south of the axial valley dredges with precipitates. All off-axis dredges recovered basalt coated with hydrothermal precipitates. The poor crystallinity of the encrustations makes zonation determinations based on mineralogy difficult. Fe oxyhydroxides, in particular, are commonly amorphous though Fe staining on the basalts is ubiquitous. The major mineralogical zonation observed is an increase in abundance of Mn oxides away from the axial valley, and a corridor of boehmite from axial valley to off-axis region.

The mineralogy of President Jackson Seamounts differs from Gorda Ridge precipitates mainly by the presence of abundant quartz and zeolites. Quartz, if analogous to that identified in hydrothermal deposits from seamounts near  $21^{\circ}\text{N}$ , East Pacific Rise (EPR), probably formed by recrystallization of opal (Alt et al., 1987). Zeolites probably represent relatively low temperature ( $<150^{\circ}\text{C}$ ) weathering (Thompson, 1983).

### Chemistry

Atomic absorption analyses for samples from cruise L5-85-NC and one sample from OSU cruise W7605B are listed in Table II-7 for on-axis, off axis and seamount samples. A ternary plot with apices Al, Fe and Mn (Fig. II-4) is consistent with the previously described mineralogical analyses showing the mineral encrustations are mixtures of Fe oxyhydroxides, Mn oxides and clays (represented by Al). The chemistry of end member minerals recovered from other hydrothermal areas are shown for comparison.

The highest concentrations of Cu, Ni, Zn, Co and Ba generally occur in samples high in Mn indicating these elements are contained in Mn oxide compounds (Calvert and Price, 1977, Toth, 1980, Chave et al., 1986). Figure II-5 shows plots of these elements versus Mn. From these plots the following conclusions are drawn:

- (1) President Jackson Seamount precipitates have higher Fe/Mn and Co/Mn ratios (Fig. II-5f,g) and slightly lower Zn/Mn ratios (Fig. II-5b) than Gorda Ridge precipitates.
- (2) Ni and Zn are strongly correlated with Mn, reflecting their incorporation in Mn oxides (Fig. II-5a,b). However, anomalous Ni enrichment (about 1,000 ppm above the dominant Ni/Mn trend) in sample 4D-1 implies excess Ni is incorporated in a mineral other than Mn oxide. The relatively high Al content in this sample (Fig. II-4) suggests its probable incorporation in clays.
- (3) Cu, Co and to a lesser extent Ba versus Mn plots (Fig. II-5c,d,e,g) are characterized by two separate trends. The more enriched samples reflect incorporation of these elements in clays and/or Fe oxyhydroxides.

Si and Al are generally negatively correlated with Mn (Fig. II-5h, i).

A ternary plot with end members Co, Cu and Ni (Fig. II-6) shows the enrichment in Ni relative to Cu and Co of all Gorda Ridge samples and the enrichment of Co in President Jackson Seamount samples relative to Gorda Ridge samples. The trace metal proportions in hydrothermal nontronite from the Juan de Fuca Ridge is plotted for comparison. Also plotted are compositions of sulfides microprobed in Gorda Ridge basalts dredged from the ridge axis near the GR-14 area. Two are representative Ni-rich sulfides and one is an unusually Cu-rich sulfide. An average of twelve analyses of basalt sulfides from the FAMOUS area of the Mid-Atlantic Ridge are plotted for comparison. The relative proportions of these elements in primary basalt sulfides bracket the hydrothermal encrustations in Gorda Ridge samples and demonstrate that basalt sulfide is a potential source for trace metals in the precipitates. Co enrichment in President Jackson Seamount samples relative to Gorda Ridge samples reflects the enhanced oxidation of  $\text{Co}^{2+}$  to  $\text{Co}^{3+}$  which substitutes for  $\text{Mn}^{4+}$  in greater quantity in Mn oxide minerals (Burns, 1976, Chave et al., 1986). Trace metal enrichment by hydrogenetic growth should result in greater enrichment of Co relative to Ni (Halbach and Puteanus, 1984) and higher Co/Zn ratios in President Jackson Seamount precipitates (Fig. II-7) reflect seawater scavenging characteristic of aging hydrothermal deposits (Toth, 1980).

#### Inter-Element Correlations

Correlation matrices were prepared in two sets (Appendix I). In the first set, Ba, Co, Li, Rb and Sr were not considered since these elements were not determined in several samples ("nd" in Table II-7). These elements were included in the second set but samples with undetermined elements were deleted. In both sets, axis/off axis samples and seamount samples were considered combined in one matrix and in separate matrices. Depth and approximate age of the underlying basalt, estimated by distance from the ridge

axis were included as variables. It was assumed that the seamounts formed on the spreading ridge.

Studies of ferromanganese crusts show that certain elemental concentrations covary either positively or negatively with water depth at collection site (Chave et al., 1986, Cronan, 1977, Hein et al., 1985). In particular, according to these researchers, Co exhibits a strong, positive correlation with depth. A correlation between an element and age bears the implied assumption that the hydrothermal precipitate formed from hydrothermal activity on the ridge axis and implies that it is enriched in the hydrothermal precipitate by aging of the encrustation. The Gorda Ridge samples have a greater alumino-silicate fraction than President Jackson Seamount samples so that depth and age tend to correlate positively and negatively respectively with elements associated with this fraction such as Al, Ti, Mg, and Ca.

Elements associated with hydrogenous accumulations (Mn, and the manganophile elements) are not correlated with either depth or age. This lends credence to the selectivity of the sampling which was intended to examine hydrothermal deposits rather than hydrogenous, oxic or suboxic deposits described by Dymond et al., 1984. Still, since hydrothermal deposits are presumably effected by depth of origin as suggested by variations in solution chemistry at least partially attributable to depth (Von Damm et al., 1987) and in addition are considered to form a continuum with hydrogenous deposits (Fleet, 1983, Toth, 1980) the lack of correlation is puzzling. A detailed discussion of both correlation sets follows:

Set I: All samples, but leaving out elements Ba, Co, Li, Rb, and Sr.

(a) For all samples combined, significant positive correlations exist between Ti and Al. Mn correlates with Ni and Zn. No significant correlations are observed for Ca, Cu, K, Mg, Na or Si.

(b) In the matrix for axis/off axis samples, more inter-element correlations are observed. Positive correlation between Ti and Al is preserved. Mn still correlates with Ni and Zn and Cu joins the manganophile group. Fe correlates with K. Negative correlations are observed between Fe and Al. Si has a strong negative correlation with Mn, Zn, Cu and to a lesser extent, Ni. No significant correlations are observed for Ca, Mg or Na.

(c) Seamount samples differ from the axis/off axis samples. Positive correlations between Mn, Ni and Zn are lowered. Negative correlations between Si and Mn, Ni and Zn are preserved, but the negative correlation with Cu disappears and is replaced by Fe. No significant correlations are observed for Al, Cu, K or Na.

Set II: Only samples for which all elements were determined.

(a) For all samples combined (minus samples with "nd" elements), Al, Ca, Ti and Mg are positively correlated. Another group correlates Mn with the manganophile elements Ba, Ni, Zn, Li and possibly Sr. Weak correlations are inferred between Co, Cu and possibly Fe and Sr. K and Rb are strongly correlated. Negative correlations are strongest between Si and Mn and the manganophile elements. Na shows no interelement correlations.

(b) In the matrix for axis/off axis samples, there are several changes in elemental affinities. The positive correlation between Al, Ca and Ti is preserved, but the correlation with Mg disappears. Co and Cu join the manganophile elements listed above that correlate with Mn. Fe correlates with K, Na and Rb. Negative correlations are strongest between Si and Mn and the manganophile elements. Al also correlates negatively with Fe, K, Mn and the manganophile elements.

(c) Like Set I, seamount samples differ from the axis/off axis samples by fewer interelement correlations. Positive correlations are between Mn, Co, Ni, Zn, Sr and Ba. Cu correlates weakly with Ni and Co. A negative correlation between Si and Fe, Mn and Ni is apparent. The elements Ca, Mg, K, Li, Na and Al lose their correlations.

The strong correlations that exist with either treatment of the data are: (1) positive correlations between Ti and Al and (2) positive correlations between Mn, Zn, and Ni.

## Discussion

Hydrothermal precipitates on basalts from the GR-14 area on the Gorda Ridge are mineralogically and chemically similar to hydrothermal deposits from other off-axis hydrothermal fields such as the Galapagos Mounds and the TAG hydrothermal field and Transform Fault "A" on the Mid-Atlantic Ridge. The deposits lie on oceanic crust with unknown minimum age on the Gorda Ridge axis up to a maximum age of 0.2 m.y. for off-axis samples, based on distance from the spreading axis and a half-spreading rate of 2.9 cm/yr (Riddihough, 1980). This is considerably younger than analogous deposits studied from the TAG hydrothermal field on the Mid-Atlantic Ridge (0.8 m.y. to 1.4 m.y.) (Thompson et al., 1985) or from the Galapagos mounds (0.5 m.y. to 0.9 m.y.) (Williams et al., 1979).

### Mineralogy

Three principal mineral phases identified by Corliss et al. (1978) in the Galapagos mounds and Thompson et al., (1985) at the TAG hydrothermal field were highly-crystalline Mn oxides (todorokite and birnessite), well crystallized nontronite and amorphous Fe oxyhydroxides. In contrast, the mineralogy of hydrothermal precipitates on basalts from the GR-14 area are less crystalline.

The todorokite identified in these samples may be a precursor to collapsed birnessite recovered from the TAG area. The appearance of birnessite as an artifact produced by the collapse of todorokite as suggested by Dymond et al. (1984) could not be fully evaluated in these samples because mixtures of minerals rendered accurate assignment stabilizing elements to Mn oxides uncertain. It is possible that with increasing distance from a high temperature area, the Mn oxide more closely resembles the form of deep sea nodule Mn oxide which is typically todorokite.

Several of the mineral precipitates identified in this study require restricted thermal and chemical environments for their genesis. Temporal changes in fluid chemistry may result in the formation of a sequence of clay minerals. Mg-rich smectites are expected to precipitate under high water/rock ratios from solutions enriched in Mg by interaction with seawater (Scheidegger and Stakes, 1978). Experimental data indicate that nontronite (an Fe-rich smectite) is formed from solutions relatively low in silica and rich in reduced iron ( $\text{Fe}^{2+}$ ) (Harder, 1976). Kaolinite and boehmite which coexist in several samples imply extremely acid conditions (Deer et al., 1966, Loughnan, 1969). The presence of talc (W7605B-4D and L5-85-NC-39D) indicates that the temperatures of deposition were

probably in the range of 270-280°C and that the fluid from which it precipitated was relatively silica-rich (Koski et al., 1985, Lonsdale, 1980).

The presence of both albite and clinocllore in some samples indicates temperatures of deposition at about 300°C. If both minerals precipitated together in equilibrium, then the fluid was characterized by low Fe concentration and Mg concentration restricted to a very narrow range (Koski et al., 1985). However, mass transfer calculations indicate that albite and clinocllore form under different water/rock ratios which suggests changing conditions between deposition of the two minerals, with albite preserved under conditions compatible with clinocllore formation (Gitlin, 1985).

Iron staining on seafloor basalts is very common and can reflect the final stages of low temperature alteration (Honnorez, 1980, Thompson, 1983). However, secondary pyrrhotite still preserved and identified in hand sample (Ship's Records on L5-85-NC-3D) and pyrite tentatively identified in samples L5-85-NC-6D and L5-85-NC-13D support the assertion that some of the iron oxyhydroxides reflect low temperature alteration of sulfides (Hekinian et al., 1980). Pyrrhotite indicates that the  $fs_2$  and  $fo_2$  is relatively low compared to pyrite (Koski et al., 1985).

Sample 5-55 from OSU cruise W7605B is very rich in Mg without corresponding enrichment in Al, or Mn (Table II-7). One possible explanation is the formation of a brucite  $Mg(OH)_2$  or magnesium silicate,  $MgSi(OH)_6$  (Hajash and Chandler, 1981). Magnesium silicate forms in basalt-seawater interaction experiments (Hajash and Chandler, 1981) but was not identified by XRD. Perhaps it is amorphous or peak overlap with other clay minerals prevented its identification.

### Chemistry

The overall lack of correlation or inconsistency of correlation between the majority of elements reflects their incorporation in more than one phase. Cu is not strongly correlated with Mn and the manganophile elements suggesting the additional association of Cu with both aluminosilicates and Fe oxides (Alpin and Cronan, 1985). The negative correlation between Si and Al in President Jackson Seamount samples and relatively low positive correlation in Gorda Ridge samples results from the additional presence of quartz/opal in the precipitates which is greater in the seamount samples. Mg may be incorporated in the Mn oxide phase (Calvert and Piper, 1984, Chave et al., 1986) as well as clays which could account for its poor correlation with Al. Manganese oxides precipitating from a hydrogenous source usually contain an alumino-silicate fraction (Bischoff et al., 1981), but the negative correlation between Al, Si and Mn (Fig. II-5, Appendix I) is evidence for the dominant separation of Mn oxides from alumino-silicates. The relative purity of

hydrothermal end member mineral phases (Fig. II-4) is further evidence of the hydrothermal origin of the precipitates.

It is potentially significant that both Ni and Zn are strongly correlated since Zn in Fe-Mn deposits and metalliferous sediments is a good indicator of hydrothermal processes (Toth, 1980, Metz et al., 1988). This suggests a hydrothermal origin for Ni. Scott et al., (1978) have attributed Ni-enrichments in sediments at TAG relative to East Pacific Rise sediments to hydrothermal activity at a slow spreading ridge. However, a recent discussion of the geochemistry of Ni in a metalliferous core from the TAG hydrothermal field contradicts this hypothesis (Metz et al., 1988). Metz et al., (1988) demonstrate that the Ni enrichments observed in metalliferous sediments can be explained by seawater scavenging and that Cu enrichment is the most indicative of hydrothermal contribution.

The relatively low Co/Zn ratio of Gorda Ridge samples also attests to their hydrothermal character (Table II-7, Fig. II-7). Figure II-7 shows the chemical similarity between hydrothermal precipitates from the Gorda Ridge and samples from the Galapagos Mounds, Transform Fault "A" on the Mid-Atlantic Ridge and hydrothermal crusts studied by Toth (1980). Detailed trace metal chemistry was not available for the TAG deposits studied by Rona et al. (1984) and Thompson et al. (1985). President Jackson Seamount samples are chemically similar to seawater-enriched ferromanganese crusts studied by Toth (1980). The increased abundance of zeolites and higher Co/Zn ratios in President Jackson Seamount precipitates reflect modification by low temperature weathering and seawater scavenging characteristic of aging hydrothermal deposits.

The general lack of correlation between Fe and Mn confirms that Fe is incorporated in other mineral phases in addition to Mn oxides. The high Fe/Mn ratios of many samples (Table II-7, Figure II-5f) probably results from extreme fractionation of Fe and Mn typical of hydrothermal areas where Fe precipitates more rapidly as Fe-rich sulfides, clays and oxyhydroxides prior to the precipitation of Mn oxides (Corliss et al., 1978, Hoffert et al., 1978, Lyle, 1981, Thompson et al., 1985).

Samples with high Fe/Mn ratios are believed to be close to the hydrothermal vent sites because of the extreme fractionation between Fe and Mn. Also, samples with high Cu, Ni, Co, Zn, or Ba/Mn ratios indicate that these elements are contained in other mineral phases besides Mn oxides, such as sulfides, sulfates, or their weathering products, clays and Fe oxyhydroxides (Robertson and Boyle, 1983). Thus we may interpret samples with both high Fe/Mn ratios and high trace metal/Mn ratios to lie closest to hydrothermal vent sites.

Figure II-8 presents the abundance of trace metals with respect to Fe and Mn in a ternary diagram after Bonatti et. al. (1972). Several samples plot in the hydrothermal



field of Bonatti et al., (1972) and many samples plot in the fields (labeled hydrogenous and Fe-Mn crusts) interpreted as deposits enriched with trace metals by seawater (Toth, 1980). An analysis of a Cu-rich gossan overlying the Cyprus massive sulfide deposit is shown in Figure II-8 as an example of the potential enrichment from the weathering of sulfides. The line represents the maximum amount of trace metals allowed in the tunnel structure of todorokite (Halbach et al., 1980). Samples above this limit are presumably enriched in trace metals above that associated with hydrogenetic growth (Halbach et al., 1980).

Two samples with very high Fe/Mn ratios (4D-1 and 13D-2) also have high Cu + Ni + Co relative to Fe and Mn and plot above the limit of hydrogenetic growth (Fig. II-8). Also these samples contained the thickest and most diverse deposits allowing three subsamples to be taken. The anomalous enrichment in trace metals without concurrent enrichment in Mn suggests the trace metals are contained in sulfides, sulfates or their weathering products implying nearby high temperature hydrothermal venting. These two locations are the best prospects for hydrothermal vent sites, based on samples in this study. Dredge L5-85-NC-13D was the closest dredge to the recently discovered Sea Cliff Hydrothermal Field. This vent field was found along the 2700 m contour on the western wall of a row of linear hills in the GR-14 area (Rona et al., 1988) (Fig II-1a) and may have been the source of metals in sample 13D-2. Almost due east from the Sea Cliff Hydrothermal Field dredge L5-85-NC-4D intersects the 2600 m contour of a similar, but smaller, row of linear hills. This area should be targeted for future explorations for hydrothermal activity.

The discovery of polymetallic sulfides on seamounts near the East Pacific Rise (Lonsdale et al., 1982, Alt et al., 1987) and their possible preservation by burial during subsequent eruptions or caldera collapse (Batiza, 1985) in addition to relatively shallow Co-rich ferromanganese crusts make seamount hydrothermal activity potentially economically attractive. Several locations on the President Jackson Seamounts are potential sites for hydrothermal deposits (29D, 31D, 33D and 35D). The high Fe/Mn and trace metal/Mn ratios in 33D and 35D make these especially favorable targets and the extreme Fe/Mn ratios and Si/Al ratio in hydrothermal precipitates on a sample from 31D (a coarse-grained "sandstone" of volcanic material) also establish it as a favorable target.

#### Nickel Enrichment

Nickel-rich coatings on submarine basalts are most frequently associated with Mn oxides formed by hydrogenous accumulation (Toth, 1980). This view is supported by analyses of hydrothermal vent waters at 21°N, East Pacific Rise that contain no detectable

nickel (Von Damm et al., 1985). This alone is not conclusive evidence of the immobility of Ni since although Cu mobilization has been observed in vent water from 21°N, East Pacific Rise (Von Damm et al., 1985) and in seawater-basalt interaction experiments (Seyfried and Mottl, 1982, Seyfried and Janecky, 1985), analyses of vent waters at the Juan de Fuca Ridge contained no detectable copper (Von Damm et al., 1987). Studies of metabasalts (Humphries and Thompson, 1978) and alteration crusts on basalt (Howard and Fisk, 1988) provide some evidence for the mobilization of nickel by hydrothermal processes. The apparent immobility of Ni is puzzling considering the seemingly readily available source of Ni from olivine and Cu-Ni sulfides in basalts.

The mobility of Ni in basalt-seawater interaction experiments is still indeterminant. Relatively high Ni concentrations in experiments run at 200°C by Bischoff and Dickson (1975) have since been attributed to contamination (Seyfried and Mottl, 1982). Experiments by Seyfried and Mottl (1982) still produced uncertain results. Two solution aliquots from Seyfried and Mottl's (1982) experiments yielded detectable, though transient, Ni concentrations thought to result from leaching of basalt. These experiments suggest that some Ni mobilization may occur, perhaps under very specific hydrothermal conditions possibly accidentally and unknowingly duplicated in the laboratory.

Traditionally, Ni-rich hydrothermal deposits on land are associated with ultramafic rocks (Blain and Andrews, 1977). The extent to which hydrothermal fluids at mid-ocean ridges are affected by interaction with deeper Ni-rich ultramafics is unknown, but peridotite-seawater interaction experiments show that solution chemistry is affected differently than in basalt-seawater interaction (Seyfried and Dibble, 1980, Janecky and Seyfried, 1986). Alkaline solutions may form that enhance the formation of metal-complexing brines (Rona et al., 1987), and variations in the Mg-SiO<sub>2</sub> ratios in solution can explain the observed precipitation of massive sepiolite (Mg-silicate) in fracture zones (Bonatti et al., 1983, Janecky and Seyfried, 1986). Bonatti et al., (1983) ruled out the formation of sepiolite from seawater-type solutions or basalt-seawater interaction since seawater is undersaturated relative to this mineral and basalt-seawater interaction produces extremely Mg-depleted solutions. Bonatti et al. (1983) instead argue that seawater interaction with ultramafic rocks will tend to increase the concentration of Mg<sup>2+</sup> and SiO<sub>2</sub> in solution resulting in fluid compositions compatible with sepiolite precipitation.

Hekinian et al. (1980) propose that an immiscible sulfide melt could separate from a silicate magma and because sulfide minerals crystallize at a lower temperature (about 800° to 1000°C) than basaltic minerals (1050° to 1200°C), a sulfide magma could "enter cracks and fissures on the ocean floor or accumulate in pockets near a magma chamber." The composition of sulfides in tholeiitic basalts from the Gorda Ridge have similar Cu/Ni

ratios as the hydrothermal precipitates on the basalts (Fig. II-6). Since processes of dissolution and precipitation could cause differential fractionation of Cu and Ni, this alone is not conclusive evidence for a genetic relationship between hydrothermal deposits and sulfide segregates. However, it does provide for interesting speculation.

On the Gorda Ridge axis near the GR-14 area, recovery of basalts containing gabbroic xenoliths (Davis and Clague, 1988) implies a deeper source of eruptions that may open conduits for deeper penetration of seawater and an additional source of Ni besides Ni leached from locally altered basalts (Howard and Fisk, 1988). Evidence for deep circulation of hydrothermal fluids is reported in ophiolites, slices of oceanic crust thrust up onto continents. In the Josephine ophiolite, evidence for hydrothermal circulation into the ultramafic section (at 4 to 5 km depth) has been documented by Kimball (1988).

An early study of hydrothermal sediments from the TAG hydrothermal field on the Mid-Atlantic Ridge suggested Ni enrichments relative to East Pacific Rise sediments could reflect differences in water circulation in the hydrothermal systems of fast and slow spreading ridges (Scott et al., 1978). If deeper seismicity at slower spreading ridges (Huang and Solomon, 1988), reflects the position of the cracking front (ie. the brittle to ductile transition in the crust) and thus the depth of hydrothermal circulation (Lister, 1983, Sleep, 1983), it is possible that fluids at slow spreading ridges interact with more primitive crust potentially mobilizing elements, such as Ni, that are enriched in deeper crustal regions (Rona, 1988, pers. comm.). Seismic velocities on the northern Gorda Ridge reveal an upper crustal thickness of 3.0 km, lower crustal thickness of up to 3.5 km and a mantle transition at about 5.2 km while focal depths of earthquakes are as deep as 20 km (Solano, 1984). Although the northern Gorda Ridge has an intermediate spreading rate (Riddihough, 1980) its geomorphological features are similar to the slower spreading Mid-Atlantic Ridge (Atwater and Mudie, 1973, Crane and Ballard, 1981). This indicates the Gorda Ridge may have a hydrothermal circulation system similar to slower spreading ridges. Thus the Ni enrichment in deposits in this region coupled with the tentative identification of sepiolite in 4D-1A and 4D-1, may reflect mineralogical and chemical signatures characteristic of deeper circulation of seawater.

## Conclusions

The mineral encrustations collected from the surfaces of Gorda Ridge basalts in the GR-14 area are of hydrothermal origin. The hydrothermal origin of these deposits is apparent considering Fe and Mn fractionation and low Co/Zn ratios. The hydrothermal signature is not evident in Si/Al ratios possibly because of low Si/Al ratio in some of the "precipitates" (eg. boehmite, kaolinite and chlorite). Some precipitates, such as Fe oxyhydroxides, Mn oxides and clays are considered direct precipitates from hydrothermal solutions by analogy with other deposits at other ridges (TAG and Galapagos mounds) but Fe oxyhydroxides and Fe-rich clays may also represent weathering of sulfides and sulfates deposited during high temperature venting. Other minor deposits such as boehmite, some clays and possibly talc may represent alteration of the underlying basalt. Minerals such as talc and pyrrhotite reflect high temperature (close to 300°C) hydrothermal activity.

Two geochemically anomalous regions have been targeted for further investigation as likely sites for high temperature hydrothermal activity. One site is at 13D near a fault scarp on the east wall of the axial valley. The anomalous chemistry at this site could be associated with the recently discovered Sea Cliff Hydrothermal Field or another vent field closer to the axial valley may remain undiscovered. The other target is located at 4D near a fault scarp to the east of the Sea Cliff Hydrothermal Field. Ni enrichment in samples from 4D may reflect deep circulation of seawater in the oceanic crust.

Several sites on the President Jackson Seamounts are potential sites for hydrothermal deposits (29D, 31D, 33D and 35D). The high Fe/Mn and trace metal/Mn ratios in 33D and 35D make these especially favorable targets and the extreme Fe/Mn ratios and Si/Al ratio in hydrothermal precipitates on a sample from 31D (a coarse-grained "sandstone" of volcanic material) also establish it as a favorable target.

Table II-1

Minerals commonly associated with hydrothermal deposits.

Oxides, hydroxides, oxyhydroxides	Silicates	Sulfides	Sulfates
<u>Fe</u> goethite lepidocrocite hematite	<u>smectite</u> nontronite quartz opal	<u>Fe</u> pyrite pyrrhotite marcasite	anhydrite barite
<u>Mn</u> birnessite todorokite $\delta$ MnO <sub>2</sub>	albite <u>zeolites</u> phillipsite analcite <u>chlorite</u> clinochlore	<u>Cu-Fe</u> chalcopyrite cubanite <u>Zn</u> sphalerite wurtzite	native sulfur

Additional minerals that may be present in small quantities.

Oxides, hydroxides, oxyhydroxides	Silicates	Sulfides	Sulfates
<u>Fe</u> limonite akaganéite maghemite- magnetite	<u>clays</u> sepiolite saponite vermiculite celadonite	<u>Cu-Fe</u> covellite chalcopyrrhotite bornite digenite idaïite chalcocite valleriite	gypsum jarosite natro- jarosite alunite anglesite caminite Cu-Fe
<u>Mn</u> ranceite natrobirnessite sulfates nsutite manjiroite manganite	<u>serpentine</u> amesite lizardite  talc <u>zeolites</u> stilbite heulandite clinoptilolite erionite	galena	Zn sulfates
<u>Al</u> boehmite corundum*			
<u>Ti</u> rutile anatase			

\* tentatively identified by Haymon and Kastner (1981).

Other minerals sometimes associated with hydrothermal activity that are likely to be present in small quantities are chlorides (atacamite and Fe-chlorides), carbonates (calcite, manganosiderite, magnesite), arsenides (loellingite, arsenopyrite), sulfosalts (tetrahedrite, tennantite, jordanite), and rare minerals: native bismuth, cinnabar, argentite, cassiterite and bismuth telluride.

(Brett et al., 1987, Clague et al., 1984, Haymon and Kastner, 1981, 1986a, 1986b, Hekinian and Fouquet, 1985, Hekinian et al., 1980, Howard et al., 1988, Koski et al., 1984, 1985, 1988, Oudin, 1983, Singer and Stoffers, 1981, Thompson et al., 1985).

Table II-2: Location and depth of dredge stations\* from which samples were selected.

Dredge	Location	Depth (m)
<u>Gorda Ridge OSU Cruise W7605B:</u>		
3D	42° 44' N, 126° 46' W	3000
4D	42° 33' N, 126° 51' W	3666
5D	42° 28' N, 126° 55' W	3690
<u>Gorda Ridge USGS Cruise L5-85-NC:</u>		
On axis:		
38D	42° 47.16' N, 126° 43.24' W	3045
39D	42° 45.96' N, 126° 44.08' W	3031
40D	42° 45.57' N, 126° 44.65' W	3026
42D	42° 47.92' N, 126° 42.09' W	3141
43D	42° 45.00' N, 126° 45.00' W	2994
44D	42° 45.54' N, 126° 44.83' W	2994
45D	42° 42.29' N, 126° 45.42' W	3520
Off axis:		
2D	42° 45.70' N, 126° 42.08' W	2745
3D	42° 45.23' N, 126° 40.65' W	2682
4D	42° 45.55' N, 126° 41.29' W	2675
6D	42° 45.30' N, 126° 42.13' W	2690
7D	42° 45.54' N, 126° 42.20' W	2594
8D	42° 45.66' N, 126° 42.37' W	2734
10D	42° 43.38' N, 126° 42.59' W	2719
11D	42° 44.93' N, 126° 43.25' W	2720
13D	42° 45.55' N, 126° 43.97' W	3075
President Jackson Seamounts:		
29D	42° 50.35' N, 128° 12.21' W	2150
32D	42° 44.32' N, 128° 05.69' W	1626
33D	42° 44.04' N, 128° 06.40' W	1563
34D	42° 32.00' N, 127° 47.00' W	2482
35D	42° 24.75' N, 127° 41.01' W	2274
36D	42° 25.66' N, 127° 40.76' W	1978

\* Locations and depths are from start of dredge.

Table II-3: Mineralogy of Gorda Ridge axis precipitates from OSU cruise W7605B.

Dredge	Sample ID	Color	Mineralogy
3D	3D-2	white	albite clays
	3D-11	brown	Mn oxide
	3D-13	brown	Mn oxide
4D	4D-8	brown	Mn oxide boehmite
	4D-10	red, green, brown	clay (nontronite*) todorokite
	4D-14	yellow, white, brown	albite talc
5D	5D-13	yellow, white	albite illite Mn oxide
	5D-31	brown	Mn oxide
	5D-32	orange	goethite
	5D-55 †	yellow	clinochlore albite Mn oxide

\* not positively identified, but has major peak present.

† glycolated for clay identification.

Fe oxyhydroxides are ubiquitous.

Table II-4: Mineralogy of Gorda Ridge axis precipitates from cruise L5-85-NC.

Dredge	Sample ID	Color	Mineralogy
38D	38D-1	grey	albite smectite
39D	39D-3 ‡	yellow	albite talc smectite/chlorite (both di- & trioctahedral) natrojarosite* gypsum*
40D	40D-1	grey, tan	albite clays boehmite
42D	very slight hydrothermal alteration		
43D	43D-1	white, tan	albite clays* (mostly amorphous)
44D	44D-1	white, tan	albite gypsum clays
45D	45D-1	grey	albite clays

\* not positively identified, but has two major peaks present.

‡ glycolated and heat treatments for clay mineral identification.  
Fe oxyhydroxides are ubiquitous.



Table II-5: Mineralogy of Gorda Ridge off-axis precipitates from cruise L5-85-NC.

Dredge	Sample ID	Color	Mineralogy
2D	2D	tan, yellow, white	boehmite albite kaolinite smectite
3D	3D-1 †	white	albite kaolinite boehmite chlorite illite* smectite*
	3D-2	tan, brown	albite Mn oxide
4D	4D-1A ‡	grey	albite smectite clinochlore sepiolite* goethite
	4D-1	yellow	phillipsite chlorite sepiolite* illite
	4D-1B	brown	todorokite birnessite goethite kaolinite
6D	6D-1A	tan	albite kaolinite
	6D-1 †	orange, tan	albite kaolinite chlorite pyrite*
7D	7D-1	white	albite kaolinite gypsum* calcite*
	7D-2	yellow, white	albite* kaolinite* (mostly amorphous)

Table II-5 (continued)

	7D-3	blue-green	albite nontronite* kaolinite illite gypsum* goethite*
8D	8D-2 ‡	green, brown	albite dioctahedral smectite (nontronite) Mn oxide chlorite kaolinite* illite
10D	10D-1	brown, yellow, tan	Mn oxide (mostly amorphous)
	10D-2	brown	$\delta$ -MnO <sub>2</sub> todorokite*
11D	11D-1 †	yellow, white, brown	albite chlorite* illite* (mostly amorphous)
13D	13D-1 †	brown, yellow, white	kaolinite illite* pyrite*
	13D-2 †	white, brown	albite gypsum* kaolinite illite
	13D-3	brown, yellow	pyrite* (mostly amorphous)

\* not positively identified, but has major peak(s) present.

Mn oxide - inferred from precipitate color or chemistry.

† glycolated for clay mineral identification.

‡ glycolated and heat treatments for clay mineral identification.

Fe oxyhydroxides are ubiquitous.

Table II-6: Mineralogy of President Jackson Seamount precipitates from cruise L5-85-NC.

Dredge	Sample ID	Color	Mineralogy
29D	29D	yellow, brown	quartz albite illite zeolites heulandite* natrolite* clinoptilolite* clays todorokite
	29D-1	brown	quartz mixed-layer clays heulandite (large peak at 2.96Å) todorokite*
33D	33D-1	yellow	quartz albite goethite phillipsite kaolinite illite
34D	34D	orange, brown	quartz (mostly amorphous) Mn oxide
34D	34D-3	red, brown	quartz Mn oxide (birnessite* $\delta$ -MnO <sub>2</sub> ) mixed layer clay
(celadonite?)			goethite
35D	35D-1	yellow	quartz albite mixed-layer clay
36D	36D-2	yellow, brown	quartz albite todorokite

\* not positively identified, but has two major peaks present.

? identification suggested from chemistry.

Mn oxide- inferred from chemistry and color.

Fe oxyhydroxides are ubiquitous.

Table II-7: Atomic absorption analyses of hydrothermal precipitates from the Gorda Ridge and the President Jackson Seamounts.

Sample ID	Al(%)	Ba	Ca(%)	Co	Cu	Fe(%)	K(%)	Li	Mg(%)	Mn(%)	Na(%)	Ni	Rb	Si(%)	Sr	Ti(%)	V	Zn	Fe/Mn	Si/Al	Co/Zn
Axis samples:																					
39D-3	7.59	nd	3.67	nd	120	3.67	0.220	nd	12.30	0.080	2.08	80	nd	24.10	nd	0.72	nd	80	45.88	3.18	-
40D-1	8.70	200	7.33	48	55	5.81	0.225	6	5.37	0.137	2.21	122	6	22.90	119	0.74	250	63	42.41	2.63	0.76
43D-1	6.19	MDL	2.58	nd	57	2.36	0.374	9	1.47	0.239	1.10	120	35	24.00	72	0.63	160	64	9.87	3.88	-
44D-1	10.50	nd	7.46	nd	132	5.66	0.178	nd	6.80	0.068	1.80	220	nd	24.10	nd	1.10	nd	154	83.24	2.30	-
5-55*	3.39	MDL	0.35	nd	332	8.90	0.490	24	15.70	0.331	0.85	111	nd	19.10	43	0.68	nd	286	26.89	5.63	-
Off-axis samples:																					
3D-2	5.74	1500	1.69	193	216	8.43	1.160	26	1.77	4.560	2.09	1170	45	24.60	442	0.50	90	281	1.85	4.29	0.69
4D-1	10.20	nd	1.01	nd	137	4.87	0.575	nd	1.77	0.061	0.58	1400	nd	28.10	nd	1.28	nd	220	79.84	2.75	-
4D-1A	9.01	300	4.24	55	183	6.69	0.599	19	4.08	0.500	1.94	510	19	21.70	164	1.04	130	275	13.38	2.41	0.20
4D-1B	3.55	1800	1.59	344	645	5.83	1.010	150	1.96	24.300	2.00	5730	24	12.10	545	0.35	420	2390	0.24	3.41	0.14
6D-1	5.32	800	2.76	91	496	13.10	1.100	30	3.12	2.580	2.57	927	48	20.20	331	0.46	200	256	5.08	3.80	0.36
6D-1A	7.42	MDL	3.15	82	285	7.73	0.906	41	6.16	1.590	1.78	930	38	21.50	205	0.74	160	192	4.86	2.90	0.43
7D-1	13.40	nd	2.84	nd	271	2.48	0.370	nd	2.26	0.256	2.82	90	nd	19.40	nd	0.87	nd	184	9.69	1.45	-
8D-1	3.88	1010	1.42	196	333	12.70	1.430	42	2.84	4.93	2.56	1340	53	19.96	359	0.40	nd	522	2.58	5.14	0.38
8D-2	10.00	480	2.28	208	659	6.28	0.529	16	3.30	4.86	4.30	1470	14	15.00	377	1.20	nd	406	1.29	1.50	0.51
10D-1	5.45	800	2.77	234	436	10.60	1.070	32	4.35	7.49	1.94	2440	35	17.60	468	0.61	250	670	1.42	3.23	0.35
10D-2	3.21	1600	1.77	462	428	11.90	1.030	50	2.08	13.70	2.79	3480	34	14.90	722	0.41	360	1090	0.87	4.64	0.42
11D-1	8.12	400	4.84	54	310	6.50	0.780	29	4.87	1.42	2.37	433	36	22.30	170	0.69	40	244	4.58	2.75	0.22
13D-1	8.16	820	4.16	82	157	7.56	0.976	30	3.53	0.82	2.29	158	44	22.86	206	0.89	nd	218	9.22	2.80	0.38
13D-2	12.30	10	6.36	103	192	2.64	0.144	17	4.17	0.06	1.57	137	10	21.73	140	0.84	nd	200	44.00	1.77	0.52
13D-3	7.40	MDL	5.87	nd	477	5.95	0.214	MDL	3.78	1.82	1.81	460	20	24.30	220	0.93	290	277	3.27	3.28	-
Seamount samples:																					
29D	5.29	700	1.16	702	229	14.00	1.630	39	0.22	3.740	2.15	851	59	20.20	377	0.50	240	234	3.74	3.82	3.00
29D-1	2.82	200	1.78	499	250	19.10	1.860	17	2.49	1.970	1.44	573	60	21.10	206	0.28	190	141	9.70	7.48	3.54
29D-2	2.84	400	0.82	611	286	20.10	1.710	36	1.93	3.460	1.50	918	55	19.60	290	0.32	220	286	5.81	6.90	2.14
31D-1	0.35	200	0.14	26	21	7.93	0.75	9	0.81	0.101	0.57	21	31	37.3	35	0.04	MDL	29	78.51	106.57	0.90
32D-1	2.15	1100	1.77	1810	183	22.20	0.608	10	1.32	10.000	1.64	1910	16	12.40	1100	0.69	690	505	2.22	5.77	3.58
33D-1	6.30	MDL	2.08	450	623	18.30	0.239	28	1.38	2.100	2.51	900	62	17.70	166	0.21	MDL	159	8.71	2.81	2.83
34D	3.09	500	2.95	2380	3270	17.90	0.967	22	2.34	8.190	2.29	2430	25	14.50	618	0.48	340	291	2.19	4.69	8.18
34D-3	3.59	1300	1.01	408	795	19.50	2.270	63	2.47	4.900	1.32	2290	87	17.70	218	0.25	340	435	3.98	4.93	0.94
35D-1	7.82	1000	3.55	118	124	8.10	1.44	38	3.12	0.397	1.94	235	71	23.90	209	0.66	MDL	158	20.40	3.06	0.75
36D-1A	4.01	900	3.23	665	164	12.70	1.14	31	2.62	4.61	2.32	1050	38	19.02	449	0.40	nd	323	2.75	4.74	2.06
36D-2	7.76	1300	1.84	696	333	9.83	1.53	61	2.73	3.64	1.94	1160	59	21.30	336	0.57	260	279	2.70	2.74	2.49

MDL = minimum detection limit (assuming 1g of sample/ml of solution analyzed, this is 5ppm for Ba and V, and 1ppm for Li).

nd = not determined.

\* W7605B, all others from L5-85-NC.

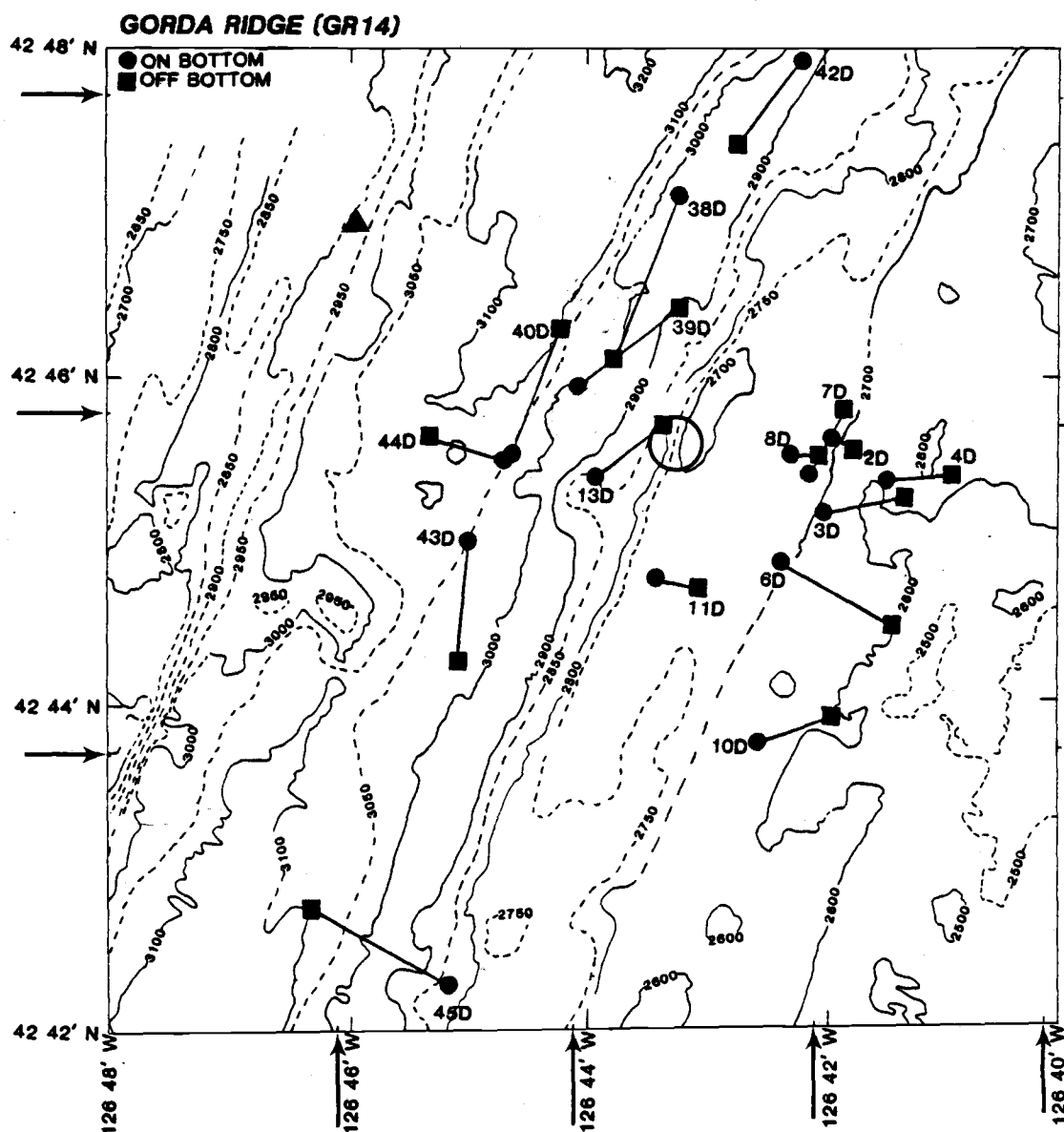


Fig. II-1: Detailed bathymetric maps showing sample locations after NOAA SEABEAM for the (a) GR-14 area and (b) President Jackson Seamounts. OSU samples except for W7605B-3D (▲) are to the south of the map area. Arrows show latitudinal shift to the south and longitudinal shift to the west from readjustment of SEABEAM navigation (Rona and Clague, 1989, in prep). Circled area near 13D is the location of the Sea Cliff Hydrothermal Field. Contour interval = 50m.

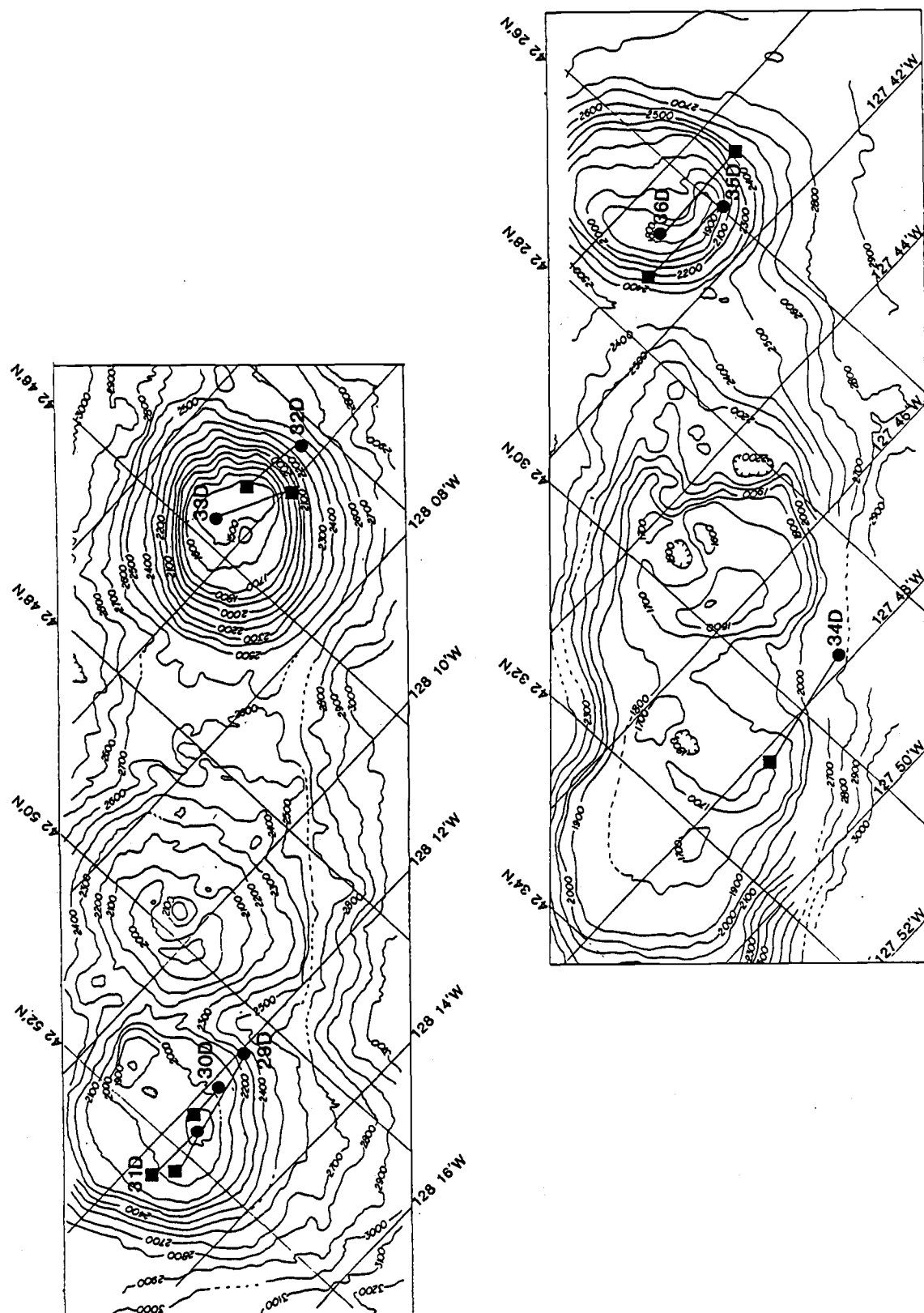


Fig. II-1b

Fig. II-2: (a) X-ray diffractogram of sample L5-85-NC-4D-1B showing two major peaks for todorokite (labeled T). Other major peaks are from the  $\text{SiO}_2$  internal standard. (b) X-ray diffractogram of sample W7605B-5D-55 showing the major peaks for clinocllore (labeled C). Other peaks are from the  $\text{SiO}_2$  internal standard. (c) X-ray diffractogram of sample W7605B-4D-14 showing the major peaks for talc. Other peaks present belong to albite and the  $\text{SiO}_2$  internal standard.

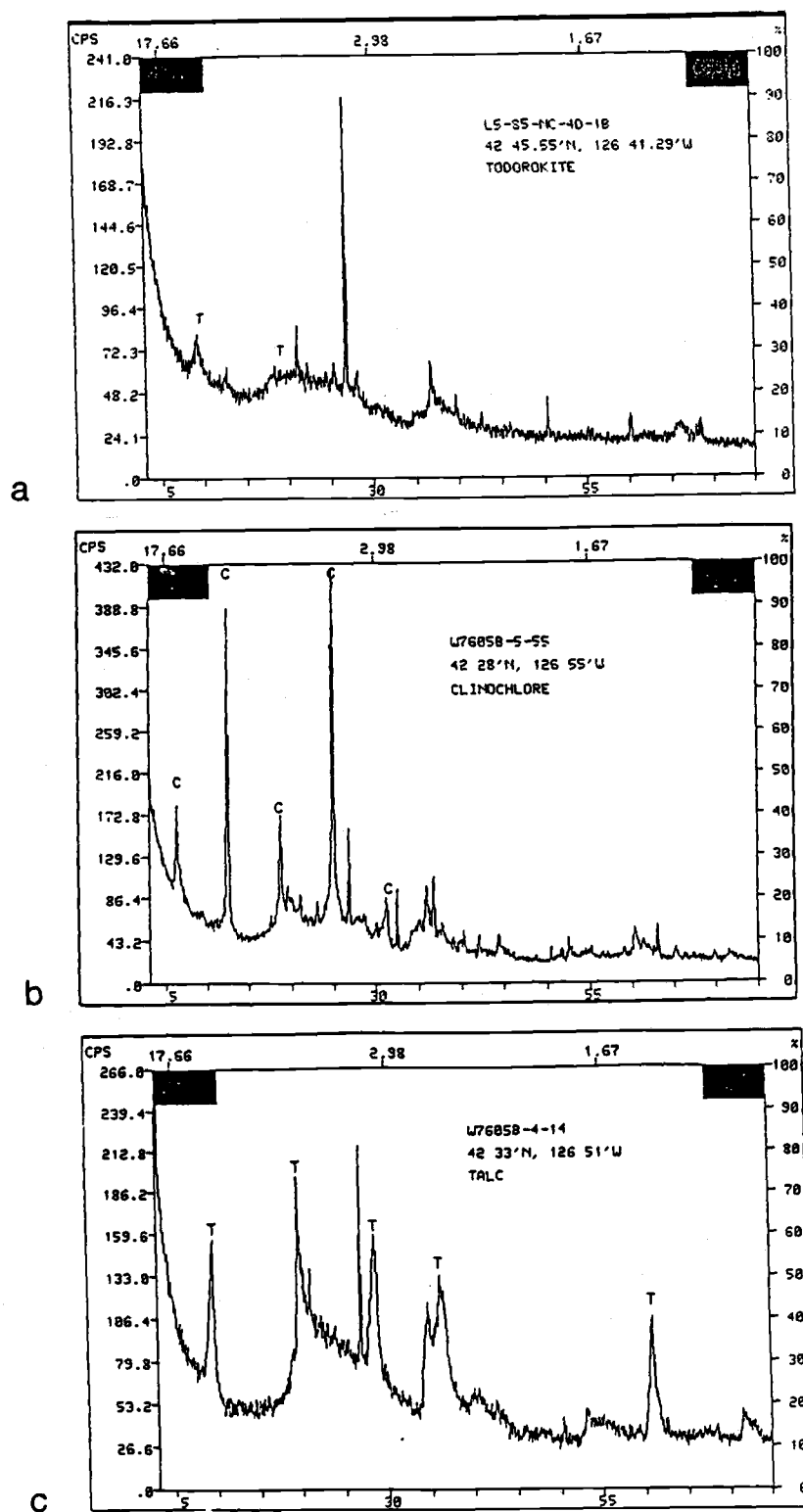


Fig. II-2



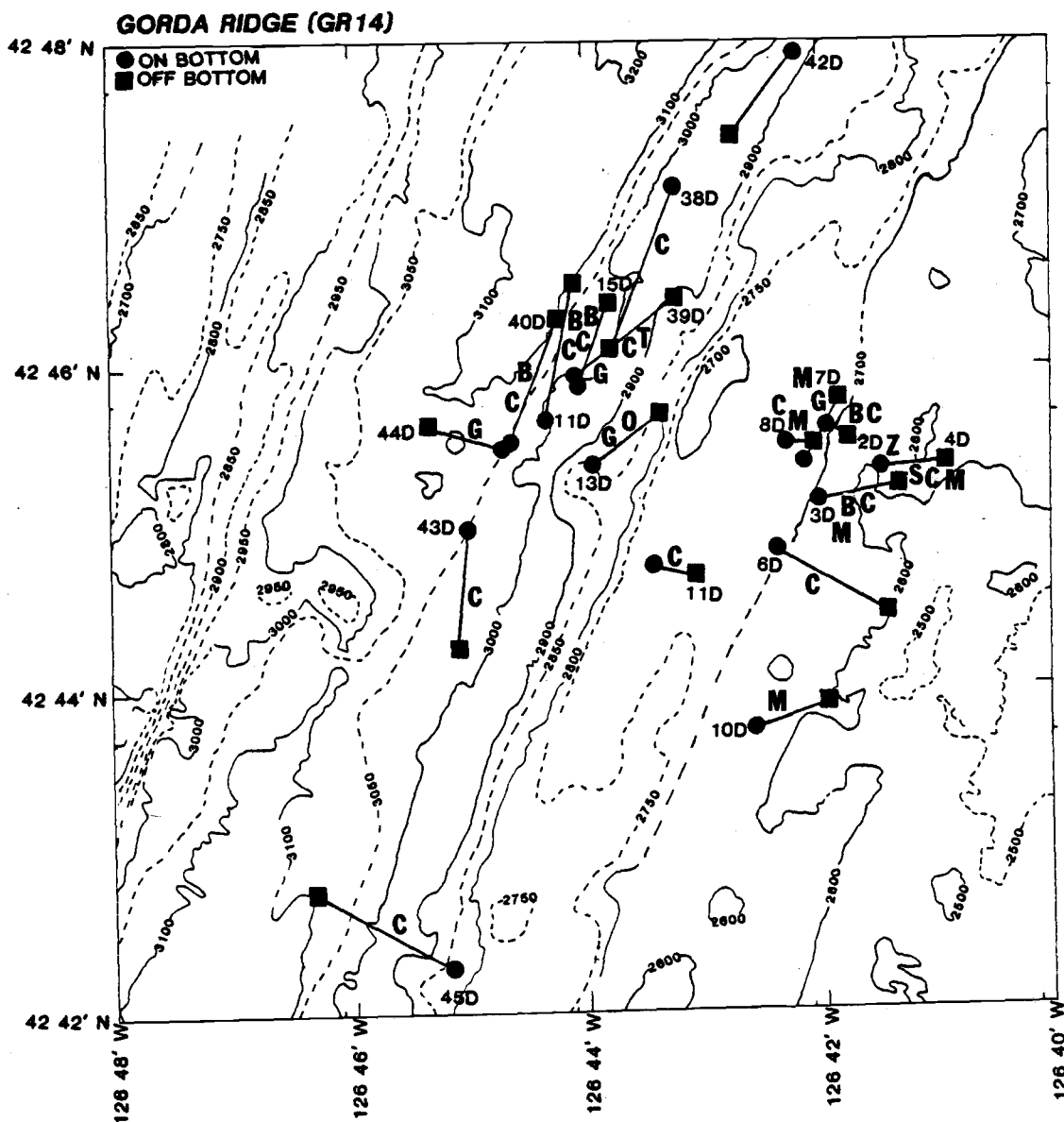


Fig. II-3: Bathymetric maps with location of major minerals identified in hydrothermal precipitates from (a) GR-14 and (b) President Jackson Seamounts. Fe oxyhydroxides are present in all samples. For (b) quartz is present in all samples. B = boehmite, C = clays, G = gypsum, M = Mn oxide, S = sepiolite (?). The location of tentatively identified sepiolite is shown to facilitate discussion in the text.

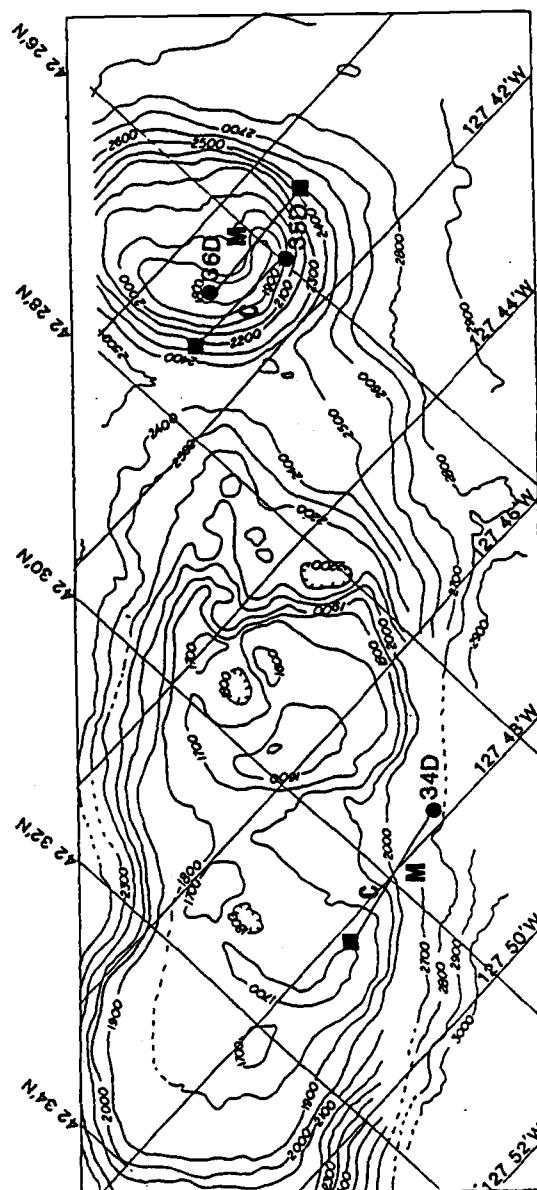
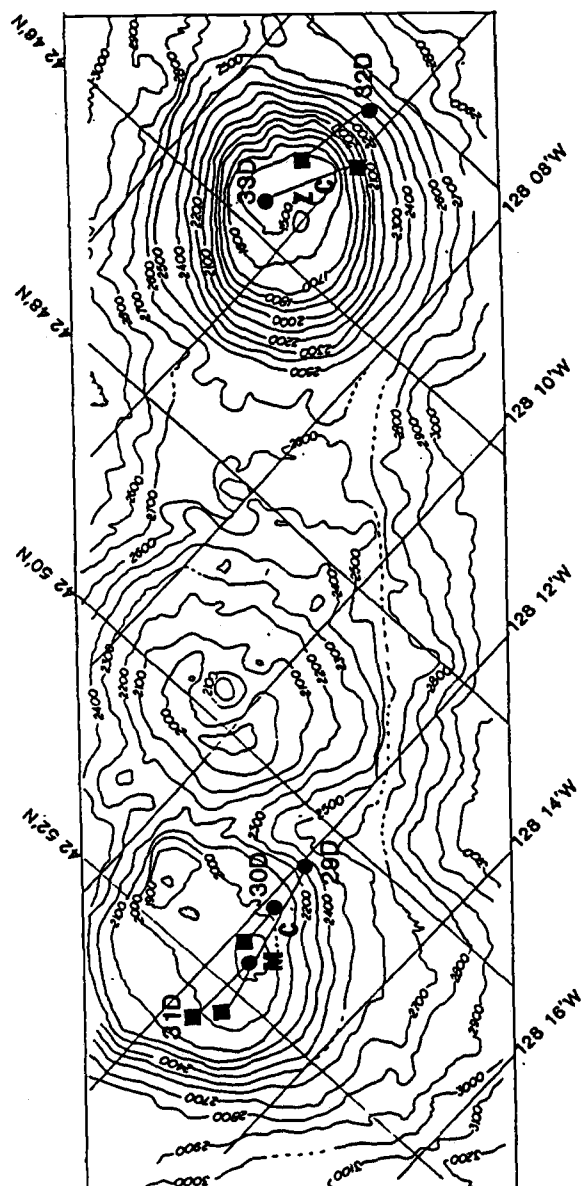


Fig. II-3b

Fig. II-4: Ternary plot with apices Al, Fe and Mn. ● are Gorda Ridge axis samples. ■ are off-axis samples. ▲ are President Jackson Seamount samples. Positions of hydrothermal deposits from the Galapagos Mounds (○), TAG Hydrothermal Field (◇), and Transform Fault "A" on the Mid-Atlantic Ridge (□) are from Thompson et al., 1985. Al-rich smectite from the East Pacific Rise (S) is from Haymon and Kastner, 1986b. Mid-ocean ridge basalt (MORB) (★) from OSU dredge, W7605B-4D are shown for comparison. N = nontronite, F = Fe oxyhydroxide, B = birnessite. Identification numbers of samples discussed in the text are also shown.

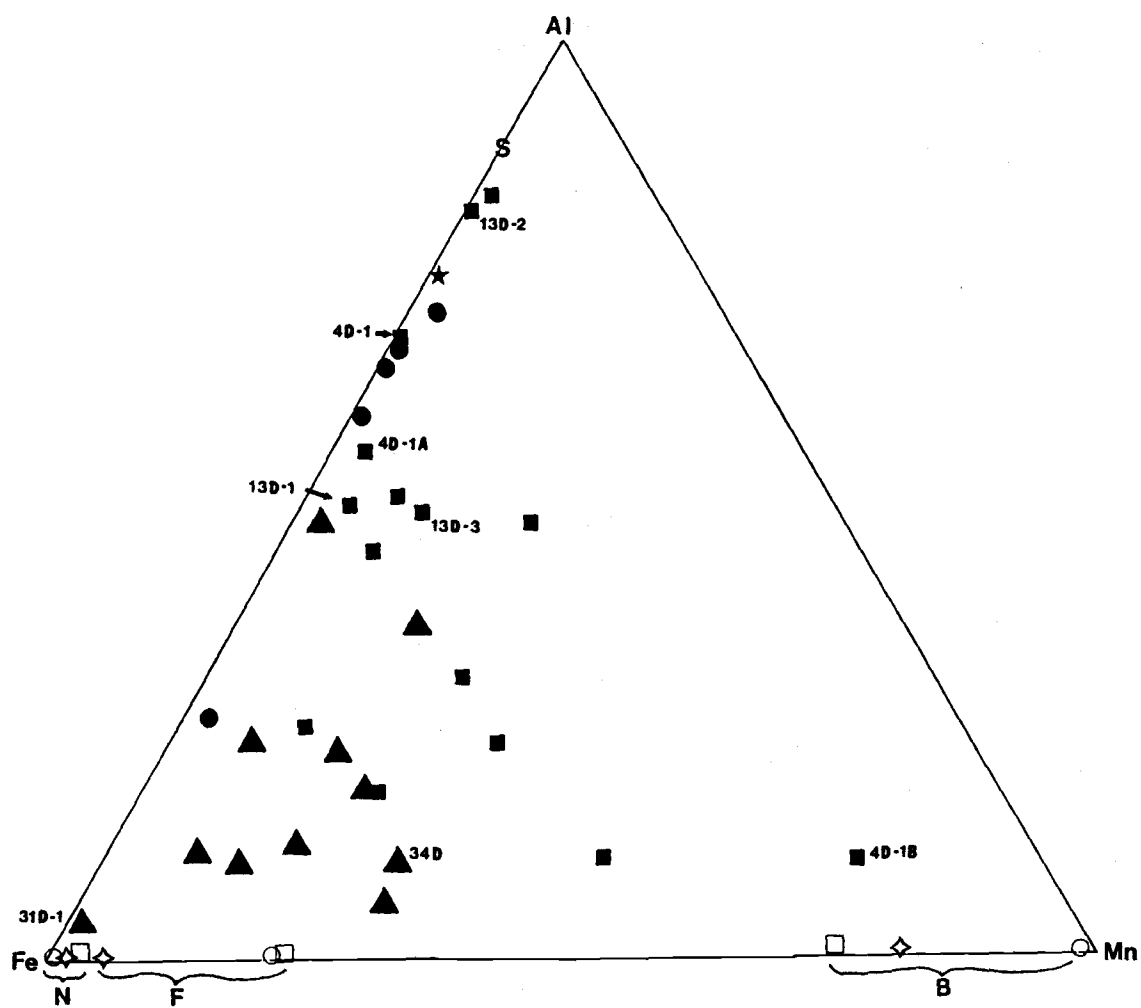


Fig. II-4

Fig. II-5: Elements versus Mn plots for Gorda Ridge on axis, off axis and President Jackson Seamount samples. Ni and Zn are strongly correlated with Mn. Hydrothermal precipitates from 4D show an extreme range of chemistry. One subsample (4D-1B) has the highest Mn and Ni concentration and another subsample (4D-1) has an anomalously high Ni/Mn ratio (a). Zn is strongly correlated with Mn (b). Cu, Co and Ba show two trends with increasing Mn (c,d,e,g). Cu versus Mn is also shown with expanded scale to better illustrate the secondary trend (d). Fe/Mn and Co/Mn are enriched in seamount samples relative to Gorda Ridge samples (f,g) and Si and Al correlate negatively with Mn (h,i). Symbols same as in Fig. II-4.

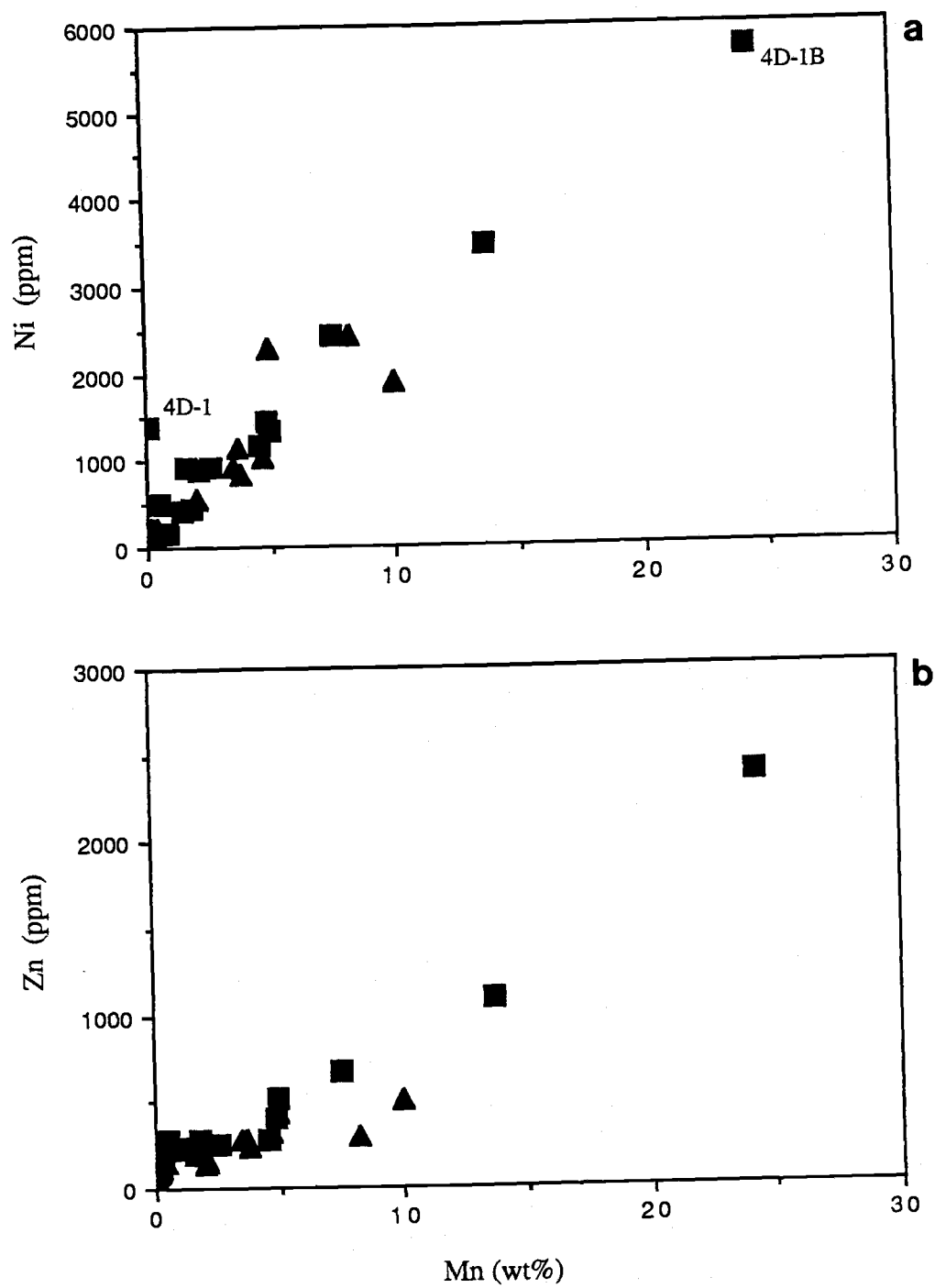


Fig. II-5

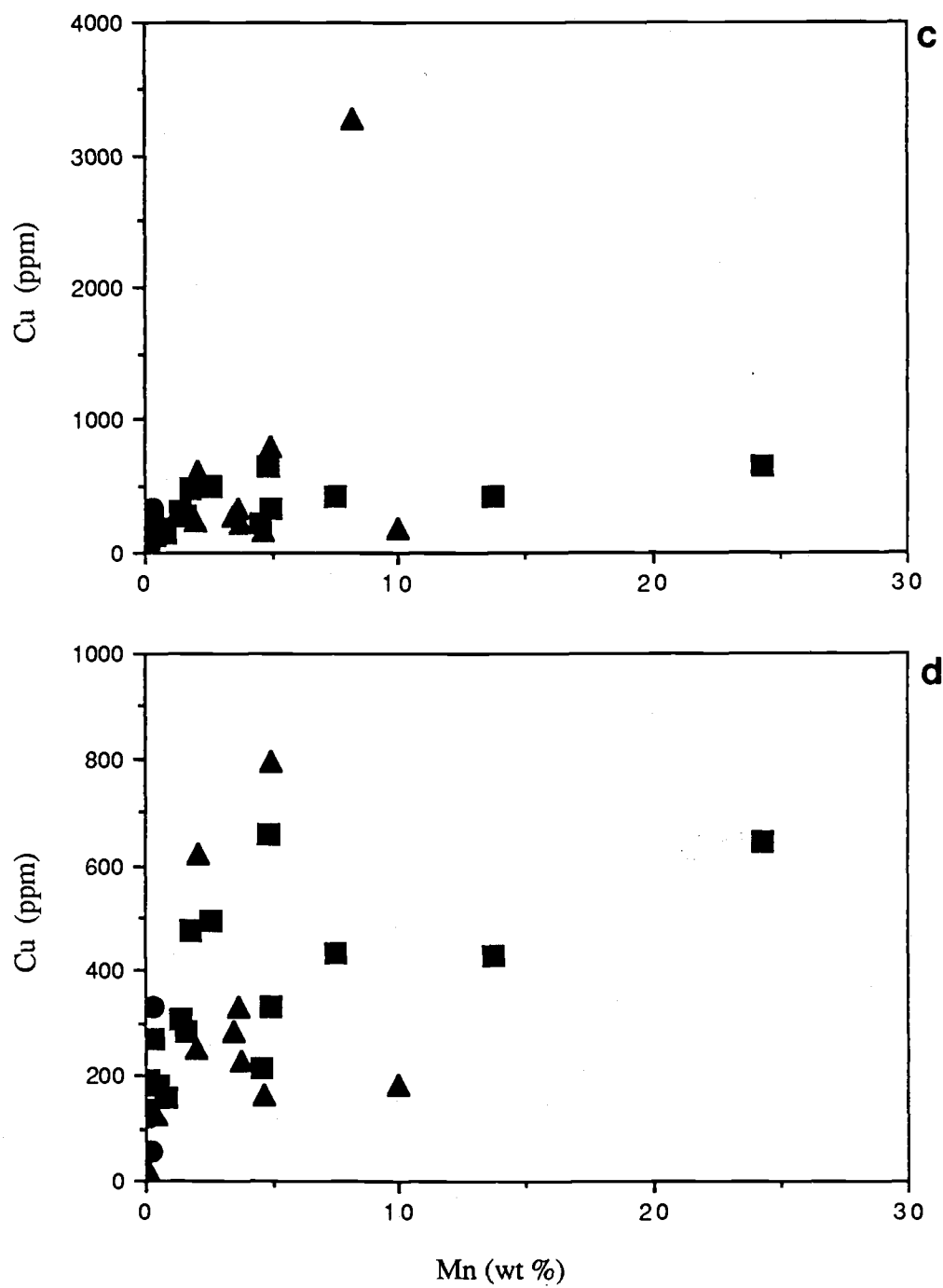


Fig. II-5 (continued)

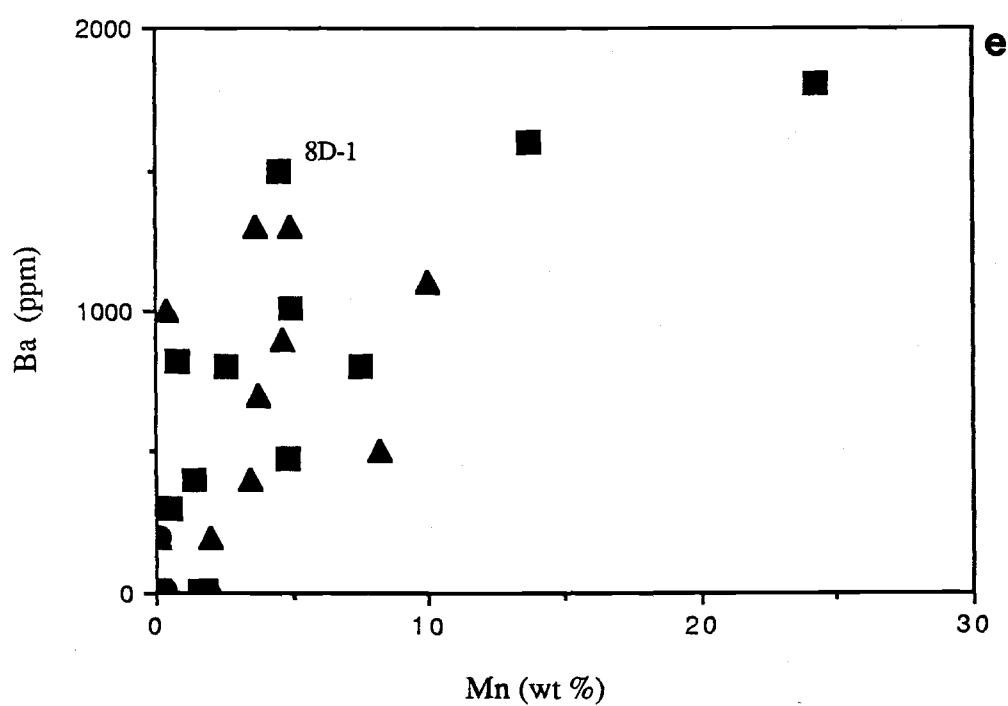
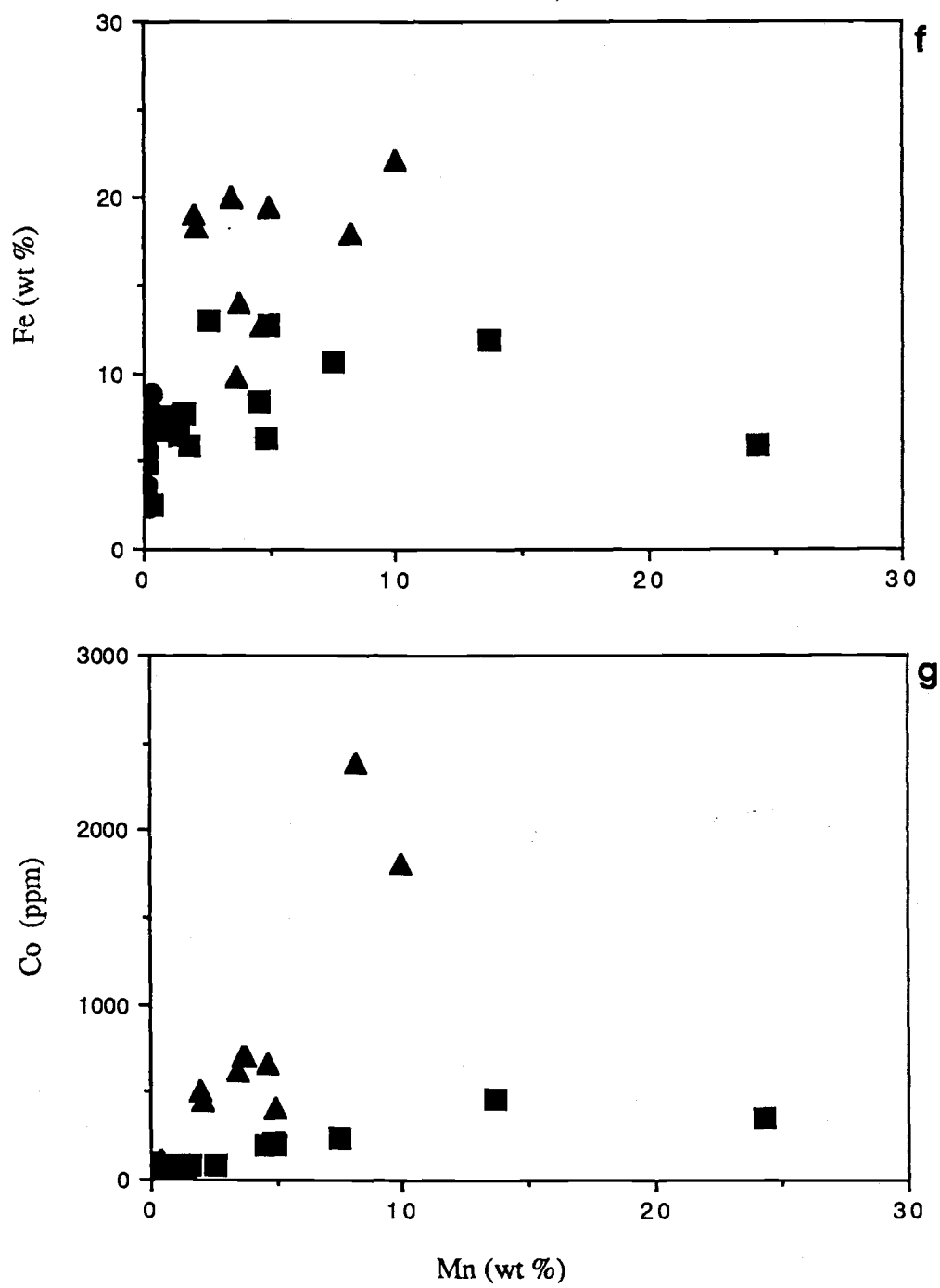


Fig. II-5 (continued)





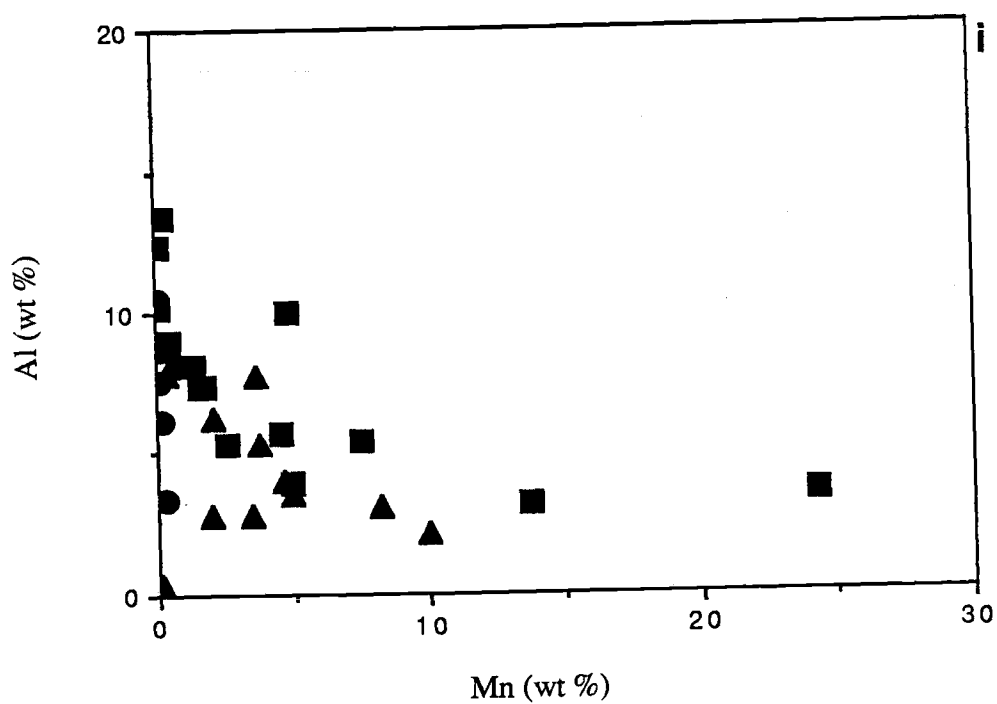
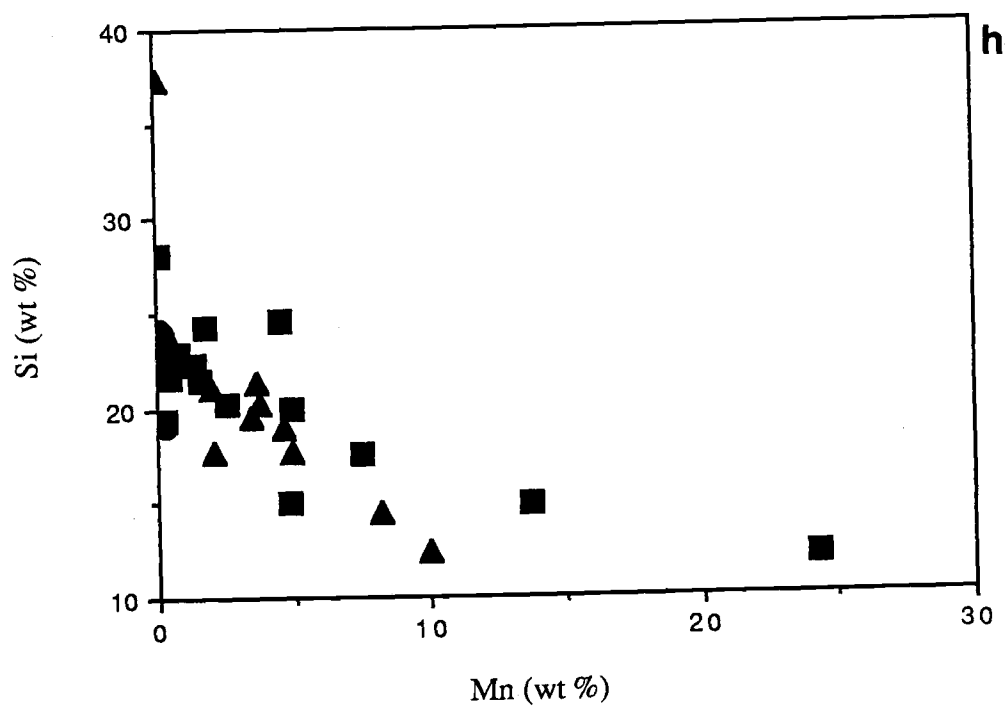


Fig. II-5 (continued)

Fig. II-6: Ternary plot with apices Co, Cu and Ni showing relative enrichment of all samples in Ni, and enrichment in President Jackson Seamount samples in Co relative to Gorda Ridge samples. Ni-rich sulfides in basalts (in addition to olivine) are a potential source of Ni in hydrothermal precipitates. Symbols same as in Fig. II-4 for samples from this study. ○ = Juan de Fuca Ridge nontronite (Murnane and Clague, 1983), ◇ = Galapagos mounds deposits (Corliss et al., 1978). From Transform Fault "A", A = hydrothermal Fe-Mn concretions, (A) = Fe-Mn coatings on basalts, C = clay, (S) = metalliferous sediment. (Hoffert et al., 1978), \* = average of 12 sulfide analyses from FAMOUS area Mid-Atlantic Ridge (Czamanske and Moore, 1977). ●<sup>5</sup> ●<sup>9</sup> = sulfides in basalt from OSU dredge sample W7605B-5-18 and USGS dredge sample KK2-83-NP-9-1, □ = seawater and ★ = basalt from Reeves and Brooks, 1978.

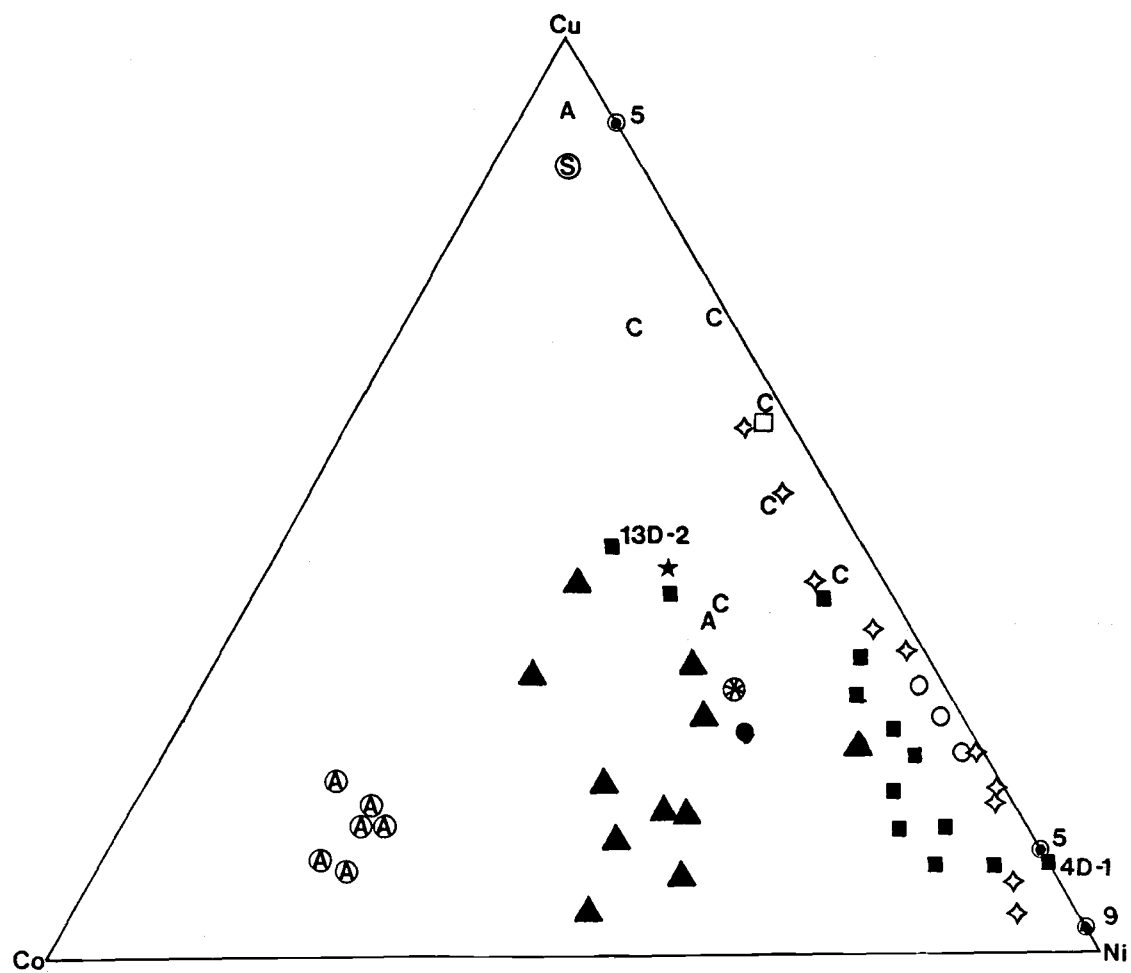


Fig. II-6

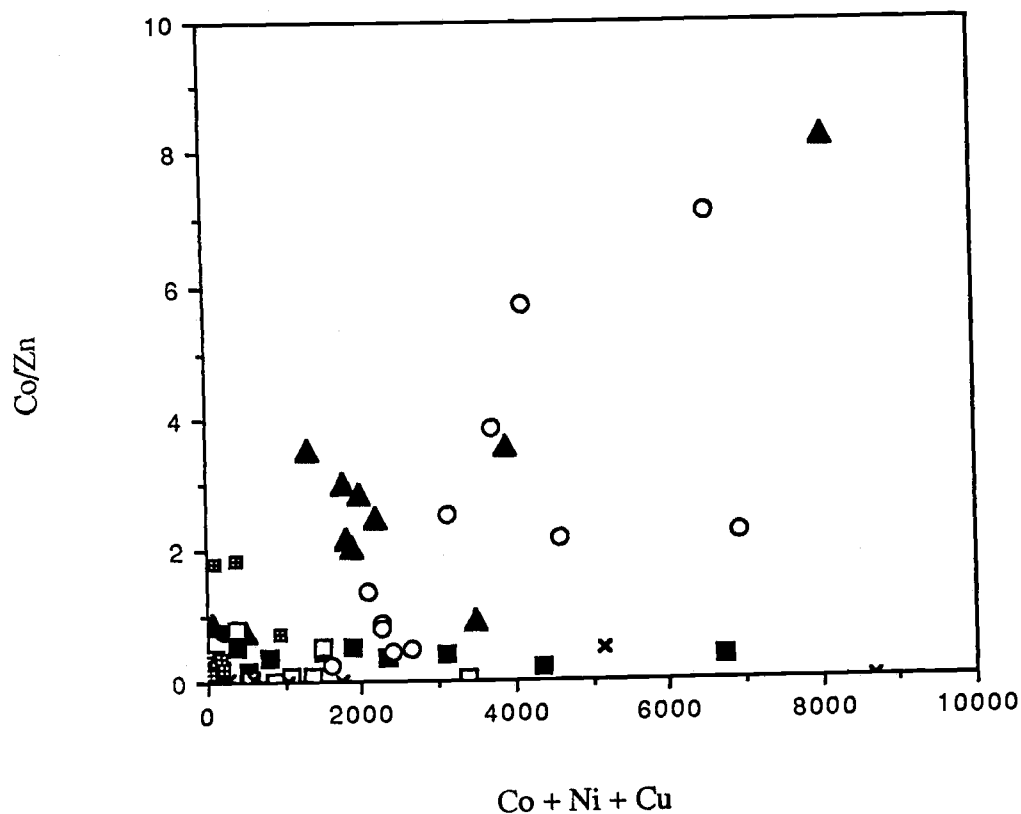


Fig. II-7: Co/Zn versus Co + Ni + Cu. Symbols same as in Fig. II-4 for samples from this study. Additional samples are  $\square$  hydrothermal crusts and  $\circ$  ferromanganese crusts from Toth (1980),  $\times$  Galapagos Mounds hydrothermal deposits from Corliss et al. (1978) and  $\square$  Transform Fault "A" ferromanganese concretions, clays and metalliferous sediment from Hoffert et al. (1978).

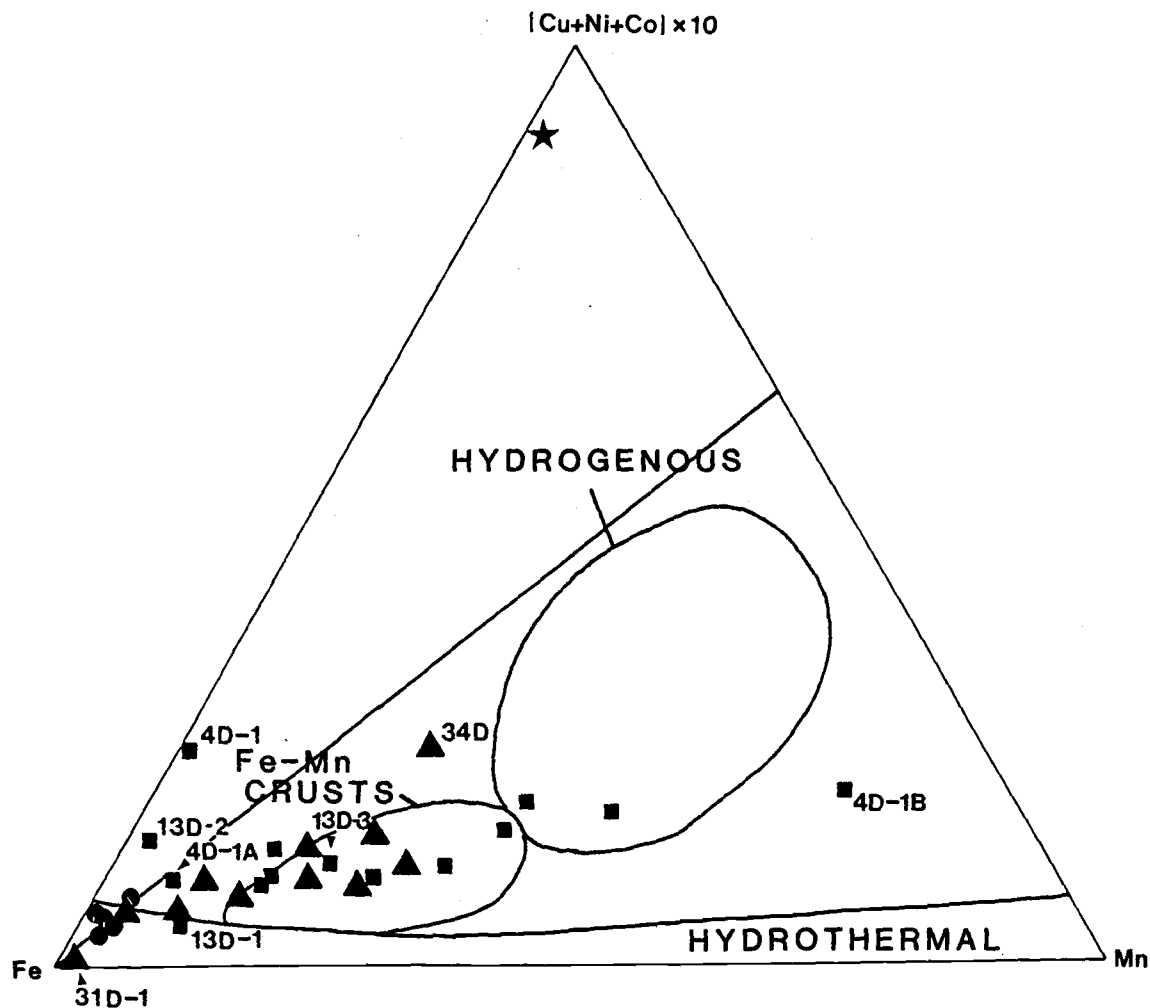


Fig. II-8: Ternary plot with apices Fe, Mn and  $(\text{Cu}+\text{Ni}+\text{Co}) \times 10$  after Bonatti et al. (1972). Hydrothermal, hydrogenous and Fe-Mn crust fields are from Toth, (1980). ★ = Cu-rich gossan overlying Cyprus massive sulfide deposits (Robertson and Boyle, 1983). Line designates the position of maximum  $(\text{Cu}+\text{Ni}+\text{Co}+\text{Zn})$  in todorokite from Halbach et al. (1981). Symbols same as in Fig. II-4. Identification numbers of samples discussed in the text are also shown.

## References

- Alt, J.C., Lonsdale, P., Haymon, R. and Muehlenbachs, K. (1987) Hydrothermal sulfide and oxide deposits on seamounts near 21°N, East Pacific Rise. *Geol. Soc. Am. Bull.* 98, 157-168.
- Alpin, A.C. and Cronan, D.S. (1985) Ferromanganese oxide deposits from the Central Pacific Ocean I. Encrustations from the Line Islands Archipelago. *Geochim. Cosmochim. Acta.* 49, 427-436.
- Arcyana, (1975) Transform fault and rift valley geology from bathyscaph and diving saucer. *Science* 190, 108-116.
- Atwater, T. and Mudie, J.D. (1973) Detailed near-bottom geophysical study of the Gorda Rise. *J. Geophys. Res.* 78, 8665-8686.
- Batiza, R. (1985) Qualitative assessment of polymetallic sulfide mineral deposits on seamounts. *Mar. Min.* 5, 181-191.
- Bischoff, J.L. (1980) Geothermal system at 21°N, East Pacific Rise: Physical limits on geothermal fluid and role of adiabatic expansion. *Science* 207, 1465-1469.
- Bischoff, J.L. and Dickson, F.W. (1975) Seawater-basalt interaction at 200°C and 500 bars: Implications for origin of sea-floor heavy metal deposits and regulation of seawater chemistry. *Earth Planet. Sci. Lett.* 25, 385-397.
- Bischoff, J.L., Piper, D.Z. and Leong, K. (1981) The alumino-silicate fraction of North Pacific manganese nodules. *Geochim. Cosmochim. Acta.* 45, 2047-2063.
- Blain, C.F. and Andrews, R.L. (1977) Sulfide weathering and the evaluation of gossans in mineral exploration. *Minerals Sci. Engng.* 9, 119-150.
- Bonatti, E., Kraemer, T. and Rudell, H. (1972) Classification and genesis of submarine iron-manganese deposits, p.149-166. In: D.R. Horn (ed.) *Papers on a Conference about Ferromanganese Deposits on the Ocean Floor*. Washington, D.C., National Science Foundation.
- Bonatti, E., Simmons, E.C., Breger, D., Hamlyn, P.R. and Lawrence, J. (1983) Ultramafic rock/seawater interaction in the oceanic crust: Mg-silicate (sepiolite) deposit from the Indian Ocean floor. 62, 229-238.
- Brett, R., Evans, H.T.Jr., Gibson, E.K. Jr., Hedenquist, J.W., Wandless, M.-V. and Sommer, M.A. (1987) Mineralogical studies of sulfide samples and volatile concentrations of basalt glasses from the southern Juan de Fuca Ridge. 92, 11,373-11,379.
- Brindley, G. W. and Brown, G. (1980) *Crystal Structures of Clay Minerals and their X-ray Identifications*. Spottiswoode Ballantyne Ltd.
- Burns, R.G. (1976) The uptake of cobalt into ferromanganese nodules, soils and synthetic manganese (IV) oxides. *Geochim Cosmochim Acta.* 40, 95-102.

- Calvert, S.E. and Piper, D.Z. (1984) Geochemistry of ferromanganese nodules from DOMES Site A northern equatorial Pacific: multiple diagenetic sources in the deep sea. *Geochim. Cosmochim. Acta.* 48, 1913-1928.
- Calvert, S.E. and Price, N.B. (1977) Geochemical variation in ferromanganese nodules and associated sediments from the Pacific Ocean. *Mar. Chem.* 5, 43-74.
- Chave, K.E., Morgan, C.L. and Green, W.J. (1986) A geochemical comparison of manganese oxide deposits of the Hawaiian Archipelago and Deep Sea. *Applied Geochemistry* 1, 233-240.
- Clague, D.A., Friesen, W., Quinterno, P., Holmes, M., Morton, J., Bouse, R., Morgenson, L., and Davis, A. (1984) Preliminary geological, geophysical and biological data from the Gorda Ridge. U.S. Geol. Survey Open-File Report 84-364, 48p.
- Collier, R.W., Holbrook, S. H. and Robbins, J.M. (1986) Studies of trace metals and active hydrothermal venting on the Gorda Ridge. Oregon Department of Geology and Mineral Industries, Open-File Report 0-86-13.
- Corliss, J.B., Lyle, M., Dymond, J. and Crane, K. (1978) The chemistry of hydrothermal mounds near the Galapagos Rift. *Earth Planet Sci Lett.* 40, 12-24.
- Craig, J.D., Andrews, J.E. and Meylan, M.A. (1982) Ferromanganese deposits in the Hawaiian Archipelago. *Mar. Geol.* 45, 127-157.
- Crane, K. and Ballard, R.D. (1981) Volcanics and structures of the FAMOUS-Narrowgate rift: Evidence for cyclic evolution: AMAR I. *J. Geophys. Res.* 86, 5112-5124.
- Cronan, D.S. (1977) Deep-sea nodules - distribution and geochemistry. In: G.P. Glasby (Ed.) *Marine Manganese Deposits*. Elsevier, Amsterdam, pp. 11-44.
- Czamanske, G.K. and Moore, J.G. (1977) Composition and phase chemistry of sulfide globules in basalt from the Mid-Atlantic Ridge rift valley near 37°N lat. *Geol. Soc. Am. Bull.* 88, 587-599.
- Davis, A. and Clague, D.A. (1988) Petrology of gabbroic xenoliths from the northern Gorda Ridge. *EOS* 69, 1493.
- Deer, W.A., Howie, R.A. and Zussman, J. (1966) *An Introduction to the Rock-Forming Minerals*. J. Wiley and Sons, 528p.
- Dymond, J., Lyle, M., Finney, B., Piper, D.Z., Murphy, K., Conard, R. and Pisias, N. (1984) Ferromanganese nodules from MANOP Sites H, S, and R - control of mineralogical and chemical composition by multiple accretionary processes. *Geochim Cosmochim Acta*, 48, 931-949.
- Feely, R.A., Lewison, M., Massoth, G.J., Robert-Baldo, G., Lavelle, J.W., Byrne, R.H., Von Damm, K.L., Curl, H.C.Jr. (1987) Composition and dissolution of black smoker particulates from active vents on the Juan de Fuca Ridge. *J. Geophys. Res.* 92, 11347-11363.



- Fleet, A.J. (1983) Hydrothermal and hydrogenous ferro-manganese deposits: Do they form a continuum? The rare earth element evidence. In: *Hydrothermal Processes at Mid-Ocean Spreading Centers* (eds. P.A. Rona, K. Bostrom, L. Laubier and E.L. Smith) pp. 535-556.
- Gitlin, E. (1985) Sulfide remobilization during low temperature alteration of seafloor basalt. *Geochim Cosmochim Acta*. 49, 1567-1579.
- Hajash, A. and Chandler, G.W. (1981) An experimental investigation of high temperature interactions between seawater and rhyolite, andesite, basalt and peridotite. *Contrib. Min. Petrol.* 78, 240-254.
- Halbach, P., Hebisch, Udo, and Scherhag, C. (1981) Geochemical variations of ferromanganese nodules and crusts from different provinces of the Pacific Ocean and their genetic control. *Chem Geol.* 34, 3-17.
- Halbach, P. and Puteanus, D. (1984) The influence of the carbonate dissolution rate on the growth and composition of Co-rich ferromanganese crusts from Central Pacific seamount areas. *Earth Planet. Sci. Lett.* 68, 73-87.
- Harder, H. (1976) Nontronite synthesis at low temperatures. *Chem. Geol.* 18, 169-180.
- Haymon, R.M. (1983) Growth history of hydrothermal black smokers. *Nature* 301, 695-698.
- Haymon, R.M. and Kastner, M. (1981) Hot spring deposits on the East Pacific Rise at 21°N: preliminary description of mineralogy and genesis. *Earth Planet. Sci. Lett.* 53, 363-386.
- Haymon, R.M. and Kastner, M. (1986a) Caminite: A new magnesium-hydroxide-sulfate-hydrate mineral found in a submarine hydrothermal deposit, East Pacific Rise, 21°N. *Am. Min.* 71, 819-825.
- Haymon, R.M. and Kastner, M. (1986b) The formation of high temperature clay minerals from basalt alteration during hydrothermal discharge on the East Pacific Rise axis at 21°N. *Geochim Cosmochim Acta*, 50, 1933-1939.
- Hein, J.R., Manheim, F.T., Schwab, W.C. and Davis, A.S. (1988) Ferromanganese crusts from Necker Ridge, Horizon Guyot and S.P. Lee Guyot: Geological considerations. *Mar. Geol.* 78, 225-283.
- Hekinian, R., Fevier, M., Bischoff, J.L., Picot, P., and Shanks, W.C. (1980) Sulfide deposits from the East Pacific Rise near 21°N. *Science* 207, 1433-1444.
- Hekinian, R. and Fouquet, Y. (1985) Volcanism and metallogenesis of axial and off-axial structures on the East Pacific Rise near 13°N. *Econ. Geol.* 80, 221-249.
- Herzig, P.M., Becker, K.P., Stoffers, P., Backer, H. and Blum, N. (1988) Hydrothermal silica chimney fields in the Galapagos Spreading Center at 86°W. *Earth Planet. Sci. Lett.* 89, 261-272.

- Hoffert, M. Perseil, A., Hékinian, R., Choukroume, P., Needham, H.D., Francheteau, J. and Le Pichon, X. (1978) Hydrothermal deposits samples by diving saucer in Transform Fault "A" near 37°N on the Mid-Atlantic Ridge, Famous area. *Oceanol. Acta.* 1, 73-86.
- Honnorez, J. (1980) The aging of the oceanic crust at low temperature. In: *The Sea* (ed. C. Emiliani) Vol. 7, Chap. 15 pp. 525-587. Wiley-Interscience.
- Howard, K.J. and Fisk, M.R. (1988) Hydrothermal alumina-rich clays and boehmite on the Gorda Ridge. *Geochim. Cosmochim. Acta.* 52, 2269-2279.
- Howard, K.J., Fisk, M.R. and Lyle, M. (1988) Weathered sulfide chimneys from the Escanaba Trough, Gorda Ridge. *EOS.* 69, 1484.
- Huang, P.Y. and Solomon, S.C. (1988) Centroid depths of mid-ocean ridge earthquakes: dependence on spreading rate. *J. Geophys. Res.* 93, 13445-13478.
- Humphries, S. and Thompson, G. (1978) Trace element mobility during hydrothermal alteration of oceanic basalts. *Geochim. Cosmochim. Acta.* 42, 127-136.
- Ingram-DePaolo, B.L. and Hein, J.R. (1988) Sr isotopes in hydrogenetic and hydrothermal Fe-Mn crusts. *EOS* 69, 1489.
- Janecky, D.R. and Seyfried, W.E. Jr. (1986) Hydrothermal serpentinization of peridotite within the oceanic crust: Experimental investigations of mineralogy and major element chemistry. *Geochim. Cosmochim. Acta.* 50, 1357-1378.
- Jannash, H.W. (1983) Microbial processes at deep sea hydrothermal vents. In: *Hydrothermal Processes at Mid-Ocean Spreading Centers* (eds. P.A. Rona, K. Bostrom, L. Laubier and E.L. Smith) pp. 677-710.
- Kimball, K.L. (1988) High-temperature hydrothermal alteration of ultramafic cumulates from the base of the Josephine Ophiolite, NW California. *J. Geophys. Res.* 93, 4675-4687.
- Koski, R.A., Clague, D.A. and Oudin, E. (1984) Mineralogy and chemistry of massive sulfide deposits from the Juan de Fuca Ridge. *Geol. Soc. Am. Bull.* 95, 930-945.
- Koski, R.A., Lonsdale, P.F., Shanks, W.C., Berndt, M.E., and Howe, E.E. (1985) Mineralogy and geochemistry of a sediment-hosted hydrothermal deposit from the southern trough of Guaymas Basin, Gulf of California. *J. Geophys. Res.* 90, 6695-6707.
- Koski, R.A., Shanks, W.C., III, Bohrsen, W.A. and Oscarson, R.L. (1988) The composition of sediment-hosted massive sulfide deposits from the Escanaba Trough, Gorda Ridge: Implications for fluid-sediment interaction and depositional processes. *Can. Min.* 26, 655-673.
- Krauskopf, K.B. (1957) Separation of manganese from iron in sedimentary processes. *Geochim. Cosmochim. Acta.* 12, 61-84.

- Lister, C.R.B. (1983) The basic physics of water penetration into hot rock. In: Hydrothermal Processes at Mid-Ocean Spreading Centers (eds. P.A. Rona, K. Bostrom, L. Laubier and E.L. Smith) pp.141-168. Plenum Press.
- Lonsdale, P. (1977) Structural geomorphology of a fast-spreading rise crest, the East Pacific Rise near 3° 25'S. *Mar. Geophys. Res.* 3, 251-294.
- Lonsdale, P., Batiza, R. and Simkin, T. (1982) Metallogenesis at seamounts on the East Pacific Rise. *J. Mar. Technol. Soc.* 16, 54-61.
- Lonsdale, P., Bischoff, J.L., Burns, V.M., Kastner, M. and Sweeney, R.E. (1980) A high temperature deposit on the seabed at a Gulf of California spreading center. *Earth Planet. Sci. Lett.* 49, 8-20.
- Loughnan, F.C. (1969) Chemical weathering of the silicate minerals. Elsevier, 154p.
- Lyle, M., Dymond, J. and Heath, G.R. (1977) Copper-nickel enriched ferromanganese nodules and associated crusts from the Bauer Basin, northwest Nazca plate. *Earth Planet. Sci. Lett.* 35, 55-64.
- Lyle, M. (1981) Formation and growth of ferromanganese oxides on the Nazca plate. In: *Geol Soc. Am. Mem.*
- Metz, S., Trefrey, J.H. and Nelson, T.A. (1988) History and geochemistry of a metalliferous sediment core from the Mid-Atlantic Ridge at 26°N. *Geochim. Cosmochim. Acta.* 52, 2369-2378.
- Murnane, R. and Clague, D.A. (1983) Nontronite from a low-temperature hydrothermal system on the Juan de Fuca Ridge. *Earth Planet. Sci. Lett.* 65, 343-352.
- Norton, S.A. (1973) Laterite and bauxite formation. *Econ Geol.* 68, 353-361.
- Oudin, E. (1983) Hydrothermal sulfide deposits on the East Pacific Rise (21°N) Part I: Descriptive mineralogy. *Mar. Min.* 4, 39-72.
- Perkin-Elmer (1982) Analytical methods for atomic absorption spectrophotometry. Perkin-Elmer Corporation, Norwalk, CT.
- Petersen, U. (1971) Laterite and bauxite formation. *Econ. Geol.* 66, 1070-1071.
- Reeves, R.D. and Brooks, R.R. (1978) Trace Element Analysis of Geologic Materials. Wiley, New York. 421p.
- Riddihough, R. (1980) Gorda plate motions from magnetic anomaly analysis. *Earth Planet. Sci. Lett.* 51, 163-170.
- Robertson, A.H.F. and Boyle, J.F. (1983) Tectonic setting and origin of metalliferous sediments in the Mesozoic Tethys Ocean. In: Hydrothermal Processes at Mid-Ocean Spreading Centers (eds. P.A. Rona, K. Bostrom, L. Laubier and E.L. Smith) pp. 595-664.
- Rona, P.A. and Clague, D.A. (1989) Geologic control of hydrothermal discharge on the northern Gorda Ridge (in prep).

- Rona, P.A. and Gorda Ridge Technical Task Force Working Group B (1988) Hydrothermal activity on the Gorda Ridge. EOS 69, 1588.
- Rona, P.A., Thompson, G., Mottl, M.J., Karson, J.A., Jenkins, W.J., Graham, D., Mallette, M., Von Damm, K., and Edmond, J.M. (1984) Hydrothermal activity at the Trans-Atlantic Geotraverse Hydrothermal Field, Mid-Atlantic Ridge Crest at 26°N. J. geophys. Res. 89, 11365-11377.
- Rona, P.A., Widenfalk, L. and Bostrom, K. (1987) Serpentinized ultramafics and hydrothermal activity at the Mid-Atlantic Ridge crest near 15°N. J. Geophys. Res. 92, 1417-1427.
- Scheidegger, K.F. and Stakes, D.S. (1978) X-ray diffraction and chemical study of secondary minerals from DSDP Leg 51, Sites 417A and 417D. p. 1253-1263. In: T. Donnelly, J. Francheteau, W. Bryan, P. Robinson, M. Flower, M. Salisbury, et al., Initial Reports of the Deep Sea Drilling Project, v. 51,52,53, Part 2: Washington (U.S. Government Printing Office).
- Scott, M.R., Scott, R.B., Morse, J.W., Betzer, P.R., Butler, L.W. and Rona, P.A. (1978) Metal enriched sediments from the TAG Hydrothermal Field. Nature. 276, 811-813.
- Seyfried, W.E. and Dibble, W.E. Jr. (1980) Seawater-peridotite interaction at 300°C and 500 bars: implications for the origin of oceanic serpentinities. Geochim. Cosmochim. Acta 44, 309-321.
- Seyfried, W.E. Jr., and Janecky, D.R. (1985) Heavy metal and sulfur transport during subcritical and supercritical hydrothermal alteration of basalt: Influence of fluid pressure and basalt composition and crystallinity. Geochim. Cosmochim. Acta 49, 2545-2560.
- Seyfried, W.E. Jr. and Mottl, M.J. (1982) Hydrothermal alteration of basalt by seawater under seawater-dominated conditions. Geochim. Cosmochim. Acta 46, 985-1002.
- Singer, A. and Stoffers, P. (1981) Hydrothermal vermiculite from the Atlantis II Deep, Red Sea. Clays and Clay Min. 29, 454-458.
- Sleep, N.H. (1983) Hydrothermal convection at ridge axes. In: Hydrothermal Processes at Mid-Ocean Spreading Centers (eds. P.A. Rona, K. Bostrom, L. Laubier and E.L. Smith) pp. 71-82.
- Solano, A.E. (1984) Crustal Structure and Seismicity of the Gorda Ridge. PhD thesis Oregon State Univ. Corvallis, OR. 185p.
- Spiess, F.N., Macdonald, K.C., Atwater, T., Ballard, R., Carranza, A., Cordoba, D., Cox, C., Diaz-Garcia, V., Francheteau, J., Guerrero, J., Hawkins, J., Haymon, R., Hessler, R., Juteau, T., Kastner, M., Larson, R., Luyendyk, B., Macdougall, J., Miller, S., Normark, W., Orcutt, J. and Rangan, C. (1980) East Pacific Rise: Hot springs and geophysical experiments. Science. 207, 1421-1433.

- Starkey, H.C., Blackmon, P.D. and Hauff, P.L. (1984) The routine mineralogical analysis of clay-bearing samples. U.S. Geol. Survey Bull. 1563. U.S. Government Printing Office, Washington.
- Stumm, W. and Morgan, J.J. (1981) Aquatic Chemistry 2nd ed. 780pp. J. Wiley and Sons, New York, N.Y.
- Thompson, G. (1983) Basalt-seawater interaction. In: Hydrothermal Processes at Mid-Ocean Spreading Centers (eds. P.A. Rona, K. Bostrom, L. Laubier and E.L. Smith) pp. 225-278.
- Thompson, G., Mottl, M.J. and Rona, P.A. (1985) Morphology, mineralogy and chemistry of hydrothermal deposits from the TAG area, 26°N Mid-Atlantic Ridge. Chem. Geol. 49, 243-257.
- Tivey, M.K. and Delaney, J.R. (1986) Growth of large sulfide structures on the Endeavor segment of the Juan de Fuca Ridge. Earth Planet. Sci. Lett. 77, 303-317.
- Tomasson, J. and Kristmannsdottir, K. (1972) High temperature alteration minerals and thermal brines, Reykjanes, Iceland. Contrib. Min. Petrol. 36, 123-134.
- Toth, J.R. (1980) Deposition of submarine crusts rich in manganese and iron. Geol. Soc. Am. Bull. 91, 44-54.
- Valeton, I. (1972) Bauxites. Elsevier. 226pp.
- Von Damm, K.L., Edmonds, J.M., Grant, B., Measures, C.I., Walden, B. and Weiss, R.F. (1985) Chemistry of submarine hydrothermal solutions at 21°N, East Pacific. Geochim. Cosmochim. Acta. 49, 2197-2220.
- Von Damm, K.L. and Bischoff, J.L. (1987) Chemistry of hydrothermal solutions from the southern Juan de Fuca Ridge. J. Geophys. Res. 92, 11334-11346.
- Wakeham, S.E. (1978) Petrochemical patterns in young pillow basalts dredged from the Juan de Fuca and Gorda ridges, M.S. thesis, Oregon State Univ., Corvallis.
- Williams, D. L., Green, K., van Andel, T-j H., Von Herzen, R.P., Dymond, J.R. and Crane, K. (1979) The hydrothermal mounds of the Galapagos Rift: Observations with DSRV Alvin and detailed heat flow studies. J. Geophys. Res. 84, 7467-7484.

### CHAPTER III

#### HYDROTHERMAL ALUMINA-RICH CLAYS AND BOEHMITE ON THE GORDA RIDGE

### Abstract

Hydrothermal alteration of basalt on the northern Gorda Ridge produced an alteration crust up to 1mm thick that can be divided into two layers based on mineralogy. An inner layer next to the basalt surface is an Al-rich interlayered smectite/chlorite similar to high temperature Al-rich clays recovered from the East Pacific Rise, 21°N with minor quartz, zeolite (phillipsite ?) and relict plagioclase. An exterior layer of boehmite,  $\text{AlO}(\text{OH})$  and minor anatase results from severe leaching of the underlying clays. The alteration crust is progressively enriched in Al, Ti, V, and Cr from interior to exterior by residual weathering. The presence of boehmite and absence of a silica-rich phase in the exterior of the crust indicates the hydrothermal fluids were silica undersaturated or silica was maintained in solution by extremely acidic fluids. This constitutes the first reporting of boehmite as a major alteration mineral in a mid-ocean ridge hydrothermal environment.

## Introduction

Alteration of basalts at mid-ocean ridges by circulation of hydrothermal fluids typically produces Al-poor hydrothermal clays enriched in  $\text{Fe}^{3+}$  in lower temperature, more oxidizing environments or clays enriched in  $\text{Mg}^{2+}$  in higher temperature, more reducing environments (Tomasson and Kristmannsdottir, 1972, Hekinian, 1982, Peterson et al., 1986). These clays are similar to smectites and mixed-layer chlorite/smectite commonly produced in basalt-seawater interaction experiments in which leaching of basalt and transfer of elements (esp. Si, Ca, K, and transition metals) into solution has been well documented (Hajash and Archer, 1980, Seyfried and Mottl, 1982, Seyfried and Bischoff, 1981, Rosenbauer and Bischoff, 1983). Al-rich clays produced by alteration of basalts in mid-ocean ridge settings have usually been associated with low temperature alteration (Scheidegger and Stakes, 1980, Alt and Honnorez, 1984). However, recent studies of Al-rich clays produced by the interaction of basalt and hydrothermal fluids on the East Pacific Rise, 21°N, indicate that aluminous alteration assemblages may result from high temperature hydrothermal activity with formation temperatures near 300°C (Haymon and Kastner, 1986).

Recent water-column surveys in the axial valley of the northern Gorda Ridge discovered anomalies in helium-3, radon-222, methane, dissolved manganese and particulate iron and anhydrite, strong indications of nearby hydrothermal venting (Baker et al., 1987). The highest Mn and thermal anomalies recorded during these surveys were on the east wall of the axial valley at 42° 45'N, 126° 44'W, a site designated GR-14 (Collier et al., 1986). NOAA camera tows in the GR-14 area revealed white material coating basalts within the axial valley (Rona and Clague, in prep). The mineralogy and chemistry of samples recovered from this area indicate that they include Al-rich clays similar to material recovered from the East Pacific Rise, 21°N, but the GR-14 samples have more extreme enrichment of Al. These materials may represent intense hydrothermal alteration of basalt under conditions uncommon at other ocean ridges. This paper presents the mineralogy and chemical composition of the alteration assemblage and discusses its implications for the nature of hydrothermal activity on the northern Gorda Ridge.



### Tectonic Setting

The Gorda Ridge is an approximately 300 km long segment of spreading ocean ridge located about 200 km off the coast of Oregon and California (Fig. III-1). The ridge is bounded to the north by the Blanco Fracture Zone (43.0°N) and to the south by the Mendocino Fracture Zone (40.4°N). The Gorda axial valley is flanked by steep normal fault blocks which rise to as much as 1500m above the median valley (Atwater and Mudie, 1973, Rona and Clague, 1986). The average depth of the axial valley is more than 3,000m and one depression near the GR-14 area (42.5°N) is more than 3,900m deep (Malahoff et al., 1982). Right lateral offsets at 42.0°N and 41.6°N divide the Gorda Ridge into three segments with varied spreading rates (Atwater and Mudie, 1973, Northrop, 1968, Riddihough, 1980, 1984). The northern segment spreads at about 28mm/yr half rate and the southern two segments spread at about 12mm/yr half rate (Riddihough, 1980).

The northern segment of the Gorda Ridge is relatively sediment starved, despite its proximity to the Oregon continental margin, and most closely resembles portions of the mid-Atlantic Ridge (cf. Crane and Ballard, 1981). At the ridge junction with the Blanco Fracture Zone is a V-shaped valley just south of which is an axial high (3100m, 42° 44'N, 126° 45'W) where several volcanic cones, fresh pillow flows, sheet flows and deep fissures in pillow lavas indicate recent volcanism (A. Malahoff, 1985, pers. comm., Rona and Clague, 1986). The samples described in this study were dredged from the east wall of the axial valley in this vicinity.

### Sample Location and Description

The location of dredges in the GR-14 study area from USGS cruises L3-86-NC and L5-85-NC are shown in Figure III-2. During the August 1986 cruise (L3-86-NC), two dredges within the ridge axis recovered basalt samples from a site where NOAA June, 1986 camera tows revealed white material coating the basalts. One sample from each dredge was selected for study (L3-86-NC-11D and L3-86-NC-15D) (Fig. III-2). Both samples were coated with a friable encrustation about 0.5-1 mm thick on all surfaces except the glassy margin. A cross-section of the crust shows its sharp contact with the underlying, relatively unaltered basalt and an interior dark green layer (about 0.2 to 0.5 mm) of hydrothermal clays that changes abruptly to an exterior white layer (about 0.5 to 0.8 mm) of boehmite. The thickness of the alteration crust is less (about 0.2 to 0.5 mm) on sample 11D. A thin white dusting occurred intermittantly on both palagonatized and fresh glass surfaces and red and brown stains of presumably Fe and Mn hydroxides/oxyhydroxides mottled these surfaces.

The basalts are considerably more altered than those typically found on the ridge axis. It is possible that they are older than their site of collection implies since they may be part of a talus slope which crumbled from a nearby mound on the east wall of the axial valley (Rona and Clague, 1986). However, preservation of quenched exterior surfaces of pillows with fresh basaltic glass observed on portions of several samples testifies to their relative youth (Howard and Fisk, 1986, P. Rona and D. Clague, 1987, pers. comm.) and suggests they may have formed as part of an off-axis eruption.

Minor amounts of boehmite were also identified by X-ray diffraction in hydrothermal precipitates and surficial alteration on basalts in samples recovered within the GR-14 area during USGS cruise L5-85-NC (Howard and Fisk, 1986) and in hydrothermal precipitates on basalts collected within the Gorda Ridge axis about 80 km south of GR-14 (Clague et al., 1984).

## Petrography

Petrographic examination of polished thin sections of encrusted basalt samples show relatively unaltered basalt changing to altered crust with virtually no change in basalt textures. Alteration material as pseudomorphs in needle-like plagioclase laths, indicates complete replacement of basalt microphenocrysts and glass by clay minerals (Fig.III- 3). This type of replacement implies quiet conditions in which alteration proceeded by molecular diffusion rather than mechanical erosion similar to that associated with later stage palagonitization (Honnorez, 1980). The greater preservation of the basaltic glass relative to the crystalline groundmass is apparently the result of greater ease of hydrothermal fluid percolation and diffusion around crystal boundaries which tends to quickly alter the crystalline matrix.

Relict plagioclase phenocrysts, often with euhedral rims, have resorbed interiors and are altering to zeolites. The groundmass is apparently more susceptible to alteration since larger plagioclase phenocrysts (up to 0.1 mm) are occasionally unaltered. Microprobe analyses reveal similar composition for larger plagioclase phenocrysts in both unaltered basalt (An79) and alteration crusts (An82). Vesicles still present in the alteration crust are filled with zeolites and occasionally dark blue to opaque minerals formed at a later stage in vesicles and fractures. Reddish Fe staining occurs interstitially throughout the cloudy weathered crust and increases in abundance towards the interior of the crust. The polished section for 15D shows the alteration crust in direct contact with basalt glass as well as massive finely crystalline basalt.

## Analytical Techniques

Samples from L3-86-NC-11D and L3-86-NC-15D were prepared in the same manner for X-ray diffraction and atomic absorption (AA) analysis. White material was scraped from the outermost surface of each sample. A second transition layer of white material grading into green material was scraped off. Finally, a third layer of dark green material closest to the basalt surface was removed. Several portions of each sample were analyzed to determine mineralogic variability within the crust. A split from each layer was reserved for AA analysis.

For each of the three layers, one random, air dried powder mount (room temperature) and one oriented, Mg-saturated mount were prepared on glass disks. Samples were analyzed from  $2^\circ - 100^\circ 2\theta$  at  $1^\circ 2\theta/\text{min}$  on a SCINTAG X-ray diffractometer using Cu-K $\alpha$  radiation. The oriented mounts were treated with ethylene glycol and the random mounts were heated to  $350^\circ\text{C}$  and  $550^\circ\text{C}$ . After each treatment, samples were analyzed from  $2^\circ - 30^\circ 2\theta$ .

Polished sections of unaltered basalt and alteration crust for microprobe analysis and scanning electron microscopy were prepared for each sample. Microprobe analyses were performed on the University of Oregon ARL/EDX microprobe using 15KV accelerating voltage and  $.15\ \mu\text{A}$  sample current. A basaltic glass standard and a defocused beam of 10 microns was used except for plagioclase analyses for which the standard Lake Co. Labradorite and a spot diameter of 1 micron was used. Each analysis was corrected using the standard Bence and Albee (1968) and Albee and Ray (1970) corrections.

Atomic absorption analyses were performed on a Perkin-Elmer 5000 atomic absorption spectrometer using standard techniques (Fukui, 1976). The samples were analyzed for a total of 22 elements. The precision and accuracy for atomic absorption analyses compared with consensus values for the three standards G-2, GSP-1 and BCR-3 is listed in Table III-1.

## Results

### (A) Mineralogy

Both samples 11D and 15D are virtually identical mineralogically. A detailed description of the layers in the alteration crust follows.

#### Inner Layer

The inner layer (adjacent to basalt) is composed of interlayered smectite-chlorite as well as some discrete smectite and chlorite (Fig.III-4). Minor quartz and possibly phillipsite, lizardite or kaolinite and trace amounts of talc were also identified in X-ray diffractograms. In the random mounts, multiple peaks within the d-spacing range of 11Å to 15Å (at least four peaks are discernable in each sample) signify the presence of an expandable clay with interlayers in various states of hydration and/or containing different interlayer cations. The most prominent reflections in this region occur at 12.4Å and 13.8Å in sample 15D and at 12.8Å and 14.4Å in sample 11D.

The broad, asymmetrical profiles of the diffraction peaks in the oriented mounts as well as reflections between 26Å - 30Å are characteristic of mixed-layer clays (Brown and Brindley, 1980). Glycolation shifted the 001 basal reflection from 14.3Å to 16.4Å in sample 15D and from 14.5Å to 16.6Å in sample 11D. Heating of the random mount to 350°C collapsed the 12Å smectite peak to 10Å but left the 14Å chlorite peaks undisturbed. Heating to 550°C destroyed reflections at 7Å and reduced the 3.5Å peak. Though this may imply the presence of some kaolinite, it is not conclusive since these peaks associated with chlorite characteristically disappear at this temperature as well. The irregular interlayering of chlorite and smectite is evident from the non-integral basal diffractions in the ethylene-glycol solvated mounts (16.4, 7.14, 4.77, 3.56 for sample 15D and 16.6, 7.14, 4.77, 3.56 for sample 11D). The similarity to aluminous clay samples from the East Pacific Rise, 21°N is striking (Table III-2). Haymon and Kastner (1986) suggest the EPR, 21°N clay formed when low pH hydrothermal fluids altered basaltic glass and plagioclase at high temperatures (295°C-360°C). They also suggest that the collapsed d-spacing for the smectite to only 12Å from the usual 14Å - 15Å for the non-glycolated oriented pattern results from irreversible dehydration of the smectite on the seafloor by heating above about 300°C. This interpretation may also be valid for Gorda Ridge clay alteration.

The 060 peaks at 1.49Å and 1.53Å indicate that both dioctahedral and trioctahedral clays are present, which precludes further subdivision of clay minerals by techniques

used in this study. However, the apparent degradation of the  $1.49\text{\AA}$  peak after heat treatment may be an indication of dioctahedral smectite. The aluminous smectite is most likely a beidellitic smectite with most of the interlayer brucite replaced by gibbsite.

In addition to the clays, weak reflections occur for quartz ( $3.34\text{\AA}$ ) and phillipsite ( $7.15\text{\AA}$  and  $3.2\text{\AA}$ ). Although plagioclase altering to zeolite was definitely identified optically, the highest intensity peak for plagioclase at  $3.2\text{\AA}$  overlaps the secondary phillipsite peak and precludes conclusive identification of phillipsite. The  $7.2\text{\AA}$  peak may be associated with the serpentine mineral, lizardite, or kaolinite. A reflection at  $9.36\text{\AA}$ , intensified during heat treatments in sample 15D, represents the presence of trace amounts of talc. The absence of this peak in other splits of the same sample probably results from sample inhomogeneity and further suggests that the talc occurs as a localized alteration of olivine which is later replaced by mixed-layer clays.

#### Outer Layer

The exterior white layer of both samples is composed of well-crystallized boehmite, an aluminous oxyhydroxide,  $\text{AlO}(\text{OH})$ , (Fig. III- 5) which to our knowledge is rarely reported in mid-ocean ridge environments, but is not uncommon in Gorda Ridge hydrothermal precipitates studied to date (Clague et al., 1984, Howard and Fisk, 1986) (Fig. III- 5). The oriented mount revealed 12 reflections for the mineral boehmite. A strong reflection at  $3.51\text{\AA}$  and weaker reflections at  $2.38\text{\AA}$  and  $1.9\text{\AA}$  are evidence for the presence of anatase, a titanium oxide stabilized by low concentrations of alkalis (Kessman, 1966). Anatase has been observed as a common alteration mineral on land replacing ilmenite and titanomagnetite in metamorphosed basalts (Yang, 1987). Apparently its only prior documentation in a mid-ocean ridge environment is in recently studied sulfide chimneys from the Juan de Fuca Ridge (Brett et al., 1987). A region of broad, ill-defined reflections between  $5.7\text{\AA}$  and  $6.0\text{\AA}$  in some samples remains unidentified but may correspond to the presence of zeolites. The sharpness of the XRD peaks indicates that the boehmite is well-crystallized. Experimental synthesis of boehmite shows the degree of crystallinity is generally correlated with increasing heating time or temperature (Tettenhorst and Hofman, 1980). The X-ray powder diffraction pattern produced by boehmite from both samples most closely resembled diffraction patterns produced from boehmite synthesized between  $150^\circ\text{C}$  -  $250^\circ\text{C}$ , the highest temperature experiments made by Tettenhorst and Hofman (1980). Wolska and Szajda (1980) conducted hydrothermal experiments in which originally amorphous aluminum hydroxide

coprecipitated with  $\text{Fe}^{3+}$  ions as  $\text{Al}_{0.5}\text{Fe}_{0.5}(\text{OH})_3$  transforms into aluminum hydroxide crystalline phases which are not observed in products of aging of pure aluminum hydroxide. Notably, in the presence of  $\text{Fe}^{3+}$  hydroxide, increasing temperature produces well crystallized boehmite instead of the usually formed pseudoboehmite (Wolska and Szajda, 1980). Since boehmite is isostructural with lepidocrocite, the substitution of  $\text{Al}^{3+}$  for  $\text{Fe}^{3+}$  to form boehmite may proceed without great difficulty in a hydrothermal environment where Fe is removed in solution.

The transition zone between the exterior boehmite layer and interior clays is mainly a mixture of boehmite and clays. However, in sample 15D, additional mineral phases present include talc, illite, plagioclase, and phillipsite.

### (B) *Chemical Compositions of Crusts*

Atomic absorption analyses of the alteration crust show that the major chemical constituents of both 11D and 15D are nearly identical indicating conditions of formation were similar (Table III-3). The chemical variation from interior to exterior shows the following trends: silica, iron, magnesium, calcium and sodium decrease away from the basalt/crust interface while aluminum and titanium increase (Fig. III-6). Variations in trace elements are also similar between the two crusts. The most notable trace element variation in both samples is the increase in chromium and vanadium from interior of the crust to exterior. In both samples, Ni concentration is highest in the transition zone, but there is an overall decrease from the interior to the exterior. Studies of basalt-seawater interaction at  $300^\circ\text{C}$  have shown that V, Cr, and Ni are among the least mobile of the transition metals (Seyfried and Mottl, 1982). The increase in V and Cr at the exterior of the crust is probably the result of enrichment by intense leaching of other more mobile elements. However, the overall decrease in Ni concentration from interior to exterior suggests that some of the Ni is being mobilized and leached by the hydrothermal fluid. This is consistent with the results of Humphris and Thompson (1978) which show some evidence for mobilization of Ni in oceanic metabasalts as well as previous analyses of hydrothermal precipitates from GR-14 that show significant enrichment in Ni (Howard and Fisk, 1986). Zn, Cu, and possibly Co, show evidence of removal by hydrothermal fluids. Co and Zn concentrations decrease from interior to exterior in both samples. There is a higher concentration of Cu in the inner layer of sample 15D and a greater decrease in Cu towards the exterior compared to sample 11D in which Cu concentration remains approximately constant from interior to exterior. Li and Sr are both significantly

depleted in the outermost layer of the crust. This contrasts with  $K_2O$  concentration which is maintained essentially the same throughout the altered crust. Only the inner layer of sample 15D contained detectable Ba.

Microprobe analyses of altered crusts, basaltic glass and groundmass (Table III-4) show dramatic changes in the concentration of major elements with distance from the basalt/crust interface (Fig. III- 6). Chemical analyses of the basalts show they are oceanic tholeiites. Their  $K_2O$  content (~0.2 wt%) is slightly higher than other reported microprobe analyses from this vicinity of the Gorda Ridge axis (Clague et al., 1984, Davis and Clague, in press) implying only slight seawater alteration. Although microprobe analyses indicate that sample 11D is more Mg-rich than sample 15D, this is probably the result of sample inhomogeneity since the chemical similarity between the crusts is apparent from AA analyses of the three layers; analyses which are more representative of the entire layer (Table III-3). Comparison of microprobe analyses and AA analyses show that some portions of the crust are more aluminous than others. This may indicate that the originally Mg or Fe-rich clays (chlorite/saponite/nontronite) are converted to Al-rich clays. For example, talc and brucite layers in chlorite may transform into pyrophyllite and gibbsite layers. This is further supported by the inverse relationship of  $Al^{3+}$  and  $Mg^{2+}$  concentrations (Fig. III-6). Mixtures of minerals renders calculation of clay mineral formulas based on microprobe analyses, inappropriate.

### (C) *Scanning Electron Microscopy (SEM)*

Identification of minor phases in the alteration crust were made with SEM backscattering electron images. In Figure III-7a, energy dispersive analysis (EDS) of brighter crystals on fan-shaped clays showed high concentrations of Si. This supports the identification of quartz observed as minor peaks in X-ray diffractograms. Crosscutting relationship between quartz and clays indicates quartz crystallized subsequent to clay formation. The anhedral appearance of these quartz grains suggests they may have undergone dissolution by Si undersaturated hydrothermal fluids. In Figure III-7b, qualitative EDS analysis showed high concentrations of Ti on brighter crystals within a matrix of boehmite/clays. These are probably tiny crystals of anatase for which XRD peaks were hidden by clay peaks in the inner layer but which appeared in the X-ray diffractogram of the boehmite layer (Fig. III-5). A Si-rich phase was not observed in the exterior regions of the crust.



## Discussion

### *Formation of Al-rich Clays*

Mineralogical and chemical similarities between the Al-rich clays in this study and from the EPR, 21°N imply similar conditions of formation at the two sites. The formation of high temperature Al-rich clays from basalt alteration has been previously described by Haymon and Kastner (1986) who propose that they were produced by the "interactions of seafloor basalt with extremely reducing, Mg-poor black smoker solutions and normal seawater". Minimum temperatures of formation of the GR-14 clays may be set by the transition between smectite and chlorite dominated assemblages at about 200-230°C (Tomasson and Kristmannsdottir, 1972). However, identification of talc and discrete chlorite places the temperature of formation at about 270-280°C from oxygen isotope determinations of these phases in other hydrothermal systems (Kristmannsdottir, 1977, Lonsdale et al., 1980, Koski et al., 1985). Evidence from seawater-basalt interaction experiments indicate not only high temperatures of formation, but also high water/rock ratios. Smectite is the only clay mineral reported by Seyfried and Mottl (1982) in experiments run at 200°C, but at 300°C, interlayered smectite/chlorite was produced. Of further significance in the 300°C experiments was the identification of quartz as an alteration product at very high water/rock ratio (125). The presence of quartz in the inner layer of the alteration crust probably precipitated in response to the formation of chlorite which releases free silica implying the fluid was initially saturated with respect to quartz (Mottl, 1983). Also, under seawater-dominated conditions, (water/rock ratios = 125, 62) clay compositions were not as depleted in K<sub>2</sub>O as in experiments conducted under rock-dominated conditions (water/rock ratio = 50). Seyfried and Mottl (1982) suggest this may result from incorporation of K<sub>2</sub>O into clays during cooling of the altering fluids, providing a possible mechanism for maintenance of a somewhat constant K<sub>2</sub>O content throughout the alteration crust.

Substantial chemical inhomogeneity of the GR-14 inner layer Al-rich clays is apparent in microprobe analyses and probably reflects the incomplete alteration of initially Mg-rich clays to Al-rich clays and boehmite. The original chemistry of the Gorda Ridge clays is obscured because of this overprinted alteration and because of mixtures of minerals in the altered crust. Although we favor formation of these crusts by a process of residual enrichment, minor contribution from altering fluid is possible. Both of these possibilities are discussed below.

### *Residual Enrichment*

Several lines of evidence indicate that leaching of Si (and other mobile elements) by hydrothermal fluids and not hydrothermal precipitation of Al are responsible for the formation of the Al-rich alteration crusts. Although Al and Ti can dissolve and reprecipitate under similar conditions, they frequently do not (Loughnan, 1969, Valetton, 1972). Thus the constancy of the  $\text{TiO}_2/\text{Al}_2\text{O}_3$  ratio from the basalts and throughout the alteration crusts (Table III-3), implies that the Al and Ti enrichment of the crusts is predominantly a process of residual enrichment. Ti, occurring as submicroscopic dispersed anatase, is commonly enriched in clays and boehmite produced by residual weathering (Goldschmitt, 1958) and residual crystals are observed by both XRD and SEM analysis. The Ti is probably derived from the breakdown of mafic minerals (eg. augite and titanomagnetite) in the basaltic groundmass. SEM images of hydrothermal Al-rich clays from the EPR, 21°N revealed globular morphology typically associated with precipitation from a gel or colloid (Haymon and Kastner, 1986). Since this morphology was not observed in the GR-14 alteration crusts, it may provide further evidence that there was little, if any, contribution from the hydrothermal fluids.

### *Proximity to Hydrothermal Vents*

It is apparent from the chemistry of hydrothermal solutions from the EPR, 13°N and 21°N, that the extreme acidity (pH 3-3.5) of these 350°C hydrothermal fluids is not only capable of intense alteration of basalt producing clay encrustations up to 1mm thick, but also, of mobilizing Al, a typically immobile cation, until it is enriched a thousand times in vent fluids over normal seawater concentrations (Michard et al., 1984, Von Damm et al., 1985). Mineralogical studies have further supported the transport and redeposition of Al as Al-Si gels very close to high temperature vent sites (Oudin, 1983). The high temperature Al-rich clays from the EPR, 21°N, were within 2 km of a black smoker vent field (Haymon and Kastner, 1986). Clearly, however, for these clays to have formed at such high temperatures, they must have formed close to a very high temperature vent. Cole (1983) found Al-rich authigenic smectite in the brine pools of the Atlantis II Deep, Red Sea that formed under higher temperatures (150-200°C) than Fe-rich, Al-poor nontronites from the same area. Cole (1983) interpreted these clays to have been closest to the source of the hydrothermal input into the brine pool supplying Al and Si. Besides the mobilization of Al, evidence for mobilization of Ti in some hydrothermal solutions is apparent from documentation of anatase in sulfide chimneys from the Juan de Fuca Ridge

(Brett et al., 1987). Therefore, despite the constancy of the  $\text{TiO}_2/\text{Al}_2\text{O}_3$  ratio, the possible addition of some minor Al or Ti from hydrothermal sources cannot be completely disregarded. The presence of a fine dusting of boehmite on fresh glass surfaces and the discovery of an Al oxyhydroxide in the water column in the GR-14 area (T. Nelson, 1986, pers. comm.) suggest it may form as a hydrothermal precipitate similar to Al-Si gels that have been observed on the EPR by Oudin (1983).

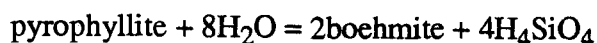
### *Occurrence of Boehmite*

Boehmite is usually associated with bauxite deposits typically formed in tropical or subtropical environments where the underlying rocks are rich in Al and low in Fe and Si (Valeton, 1972, Guilbert and Park, 1986) and is frequently associated with its dimorph diaspore and kaolinite. Boehmite is considered metastable in the presence of  $\text{H}_2\text{O}$  but its conversion rate to more stable diaspore is very slow (Kennedy, 1959, Delany and Helgeson, 1978). Petersen (1971) pointed out the importance of the  $\text{Al}_2\text{O}_3/\text{SiO}_2$  ratio of groundwater in determining whether kaolinite or bauxite would form, and that the relatively low  $\text{SiO}_2$  content of basalts makes them favorable for bauxite formation. Boehmite can only form in solutions unsaturated in silica with respect to quartz (Rafal'skiy and Alekseyev, 1986). Norton (1973) has determined that highly reducing conditions are necessary to separate Fe from Al to form bauxites instead of more iron-rich deposits, termed laterites. Boehmite has also been identified as a hydrothermal alteration product of feldspar (Shelley et al., 1977, Deer et al., 1966).

The occurrence of boehmite in mid-ocean ridge environments has not been commonly reported at other localities besides the Gorda Ridge probably because such intense leaching is rare. Boehmite was tentatively identified by Bass (1976) in basaltic vein material at DSDP site 319A (113-114 cm depth) where it was interpreted as an alteration of some earlier vein component. Since diaspore has not been observed in samples containing boehmite, perhaps boehmite reverts to clays rather than diaspore after the cessation of hydrothermal activity. Boehmite may only exist temporarily close to its environment of formation. Such retrograde reactions by a process of resilication would be expected based on the stability relations in the system  $\text{Al}_2\text{O}_3\text{-SiO}_2\text{-H}_2\text{O}$  (Fig. III-8) (Hemley et al., 1980).

Since the smectite structure is analogous to pyrophyllite, ignoring substitutions in both octahedral and tetrahedral sheets and the lack of electrical neutrality, the pyrophyllite field can be taken as the approximate stability field for Al-rich clays.

Observations from Fig. 8 are: (1) boehmite forms at relatively low Si activity compared to the Al-rich, sheet silicate, pyrophyllite and (2) at higher temperatures, boehmite occurs at a lower degree of quartz undersaturation. The latter may be important since hydrothermal fluids are approximately buffered at quartz saturation (Von Damm et al., 1983) and at higher temperatures, higher Si activity would be required to stabilize boehmite. Two possible mechanisms could account for the presence of boehmite. First, an increase in temperature will encourage the formation of boehmite by the following desilication reaction:



(Hemley et al., 1980). In this case, the silica activity need not be reduced. The assemblage pyrophyllite-diaspore has been observed at the Matsukawa geothermal field in Japan where it was interpreted to be a relict assemblage formed at above 310°C (Sumi, 1968, cited by Browne, 1978, Sumi and Takashima, 1976). Second, mixing of a hydrothermal end member and normal seawater would (a) reduce the temperature of the solution, (b) reduce the silica activity, and (c) increase the pH of the solution.

Clays can be converted to gibbsite by a process of desilication at temperatures below about 140°C (Deer et al., 1966) but both the temperature and acidity of submarine hydrothermal solutions favor the formation of boehmite over gibbsite. The structure of boehmite makes it much more resistant to attack by very acidic hydrothermal fluids whereas gibbsite is much more soluble in solutions at pH values below 4 (Loughnan, 1969, Tole, 1987) and at higher temperatures (140°C - 200°C), gibbsite is dehydrated to form boehmite by the reaction:



(Bowers et al., 1984, Deer et al., 1966).

### *Stages of Alteration*

The formation of the interlayered clays at GR-14 probably represents an initial stage of alteration of basalt to clays commonly observed at other ocean ridges near high-temperature hydrothermal venting. Initially, these clays may have been similar to Mg-rich interlayered smectite/chlorite produced in seawater-basalt interaction experiments at 300°C (Seyfried and Mottl, 1982). What is unusual, however, is that sufficient intensity and duration of hydrothermal activity or a change in the thermo-chemical regime of the system has led to intensive leaching of the clay alteration to form high Al-clays and finally boehmite.

Hydrothermal alteration of the basalts in this study can be viewed as a dynamic process which can be divided into several stages. First, alteration began under "seawater dominated" conditions producing Mg-rich and possibly some Fe-rich interlayered chlorite/smectite. Fe was leached until the fluid reached saturation or cooled enough to precipitate amorphous Fe-oxyhydroxides. Mg was stripped from seawater and extremely low pH solutions prevailed. The fluid was at or above quartz saturation and crystallization of some quartz took place. Second, the temperature of the fluid rose and either entrainment of normal seawater allowed Si concentrations to drop below quartz saturation, or the extreme acidity (pH ~3-4) tended to maintain Si in solution (Seyfried and Mottl, 1982) and extensive leaching of all elements except Al, Ti, V, and Cr, encouraged crystallization of boehmite and anatase. Finally, cooling of the solutions allowed precipitation of Fe oxyhydroxides in the interstices and then Fe and Mn oxyhydroxides superficially, and K was incorporated in clays.

The implication that the hydrothermal fluid responsible was quartz undersaturated is unusual considering that the dissolved  $\text{SiO}_2$  concentration is often buffered by quartz solubility (Von Damm et al., 1985). At the Matsukawa geothermal field in Japan, the Al-rich assemblage pyrophyllite-diaspore was also accompanied by the precipitation of quartz indicating the hydrothermal fluids were in equilibrium with quartz (Sumi, 1968). If we accept that the system is saturated with respect to quartz, then perhaps the sluggish kinetics of quartz nucleation and growth allows for continued leaching of Si without precipitation of quartz. Alternatively, a shift to rock dominated conditions (water/rock ratios  $\leq 50$ ) could allow silica concentrations to drop below quartz saturation (Seyfried and Mottl, 1982). This could be achieved by long term flow in the same conduits allowing sealing of conduits by secondary mineral formation. Such conditions might also create silica undersaturated fluids since prolonged hydrothermal flow within the same conduits could result in decreased interaction between hydrothermal fluids and fresh basalt and increased interaction between hydrothermal fluids and progressively Si-depleted secondary minerals.

## Conclusions

(1) Hydrothermal alteration of basalts at the northern Gorda Ridge produced an alteration crust about 0.5 to 1 mm thick that can be roughly divided into two layers based on mineralogy. The inner layer of alteration crust is high aluminum interlayered smectite/chlorite similar to high temperature clays produced by basalt alteration on the EPR, 21°N. However, the Gorda Ridge clays have been even more severely leached to produce an outer layer of white boehmite,  $\text{AlO}(\text{OH})$  that is also high in Ti incorporated in anatase. The alteration crusts are enriched in Al, Ti, V, and Cr by a process of residual weathering.

(2) Minimum temperature of formation is 200-230°C, based on the shift from smectite to chlorite dominated assemblages, but could be closer to about 270-280°C, based on the presence of talc, discrete chlorite, and Al-rich clays similar to high temperature (295-360°C) aluminous clays from the EPR 21°N.

(3) In the process of hydrothermal alteration of seafloor basalts to produce the inner layer clays, the silica activity is within the range approximately equal to the stability of pyrophyllite and the fluids are buffered at quartz saturation. The stability relations argue that either increasing temperature or decreasing fluid temperature coupled with a drop in silica activity will convert Al-rich clay (represented by pyrophyllite) to boehmite. The outer layer most probably represents extreme leaching of the underlying clays by hydrothermal fluids that are undersaturated with respect to silica or pH is so low ( $\leq 4$ ) that Si remains in solution.

(4) The presence of fresh glass on quenched pillow surfaces on some samples is an indication of their relative youth. The extreme degree of alteration shows they have been exposed to intense hydrothermal alteration. Because these samples form part of a talus pile on the east side of the axial valley, it may be that they formed as part of an off-axis eruption.

(5) The intensity of leaching in this area may be important for the formation of metalliferous deposits nearby. The apparent mobility of Ni suggests a source for nearby Ni-rich hydrothermal precipitates observed in the GR-14 area.

(6) If Al is contributed from a hydrothermal fluid enriched in Al, it may be that proximity to the vent site has contributed to the observed high Al content in the crusts. However, the constancy of the  $\text{TiO}_2/\text{Al}_2\text{O}_3$  ratio from the basalt through the alteration crust implies it is a relatively minor contribution.

(7) Finally, in view of the high Al measured in vent waters at other spreading ridges, high temperature aluminous alteration assemblages reported from this study and from the East Pacific Rise, 21°N, and Al oxyhydroxide reported in the water column in the GR-14 area, the interpretation of high Fe/Al ratios in water column particulates, sediments, or hydrothermal crusts as an indicator of proximity to vent sites should be used with caution.

Table III-1. Average of three atomic absorption analyses (this study) of U.S. Geological Survey standard rocks; G-2, GSP-1, and BCR-3, compared with consensus values (Gladney and Burns, 1983). % RSD = % relative standard deviation.

Element (wt %)	G-2				GSP-1				BCR-3			
	This study	% RSD	Consensus	% RSD	This study	% RSD	Consensus	% RSD	This study	% RSD	Consensus	% RSD
Al	8.11	1.32	8.15	1.47	7.91	1.33	8.02	1.87	7.23	0.92	7.21	1.80
Ba	0.210	0.20	0.187	1.06	0.146	2.09	0.131	0.76	0.0766	3.09	0.068	2.36
Ca	1.35	1.77	1.41	4.96	1.41	1.94	1.46	4.79	5.04	2.30	4.97	2.21
Co	0.0006	42.98	0.0005	8.70	0.0012	43.30	0.0007	12.31	0.0047	6.61	0.0036	4.41
Cr	0.0009	12.37	0.0009	22.22	0.0010	22.05	0.0013	20.00	0.0004	--	0.0018	--
Cu	0.0010	12.69	0.0011	27.27	0.0033	2.97	0.0034	14.71	0.0016	3.95	0.0019	21.05
Fe	1.83	1.14	1.87	3.74	2.92	1.22	3.01	2.99	9.32	0.54	9.38	2.35
K	3.67	1.73	3.73	3.22	4.51	1.32	4.57	2.63	1.41	0.82	1.40	5.00
Li	0.0032	1.62	0.0036	13.89	0.0028	1.74	0.0031	12.90	0.0011	3.90	0.0013	31.01
Mg	0.440	1.82	0.460	8.69	0.576	2.46	0.596	7.89	2.11	1.37	2.08	4.81
Mn	0.0253	1.88	0.0260	15.38	0.0305	2.06	0.0310	12.90	0.1518	1.11	0.141	6.38
Na	3.00	1.50	3.02	2.98	2.05	0.95	2.08	3.37	2.36	1.13	2.43	3.29
Pb	--	--	--	--	0.0051	--	0.0054	12.96	--	--	--	--
Rb	0.0179	5.70	0.0168	--	0.0270	1.51	0.0254	0.79	0.0050	3.97	0.0047	1.27
Si	32.2	1.32	32.2	0.87	30.97	1.28	31.46	0.73	25.2	0.98	25.3	0.95
Sr	0.0504	0.05	0.0478	0.63	0.0246	1.85	0.0234	1.28	0.0361	1.71	0.0330	1.52
Ti	0.31	3.27	0.30	7.46	0.4262	2.50	0.3930	6.11	1.53	1.39	1.33	4.51
V	0.0020	--	0.0035	--	0.0082	31.57	0.0053	13.21	0.0450	--	0.0404	--
Zn	0.0085	2.71	0.0085	8.24	0.0103	1.05	0.0103	8.74	0.0132	1.40	0.019	0.78

(-- = not determined)



Table III-2. Comparison of basal reflections for Gorda Ridge (GR-14)  
Al-rich chlorite/smectite and East Pacific Rise, 21°N Al-rich  
chlorite/smectite.

	GR-14		EPR, 21°N*
	L3-86-NC-11D	L3-86-NC-15D	
00l	d(Å)	d(Å)	d(Å)
001	14.5	14.3	14.6
002	7.14	7.14	7.23
003	4.77	4.77	4.84
004	3.56	3.56	3.51
Glycolated			
001	16.6	16.4	15.36

\* Sample 923 R-3 from Haymon and Kastner (1986)

Table III-3. Atomic absorption analyses of alteration crusts from Gorda Ridge, GR-14.

Sample L3-86-NC-11D			
	11D-C (inner layer)	11D-B (transition zone)	11D-A (outer layer)
SiO <sub>2</sub> (wt %)	44.5	36.4	18.19
TiO <sub>2</sub>	2.3	3.0	5.1
Al <sub>2</sub> O <sub>3</sub>	25.5	35.34	60.5
FeO*	7.37	3.10	1.39
MgO	11.54	9.98	1.98
CaO	1.88	0.52	0.79
K <sub>2</sub> O	0.39	0.37	0.34
Na <sub>2</sub> O	1.66	1.08	0.86
SUM	95.14	89.79	89.95
Ba (ppm)	0	0	0
Co	57	23	20
Cr	450	610	1060
Cu	60	64	68
Li	9	15	2
Mn	236	211	193
Ni	290	330	170
Rb	6	4	4
Sr	30	20	0
V	400	500	700
Zn	66	46	41
TiO <sub>2</sub> /Al <sub>2</sub> O <sub>3</sub>	0.09	0.08	0.08
Al <sub>2</sub> O <sub>3</sub> /SiO <sub>2</sub>	0.57	0.97	3.19
MgO/SiO <sub>2</sub>	0.26	0.27	0.10
Al <sub>2</sub> O <sub>3</sub> /MgO	2.21	3.54	30.56
Sample L3-86-NC-15D			
	15D-C (inner layer)	15D-B (transition zone)	15D-A (outer layer)
SiO <sub>2</sub> (wt %)	40.2	37.64	14.55
TiO <sub>2</sub>	2.13	2.81	5.42
Al <sub>2</sub> O <sub>3</sub>	24.38	32.7	63.32
FeO*	6.85	3.27	0.46
MgO	15.0	11.6	1.1
CaO	1.64	0.32	0.16
K <sub>2</sub> O	0.27	0.34	0.35
Na <sub>2</sub> O	1.14	0.94	0.48
SUM	91.61	89.62	85.84
Ba (ppm)	60	0	0
Co	58	52	25
Cr	447	537	939
Cu	230	137	32
Li	15	22	5
Mn	113	162	74
Ni	370	480	70
Rb	3	5	5
Sr	30	20	10
V	400	500	900
Zn	108	90	22
TiO <sub>2</sub> /Al <sub>2</sub> O <sub>3</sub>	0.09	0.09	0.09
Al <sub>2</sub> O <sub>3</sub> /SiO <sub>2</sub>	0.61	0.87	3.19
MgO/SiO <sub>2</sub>	0.37	0.31	0.10
Al <sub>2</sub> O <sub>3</sub> /MgO	1.63	2.82	30.56

Cd, Pb and As were not detected. \*all iron calculated as FeO

Table III-4. Microprobe analyses from samples L3-86-NC-11D and L3-86-NC-15D, Gorda Ridge, GR-14.

L3-86-NC-11D							
Oxides (wt%)	Glass*	Alteration Crust					
		Smectite/Chlorite				Boehmite	
		interior		exterior			
SiO <sub>2</sub>	48.63	45.45	35.54	31.25	30.47	14.41	7.21
TiO <sub>2</sub>	1.16	1.49	2.93	1.04	1.59	0.87	0.82
Al <sub>2</sub> O <sub>3</sub>	15.76	17.49	16.16	23.95	24.61	23.31	25.43
FeO	8.30	5.30	6.47	1.31	0.72	0.05	0.05
MnO	0.16	0.04	0.04	0.04	0.04	0.04	0.04
MgO	9.13	14.81	24.07	11.04	10.66	0.13	0.08
CaO	13.04	4.17	0.23	0.16	0.17	0.16	0.16
Na <sub>2</sub> O	2.90	2.36	0.48	2.78	1.10	0.61	0.21
K <sub>2</sub> O	0.20	0.14	0.09	0.15	0.28	0.32	0.17
Cr <sub>2</sub> O <sub>3</sub>	0.06	0.05	0.11	0.05	0.05	0.05	0.07
SUM	99.34	91.31	86.12	71.76	69.70	39.95	34.25
H <sub>2</sub> O	0.66	8.69	13.88	28.24	30.30	60.05	65.75
(by diff.)							
TiO <sub>2</sub> /Al <sub>2</sub> O <sub>3</sub>	0.07	0.09	0.18	0.04	0.06	0.04	0.03
Al <sub>2</sub> O <sub>3</sub> /SiO <sub>2</sub>	0.32	0.38	0.45	0.77	0.81	1.62	3.53
MgO/SiO <sub>2</sub>	0.19	0.33	0.68	0.35	0.35	0.01	0.01
Al <sub>2</sub> O <sub>3</sub> /MgO	1.73	1.18	0.67	2.17	2.31	146	159
Distance(mm)	0.0	0.06	0.06	0.43	0.45	0.35	0.36

L3-86-NC-15D						
Oxides (wt%)	Glass*	Alteration Crust				
		From Smectite/Chlorite to Boehmite (interior to exterior)				
SiO <sub>2</sub>	49.17	39.33	36.53	28.49	10.12	9.12
TiO <sub>2</sub>	1.38	2.10	2.43	4.30	3.44	5.23
Al <sub>2</sub> O <sub>3</sub>	15.73	23.17	24.10	36.93	41.12	36.47
FeO	8.28	4.57	1.94	0.52	0.09	0.12
MnO	0.18	0.04	0.04	0.04	0.04	0.04
MgO	8.69	5.80	6.33	0.66	0.45	0.75
CaO	12.19	0.17	0.17	0.16	0.16	0.16
Na <sub>2</sub> O	2.66	0.74	0.90	0.58	0.56	0.76
K <sub>2</sub> O	0.20	0.32	0.23	0.37	0.13	0.17
Cr <sub>2</sub> O <sub>3</sub>	0.05	0.05	0.07	0.10	0.12	0.13
SUM	98.53	76.29	72.73	72.16	56.25	52.96
H <sub>2</sub> O	1.47	23.71	27.27	27.84	43.75	47.04
(by diff.)						
TiO <sub>2</sub> /Al <sub>2</sub> O <sub>3</sub>	0.09	0.09	0.10	0.12	0.08	0.14
Al <sub>2</sub> O <sub>3</sub> /SiO <sub>2</sub>	0.32	0.59	0.65	1.30	4.06	4.00
MgO/SiO <sub>2</sub>	0.18	0.15	0.17	0.02	0.04	0.08
Al <sub>2</sub> O <sub>3</sub> /MgO	1.81	3.99	3.81	56	91	49
Distance(mm)	0.0	0.07	0.21	0.4	0.8	0.8

\*average of two analyses

Distance = distance from interior (basalt/crust interface).

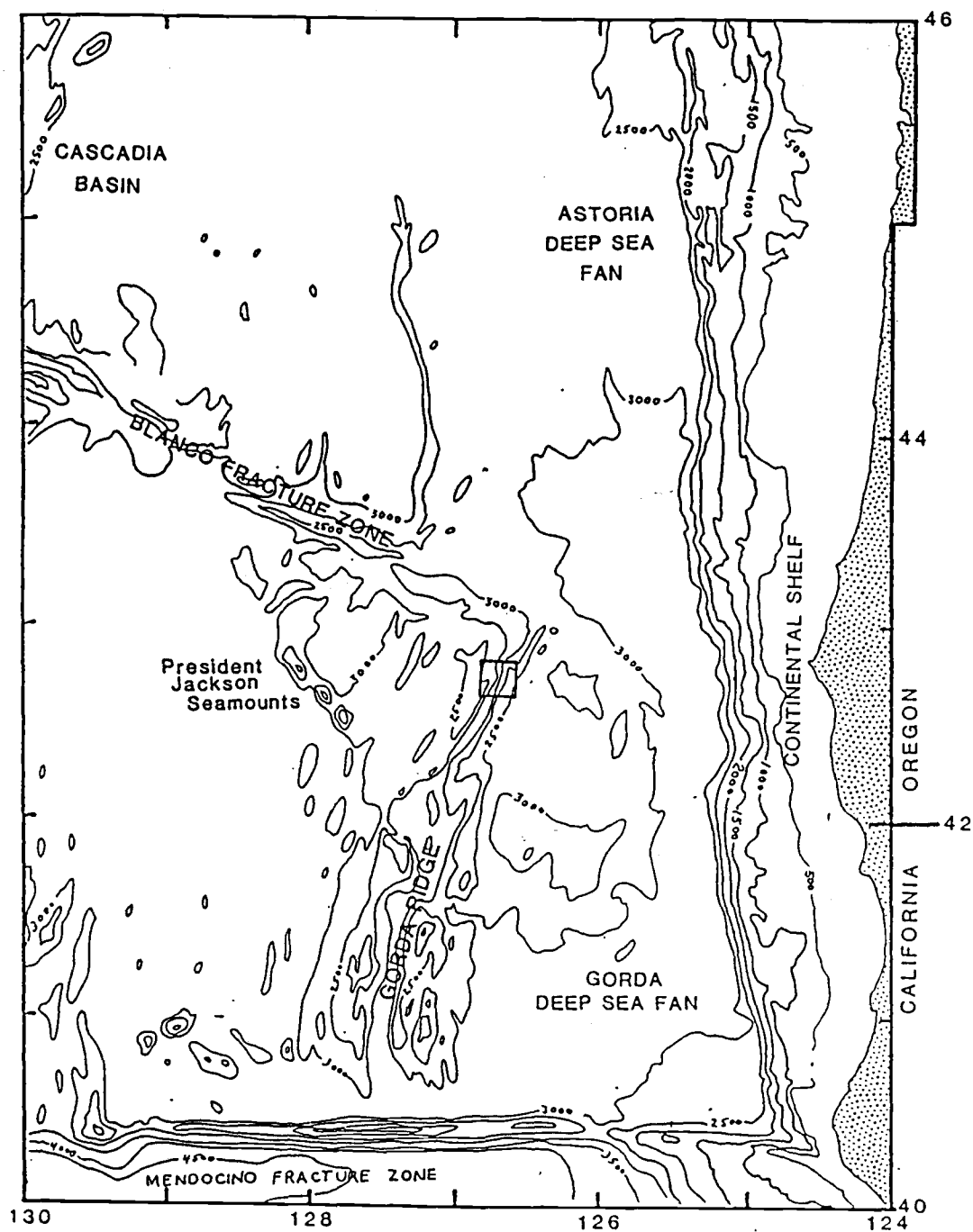


Fig. III-1: Location of the Gorda Ridge off the coast of Oregon and California from Wilde et al., 1978, 1979. Area outlined is the GR-14 study area. Contour interval = 500m.

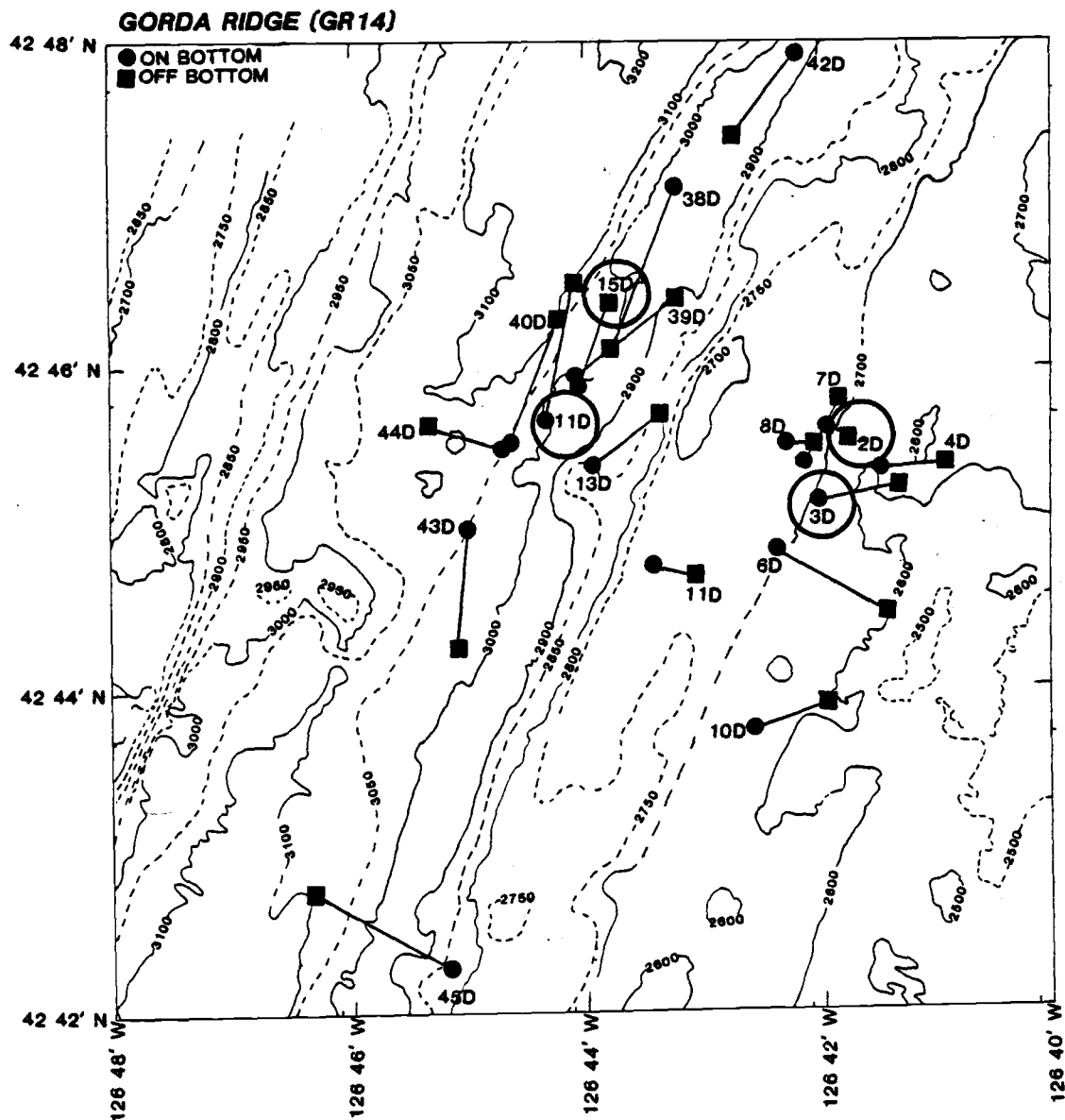


Fig. III-2: Bathymetric map of the northern Gorda Ridge from NOAA SEABEAM. with locations of L3-86-NC and L5-85-NC dredges on the USGS R/V S.P. Lee. Circled dredge numbers recovered boehmite. Circled dredges 11D and 15D contained material used in this study. Contour interval = 50m.

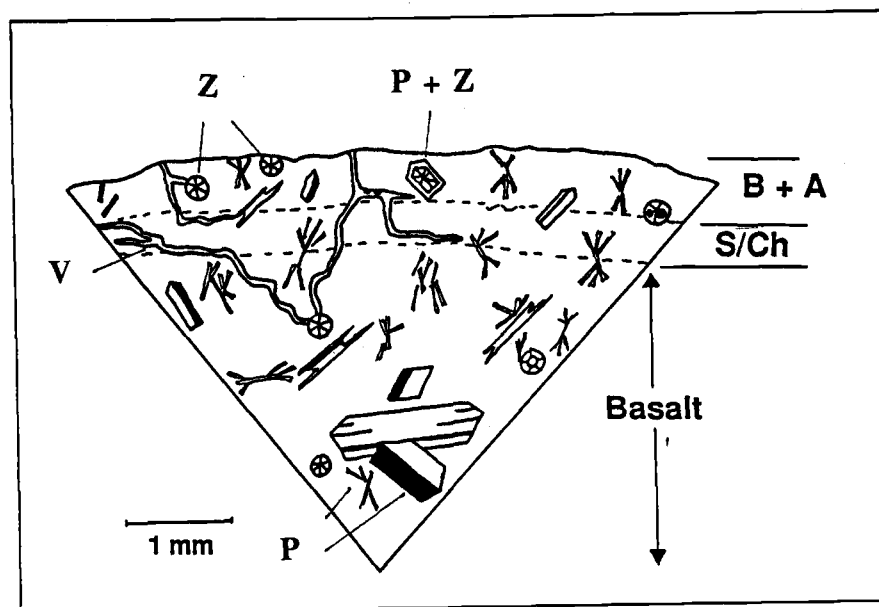


Fig. III-3: Drawing of basalt and alteration crust with mineralogy and textures observed in thin section. Relatively unaltered dark grey basalt changes into an interior dark green layer and then into an exterior white layer. Dashed lines indicate alteration fronts between these layers. In thin section both layers pseudomorph basalt texture but are distinguished by increased light transmission (from interior to exterior) and reddish, oxidized appearance. S/Ch = inner layer of smectite/chlorite. B+ A = the exterior layer of boehmite and anatase. P = plagioclase phenocrysts and microphenocrysts, Z = zeolite, V = vein. See text for petrographic description.

Fig. III-4: X-ray diffractograms of the inner layer of sample L3-86-NC-11D (  $0^\circ$  to  $30^\circ 2\theta$ ) showing the presence of smectite/chlorite interlayered clays. Numbers above peaks are d-spacings in Å. S/Ch = interlayered smectite/chlorite, P = plagioclase, and C = corundum standard. (a) random mount (b) oriented mount (air dried) (c) oriented mount (ethylene glycolated) (d) oriented mount heated to  $350^\circ\text{C}$ .

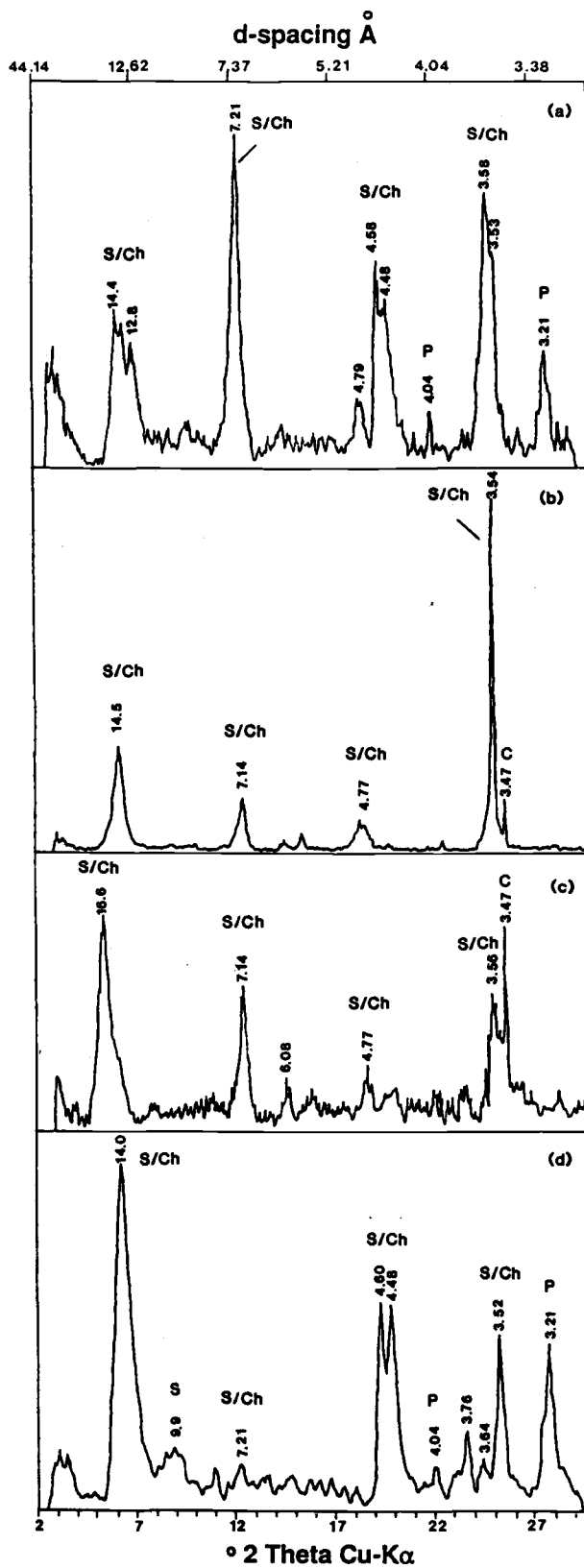


Fig. III-4



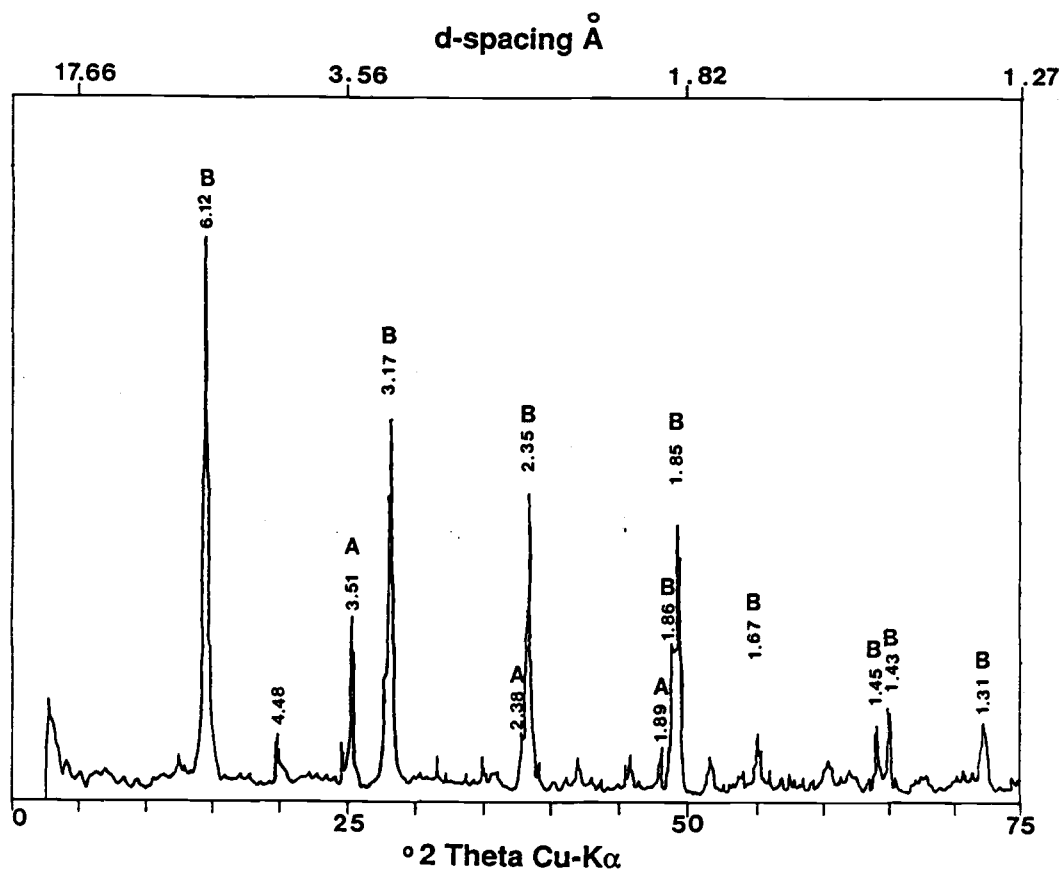


Fig. III-5: X-ray diffractogram of outer layer of sample L3-86-NC-15D from the northern Gorda Ridge showing the presence of boehmite,  $\text{AlO}(\text{OH})$  and anatase. Numbers above peaks are d-spacings in Å. B = boehmite, A = anatase.

Fig. III-6: Major element oxides from microprobe analyses versus distance from the basalt/crust interface (inner) to the exterior (outer) of sample 15D. Distance = 0 mm corresponds to basalt glass composition. Error bars are given for analyses with errors greater than the size of the data point.

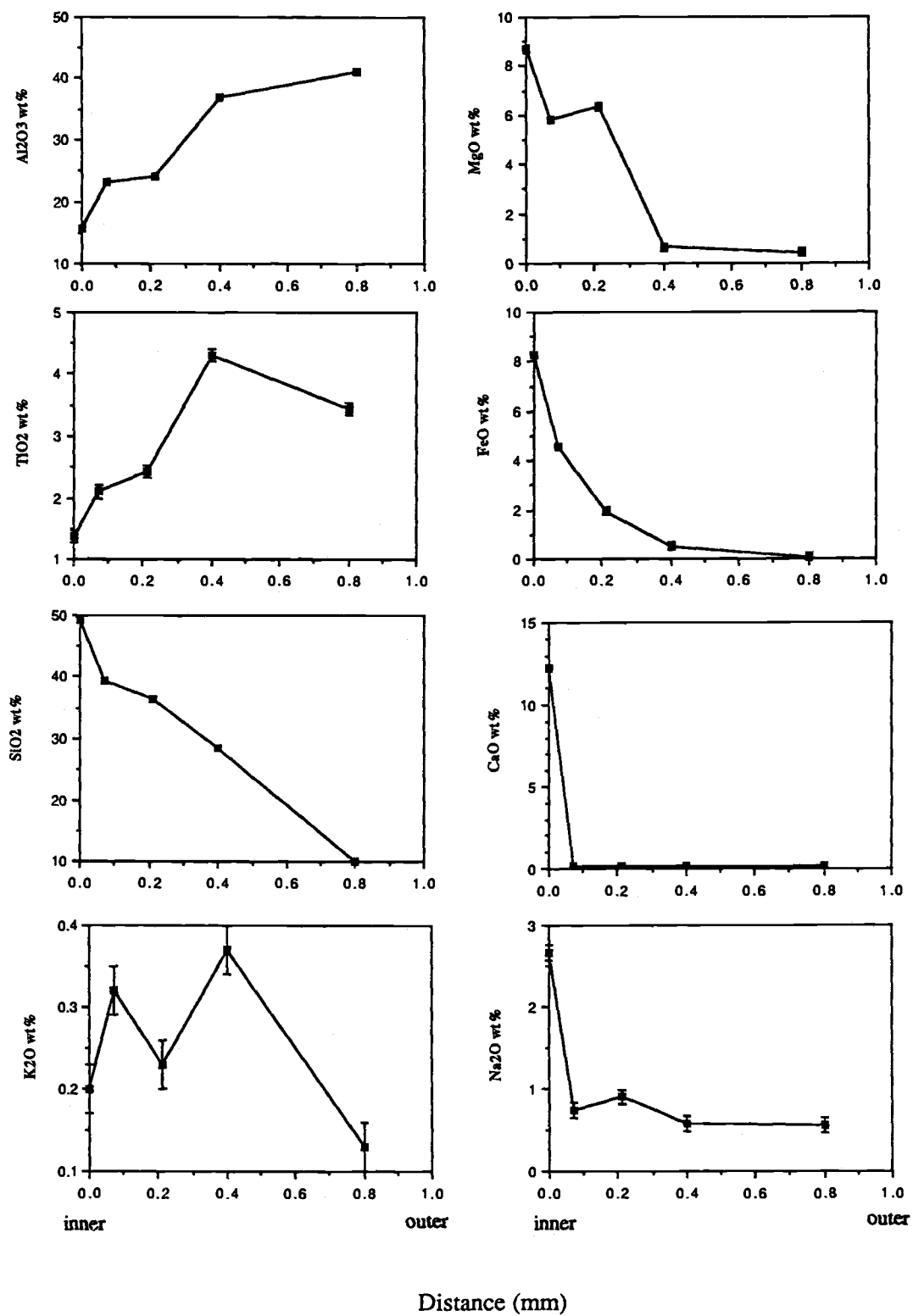


Fig. III-6

Fig. III-7: SEM electron backscattering images of Gorda Ridge hydrothermal alteration crusts. (a) Quartz grains on clay background possibly showing effects of dissolution destroying crystal boundaries. Scale bar = 20 microns. (b) Anatase crystals on background of boehmite/clay. Scale bar = 1 micron.



Fig. III-7 (a)



Fig. III-7 (b)

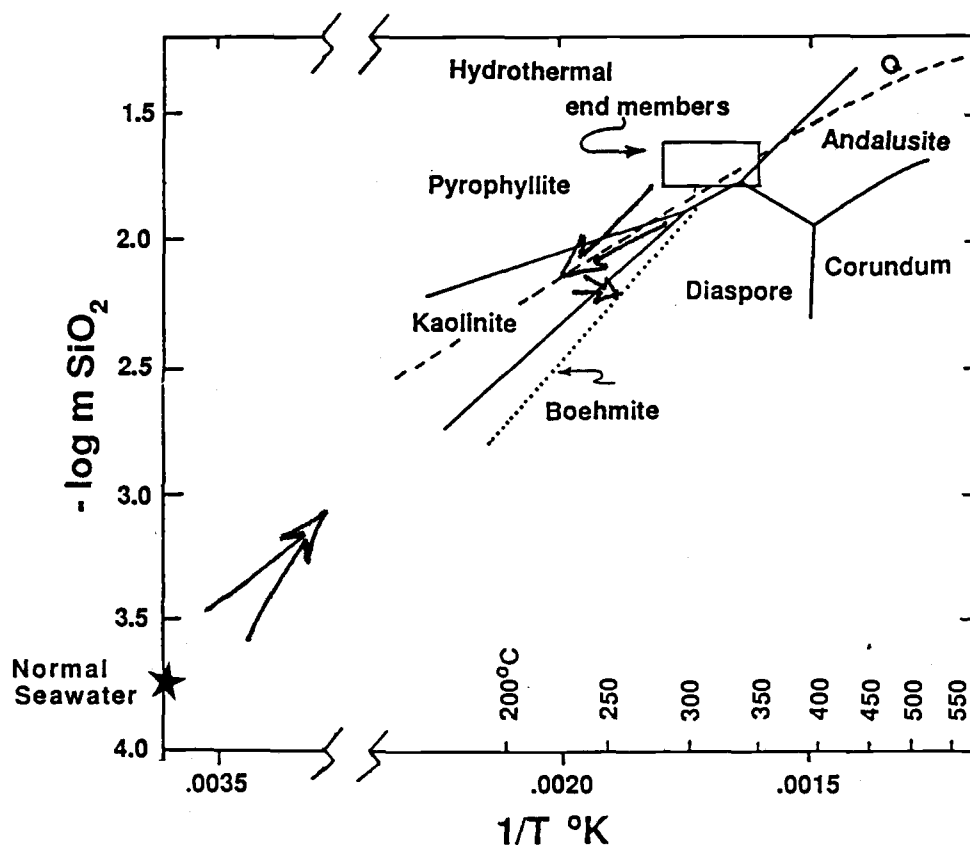


Fig. III-8: Phase relations in the system  $\text{Al}_2\text{O}_3\text{-SiO}_2\text{-H}_2\text{O}$  at 1 kb from Hemley et al., 1980 with expanded scale to incorporate the position of normal seawater collected between 2600-3000 m in the GR-14 area (B. Collier for J. Trefry, pers. comm., 1988). The plotted rectangle for hydrothermal end members incorporates data from Edmond et al., 1979, Michard et al., 1984, Von Damm et al., 1985 and Von Damm and Bischoff, 1987. Arrows generalize the necessary conditions for the formation of boehmite. The dashed line labeled Q is quartz saturation.  $m$  = micromoles/kg.

## References

- Albee A.L. and Ray L. (1970) Correction factors for electron probe microanalysis of silicates, oxides, carbonates, phosphates and sulfides. *Anal. Chem.* 42, 1408-1414.
- Alt J.C. and Honnorez J. (1984) Alteration of the upper oceanic crust, DSDP site 417: mineralogy and chemistry. *Contrib. Min. Petrol.* 87, 149-169.
- Atwater T.M. and Mudie J.M. (1973) Detailed near-bottom geophysical study of the Gorda Rise. *J. Geophys. Res.* 78, 8665-8686.
- Baker E.T., Massoth G.J., Collier R.W., Trefry J.H., Kadko D., Nelsen T.A., Rona P.A. and Lupton J.E. (1987) Evidence for high-temperature hydrothermal venting on the Gorda Ridge, Northeast Pacific Ocean. *Deep Sea Res.* 34, 1461-1476.
- Bass M.N. (1976) Secondary minerals in oceanic basalt, with special reference to Leg 34, Deep Sea Drilling Project. In Yeats, R.S., Hart, S.R., et al., 1976. Initial Report of the Deep Sea Drilling Project, Volume 34, Washington (U.S. Government Printing Office), pp. 393-432.
- Bence A.E. and Albee A.L. (1968) Empirical correction factors for electron microanalysis of silicates and oxides. *J. Geol.* 76, 382-403.
- Bowers T.S., Jackson K.J. and Helgeson H.C. (1984) Equilibrium activity diagrams for coexisting minerals and aqueous solutions at pressures and temperatures to 5kb and 600°C. Springer-Verlag, 397 p.
- Brett R., Evans H.T., Gibson E.K., Hedenquist J.W., Wandless M.-V. and Sommer M.A. (1987) Mineralogical studies of sulfide samples and volatile concentrations of basalt glasses from the southern Juan de Fuca Ridge. *J. Geophys. Res.* 92, 11,373-11,379.
- Brown G. and Brindley G.W. (1980) X-ray diffraction procedures for clay mineral identification. In: *Crystal structures of clay minerals and their X-ray identifications*, (eds. G.W. Brindley and G. Brown), Chap. 5, pp. 305-359. Spottiswoode Ballantyne Ltd.
- Browne P.R.L. (1978) Hydrothermal alteration in active geothermal fields, *Ann. Rev. Earth Planet Sci.*, 6, 229-250.
- Clague D.A., Friesen W., Quintero P., Morgenson L., Holmes M., Morton J., Bouse R. and Davis A. (1984) Preliminary geological, geophysical and biological data from the Gorda Ridge. U.S. Geol. Survey Open File Report, 84-364, 33 p.
- Cole T.G. (1983) Oxygen isotope geothermometry and origin of smectites in the Atlantis II Deep, Red Sea. *Earth Planet Sci. Lett.* 66, 166-176.
- Collier R.W., Holbrook S.H. and Robbins J.M. (1986) Studies of trace metals and active hydrothermal venting on the Gorda Ridge. Oregon Department of Geology and Mineral Industries, Open-File Report 0-86-13.



- Crane K. and Ballard R.D. (1981) Volcanics and structures of the FAMOUS-Narrowgate rift: Evidence for cyclic evolution: AMAR I. *J. Geophys. Res.* 86, 5112-5124.
- Davis A. and Clague D.A. Geochemistry, mineralogy and petrogenesis of lava from the Gorda Ridge between latitude 43°N and 41°N. *J. Geophys. Res.* (in press).
- Deer W.A., Howie R.A. and Zussman J. (1966) An introduction to the rock-forming minerals. Wiley and Sons, 528 p.
- Delany J.M. and Helgeson H.C. (1978) Calculation of the thermodynamic consequences of dehydration in subducting oceanic crust to 100kb and >800°C. *Am. Jour. Sci.*, 278, 638-686.
- Edmond J.M., Measures C.I., McDuff R.E., Chan L.H., Collier R.W., Grant B., Gordon L.I. and Corliss J.B. (1979) Ridge crest hydrothermal activity and the balances of the major and minor elements in the ocean: The Galapagos data. *Earth Planet. Sci. Lett.* 46, 1-18.
- Fukui S. (1976) Laboratory techniques used for atomic absorption spectrophotometric analysis of geologic samples, Oregon State University Reference 76-10.
- Gladney E.S. and Burns C.E. (1983) 1982 compilation of elemental concentrations in eleven United States Geological Survey rock standards. *Geostandards Newsletter*. 7, 3-17.
- Goldschmidt V.M. (1968) *Geochemistry*. Oxford Clarendon Press, 730 p.
- Guilbert J.M. and Park C.F., Jr. (1986) *The Geology of Ore Deposits*. W.H. Freeman, 985 p.
- Hajash A. and Archer P. (1980) Experimental seawater/basalt interactions: effects of cooling. *Contrib. Mineral. Petrol.*, 75, 1-13.
- Haymon R.M. and Kastner M. (1986) The formation of high temperature clay minerals from basalt alteration during hydrothermal discharge on the East Pacific Rise axis at 21°N. *Geochim Cosmochim Acta*. 50, 1933-1939.
- Hekinian R. (1982) *Petrology of the ocean floor*. Elsevier Scientific Publishing Co. 393p.
- Hemley J.J., Montoya J.W., Marienko J.W. and Luce R.W. (1980) Equilibria in the system  $\text{Al}_2\text{O}_3\text{-SiO}_2\text{-H}_2\text{O}$  and some general implications for alteration processes. *Econ. Geol.* 75, 210-228.
- Honnorez J. (1980) The aging of the oceanic crust at low temperature. In: *The Sea* (ed. C. Emiliani), Vol.7, Chap. 15, 525-587. John Wiley Interscience.
- Howard K.J. and Fisk M.R. (1986) Hydrothermal precipitates from basalts on the Gorda Ridge and the President Jackson Seamounts. Oregon Department of Geology and Mineral Industries, Open-File Report 0-86-18.

- Humphris S.E. and Thompson G. (1978) Trace element mobility during hydrothermal alteration of oceanic basalts. *Geochim. Cosmochim. Acta.* 42, 127-136.
- Kennedy G.C. (1959) Phase relations in the system  $\text{Al}_2\text{O}_3\text{-H}_2\text{O}$  at high temperatures and pressures. *Am. Jour. Sci.* 257, 563-573.
- Kessman I. (1966) Zur hydrothermalen synthese von Brookit. *Zeitschrift für anorganische und allgemeine Chemi.* 346, 30-43.
- Koski R.A., Lonsdale P.F., Shanks W.C., Berndt M.E. and Howe S.S. (1985) Mineralogy and geochemistry of a sediment-hosted hydrothermal sulfide deposit from the southern trough of Guaymas Basin, Gulf of California. *J. Geophys. Res.* 90, 6695-6707.
- Kristmannsdottir H. (1977) Types of clay minerals in hydrothermally altered basaltic rocks, Reykjanes, Iceland. *Jökull.* 26, 30-39.
- Lonsdale P.F., Bischoff J.L., Burns V.M., Kastner M. and Sweeney R.E. (1980) a high temperature hydrothermal deposit on the seabed at a Gulf of California spreading center. *Earth Planet Sci. Lett.* 49, 8-20.
- Loughnan F.C. (1969) Chemical weathering of the silicate minerals. Elsevier Publishing Co. Inc., 154 p.
- Malahoff A., Embly R., Hammond S., Ryan W. and Crane K. (1982) Juan de Fuca and Gorda Ridge axial ridge morphology and tectonics from combined SEABEAM and SEA MARC data (abstr.). *EOS* 63,1147.
- Michard G., Albarede F., Michard A., Minster J.-F., Charlo J.-L. and Tan, N. (1984) Chemistry of solutions from the 13°N East Pacific Rise hydrothermal site. *Earth Planet Sci. Lett.* 67, 297-307.
- Mottl M.J. (1983) Hydrothermal processes at seafloor spreading centers: application of basalt-seawater experimental results. In: *Hydrothermal Processes at Seafloor Spreading Centers*, (eds. P.A. Rona, K. Bostrom, L. Laubier and E.L. Smith), Plenum Press, pp. 199-224.
- Northrup J., Menard H.W. and Duennebie F.K. (1968) Seismic and bathymetric evidence of a fracture zone on Gorda Ridge. *Science.* 161, 688-690.
- Norton S.A. (1973) Laterite and bauxite formation. *Econ Geol.* 68, 353-361.
- Oudin E. (1983) Hydrothermal sulfide deposits of the East Pacific Rise (21°N), Part I: Descriptive mineralogy. *Marine Mining* 4, 39-72.
- Petersen U. (1971) Laterite and bauxite formation. *Econ Geol.* 66, 1070-1071.
- Peterson C., Duncan R. and Scheidegger K. (1986) Sequence and longevity of basalt alteration at Deep Sea Drilling Project Site 597. In Leinen, M., Rea, D.K. et al., *Init Repts. DSDP, 92: Washington (U.S. Govt. Printing Office)*, 505-515.

- Rafal'skiy R.P. and Alekseyev V.A. (1986) Kinetics of reaction of silicates with aqueous solutions. *Geochemistry International*. 24, 68-77.
- Riddihough R. (1980) Gorda plate motions from magnetic anomaly analysis. *Earth Planet Sci. Lett.* 51, 163-170.
- Riddihough R. (1984) Recent movements of the Juan de Fuca plate system. *J. Geophys. Res.* 89, 6980-6994.
- Rona P.A. and Clague D.A. (1986) Geologic setting of hydrothermal activity at the northern Gorda Ridge (abstr.), *EOS* 67, 1028.
- Rosenbauer K.J. and Bischoff J.L. (1983) Uptake and transport of heavy metals by heated seawater: a summary of the experimental results. In: *Hydrothermal Processes at Seafloor Spreading Centers* (eds. P.A. Rona, K. Bostrom, L. Laubier and E.L. Smith), Plenum Press, 177-198. .
- Scheidegger K.F. and Stakes D.S. (1980) X-ray diffraction and chemical study of secondary minerals from Deep Sea Drilling Project Leg 51, holes 417A and 417D. In *Initial Reports of the Deep Sea Drilling Project Legs 51-53*, 1253-1263. U.S. Gov't. Printing Office, Washington, D.C.
- Seyfried W.E, Jr. and Bischoff J.L. (1981) Experimental seawater-basalt interaction at 300°C, 500 bars, chemical exchange, secondary mineral formation and implications for the transport of heavy metals. *Geochim. Cosmochim. Acta.* 45, 135-147.
- Seyfried W.E. and Mottl M.J. (1982) Hydrothermal alteration of baslt by seawater under seawater-dominated conditions. *Geochim. Cosmochim. Acta* 46, 985-1002.
- Shelley D., Smale D. and Tullock A.J. (1977) Boehmite in syenite from New Zealand. *Min Mag.* 41, 398-400.
- Sumi K. (1968) Hydrothermal rock alteration of the Matsukawa geothermal area northeast Japan. *Geol. Survey Japan. Report No. 225*, 42 p.
- Sumi K. and Takashima I. (1976) Absolute ages of the hydrothermal alteration halos and associated volcanic rocks in some Japanese geothermal fields. *Proc. 2nd U.N. Symp. Dev. Use Geotherm. Resour.* 1975, 1:625-34. San Francisco: United Nations, 844 p.
- Tettenhorst R. and Hofman D.A. (1980) Crystal chemistry of boehmite. *Clays. Clay Min.* 28, 373-380.
- Tole M.P. (1987) Thermodynamic and kinetic aspects of formation of bauxites. *Chem. Geol.* 60, 95-100.
- Tomasson J. and Kristmannsdottir H. (1972) High temperature alteration of minerals and thermal brines, Reykjanes, Iceland. *Contrib. Min. Petrol.* 36, 123-134.
- Valeton I. (1972) *Bauxites*. Elsevier Pub. Co., 226 p.

- Von Damm K.L. and Bischoff J.L. (1987) Chemistry of hydrothermal solutions from the southern Juan de Fuca Ridge. *J. Geophys. Res.* 92, 11,334-11,346.
- Von Damm K.L., Edmond J.M., Grant B., Measures C.I., Walden B. and Weiss R.F. (1985) Chemistry of submarine hydrothermal solutions at 21°N, East Pacific Rise. *Geochim Cosmochim Acta* 49, 2197-2220.
- Wilde P., Chase T.E., Holmes M.L., Normark W.R., Tomas J.A., McCulloch D.S. and Kulm L.D. (1978) Oceanographic data off northern California - southern Oregon, 40° to 43° North including the Gorda Deep Sea Fan. LBL Publ., 251, Lawrence Berkeley Lab. Berkeley, Calif.
- Wilde P., Chase T.E., Holmes M.L., Normark W.R., Tomas J.A., McCulloch D.S., Carlson P.R., Kulm L.D. and Young J.D. (1979) Oceanographic data off Oregon 43° to 46° North including Astoria Deep-Sea Fan. LBL Publ., 253, Lawrence Berkeley Lab, Berkeley, Calif.
- Wolska E. and Szajda W. (1980) Die bildung von kristallinem bohmit in gemeinsam gefallten AlFe(III)-Hyroxiden unter hydrothermalen bedingungen. *Monatshefte fur Chemie* 111, 1329-1334.
- Yang H.-Y. (1987) Stability of ilmenite and titanomagnetite in the presence of carbon dioxide - a thermodynamic evaluation. *Contrib. Mineral. Petrol.* 95, 202-206.

## CHAPTER IV

### WEATHERED SULFIDE CHIMNEYS FROM THE ESCANABA TROUGH, GORDA RIDGE

### Abstract

Sulfide chimneys recovered from the Escanaba Trough, southern Gorda Ridge are highly weathered, but still contain unusual trace mineralogy. Fresher portions of chimneys are dominantly lattices of boxwork pyrrhotite with interstitial minor sphalerite, chalcopyrite, isocubanite, galena and barite. Exceptions include one dominantly pyrite chimney sample and one barite chimney. In pyrrhotite-rich samples, pyrrhotite laths are frequently rimmed by Cu-Fe sulfides and sphalerite, Zn-rich rims form around Cu-Fe sulfides and galena is included in sphalerite. Small amounts of minerals previously unidentified in mid-ocean ridge hydrothermal environments include bismuth telluride, cassiterite, a Cu-Zn-Ni sulfide and cinnabar. Bismuth telluride and cassiterite are included in euhedral pyrrhotite and Cu-Zn-Ni sulfide is a replacement rim on pyrrhotite. The presence of bismuth telluride and cassiterite is evidence for the interaction of hydrothermal fluids and island arc derived sediments filling the Escanaba Trough. Arsenopyrite identified in Escanaba Trough chimney samples is not commonly reported in mid-ocean ridge hydrothermal deposits and also reflects fluid-sediment interaction. Cinnabar is a trace mineral in a barite chimney that contains fine-scale Sr zonation.

Chimney weathering is similar to that observed in sulfide deposits recovered from the Guaymas Basin, Gulf of California. Initially, pyrrhotite oxidizes to marcasite. Final products of chimney weathering include elemental sulfur, atacamite, amorphous Fe oxyhydroxides, goethite, lepidocrosite and possible (?) akaganéite. Some Fe oxyhydroxides represent direct precipitation from cooler FeOOH saturated solutions rather than in situ alteration of sulfides. Clay minerals and detrital sediments are a significant fraction of weathered chimneys.

Weathered rinds of chimneys are enriched in elements associated with clays (Al, Si, K). Enrichments of Co and As in chimney exteriors relative to chimney interiors reflect either differential precipitation or weathering processes. Enrichments in Zn, Cd and Pb reflect the increased abundance of sphalerite and galena from chimney interiors to chimney exteriors. Chemical analyses of individual chimney samples show maximum concentrations of minor elements are: Pb and Cu up to 3 wt%, As up to 1.9 wt% and Co up to 1750 ppm. The high combined metals content of Escanaba Trough deposits compared to hydrothermal deposits at other sedimented spreading ocean ridges such as Guaymas Basin, Gulf of California and Middle Valley, Endeavor Ridge may reflect differences in the degree of interaction between sediments and hydrothermal fluids or differences in sediment composition between the three regions.

## Introduction

Mid-ocean ridge massive sulfide deposits, formed by hydrothermal circulation of seawater in the oceanic crust, have now been discovered at both fast- (Koski et al., 1984, Oudin, 1983, Haymon and Kastner, 1981, Zierenberg et al., 1984) and slow- (Rona, 1986, Morton et al., 1987) spreading ridges and sediment-covered (Lonsdale et al., 1980, Koski et al., 1985, Davis et al., 1987, Morton et al., 1987) and sediment-starved ridges (Rona, 1986, Koski et al., 1984, Haymon and Kastner, 1981). Scott et al. (1978) suggested that differences in the metal content of deposits could reflect differences in hydrothermal systems between fast and slow spreading ridges. Although later studies refuted the initial evidence underlying this hypothesis (Metz et al., 1988), significant differences in metal content are found when sediment-covered and sediment-starved ridges are compared. Sediment-covered ridges generally produce greater diversity in the chemistry and mineralogy of hydrothermal deposits because of hydrothermal reactions in the sediments (perhaps associated with prolonged high temperature and slow water flow conditions) in addition to seawater-basalt interactions. In addition, surficial hydrothermal deposits at sedimented ridges usually possess a lower combined ore metal content ( $\text{Cu} + \text{Zn} + \text{Pb} + \text{Ag} + \text{Cd}$ ) compared to hydrothermal deposits at sediment-free ridge crests (Davis et al., 1987, Koski et al., 1985).

In 1985, a cooperative venture between Oregon State University, the U.S. Geological Survey and Minerals Management Service initiated exploration for hydrothermal vents in the sediment-filled Escanaba Trough, southern Gorda Ridge. Preliminary evidence of active hydrothermal vents in this region was the discovery of anomalously high heat flow ( $> 1200 \text{ mW/m}^2$ ) associated with sediment domes caused by underlying volcanic intrusions (Abbott, 1986). Subsequent dredging operations collected polymetallic sulfides in the sediments (Morton et al., 1987). The following year, the results of the above studies culminated in U.S. Navy sponsored SEACLIF submersible dives around two of the larger volcanic edifices within the Escanaba Trough. Highly weathered, inactive chimneys were discovered and sampled at both volcanic domes visited.

This report presents a discussion of the mineralogy and chemistry of weathered sulfide chimneys from the Escanaba Trough, southern Gorda Ridge collected by the submersible SEACLIF in August, 1986. Emphasis is placed upon mineralogic changes and the mobilization of elements as chimneys weather on the seafloor. Documented differences in the chemistry and mineralogy of deposits associated with active versus inactive hydrothermal areas (Styrt et al., 1981, Hekinian et al., 1980, Haymon and Kastner, 1981) provide a means for examining weathering processes of hydrothermal deposits on

the seafloor. Further comparison of Escanaba Trough deposits with other sediment-filled ridges at Middle Valley, northern Juan de Fuca Ridge and Guaymas Basin, Gulf of California, reveal that the Escanaba Trough deposits are relatively enriched in combined ore metals and are more similar to deposits studied from sediment-free ridges such as 21°N, East Pacific Rise (EPR) and southern Juan de Fuca Ridge. This significant difference challenges our understanding of the effects of sediment cover on hydrothermal deposits produced at mid-ocean ridges and may be of economic importance considering that the Escanaba Trough lies within the 200 mile offshore boundary defining the U.S. Exclusive Economic Zone.



## Tectonic Setting

The Escanaba Trough is a slowly spreading (2.3 cm/yr full rate) segment of volcanic ocean ridge located within the U.S. Exclusive Economic Zone about 300 km off the coast of northern California (Fig. III-1) (Atwater and Mudie, 1973, Riddihough, 1980). It is the southern-most segment of the three segments of ridge that comprise the 300 km long, Gorda Ridge and unlike the northern two segments, it is filled with sediments. The northern limit of the Escanaba Trough is defined by a small right-lateral offset at  $41^{\circ} 30'N$  where the axial valley narrows to 3-5 km wide (Riddihough, 1980). The Escanaba Trough is bounded to the south by the Mendocino Fracture Zone ( $40^{\circ} 24'N$ ), where the axial valley is up to 18 km wide. Within the Escanaba Trough, the water depth over the axial valley floor averages about 3,200 m and flanking ridges are between 1,200 to 1,700 m high.

A gap between the end of the ridge and the Mendocino Fracture Zone creates a channel for turbidites originating from the North American continental margin (Moore, 1970). This terrigenous sediment, up to 500m thick, fills the Escanaba Trough south of  $41^{\circ} 15'N$  where the axial valley shoals (Moore, 1970, Karlin and Lyle, 1989). The insulating blanket of sediment provides a mechanism for maintaining high temperatures in the hydrothermal system that enhance chemical exchange between the hydrothermal fluids and the sediments. Evidence of significant interaction between hydrothermal fluids and sediment at depth has been reported by Morton et al. (1987) and deposition of sulfides and sulfates in the sediment column has been documented by Karlin and Lyle (1989).

### *Sample Location*

Six volcanic centers, located by seismic reflection profiles, are spaced at 15 to 20 km intervals along the axis of the Escanaba Trough and dome the otherwise flat-lying sediments up to 100m high (Morton et al., 1987). The two largest volcanic edifices are located at  $40^{\circ} 45'N$  latitude and  $41^{\circ}N$  latitude (Fig. IV-1) and are designated Dome B and Dome D respectively. The sites of SEACLIF dive around Dome D are designated NESCA sites (for northern Escanaba) and those around Dome B are designated SESCA sites (for southern Escanaba). The locations of SEACLIF dives in the Escanaba Trough that recovered chimney fragments are shown in Fig. IV-2. Fifteen chimney fragments were examined in this study. Ten samples are from "NESCA" Dome D (five from Dive 658 and five from Dive 659) and five samples are from "SESCA" Dome B (one from Dive 661, two from Dive 662 and two from Dive 663).

At NESCA, the neovolcanic center is displaced to the eastern side of the axial valley. Dive 658 located a fault bounding Dome D to the north that contained the most extensive,

best preserved, sulfide deposits at NESCA. A barite chimney, collected at the bottom of the slope at this site, is one of the fragments described in this report (sample 658-R2-B). Large outcrops of fresh, glassy pillow basalt are located on a nearby hill and in the basin surrounding the hill. Smaller chimneys growing through the sediments were discovered at Dive 659. At SESCA, the neovolcanic center is displaced to the western side of the axial valley and has more extensive sediment cover than at NESCA. Dives 661, 662, and 663 are all located on faults bounding sediment domes.

Based on radiocarbon dating of turbidites, Karlin and Lyle (1989) determined the most recent volcanic activity at Dome B and Dome D was 2400 to 3000 years ago. This may be an approximate maximum age for chimney deposits that were built up during a post volcanic quiescent period (Spiess et al., 1980).

## Methods

### *Subsampling*

The fifteen chimney fragments were subdivided into samples based on (1) degree of alteration and (2) mineralogical variability. Generally, an outer surface that represents the weathered exterior exposed to more oxygenated seawater (designated "altered") was separated from the more protected, fresher chimney interior (designated "fresh"). One sample from the freshest portion of each chimney fragment was sampled for analysis and classified as "fresh" with the following exceptions. Samples 659-1 and 661-R1 were completely weathered throughout and subsamples of these were classified as "altered". Two additional samples from Site 659 (samples 659-3 and 659-R1-F) and one additional sample from Site 662 (659-3-2) were separated for analysis because each appeared mineralogically different. In "altered" samples, discernable differences in either hydrothermal precipitate mineralogy or alteration products from weathering, enabled further subdivision. Splits of all samples were subjected to X-ray diffraction to determine sample mineralogy and atomic absorption to determine bulk chemistry.

### *X-Ray Diffraction*

Samples were ground in a mortar and pestle and random, air-dried powder mounts were prepared on glass disks. Samples were initially analyzed from  $2^{\circ}$  to  $100^{\circ}$   $2\theta$  at  $1^{\circ}$   $2\theta/\text{min}$  on a SCINTAG X-ray diffractometer using Cu-K $\alpha$  radiation. Sample diffractograms that indicated poorly crystalline material (low signal/background ratio) were rerun by a time averaging option using  $6^{\circ}$   $2\theta/\text{min}$  and 20 consecutive scans over the same  $2\theta$  range. Peaks selected by computer were edited by hand and compared with the JCPDS files for inorganic minerals.

### *Atomic Absorption*

Atomic absorption analyses were performed on a Perkin-Elmer 5000 atomic absorption spectrometer after digestion in teflon crucibles sealed in metal bombs according to methods described by Fukui (1976). The samples were analyzed for a total of 22 elements by methods outlined in Perkin-Elmer (1982). The precision and accuracy for atomic absorption analyses compared with consensus values for the three standards G-2, GSP-1 and BCR-3 is listed in Table III-1. Analytical error compared to the above standards is: within 1% for K, Li, Co, Cu, Si and Zn; within 2% for Al, Fe, Mg, Mn, Na and Pb; within 5% for Ba; within 6% for Ca and Sr; within 10% for Ni, Rb and V at the level of the analyses; within 11% for Cr and within 18% for Ti. Analytical errors for As and Cd were not determined since their concentrations in the standards are too low to

measure. To examine relations between variables, correlation matrices were prepared for samples split into altered versus fresher chimney fragments.

### *Electron Microprobe and Scanning Electron Microscope (SEM)*

Polished sections of seven of the freshest chimney samples were prepared for microprobe analysis and scanning electron microscopy to examine primary and replacement mineralogy and the effects of alteration on sulfides. Six samples were chosen from Dome D and one from Dome B. Microprobe analyses were performed on the University of Oregon ARL/EMX microprobe using 15kV accelerating voltage and .15 $\mu$ A sample current. Each analysis was corrected using the standard Bence and Albee (1968) and Albee and Ray (1970) corrections. Scanning electron microscopy (SEM/EDS) was performed at the U.S.G.S. in Menlo Park, California.

### *Sulfur Isotopes*

Sulfur isotopes were determined on hand picked sulfides (pyrrhotite and sphalerite) and barite in Dive 658 chimney fragments. Sulfur isotope ratios are expressed as  $\delta^{34}\text{S}$  (in per mil) relative to troilite sulfur from the Canyon Diablo meteorite (defined as 0 ‰), where:

$$\delta^{34}\text{S}_x \text{ ‰} = \left( \frac{R_x}{R_{\text{std}}} - 1 \right) 10^3 ; \quad R_x = \left( \frac{{}^{34}\text{S}}{{}^{32}\text{S}} \right)_x \quad (1)$$

where x = sample and std = standard.

Measurements are precise to within  $\pm 0.2$  ‰. Isotopic compositions were standardized with an in-lab standard (Standard B) which has a value of 1.2 ‰ relative to the Canyon Diablo Troilite.  $\text{SO}_2$  gas was prepared in an extraction line at Oregon State University after converting all sulfur to  $\text{Ag}_2\text{S}$ . For sulfides, sulfur was converted to  $\text{Ag}_2\text{S}$  by reaction with graphite and precipitation with  $\text{AgNO}_3$  solution.  $\text{Ag}_2\text{S}$  was then combusted with  $\text{CuO}$  at  $1025^\circ\text{C}$  for 10 minutes to yield  $\text{SO}_2$  which was then purified to remove  $\text{H}_2\text{O}$  and  $\text{CO}_2$  (Grinenko, 1962). For barite, the sulfate was reduced to  $\text{H}_2\text{S}$  by boiling in a mixture of  $\text{HI}$ ,  $\text{H}_3\text{PO}_2$  and  $\text{HCl}$  by methods described in Thode et al., (1961), then converted to  $\text{SO}_2$  by the method described above for sulfides. Sulfur isotope ratios in  $\text{SO}_2$  were measured by mass spectrometer at Global Geochemistry in Los Angeles.

The isotopic fractionation factor between two minerals A and B is approximated by:

$$\Delta_{AB} = \delta^{34}\text{S}_A - \delta^{34}\text{S}_B = 10^3 \ln \alpha_{A-B} ; \quad \text{where } \alpha_{A-B} = \frac{R_A}{R_B} \quad (2)$$

At high temperatures the fractionation factor is unity, thus the isotopic composition of sulfides and sulfates should reflect the isotopic composition of the sulfur source (Ohmoto and Rye, 1974).

## Results

### (A) Mineralogy

The mineralogy of sulfide chimneys from the Escanaba Trough, divided between fresher interiors and weathered exteriors in direct contact with seawater, is summarized in Table IV-1. A more complete description of each subsample and selected X-ray diffractograms with mineral identifications are provided in Appendix II. Complete separation of interior fresh sulfides from weathered exteriors was not attempted for mineralogical analysis, but major differences between the two subdivisions are apparent.

#### (a) Interiors

Pyrrhotite dominates the fresher chimney interiors with the following exceptions: Sample 662 was dominantly pyrite, the interior of sample 662-R1 was dominantly lepidocrocite, four samples (658, 659-1, 661-R1, 663-R2) were primarily clays and in sample 663-R1, marcasite was the dominant iron sulfide. Sample 658-R2-B, the barite chimney, is essentially pure barite. Only hexagonal pyrrhotite was observed in X-ray diffractograms as in Guaymas Basin chimney samples studied by Koski et al., (1985).

Sphalerite, chalcopyrite/cubanite and barite are secondary in abundance in sample interiors. Sphalerite is second in abundance in all samples from NESCA Dive 659, in one sample from NESCA Dive 658 (658-R1-1A) and in sample 662. Minor galena was found mainly by NESCA Dive 659 and SESCO Dive 662. Arsenopyrite was identified by XRD only in sample 659-R1-F. Otherwise, trace phases were identified by SEM.

Four samples contain clays and three of these also contain quartz and plagioclase and/or phillipsite. These findings support the assertion of Vallier-Silver et al. (1987) that sediments are entrained in chimneys during ascent of hydrothermal fluids. However, since the thermodynamic stability of silicate minerals in hydrothermal systems has been predicted by Bowers et al., (1985) and silicates are also observed in weathered chimney deposits at 21°N, EPR (Hekinian et al., 1980) their origin remains uncertain.

In addition, the chimney deposits (samples 9 (659-R1-F) and 11 (662-R1) from this study) have a petroliferous odor associated with asphaltic petroleum incorporated into the deposits by circulating hydrothermal fluids (Kvenholden, 1986, Morton et al., 1987).

#### (b) Exteriors

In contrast to fresher sulfide-rich chimney interiors, weathered exteriors have the following characteristics: First, clays, amorphous Fe-oxyhydroxides, goethite, lepidocrocite and akaganéite are in greater abundance in the exterior portions of the chimney. Second, sphalerite and barite are more abundant in sample exteriors, consistent with decreasing temperature and increasing oxidation, respectively, outward through the

chimney walls (Haymon, 1983). Third, amorphous silica, elemental sulfur, gypsum and talc are identified primarily in sample exteriors.

### *Petrography*

Samples chosen for petrographic examination are indicated in Table IV-1. Despite the effects of weathering, the freshest samples chosen for thin section preparation showed preservation of original textures and primary mineralogy. Open boxworks of pyrrhotite characterize all samples studied petrographically except sample 662 that contained primarily colloform pyrite. Larger pyrrhotite crystals, representing the main chimney flow channels, are surrounded by smaller, skeletal interlocking pyrrhotite crystals with an abrupt change in crystal size (Fig IV-3). Interstices in the pyrrhotite framework are partially filled with barite and secondary Fe-oxyhydroxides, implying later precipitation from cooling fluids. Minor replacement of pyrrhotite by sphalerite and chalcopyrite is observed in most samples. Sphalerite with inclusions of galena confirms the earlier crystallization of the latter.

### *Scanning Electron Microscopy (SEM)*

Minerals in low abundance ( $< \sim 5\%$ ) cannot usually be identified with certainty by XRD (and may not be distinguished by petrographic techniques employed in this study.) However, minor phases may be important in determining the distribution of trace elements and their contribution to ocean chemistry. To enable identification of minor mineralogy, as well as examine sulfide weathering in more detail, SEM was used on polished thin sections. One sample from Dome B and six samples from Dome D were examined by SEM to determine minor phases, replacement textures and alteration affects (Table IV-1). The major SEM results are summarized below. Details of the observations are provided in Appendix II-3.

#### *(a) Trace Minerals*

A Sn-rich mineral included in Fe-sulfide crystallized in samples from both Dome B (Dive 662) and Dome D (Dive 659). Although identification is not certain, low Fe and S concentrations recorded by the SEM probably represent contributions from the surrounding Fe-sulfide (pyrite at Dive 662 and pyrrhotite at Dive 659) and strongly suggest the Sn is incorporated in cassiterite ( $\text{SnO}_2$ ). Another sample from Dive 659 contained an As-rich mineral intergrown with cubanite (Fig. IV-4). A significant sulfur concentration indicates the presence of arsenopyrite ( $\text{FeAs}_2\text{S}$ ) although loellingite ( $\text{FeAs}_2$ ) has also been reported in Escanaba Trough sulfide chimneys (Zierenberg et al., 1986, Koski et al., 1987). Bismuth telluride in pyrrhotite was identified in sample 658-R3-A and cinnabar was preserved in a portion of the barite chimney (658-R2-B) (Fig. IV-5).

This is the first documentation of both minerals in mid-ocean ridge hydrothermal deposits studied to date.

### *(b) Replacement Minerals*

Observations of replacement mineralogy by SEM confirm those obtained by microscopy. Pyrrhotite, chalcopyrite and cubanite often have Zn-rich rims and are replaced primarily by sphalerite. Both of the above observations are consistent with crystallization of sphalerite during later stage decrease in fluid temperature.

In sample 658-R3-A, pyrrhotite is rimmed by Ni,Cu,Zn sulfide. Incorporation of Ni in a secondary replacement sulfide is unusual considering its immobility in seawater-basalt interaction experiments (Mottl, 1983, Seyfried and Janecky, 1985) and studies of natural metabasalts (Humphries and Thompson, 1978). However, some evidence for Ni mobility during alteration of basalt is observed on the northern Gorda Ridge (Howard and Fisk, 1986, 1988). From the above observations, the following paragenetic sequence is proposed: pyrrhotite  $\rightarrow$  Cu-Fe sulfides + galena  $\rightarrow$  sphalerite  $\rightarrow$  barite.

### *(c) Alteration Minerals*

The primary type of alteration observed in the chimney fragments is the oxidation of pyrrhotite ( $\text{Fe}^{+2}\text{S}_2$ ) to marcasite ( $\text{Fe}^{+2}\text{S}_2^{-1}$ ) (Ramdohr, 1969). A decrease in the Fe/S ratio near the borders of corroding pyrrhotite crystals is evidence of this oxidation effect (Fig. IV-6). A distinct separation between pyrrhotite crystals and Fe oxyhydroxides suggest that the latter in part precipitated from solution onto pyrrhotite crystals rather than formed entirely from in situ alteration of pyrrhotite grains (Fig. IV-7). This hypothesis is consistent with the interpretation based on similar observations of altered chimney samples from the Guaymas Basin (Koski et al., 1985).

No sulfate phase was observed as an intermediate stage of alteration of pyrrhotite to Fe oxyhydroxides, but elemental sulfur is a common alteration product recorded by X-ray diffraction. Atacamite, tentatively identified in sample 8 (659-R1), is formed from the weathering of Cu-Fe sulfides (Haymon and Kastner, 1983).

## (B) Mineral Chemistry

Table IV-2 contains electron microprobe analyses of iron sulfides, cubanite, sphalerite and barite. The Fe content of pyrrhotite determined by electron microprobe (Table IV-2a) is consistent with precipitation of hexagonal pyrrhoite observed both megascopically and in X-ray diffractograms and implies temperatures of formation  $> 250^\circ\text{C}$  (Krissen and Scott, 1982). All Fe sulfides are relatively free of impurities in contrast to pyrite from 21°N, EPR that crystallized with high Zn contents (up to 4.2 wt%) attributable to minute ZnS inclusions (Zierenberg et al., 1984).

Microprobe analysis of Escanaba Trough sphalerites all have low totals (Table IV-2b). This may reflect the absence of silica in the analyses as is the case for southern Juan de Fuca Ridge and 21°N, EPR in which precipitation of amorphous silica accompanied the crystallization of zinc sulfides (Koski et al., 1984, Zierenberg et al., 1984). Sphalerites are enriched in both FeS and CuS. CuS enrichment may signify minor Cu-Fe sulfide inclusions. In sample 659-3, FeS in sphalerite ranges from 30-36 mole%, similar to Guaymas Basin sphalerites also associated with pyrrhotite. Sphalerites from both Escanaba Trough and Guaymas Basin are richer in FeS than sphalerites from the southern Juan de Fuca Ridge (Fig. IV-8) reflecting the latter's association with pyrite. Sphalerite in sample 662-1 is associated with pyrite and its FeS content is hence, less (15 mole%).

Cu-Fe sulfides are similar in chemistry to cubanite ( $\text{CuFe}_2\text{S}_3$ ) (Table IV-2c) and are slightly higher in sulfur and lower in Cu than cubanites from the Juan de Fuca Ridge (Fig IV-9). Zierenberg (pers.comm.) suggested this phase is actually cubic cubanite which could have precipitated in equilibrium with pyrrhotite (Craig and Scott, 1974, Haymon, 1983, Zierenberg et al., 1984). X-ray diffraction analysis of this sample yielded only chalcopyrite. If this was an Fe-rich chalcopyrite of high temperature origin, cooling could result in exsolution of cubanite (Deer et al., 1966) which was the mineral analyzed by microprobe. Hekinian et al. (1980) report an X-ray diffraction pattern for high temperature cubanite with two major peaks indistinguishable from a-form chalcopyrite. Microprobe analyses are required to resolve the uncertainty in Cu-Fe sulfide mineralogy.

The composition of barite from the barite chimney (658-R2-B) and from sample 662-1 provides confirmation that chemical zoning observed in SEM primarily reflects fluctuations in Sr content and to a lesser extent fluctuations in Ca content (Table IV-2d, Fig. IV-5). The Pb content of barite in both samples is consistently about 0.2 wt%.

### ← (C) Bulk Chemistry

Atomic absorption analyses of twenty-two elements of weathered sulfide chimneys from the Escanaba Trough are presented in Table IV-3. The first sixteen chimney samples are the freshest interior portions and the remaining twenty-two represent more altered portions, normally from chimney exteriors. A chemical analysis of basalt sample L1-85-NC-36D collected near Dome B is at the bottom of Table IV-3. Table IV-4 gives elemental weight percents recalculated as major oxides, sulfides and sulfates.

Iron in Table IV-4 was recalculated according to the dominant Fe-bearing mineral observed in XRD analyses. Low totals were encountered in nearly all samples because of the following: (1) barite is highly insoluble (Holland and Malinin, 1979), analyses for barium are not reliable and do not accurately reflect the amount of barite in the sample.



Nineteen of 38 samples analyzed formed precipitates during digestion for atomic absorption analyses (Table IV-3). Of the 19 precipitate samples, only seven contained enough material to analyze by XRD. Four of these seven were identified as solely barite. Two of the remaining three (659-2-2 and 659-2-1) were dominantly barite. In addition to barite, 659-2-2 contained probable cubanite and the closest match to XRD peaks in 659-2-1 was akaganéite. A red/brown precipitate from sample 659-R1-2 containing only two XRD peaks (at 3.59Å and 1.79Å) remains unidentified although both peaks are associated with barite. (2) All 38 samples contain water and possibly other elements (such as sulfur and carbon) that were not quantitatively analyzed by techniques used in this study. The organic carbon content in a chimney fragment from the Escanaba Trough was 5.6 wt% (Morton et al., 1987) and significant elemental sulfur was identified by XRD in three samples (Table IV-1). Other elements, analyzed by atomic absorption, but not considered in the recalculated analyses (eg. As is almost 2 wt% in sample 659-R1-F3) also contribute to the low totals.

Despite the low totals, chemical analyses of samples (Table IV-3) agree well with mineralogical determinations (Table IV-1) (excepting the aforementioned difficulty analyzing Ba in barite). The most abundant element, Fe, is incorporated in the most varied mineralogy; Fe-sulfides, oxyhydroxides and silicates (eg clays at Dive 661).

The Cu/Zn ratio (Table IV-3) is greater in sample interiors than exteriors consistent with greater susceptibility of Cu-Fe sulfides to oxidative weathering (Sillitoe and Clark, 1969, Alt et al., 1987). Alternatively, mineralogy of active chimneys is known to shift from interior Cu-Fe sulfides at temperatures of approximately 250°C to exterior zinc sulfides at temperatures below 250°C (Haymon, 1983). Samples rich in Si or Al contained clays, quartz and/or amorphous silica. Si/Al ratios calculated for samples with > 2 wt% Si are shown in Table IV-3. The Si/Al ratio of basalt and marine sediments is about 3.0 (Table IV-3 and Turekian and Wedepohl, 1961). Samples with Si/Al ratios significantly greater than 3.0 probably contain quartz and/or amorphous silica. The presence of amorphous silica is inferred (Table IV-1) if quartz was not identified by XRD or if amorphous silica was not previously identified megascopically.

#### (D) Sulfur Isotopes

Sulfur isotope values, determined on sulfide minerals in three chimney fragments from Dive 658, average 5.4 ‰ and range from 5.1 to 5.8 ‰ (Table IV-5). Although some mixing between pyrrhotite and sphalerite grains was unavoidable in sample 658-R3-A, sulfur isotope values should remain unaffected since both phases have the same

fractionation factor (Ohmoto and Rye, 1979). The isotopic values for coarse and fine mineral grains separated from the same samples showed little variation (Table IV-5).

## Discussion

### (A) Chimney Chemistry

Sulfide chimneys from the Escanaba Trough are compositionally heterogeneous even on the scale of a single thin section. Consequently, comparison of chemistry between samples is potentially misleading. However, a ternary diagram with apices Cu-Pb-Zn (Fig. IV-10) illustrates the large compositional range of the fresher chimney interiors and suggests that the range may be greater than at other spreading ridges.

#### *Comparison With Basalt*

A general comparison between chemistry of chimney samples and basalt (Table IV-3) yields the following observations: (1) elements that are generally enriched in chimney samples above basalt values (As, Ba, Cd, Co, Cu, Fe, Pb, and Zn) correspond well with the chemistry of identified sulfide minerals (Table IV-1) and (2) elements that are generally depleted in chimney samples relative to basalt (Al, Ca, Cr, Mg, Mn, Ni, Si, Ti and V) correspond well with elements either considered relatively immobile (Cr, Ni, V) in seawater-basalt interaction experiments (Seyfried and Mottl, 1982), or in natural hydrothermal systems (Ti and Al) (R. Haymon, pers. comm., 1986).

Most of the first group of elements are derived from basalt, but enrichment in Ba, As and Pb reflect interaction between hydrothermal fluid and sediment (Koski et al., 1988). Pb isotope analyses in chimney samples are identical to those obtained from Escanaba Trough sediments (Koski et al., 1988). Although Co enrichment may reflect seawater scavenging in older Fe-Mn deposits, enrichment in chimney exteriors probably reflects differential precipitation or weathering. Seawater-basalt interaction experiments demonstrate Co is significantly mobilized at 300°C under seawater-dominated conditions (Seyfried and Mottl, 1982).

The general depletion of Mg in chimney samples is expected since Mg is depleted in vent waters (Von Damm, 1983) and since the precipitation of Mn is not favored by reaction kinetics in reducing hydrothermal end-member solutions, it may be dispersed farther from the vent site in plumes (Seyfried and Mottl, 1982, Haymon and Kastner, 1983, Dymond and Roth, 1986, Klinkhammer and Hudson, 1986, Mottl, 1986). Ca is typically enriched in chimney material as anhydrite or, less commonly, calcite. Depletion of Ca in the inactive chimneys is probably from retrograde solubility of these minerals (Holland and Malinin, 1979), or dissolution by acidic fluids may have played a role in the case of calcite.

(3) Elements that are variably enriched or depleted in chimney samples relative to basalt are the alkali elements K, Li, Rb, and to a lesser extent Na and the alkaline earth

element, Sr. All of the above are enriched in Guaymas Basin vent waters over seawater composition (Von Damm et al., 1985b), but Sr and Na exhibit both enrichments and depletions in 21°N, EPR vent waters (Von Damm et al., 1985a). The enrichment of K, Li and Rb in Guaymas Basin hydrothermal fluids has been interpreted by Gieskes et al., (1982) to result from sediment-fluid interactions since the elemental abundances are much higher in sediments than in basalts. Their differential concentration in Escanaba Trough deposits suggests the variability in the influence of sediments on hydrothermal fluid chemistry.

#### *Inter-Element Correlations*

Table IV-5 shows correlation matrices for analytical data in Table IV-3. The upper triangular matrix contains coefficients for elemental concentrations in fresh chimney samples and the lower triangular matrix contains coefficients for elemental concentrations in more altered chimney sections.  $|R|$  values  $\geq |.7|$  are highlighted. In both matrices, no significant negative correlations are observed.

##### *(a) Interiors*

In the matrix for fresher portions of chimneys, the following positive correlations are observed: (1) Al, Ca, Mg, Si, Ti and V covary strongly ( $|R| > .9$ ) consistent with incorporation in clay minerals. (2) A strong correlation between Ba and Sr reflects the incorporation of Sr in barite. (3) The covariance of Cd, Zn and Pb is consistent with their distribution pattern in vent waters (Von Damm et al., 1985a) (4) Na correlates weakly with Al and Ca, but not at all with K. A significant absence of correlation between Cu and Fe reflects that although Cu occurs as Cu-Fe sulfide, most of the Fe is associated with Fe sulfide and oxyhydroxides. (5) Cr covaries most strongly with Ni, however, the covariance of Cr, Li, Rb, V and Ni with respect to other elements is difficult to evaluate because their concentration in all samples is low and at the measured concentrations, analytical uncertainty is high.

##### *(b) Exteriors*

The matrix for more altered portions of the chimneys generally maintains the correlations for the less altered parts with the following exceptions: (1) The correlation of Al with Si, Mg, Ca and V is weakened suggesting less influence of clays and greater increase in amorphous silica in chimney exteriors (2) Cr loses its correlation for Ni and instead correlates most strongly with Al, Si and Ti probably reflecting its immobility and increased concentration in the outer portions of the chimney by residual weathering (Howard and Fisk, 1988). (3) Cd and Zn retain their affinity but covariance with Pb is weakened. (4) Co correlates most strongly with Cu in more weathered samples. This is somewhat unexpected since Co should behave more like Zn and Cd as observed in vent

waters from 21°N, EPR (Von Damm, 1985a). It may reflect incorporation of Co as a secondary constituent in Cu sulfides by seawater scavenging and adsorption.

### *Chemical Fluxes*

Elemental fluxes between the exterior, weathered portion of the chimney and the interior, fresher portion of the chimney can result from either differential precipitation during chimney formation or weathering. Enrichment factors calculated for each element of interest were based on chemical analyses in Table IV-3 where

$$\text{Enrichment Factor} = \frac{\text{Altered} - \text{Fresh}}{\text{Fresh}}$$

The analyses of bulk samples that were subdivided were averaged and this average was when computing the enrichment factor. This helped to smooth chemical inhomogeneity in the sample. A positive enrichment factor means that the element is enriched in the altered exterior of the sample. Plots of enrichment factors for samples designated 2, 4, 6 and 11 are shown in Fig. IV-11. The elements Ba, Ni, Rb, Ti and V are not included. Ba is not included because its precipitation during digestion for atomic absorption analysis renders the analytical results uncertain. Ni, Rb, Ti and V are not included since they were frequently measured at the minimum detection limit (MDL) and analytical uncertainty for these elements is especially large at the low concentrations measured. Li is included despite the frequency of measurements at MDL since it is reliably measured at concentrations as low as 0.5 ppm and the analytical uncertainty is only 1% (J. Robbins, pers. comm., 1988). Both within individual samples and between the twelve samples studied, enrichment factors varied over three orders of magnitude.

Distinct patterns that emerge from examination of the enrichment factors in Fig. IV- 11 are consistent with either processes associated with chimney weathering or differences between chimney interiors and exteriors produced during chimney formation. Three major elemental associations are noted. (1) Enrichment in Co and As in chimney exteriors (Fig. IV-11, samples 2, 6 and 11). (2) Enrichment in Cd, Zn and Pb in chimney exteriors (Fig. IV-11, samples 2, 11). (3) Enrichment in Al and Si (Fig. IV-11, samples 4, and 6). Arsenic is most enriched in samples 11 and is significantly enriched in the exteriors of sample 2. Koski et al. (1988) found increased precipitation of As-bearing minerals arsenopyrite and loellingite in chimney exteriors. Two possible explanations are: (1) Arsenic concentration in geothermal fluids varies inversely with  $\text{PH}_2\text{S}$  and directly with temperature (Ballantyne and Moore, 1988). Decreasing temperature is expected during seawater mixing with a hydrothermal end-member solution and thus lower temperatures prevailing around chimney exteriors could result in increased precipitation of As bearing minerals. (2) Alternatively, oxidation of  $\text{As}^{\text{III}}$  to

As<sup>V</sup> favors its incorporation on Fe oxides (or presumably oxyhydroxides) after complete oxidation of H<sub>2</sub>S to SO<sub>4</sub><sup>2-</sup> (Ballantyne and Moore, 1988), a condition also more favorable around chimney exteriors. It is uncertain whether Co enrichment is produced by differential precipitation or weathering.

Other enrichments that correspond to mineralogical changes between chimney interiors and exteriors include the enrichment of Zn and Cd in sample 2 and Pb enrichment in sample 11. These observations probably reflect an increase in sphalerite and galena in chimney exteriors. This interpretation is consistent with studies of dredge samples from the Escanaba Trough in which Koski et al. (1988) describe the deposition of a low-temperature assemblage including sphalerite and galena that grew outward from the chimney outer wall.

Enrichment of Si and Al in chimney exteriors probably reflect increased incorporation of clay minerals. However, some of the enrichment in Si reflects the precipitation of amorphous silica or the presence of quartz (eg. Table IV-1, sample 12). Though quartz may result from the recrystallization of amorphous silica, the presence of plagioclase in sample 12 indicates the quartz could be of detrital origin. A detrital fraction in Escanaba Trough chimney samples has also been observed by Vallier-Silver et al. (1987) and Koski et al. (1988).

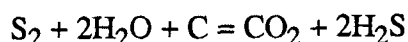
#### (B) Comparison to other ridge-crest sulfide deposits.

##### *Mineralogy and Sulfide Paragenesis*

The Escanaba Trough, southern Gorda Ridge, Guaymas Basin, Gulf of California and Middle Valley, Endeavor Ridge are all sediment-filled spreading ridges with polymetallic sulfides forming from the interaction between hydrothermal fluids, basalts and sediments. All three sediment-covered ridges have a higher proportion of non-sulfide phases (barite, opaline silica and talc) than at 21°N, East Pacific Rise or southern Juan de Fuca Ridge which are sediment-free hydrothermal deposits. In terms of major mineralogy and textures, sulfide chimneys from the Escanaba Trough are most similar to chimney samples recovered from the Guaymas Basin. Despite differing sediment chemistry, both hydrothermal systems precipitated abundant pyrrhotite and barite. Sphalerite and Cu-Fe sulfides are interstitial to the boxwork pyrrhotite texture. Pyrite is less common. Both regions contain Fe-rich sphalerite when associated with pyrrhotite, but the abundance of Zn-sulfide is greater in Escanaba Trough deposits than in Guaymas Basin deposits.

Koski et al., (1985) calculated phase relations in the system Cu-Fe-S-O at 300°C and 20MPa (Fig IV-12) to estimate the approximate  $f_{S_2}$  and  $f_{O_2}$  of the hydrothermal

fluids. The presence of pyrrhotite signifies fluids with lower sulfur fugacity than fluids that precipitate pyrite. The fluid may have been depleted in sulfur by precipitation of pyrite in volcanic turbidites as observed by Karlin and Lyle (1989). Koski et al. (1985) suggest that the lower sulfidation state may also result from the removal of  $S_2$  by reactions within the sediments such as:



Koski et al. (1985) used the diagram shown in Fig. IV-12 to show that pyrrhotite and barite represent disequilibrium assemblages. The  $fs_2$  of sphalerite in equilibrium with pyrrhotite at 300°C is estimated based on its FeS content (Scott and Barnes, 1971). The FeS contents of sphalerite (30 - 36 mole%) from the Escanaba Trough (Table IV-2c) show it could have precipitated in equilibrium with pyrrhotite and chalcopyrite. Only one sample (10, 662-1) crystallized abundant pyrite and the FeS content of associated sphalerite (15 mole%) is predictably low.

The lack of carbonate minerals in hydrothermal deposits from both Escanaba Trough and Middle Valley is in stark contrast to Guaymas Basin deposits and implies either carbonates dissolved at lower temperatures because of retrograde solubility (Holland and Malinin, 1979), or carbonate minerals dissolve in acidic solutions associated with active chimney formation or weathering of sulfides.

Barite has been identified in hydrothermal deposits from sediment-free spreading ridges (Corliss et al., 1978, Hekinian et al., 1980), but it is observed in greatest abundance at sediment-covered spreading ridges (Koski et al., 1985, Davis et al., 1987). In Guaymas Basin deposits, barium in barite could precipitate with organic carbon as it falls through the water column (Lyle, pers. comm., 1989). The barium in Escanaba Trough chimney fragments may be partially derived from this source, but feldspars in the terrigenous sediments are abundant (plag/quartz ratio is 5/1 (Karlin and Lyle, 1989)) so this is also a likely source for both Ba and Sr.

In sample 13 (663-R2), enrichment of Mg in the chimney exterior is correlated with a mineralogical shift from Fe-rich clays associated with the weathering of Fe (and possibly Cu-Fe) sulfides in the chimney interior to Mg-rich clays and talc in the chimney exterior formed when Mg-depleted hydrothermal fluids interact with Mg-rich bottom water or pore fluid (Lonsdale et al., 1980, Haymon and Kastner, 1981, Koski et al., 1984, 1985). If analogous to talc described from Guaymas Basin, its formation temperature is between 270-280°C (Lonsdale et al., 1980, Koski et al., 1985). The formation of talc may reflect sluggish discharge of hydrothermal fluids (Koski et al., 1988).

The paragenetic sequence observed in Escanaba Trough hydrothermal deposits differs from Guaymas Basin deposits in the order of Cu-Fe sulfides versus Zn-sulfide

precipitation. In contrast to Guaymas Basin, Cu-Fe sulfides precipitate earlier than Zn-sulfides in Escanaba Trough deposits. The earlier precipitation of Cu-Fe sulfides at Escanaba Trough implies temperatures of the hydrothermal fluid rose, possibly in response to sealing off of the chimneys by precipitation of anhydrite, barite and amorphous silica (Haymon and Kastner, 1983, Tivey and Delaney, 1986), at an earlier stage of chimney growth. As hydrothermal activity wanes and finally shuts down, dissolution and oxidation of chimney deposits results in mineralogical changes that are recorded in the weathered rind of Escanaba Trough deposits.

Cinnabar, identified in sample 3 (658-R2-B) (Table IV-1) may be preserved because of the lower temperatures associated with the formation of the barite chimney. Most Hg ores form at relatively low temperatures (between 100° and 200°C) and thermodynamic calculations of Varekamp and Buseck (1984) predict that cinnabar cannot coexist with pyrrhotite at temperatures between 100° and 250°C. This may account for its absence in pyrrhotite-rich chimneys.

#### *Weathering and Aging of Chimneys*

Styrt et al., (1981) summarized changes in mineralogy associated with aging of sulfide chimneys on the seafloor based on information available at that time from active and inactive chimneys at 21°N, East Pacific Rise. Styrt et al. (1981) noted the inversion of the high temperature polymorph of Zn-sulfide, wurtzite, in active chimneys to sphalerite in inactive chimneys. Hexagonal wurtzite inverted to sphalerite was not observed in polished sections of Escanaba Trough samples suggesting that precipitation of Zn-sulfides occurred below the sphalerite/wurtzite inversion temperature. This temperature is not well defined and the inversion also depends on the sulfidation state of the fluid (Scott and Barnes, 1972).

Primary sulfates described in active hydrothermal chimneys include anhydrite and barite (Hekinian et al., 1980). The retrograde solubility of anhydrite accounts for its absence in inactive chimneys, but barite persists because of its relatively low solubility (Holland and Malinin, 1979). In Escanaba Trough chimneys, complete dissolution of anhydrite may account for its absence. Gypsum, identified in sample 12 (663-R1) and tentatively identified in sample 1 (658) could be evidence of the former presence of anhydrite in Escanaba Trough chimneys since gypsum may represent hydrated anhydrite. It is not known whether the gypsum is a secondary hydration product of primary anhydrite or a primary precipitate of Ca saturated solutions on the exterior of chimney samples. Brett et al., (1987) found that anhydrite in Juan de Fuca Ridge chimney samples hydrated to gypsum within a few weeks after thin sections were prepared.



Zierenberg et al. (1986) interpreted enrichment of Ca and  $\text{SO}_4$  in Escanaba Trough pore fluids as the dissolution of anhydrite in the sediments.

Oxidation of sulfides in contact with seawater is apparent in all Escanaba Trough samples. Early rapid alteration was probably slowed as the development of an external alteration rind protected the interior from seawater oxidation. The pyrrhotite-rich samples are attacked and oxidized in a manner similar to that observed in Guaymas Basin sulfide deposits. Rims and fractures in pyrrhotite crystals are oxidized to marcasite reflecting the oxidation of  $\text{S}^{-2}$  to  $\text{S}^{-1}$ . According to Murowchick and Barnes, (1986) marcasite can form directly from pyrrhotite by leaching of Fe coupled with partial oxidation of the sulfide sulfur in situ. At Middle Valley, observations by Davis et al., (1987) suggest that the replacement of pyrrhotite by pyrite and marcasite, signifying a shift to a more oxidative environment by the entrainment of seawater, is more pronounced than at either Escanaba Trough or Guaymas Basin. Pyrrhotite/marcasite is replaced by amorphous Fe-oxyhydroxides, lepidocrocite, goethite and akaganéite. In the pyrrhotite-rich samples from Guaymas Basin, Koski et al. (1985) found that replacement of pyrrhotite by lepidocrocite occurs prior to deposition of goethite, but goethite pseudomorphs of pyrrhotite have been observed at 21°N, EPR (Zierenberg et al., 1984). The absence of goethite pseudomorphs of pyrrhotite in the Escanaba Trough samples suggests that weathering processes resembling those attacking Guaymas Basin chimneys are prevalent. In addition to in situ alteration of sulfides to Fe-oxyhydroxides, another observation shared by both Escanaba Trough and Guaymas Basin deposits is the precipitation of Fe-oxyhydroxides in response to cooling FeOOH saturated fluids.

Further evidence of the effects of oxidation include a slight depletion of Cu in the exterior of sample 8 that may signify the oxidation of Cu-Fe sulfides. Another possible contribution to the depletion of Cu is the dissolution of atacamite, although atacamite is only tentatively identified in this sample by XRD.

Secondary sulfate minerals such as Cu-Fe sulfates and Zn sulfates have been described as weathering products in chimney samples from 21°N, East Pacific Rise (Hekinian et al., 1980, Oudin, 1983) and Fe sulfates are reported in Escanaba Trough chimneys (Holmes and Zierenberg, 1989, in prep). Elemental sulfur, identified in four Escanaba Trough samples from this study, is an additional product of sulfide weathering. Holmes and Zierenberg (1989, in prep) noted that elemental sulfur is especially prevalent at the contact between sulfide chimneys and sediments.

#### *Deciphering Sediment Effects*

In the Guaymas Basin, the relatively high calcium carbonate content and sulfate reduction in the sediments raises the pH of the hydrothermal fluids and so lowers the

ability of the fluids to transport metals. Consequently, it has been suggested that higher grade ore deposits are located at depth in the sediment (Bowers et al., 1985, Koski et al., 1985, Von Damm et al., 1985b). A similar situation is proposed for the Middle Valley deposits (Davis et al., 1987). The Escanaba Trough, however, remains distinct from these other two sedimented ridges. Although sediment organic carbon content is similar to Guaymas Basin (~ 2%) (Morton and Koski, 1989, in prep), higher grade ores are deposited at the sediment-water interface, signifying the expulsion of high-temperature, low pH fluids similar to hydrothermal fluids at sediment-free ridge crests. Some chimneys from the Escanaba Trough even surpass sediment-free ridge chimney deposits in terms of ore grade (Morton and Koski, 1989, in prep).

Evidence for extensive interaction between hydrothermal fluids and sediments is convincing. In addition to the elevated Pb, (Fig. IV-12, Table IV-3) Ba and As contents in Escanaba Trough chimneys, Pb isotope analyses of chimneys and sediments are identical (Koski et al., 1986) and the presence of hydrocarbons in sulfide chimneys attests to the interaction of hydrothermal fluids with organic material in the sediment (Kvenholden et al., 1986). The above evidence suggests that sediment chemistry is enhancing the ore metal grade of Escanaba Trough sulfide deposits relative to other sediment-covered spreading ridges.

Newly identified trace minerals provide additional evidence for fluid-sediment interaction. Trace minerals bismuth telluride and cassiterite are unknown in Cyprus or 21°N, East Pacific Rise sulfide deposits, but are often found in Island Arc massive sulfide ore (Oudin et al., 1981). Cassiterite, in particular, is typically associated with acidic volcanism (Oudin et al., 1981) and native bismuth (identified in Escanaba Trough chimney samples by Koski et al., 1988) is frequently associated with Pb (Deer et al., 1966). The presence of both cassiterite and bismuth telluride is strong evidence for the interaction between hydrothermal fluids and island arc derived sediments filling the Escanaba Trough.

### (C) Sulfur Isotopes

Sulfur isotope analyses may provide information about the Escanaba Trough hydrothermal system that can explain the higher grade ores deposits. The small isotopic variation in sulfur from sulfide minerals in chimney fragments from NESCA Dive 658 indicates the hydrothermal solutions are homogenous. Mixing takes place well below the vent site, possibly within the sediments. If mixing took place near the surface, there would be a much greater variability in sulfur isotopes as observed at 21°N, EPR (Shanks and Seyfried, 1987). Also, the similarity in isotopic ratio between coarse and fine

pyrrhotite separates implies that even as conditions of formation within the chimney changed over space and time, the same isotopic exchange and mixing patterns were preserved (Styrt et al., 1981). Sulfur isotope determinations of pyrrhotite in dredge samples from the Escanaba Trough by Koski et al. (1988) cover a wider range (1.9 ‰ to 11.6 ‰), but are all from the SESCO site. It is possible that major differences between the NESCA and SESCO hydrothermal systems are revealed by such differences in sulfur isotopes.

The sulfur isotope values at NESCA are significantly heavier than chimney samples from 21°N, EPR (Kerridge et al., 1983, Styrt et al., 1981, Zierenberg et al., 1984) or Guaymas Basin (Koski et al., 1985) and most samples studied from the southern Juan de Fuca Ridge (Shanks and Seyfried, 1987) (Table IV-7). One sulfur isotope determination on the barite chimney fragment (19.4 ‰) is very close to the seawater sulfate  $\delta^{34}\text{S}$  value of approximately 20 ‰ (Ohmoto and Rye, 1979).

#### *Geothermometry*

If two minerals are in isotopic equilibrium, and their isotopic fractionation factors have been determined, temperatures of formation can be estimated by the relation between temperature and fractionation factor:

$$10^3 \ln \alpha = a \left( \frac{10^6}{T^2} \right) + b$$

where a and b are theoretically or empirically derived constants.

Fractionation equations pertinent to this study are:

$$(4) \Delta_{(\text{SO}_4\text{-H}_2\text{S})} = 6.463 \left( \frac{10^6}{T^2} \right) + 0.56 \quad (\text{Ohmoto and Lasaga, 1982})$$

$$(5) \Delta_{(\text{po,sl-H}_2\text{S})} = 0.10 \left( \frac{10^6}{T^2} \right) + 0.00 \quad (\text{Ohmoto and Rye, 1979})$$

Equation (5) is the same for pyrrhotite (po) and sphalerite (sl).

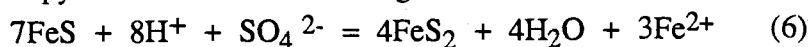
Combining equations (4) and (5) above gives the  $\Delta_{(\text{po,sl-SO}_4)}$  and the temperature calculated for coexisting po/sl and barite is 415°C. If the minerals are in equilibrium, uncertainties are  $\pm 15^\circ\text{C}$  based on the errors in a and b and  $\pm 5^\circ\text{C}$  based on analytical errors of  $\pm 0.2\text{‰}$  for  $\Delta$  values. Despite the expected disequilibrium between sulfides and sulfates in hydrothermal systems (Ohmoto and Rye, 1979, Zierenberg et al., 1984), this temperature is not unreasonable when considering that end-member hydrothermal vent waters have been measured with in situ temperatures as high as 355°C at the unsedimented 21°N, EPR. The additional insulation of the thick sediment cover in the

Escanaba Trough may have considerable effect on the local geothermal gradient, allowing the maintenance of relatively high temperatures within the sediment column. At the sedimented Middle Valley, northern Juan de Fuca Ridge, temperatures estimated for the sediment-basement contact were highest ( $>300^{\circ}\text{C}$ ) near the center of the valley (Davis et al., 1987). At Guaymas Basin, temperatures of formation determined from fluid inclusions in calcite gave a mean temperature of  $326^{\circ}\text{C}$  (Koski et al., 1985).

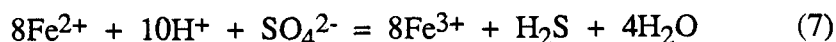
#### *Sources of Sulfur*

Since the sulfides in the chimney fragments precipitated at high temperatures, little fractionation between aqueous  $\text{H}_2\text{S}$  and sulfides is expected (Ohmoto and Rye, 1979). Thus the  $\delta^{34}\text{S}$  of the sulfides provides an approximate record of the  $\delta^{34}\text{S}$  of the hydrothermal fluid. Magmatic sulfur from mid-ocean ridge basalts has a  $\delta^{34}\text{S}$  of  $0.1 \pm 0.5$  ‰ (Sakai et al., 1980). The enrichment of  $^{34}\text{S}$  above magmatic  $^{34}\text{S}$  values requires either (1) the addition of seawater sulfate, or (2) high water/rock ratios (Shanks et al., 1981). These are not necessarily identical conditions because the precipitation of anhydrite in the crust can remove a lot of the seawater sulfate. Although no sulfur isotope determinations in Escanaba Trough sediments were made, it is unlikely that biogenically reduced sedimentary sulfur had a significant influence on the sulfur isotopic ratio of the hydrothermal fluids. Biogenic sedimentary sulfur isotopes tend to be lighter and more variable (Ohmoto and Rye, 1979). Most of the sediment in the Escanaba Trough is of terrigenous origin and is not organic rich (Karlin and Lyle, 1989). Water/rock ratios at  $21^{\circ}\text{N}$ , EPR are estimated to be relatively low, in the range of 1-5 based on chemical and isotopic data (Craig, 1980, Edmond, 1980, Von Damm et al., 1985a), but it is uncertain how the sediment cover influences the effective water/rock ratio. The presence of hydrothermal barite in the sediments (Karlin and Lyle, 1989) as well as high Ca concentrations measured in Escanaba Trough pore fluids interpreted as the dissolution of anhydrite (Zierenberg et al., 1986) increase the plausibility of mixing of reduced sulfate with magmatic derived  $\text{H}_2\text{S}$  during the ascent of hydrothermal fluid from the crust through the overlying sediments.

Shanks and Seyfried (1987) discuss the importance of the conversion of basaltic pyrrhotite to pyrite as a means of reducing seawater sulfate by the reaction:



Isotopic mass balance considerations show that this conversion results in a  $\delta^{34}\text{S}$  enrichment of 3.0 ‰ above magmatic values, assuming that sulfate is quantitatively reduced without fractionation and the resulting sulfide inherits the  $\delta^{34}\text{S}$  value of the sulfate (Shanks and Seyfried, 1987). In addition to the above reaction, ferrous iron from basalt may be a reducing agent for sulfate as expressed in the following reaction:



Shanks et al., (1981) cite the increase in the ferric/ferrous ratio in basalts during hydrothermal alteration (Humphries and Thompson, 1978) as evidence of the reduction of seawater sulfate in the crust via the above reaction. Zierenberg et al. (1984) suggest that aqueous  $\text{Fe}^{2+}$ , enriched in hydrothermal fluids, rather than  $\text{Fe}^{2+}$  in basalt, may be the source of  $\text{Fe}^{2+}$  in the above reaction. In the Escanaba Trough, previously precipitated Fe-sulfides in the sediment (Karlin and Lyle, 1989, in press) provide yet another additional source of  $\text{Fe}^{2+}$  for the above reaction.

Because the average  $\delta^{34}\text{S}$  value of 5.4‰ observed in Escanaba Trough sulfides is somewhat higher than the value predicted for conversion of basaltic derived pyrrhotite to pyrite (3.0‰) (Shanks and Seyfried, 1987), some additional fraction of seawater sulfate is required. By mass balance:

$$\delta^{34}\text{S}_{\Sigma\text{S}} = \delta^{34}\text{S}_{\text{H}_2\text{S}_i} X_{\text{H}_2\text{S}_i} + \delta^{34}\text{S}_{\text{SO}_4\text{r}} X_{\text{SO}_4\text{r}} \quad (8)$$

where  $X$  is the mole fraction,  $\text{H}_2\text{S}_i$  is the initial sulfide in the basalt,  $\Sigma\text{S}$  is the total sulfide in the system, and  $\text{SO}_4\text{r}$  is the sulfate that is reduced. Using 0.1‰ as magmatic  $\delta^{34}\text{S}$  (from Sakai et al., 1980), 19.4‰ (the  $\delta^{34}\text{S}$  composition of Escanaba Trough barite) as the isotopic composition of sulfate to be quantitatively reduced and 5.4‰ (the average  $\delta^{34}\text{S}$  of sulfides from the Escanaba Trough, Dive 658) as the isotopic composition of the total sulfide, yields approximately 27%  $\text{SO}_4^{2-}$  that must be mixed with magmatic derived  $\text{H}_2\text{S}$  to produce the  $^{34}\text{S}$  enrichment observed in Escanaba Trough sulfides. This  $\text{SO}_4^{2-}$  may be derived from the dissolution of sulfates (barite and anhydrite) in the sediments as well as admixed seawater sulfate.

## Conclusions

- (1) Sulfide chimneys from the Escanaba Trough are dominantly boxwork lattices of pyrrhotite with interstitial sphalerite, Cu-Fe sulfides, barite and amorphous silica. Temperatures of formation are  $> 250^{\circ}\text{C}$  based on the presence of hexagonal pyrrhotite.
- (2) Weathering of sulfide chimneys from the Escanaba Trough proceeds by the oxidation of pyrrhotite to marcasite and finally alteration to Fe oxyhydroxides (goethite, akaganéite and lepidocrosite) and elemental sulfur. Fe oxyhydroxides also form as precipitates from cooler  $\text{FeOOH}$  saturated solutions. These processes are similar to those observed in Guaymas Basin sulfide deposits (Koski et al., 1985).
- (3) Chemical fluxes are dominated by enrichment of Co, As, Cd, Zn, Pb, Al and Si. The chemical affinity between Zn and Cd accounts for their sympathetic correlation. This has also been reported in hydrothermal vent fluids from  $21^{\circ}\text{N}$ , East Pacific Rise (Von Damm et al., 1985). Clays account for the sympathetic variability in abundance of Al, Si and to a lesser extent, K in the chimney samples from this study. Clays may represent particulates from seawater or resuspended sediments that adhere to chimney exteriors. Alternatively, Fe oxyhydroxides from sulfide weathering and amorphous silica may combine to form clays (Harder, 1976, Lyle et al., 1977, Haymon and Kastner, 1981).
- (4) Sulfur isotopes may be influenced by sulfide-rich tuffaceous turbidites within the basin (Karlin and Lyle, 1989). In addition, the sediments have significant porewater sulfate (Zierenberg et al., 1986). Oxidation of  $\text{Fe}^{2+}$  contributed to the sediments from hydrothermal activity may be an additional source for sulfate reduction to produce  $^{34}\text{S}$ -enriched sulfides. It is likely that the heavy isotopic compositions result from the reduction of seawater sulfate or conversion of sulfates (anhydrite or barite) to  $\text{H}_2\text{S}$ , an interpretation consistent with studies of similar deposits (Shanks and Seyfried, 1987, Koski et al., 1985).
- (5) Newly identified trace minerals, cassiterite and bismuth telluride, are evidence for the interaction of hydrothermal fluids with island arc derived sediments filling the Escanaba Trough. The contribution of trace minerals in hydrothermal vent deposits to ocean chemistry has yet to be evaluated. Their presence must be considered when refining calculations of global elemental mass balances.

Table IV-1: Mineralogy of weathered sulfide chimneys from NESCA and SESCO sites, Escanaba Trough, Gorda Ridge.

NESCA			
Sample:	Interior	Mineralogy <sup>a</sup>	Exterior
Dive 658			
(1) 658	clay, qz, pl		clay, qz, pl, gp?
(2) 658-R1-1A*	po, sp, cp, ba		ba, po, sp, cp, si
(3) 658-R2-B*	ba, cn <sup>s</sup>		amorph. Mn & Fe oxyhydroxide, ba, si <sup>c</sup>
(4) 658-R3-A*	po, mc, cp, iss, sp, ba gn, Ni-Cu-Zn sulfide <sup>s</sup> bismuth telluride <sup>s</sup>		sp, ba, hm, gt, sl, si? <sup>m</sup>
(5) 658-R4-1A*	po, cp, lp, sl, gt, mc <sup>s</sup>		
Dive 659			
659-1		clay(s), si <sup>c</sup>	
(6) 659-2*	po, sp, gn, cp, mc <sup>s</sup> , ca <sup>s</sup>		ba, po, sp, cp, gn
(7) 659-3*	po, sp, cp, gn <sup>s</sup> , as <sup>s</sup>		sl, po, sp, cp
(8) 659-R1	po, sp		gt, ak, clay, si <sup>c</sup> , at?
(9) 659-R1-F (p)	po, sp, cp, sl		gt, lp, sp, cp, iss po, as, sl, ak, clays, mc?
SESCA			
Dive 661			
661-R1	clay, gt, ak, qz, pl/z		
Dive 662			
(10) 662*	py, sp, ba, gn, ca <sup>s</sup>		ba, gt, py, sp, clay, si <sup>m</sup>
(11) 662-R1 (p)	lp, po, cp, sl		sp, cp, lp, po, ba, sl
Dive 663			
(12) 663-R1	mc, cp, at, mica?		gp, gt, qz, ak?, ba, sp, pl/z?, clay
(13) 663-R2	Fe-clay, ak, lp, gt		clay, gt, py, qz, pl, talc, si <sup>m</sup>
ak: akaganéite	gn: galena	mc: marcasite	st: sulfur
as: arsenopyrite	gp: gypsum	pl: plagioclase	sp: sphalerite
at: atacamite	gt: goethite	po: pyrrhotite	z: zeolite
ba: barite	hm: hematite	py: pyrite	(phillipsite)
ca: cassiterite	iss: cubanite	qz: quartz	
cn: cinnabar	lp: lepidocrosite	si amorphous silica	
cp: chalcopyrite			

<sup>a</sup> identified by XRD unless otherwise noted and listed in approximate order of decreasing abundance. <sup>s</sup> identified by SEM. <sup>m</sup> megascopic identification (see Appendix II-1). <sup>c</sup> presence of amorphous silica predicted by Si/Al >> 3.

? tentative identification. (p) petroliferous odor.

\* samples chosen for petrographic and SEM examination.

Table IV-2a: Electron microprobe analyses of iron sulfides.

Analysis	Fe	Cu	Zn	Mn	Cd	S	SUM	Phase
NESCA								
Sample: 658-R3-A								
1	59.91	0.13	0.16	0.04	nd	38.10	98.34	po
2	61.19	0.13	0.16	0.04	nd	37.99	99.51	po
3	46.29	0.13	0.14	0.30	nd	52.45	99.32	mc
4	60.03	0.13	0.16	0.04	0.21	37.98	98.55	po
Sample: 659-3								
1	58.47	0.13	0.16	0.04	0.21	37.26	96.26	po
2	59.37	0.13	0.16	0.04	0.21	37.61	97.52	po
3	60.28	0.16	0.16	0.05	0.21	37.74	98.60	po
4	58.70	0.13	0.16	0.05	0.21	38.27	97.52	po
5	59.04	0.13	0.16	0.04	0.20	36.87	96.44	po
6	58.23	0.13	0.16	0.04	0.20	36.76	95.58	po
SESCA								
Sample: 662-1								
1	48.75	0.22	0.21	0.04	0.16	53.21	102.59	py
2	48.31	0.22	0.21	0.04	0.16	52.53	101.47	py
3	45.86	0.22	0.21	0.04	0.16	51.00	97.49	py
4	48.35	0.22	0.21	0.04	0.16	52.27	101.25	py

po = pyrrhotite, mc = marcasite, py = pyrite

\* Each analysis represents a separate grain.



Table IV-2b: Electron microprobe analyses of sphalerite.

Analysis	Fe	Cu	Zn	Mn	Cd	S	SUM	Mole% Fe
Sample: 662-1								
1	14.86	1.71	31.17	0.32	0.22	22.78	71.06	36
2	13.10	1.47	25.09	0.39	0.22	29.57	69.84	30
3	17.39	0.46	28.83	0.04	0.22	39.09	86.04	31
4	18.37	1.10	31.92	0.04	0.22	41.03	92.69	31
Sample: 662-1								
	7.30	0.67	43.72	0.04	0.31	29.93	81.96	15

Table IV-2c: Electron microprobe analyses of isocubanite from sample 658-R3-A.

Analysis	Fe	Cu	Zn	Mn	Cd	S	SUM
1	41.14	20.59	1.41	0.04	0.22	35.58	98.99
2	41.95	20.36	1.58	0.04	0.22	35.56	99.72
3	41.89	20.08	1.69	0.05	0.22	34.94	98.87
4	41.35	19.90	1.30	0.04	0.22	35.62	98.43
iss*	42.0	22.6	-	-	-	35.1	99.7

\* from Brett et al., 1987.

Table IV-2d: Electron microprobe analyses of barite. Individual crystals were analyzed twice (a and b below) to examine fluctuations in Sr and Ca.

Sample: 658-R2-B (Barite chimney)

Analysis	Ba	Sr	Ca	Pb	S	O*	SUM
1a	60.94	1.17	0.60	0.21	12.31	24.79	100.02
b	58.82	0.78	0.88	0.21	12.67	26.64	100.00
2a	59.78	0.91	0.88	0.21	12.90	25.33	100.01
b	58.79	0.75	0.84	0.21	12.52	26.90	100.01
3a	61.03	1.19	0.42	0.21	12.34	24.82	100.01
b	59.28	1.01	0.66	0.21	12.93	25.92	100.01
4a	60.31	1.09	0.38	0.21	12.80	25.24	100.03
b	60.15	0.37	0.17	0.21	12.94	26.17	100.01
5a	55.33	1.98	0.38	0.21	12.97	29.15	100.02
b	51.97	2.38	0.44	0.21	13.29	31.71	100.00
6a	53.59	1.98	0.44	0.21	13.40	30.40	100.02
b	52.23	2.48	0.65	0.21	13.57	30.87	100.01

Sample: 662-1

1a	58.14	0.73	0.22	0.21	12.35	28.36	100.01
b	56.12	1.01	0.27	0.21	12.54	29.86	100.01
2a	60.94	0.12	0.03	0.21	11.96	26.77	100.03
b	60.23	0.44	0.05	0.21	12.38	26.70	100.01
3a	61.55	1.06	0.30	0.21	11.46	25.44	100.02
b	60.31	1.46	0.47	0.21	12.59	24.97	100.01

\* Oxygen by difference.

Table		Ti	V	Zn (wt%)	Cu/Zn	Si/Al	Precip*
Sample							
(Fresh)							
1 658-1*	5570	200	0.193	0.05	3.2	Tw	
2 658-R	170	0	0.142	0.23	7.3	M w, b §	
3 658-R	0	0	0.002	0.45		M t §	
4 658-R	0	0	0.345	3.25			
5 658-R	0	0	0.041	52.20			
6 659-2-	0	0	7.590	0.16		T r/b	
7 659-3-	0	0	1.250	0.90		M r/b	
7 659-3-	0	0	5.040	0.28		M r/b	
8 659-R	0	40	4.140	0.14		M r/b	
9 659-R	0	0	2.810	0.30			
9 659-R	0	0	8.900	0.27		M r/b	
10 662-3*	0	30	5.800	0.23		T r/b	
10 662-4*	0	0	40.000	0.01		T r/b	
11 662-R1	0	0	0.673	2.12			
12 663-R1	350	0	0.079	28.61		T r/b	
13 663-R2	3260	200	0.183	1.04	3.6		
(Altered)							
1 658-2*	4510	100	0.038	0.42	3.1	Tw	
2 658-R1	0	0	2.350	0.33		M w	
3 658-R2	170	0	0.142	0.23	7.7	M w	
4 658-R3	150	0	0.585	0.92			
5 658-R4	0	0	0.172	17.56			
6 659-1	320	60	0.049	0.58	12.7		
6 659-2-1	0	0	5.870	0.31		B r/b	
6 659-2-3	0	0	3.340	0.38		M r/b	
7 659-3-3	0	0	7.340	0.22		M r/b	
8 659-R1	0	0	0.241	0.04	21.6		
9 659-R1	0	140	0.562	0.21	2.1		
9 659-R1	0	0	4.850	0.61			
661-R1	1810	50	0.012	1.22	4.1		
661-R1	520	220	0.018	0.56	9.1		
10 662-1	0	650	4.260	0.14	23.3		
10 662-2*	180	90	0.947	0.07		M w §	
11 662-R1	0	0	14.600	0.20			
12 663-R1	380	190	0.480	1.01	4.6		
12 663-R1	740	390	0.401	0.35	3.3		
12 663-R1	270	120	1.410	1.67	4.2	M r/b §	
13 663-R2	0	0	0.060	8.33	54.0		
13 663-R2	90	50	0.056	1.16			
basalt†	10600	300	0.008	0.71	3.0		
MDL (a)	0.1	0.01	0.001				
MDL (b)	50	5	0.5				

\* These sample letters denote the precipitate's color: w = white,

b = black > 2 wt%.

MDL = m

Table IV-4: Atomic absorption analyses recalculated as major oxides, sulfides and sulfate in wt%.

Sample	FeS*	ZnS	CuS	PbS	BaSO <sub>4</sub>	SiO <sub>2</sub>	TiO <sub>2</sub>	Al <sub>2</sub> O <sub>3</sub>	MgO	CaO	Na <sub>2</sub> O	K <sub>2</sub> O	SUM
(Fresh)													
658-1 <sup>1</sup>	7.59	0.03	0.02	0.00	0.16	58.18	0.95	16.03	4.53	1.40	2.66	0.25	91.80
658-R1-1A1	4.12	0.21	0.05	0.23	0.36	4.41	0.03	0.53	0.20	0.52	0.70	0.14	13.87
658-R2-B2	0.03	0.00	0.00	0.01	0.83	0.24	0.00	0.01	0.03	0.29	0.15	0.08	1.69
658-R3-A2	41.10	0.51	1.68	0.02	0.02	0.11	0.00	0.00	0.08	0.06	0.27	0.04	67.48
658-R4-1A1 <sup>1</sup>	54.80	0.06	3.21	0.00	0.01	0.00	0.00	0.01	0.02	0.02	0.07	0.00	81.75
659-2-2	41.20	11.31	1.83	2.59	0.01	0.45	0.00	0.05	0.05	0.06	0.29	0.02	81.51
659-3-1	56.30	1.86	1.70	0.05	0.00	1.45	0.00	0.00	0.04	0.04	0.09	0.01	93.86
659-3-2	27.60	7.51	2.15	1.20	0.00	0.13	0.00	0.57	0.04	0.03	0.23	0.01	55.31
659-R1-2	48.00	6.17	0.88	0.90	0.00	1.60	0.00	0.13	0.13	0.18	0.59	0.04	86.17
659-R1-F2	54.90	4.19	1.27	0.35	0.06	0.00	0.00	0.00	0.01	0.01	0.04	0.00	92.34
659-R1-F4	22.40	13.26	3.54	1.92	0.07	0.90	0.00	0.35	0.10	0.09	0.54	0.08	56.11
662-3 <sup>2</sup>	72.67	8.64	1.97	0.73	0.01	0.67	0.00	0.06	0.17	0.22	0.78	0.04	85.96
662-4 <sup>2</sup>	26.66	59.60	0.57	3.48	0.02	0.17	0.00	0.04	0.02	0.02	0.09	0.01	90.68
662-R1-2 <sup>1</sup>	46.60	1.00	2.15	0.06	0.01	0.00	0.00	0.01	0.08	0.05	0.55	0.03	70.56
663-R1-3 <sup>1</sup>	31.10	0.12	3.39	0.18	0.02	1.97	0.06	0.30	0.38	0.31	2.64	0.13	53.96
663-R2-3 <sup>1</sup>	26.50	0.27	0.29	0.88	0.34	32.30	0.55	7.88	0.72	1.45	2.09	1.56	86.22
(Altered)													
658-2 <sup>1</sup>	7.16	0.02	0.06	0.01	0.08	47.70	0.77	13.53	6.86	1.22	5.58	1.69	87.76
658-R1-1A2	34.20	1.17	3.50	0.54	0.01	4.41	0.00	0.05	0.05	0.06	1.58	0.02	65.21
658-R2-B-1	4.12	0.01	0.03	0.08	1.92	2.57	0.03	0.51	0.36	1.17	0.70	0.35	14.22
658-R3-A-1 <sup>1</sup>	43.30	0.87	0.81	0.05	0.10	3.10	0.03	0.40	0.41	0.38	0.74	0.12	68.92
658-R4-1A2 <sup>1</sup>	50.60	0.26	4.53	0.00	0.07	0.13	0.00	0.02	0.12	0.12	0.32	0.02	77.93
659-1 <sup>1</sup>	42.70	0.07	0.04	0.01	0.12	18.25	0.05	1.27	0.48	0.70	1.23	0.25	83.52
659-2-1	47.40	8.75	2.73	0.09	0.00	0.13	0.00	0.02	0.03	0.03	0.14	0.00	86.53
659-2-3	45.40	4.98	1.91	1.22	1.10	2.65	0.00	0.89	0.03	0.43	2.08	0.08	86.83
659-3-3	10.70	10.94	2.48	0.82	0.00	0.56	0.00	0.10	0.21	0.39	0.82	0.05	33.21
659-R1-1 <sup>1</sup>	48.30	0.36	0.01	0.46	0.00	6.18	0.00	0.25	0.30	0.30	1.62	0.09	78.62
659-R1-F-1 <sup>1</sup>	45.10	0.84	0.18	0.45	0.02	5.67	0.00	2.34	0.27	0.22	1.35	0.06	75.88
659-R1-F-3 <sup>1</sup>	23.30	7.23	4.43	1.20	0.24	0.53	0.00	0.13	0.08	0.08	0.50	0.05	47.78
661-R1-1 <sup>1</sup>	32.50	0.02	0.02	0.00	0.31	26.95	0.31	5.76	1.88	1.08	2.16	0.97	85.93
661-R1-2 <sup>1</sup>	42.60	0.03	0.02	0.00	0.12	18.44	0.09	1.80	0.80	0.84	1.36	0.42	84.83
662-1 <sup>2</sup>	73.53	6.35	0.87	0.89	11.77	4.83	0.00	0.18	0.49	0.95	1.22	0.12	101.20
662-2 <sup>1</sup>	5.63	1.41	0.09	1.00	0.84	2.89	0.03	0.60	0.29	0.57	0.96	0.14	14.45
662-R1-1 <sup>1</sup>	34.40	21.75	4.40	2.45	0.03	0.33	0.00	0.12	0.27	0.15	1.67	0.07	80.42
663-R1-1 <sup>1</sup>	43.10	0.72	0.73	1.28	0.88	6.78	0.06	1.29	0.61	0.84	2.24	0.21	77.26
663-R1-2 <sup>1</sup>	43.80	0.60	0.21	0.71	0.19	6.48	0.13	1.73	0.86	1.13	3.15	0.31	78.12
663-R1-4 <sup>1</sup>	35.80	2.10	3.54	0.86	0.18	6.33	0.05	1.33	0.41	0.84	1.83	0.17	68.82
663-R2-1 <sup>1</sup>	18.00	0.09	0.75	0.40	0.00	46.20	0.00	0.76	17.26	0.25	2.10	0.07	93.61
663-R2-2 <sup>1</sup>	49.40	0.08	0.10	0.24	0.05	2.13	0.02	0.28	0.19	0.16	0.97	0.08	74.93
basalt <sup>3</sup>	9.12	-	-	-	-	49.41	1.77	14.38	8.67	10.42	2.45	0.23	96.45

\* All Fe in chimney samples calculated as FeS unless <sup>1</sup> If XRD showed predominantly goethite or clay, then all Fe was calculated as Fe<sub>2</sub>O<sub>3</sub> or <sup>2</sup> If XRD showed predominantly pyrite, then all Fe was calculated as FeS<sub>2</sub>. <sup>3</sup> Fe in basalt was calculated as FeO, and SUM includes MnO = 0.17 wt%.

Table IV-5: Sulfur isotope determinations <sup>a</sup>

Sample	Description	Mineral	$\delta^{34}\text{S}$ (‰)
B-std*			1.3
658-R1-1A	fine	po	5.8
658-R1-1A	coarse	po	5.5
658-R3-A		po (sp)	5.4
658-R3-A		sp/w (po)	5.6
658-R4-1A	fine	po	5.1
658-R4-1A	coarse	po	5.1
658-R2-B		ba	19.4

<sup>a</sup> analyses provided by C.W. Field

\* C.W. Field in-lab standard.

po = pyrrhotite, sp = sphalerite, w = wurtzite

( ) = may contain some of this phase. Mixing of po and sl should not effect the sulfur isotope values since both have the same fractionation factor (Ohmoto and Rye, 1979).

Table IV-6: Correlation matrix for analytical data in Table IV-3. The top matrix is for fresher portions of sulfide chimneys and the bottom matrix is for more altered portions of chimneys.

	Al	As	Ba	Ca	Cd	Co	Cr	Cu	Fe	K	Li	Mg	Mn	Na	Ni	Pb	Rb	Si	Sr	Ti	V	Zn	
Al		-0.08	.17	.98	-.20	-.18	.46	-.44	-.39	.51	.96	.95	.05	.72	.20	-.18	1.00	1.00	-.07	1.00	.92	-.18	Al
As	-.19		-.13	-.12	.44	-.12	-.01	.27	-.13	.16	-.16	-.17	.37	-.09	-.06	.62	-.08	-.08	-.27	-.08	-.01	.41	As
Ba	-.10	-.14		.29	-.25	-.25	-.03	-.59	-.65	.33	.10	.08	-.06	.07	-.07	-.25	.17	.19	.90	.19	.20	-.23	Ba
Ca	.83	-.17	.20		-.26	-.24	.46	-.50	-.48	.56	.92	.92	.08	.78	.25	-.23	.98	.99	.06	.98	.93	-.24	Ca
Cd	-.27	.27	.19	-.30		-.17	-.22	-.08	-.20	-.20	-.20	-.19	-.02	-.31	-.20	.85	-.21	-.22	-.21	-.22	-.21	1.00	Cd
Co	-.27	.12	-.04	-.44	.16		-.20	.39	.36	-.16	-.20	-.16	-.26	-.18	-.18	-.25	-.18	-.20	-.22	-.19	-.21	-.17	Co
Cr	.73	-.36	.08	.68	-.35	-.41		.01	-.06	.13	.43	.51	-.13	.68	.82	-.26	.45	.45	-.18	.47	.34	-.21	Cr
Cu	-.33	.31	-.08	-.43	.59	.71	-.43		.51	-.33	-.41	-.36	-.02	-.10	.27	.03	-.45	-.46	-.50	-.44	-.47	-.10	Cu
Fe	-.31	-.01	-.01	-.30	-.17	.32	-.30	.10		-.19	-.30	-.40	-.36	-.31	-.15	-.17	-.38	-.39	-.62	-.38	-.29	-.22	Fe
K	.97	-.23	-.07	.87	-.28	-.34	.73	-.36	-.31		.36	.21	-.14	.53	-.03	-.03	.53	.55	-.02	.58	.76	-.17	K
Li	.91	-.29	-.09	.74	-.24	-.27	.65	-.32	-.27	.95		.95	.01	.63	.18	-.23	.96	.96	-.10	.95	.83	-.19	Mg
Mg	.31	-.23	-.08	.19	-.21	-.26	.65	-.18	-.34	.27	.24		.10	.68	.31	-.22	.93	.93	-.06	.92	.77	-.17	Mn
Mn	-.01	-.07	.51	.20	.22	-.16	-.02	-.21	-.59	.06	.10	-.18		-.05	-.05	.21	.03	.05	.07	.01	-.04	-.04	Na
Na	.84	-.07	-.06	.82	-.26	-.44	.65	-.35	-.21	.80	.65	.42	-.19		.71	-.25	.71	.74	-.12	.76	.72	-.28	Ni
Ni	.44	-.17	-.03	.41	-.17	-.22	.28	-.28	-.67	.42	.34	.11	.42	.31		-.23	.18	.20	-.10	.22	.07	-.19	Pb
Pb	-.30	.43	.16	-.20	.61	-.05	-.39	.47	-.10	-.32	-.37	-.17	-.02	.00	-.02		-.18	-.18	-.26	-.18	-.13	.85	Rb
Rb	.98	-.24	-.10	.83	-.25	-.28	.71	-.31	-.33	.99	.95	.28	.05	.78	.44	-.34		1.00	-.08	1.00	.93	-.18	Si
Si	.72	-.34	-.10	.60	-.38	-.43	.88	-.41	-.33	.72	.68	.82	-.12	.68	.24	-.38	.71		-.06	1.00	.94	-.19	Sr
Sr	-.10	-.27	.49	.15	-.09	-.26	.02	-.28	-.56	-.06	-.10	-.07	.69	-.14	.45	.03	-.08	-.10		-.08	-.09	-.19	Ti
Ti	.98	-.19	-.10	.86	-.26	-.28	.70	-.31	-.34	.98	.91	.28	.02	.83	.46	-.30	.99	.69	-.07		.95	-.19	V
V	.06	-.01	.79	.46	-.06	-.21	.26	-.27	.11	.10	-.02	-.09	.27	.21	-.02	.08	.03	.00	.33	.07		-.19	Zn
Zn	-.27	.18	.12	-.33	.93	.15	-.36	.64	-.07	-.27	-.24	-.21	.03	-.20	-.17	.73	-.25	-.38	-.11	-.25	-.10		

Table IV-7: Comparative  $\delta^{34}\text{S}$  of hydrothermal vents.

Location	$\delta^{34}\text{S}$ (‰)
Escanaba Trough <sup>1</sup>	
po/sp/w	5.1 to 5.8 (ave 5.4)
ba	19.4
po <sup>2</sup>	1.9 to 11.6 (ave 6.6)
EPR, 21°C <sup>3</sup>	
sp/w	1.9 to 4.1
an	18.96
vent fluid	3.46 to 3.70
SW	18.86
SJFR <sup>4</sup>	
po	1.6 to 5.7
vent fluid	4.0 to 7.4
Guaymas <sup>5</sup>	
po	0.88 to 2.92
ba	19.49 to 21.43
SW <sup>6</sup>	21.0
MORB <sup>7</sup>	0.1 ± 0.5

po = pyrrhotite, sp = sphalerite, w = wurtzite, ba = barite, an = anhydrite,  
SW = seawater, MORB = mid-ocean ridge basalt

1 This study (NESCA Dive 658)

2 SESCA dredge samples (Koski et al., 1988)

3 21°N, East Pacific Rise (Kerridge et al., 1983, Zierenberg et al., 1984)

4 Southern Juan de Fuca Ridge (Shanks and Seyfried, 1987)

5 Guaymas Basin (Koski et al., 1985)

6 Seawater (Rees et al., 1978)

7 Mid-ocean ridge basalt (Sakai et al., 1984)

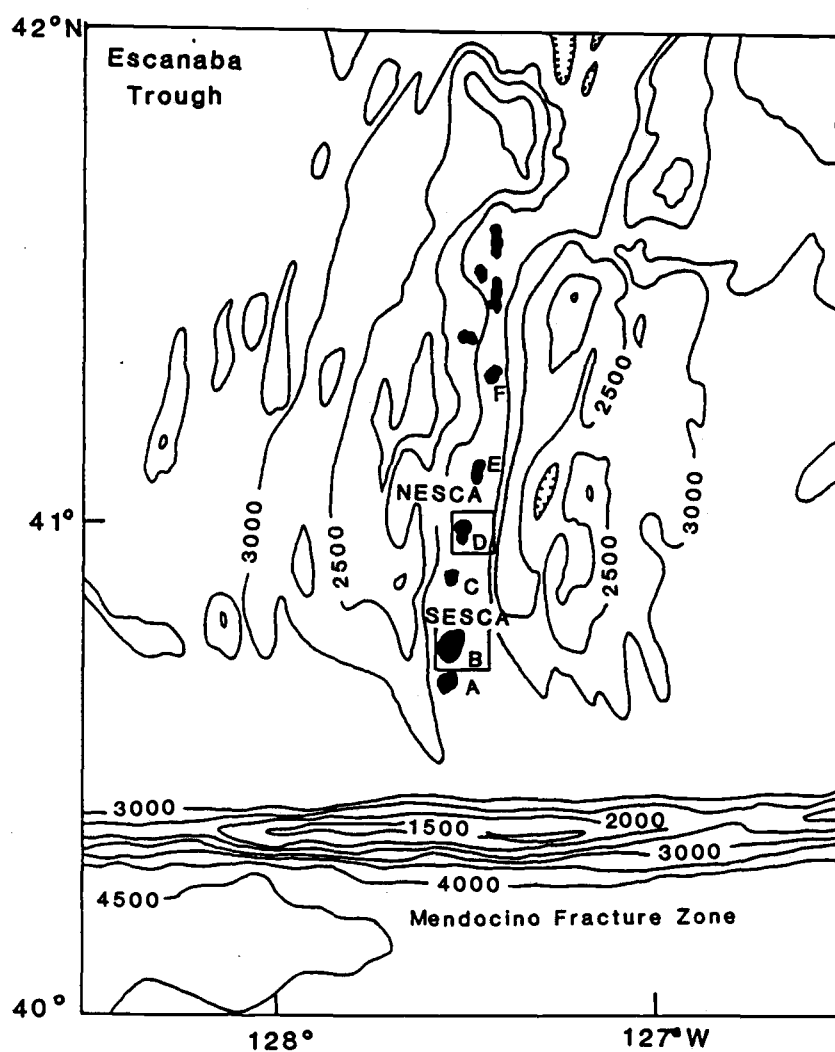


Fig. IV-1. Bathymetric map of the Escanaba Trough after Wilde et al., 1979 showing the locations of six major volcanic edifices (A through F shown in solid pattern) along the axis of the Escanaba Trough from Abbott et al., 1986. Domes B (SESCA site) and D (NESCA site) are shown in greater detail in Fig. IV-2.



Fig. IV-2. Detailed bathymetry of the (a) NESCA site (Dome D) and (b) SESCA site (Dome B) in the Escanaba Trough, southern Gorda Ridge from NOAA SEABEAM. Basalt outcrops are stippled and hydrothermal sulfide deposits are solid pattern. The unpatterned area is sediment covered. At the NESCA site, Seacliff dive sites 658 and 659 are located at map center. At the SESCA site, Seacliff dive sites 661, 662 and 663 are located in the upper right quadrant. Numbers along the top and right margins of the map are the transponder navigation grid.

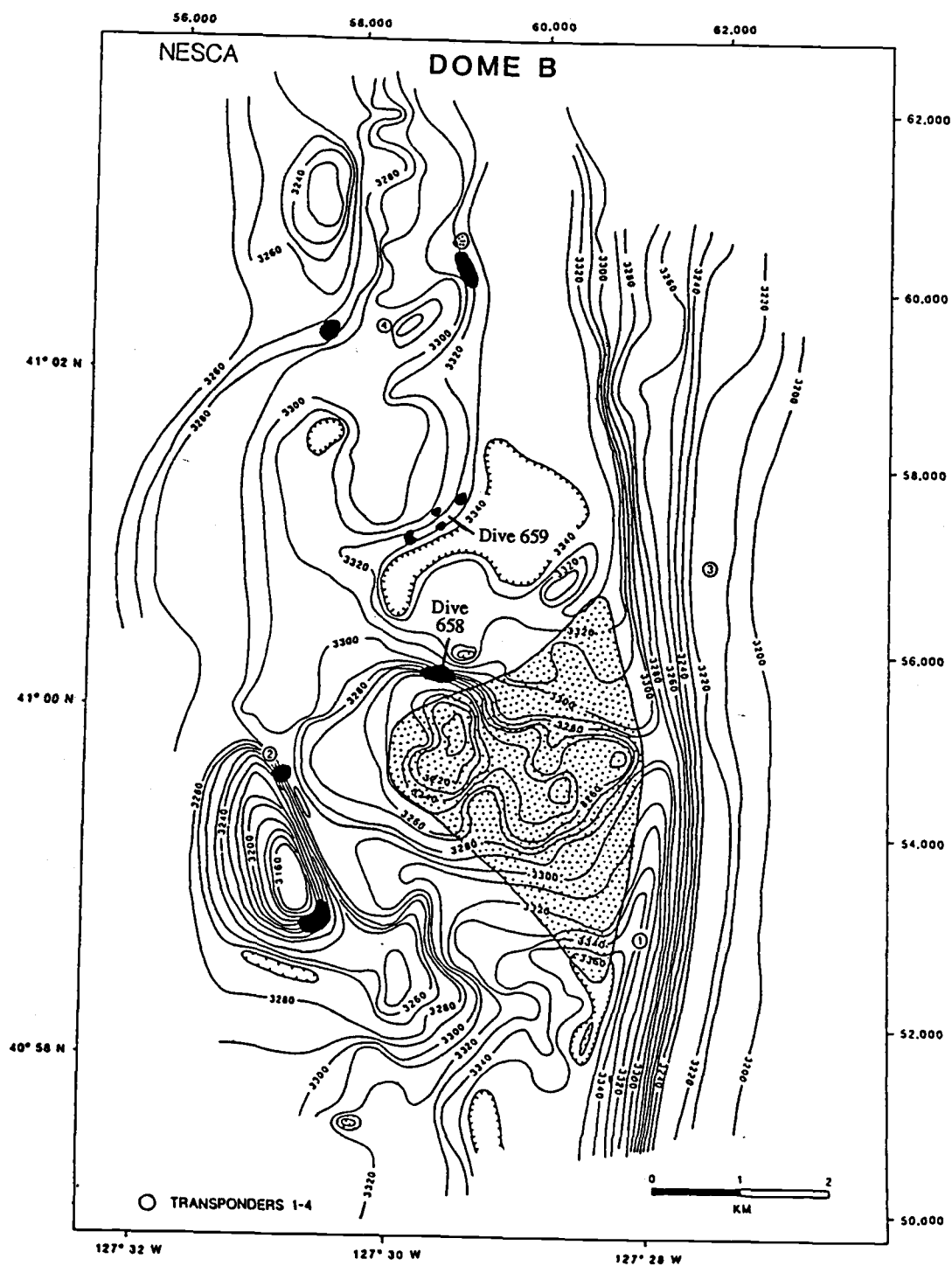


Fig. IV-2 (a)

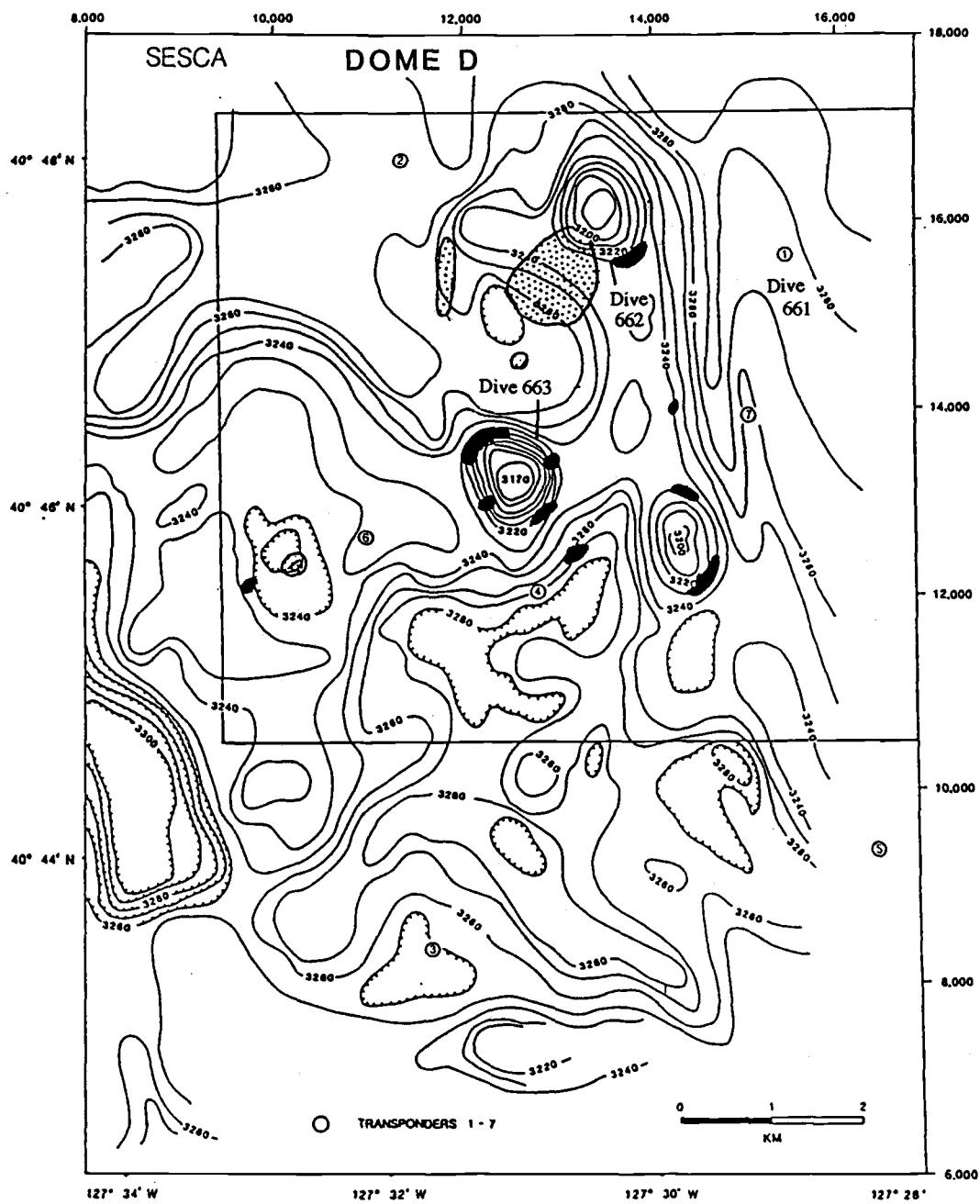


Fig. IV-2 (b)

Fig. IV-3. Photomicrograph of a polished thin section of sample 659-2 showing large boxwork pyrrhotite in chimney flow channels and abrupt change in crystal size at channel margins. Boxwork pyrrhotite crystals in this figure represent regions of flow through hydrothermal chimneys. Massive pyrrhotite forms where mixing between hydrothermal fluids and seawater inhibits growth of larger crystals. Scale bar = 2 cm.



0 1 2

Fig. IV-3

Fig. IV-4. SEM backscattering image of an As-rich mineral intergrown with isocubanite (CuFe) with Zn-rich rim from chimney sample 7 (659-3). Significant sulfur concentration indicates the presence of arsenopyrite ( $\text{Fe As}_2\text{S}$ ).

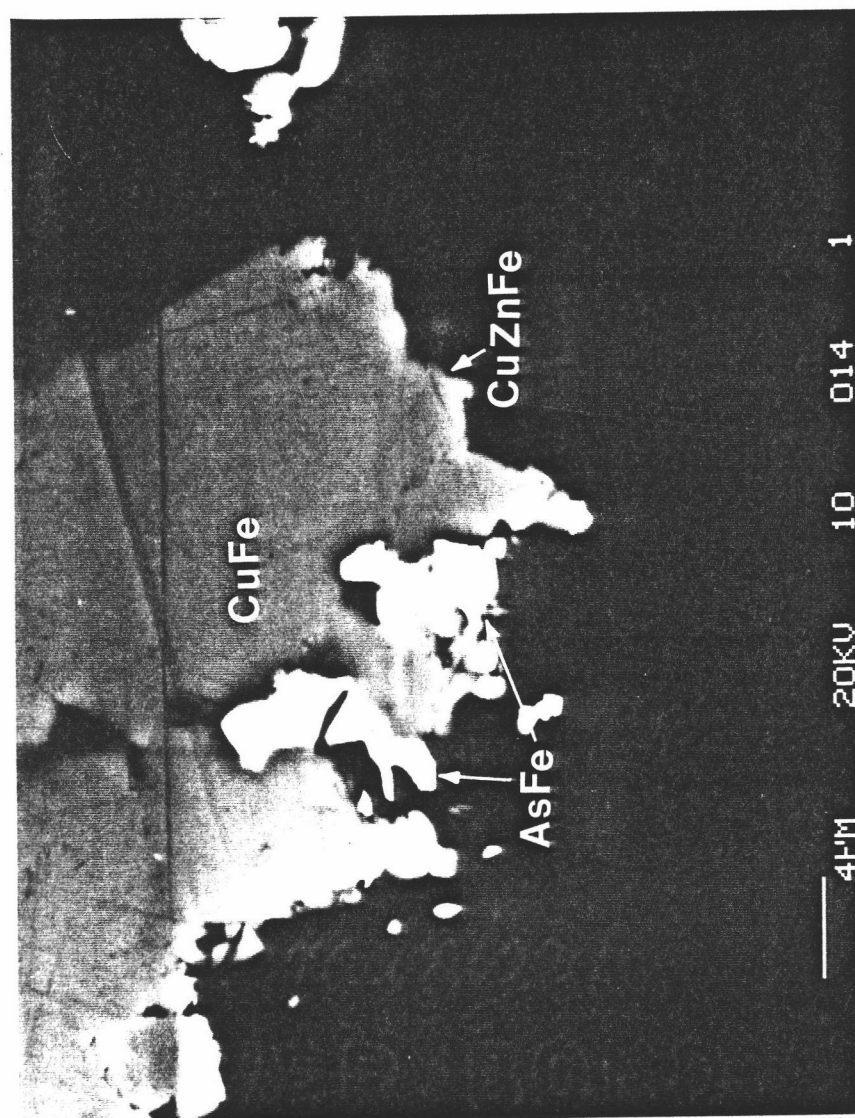


Fig. IV-4

Fig. IV-5. SEM backscattering image of barite chimney (ba) showing fine scale zonation from variable Sr content (light and dark bands) and small cinnabar crystal (HgS).



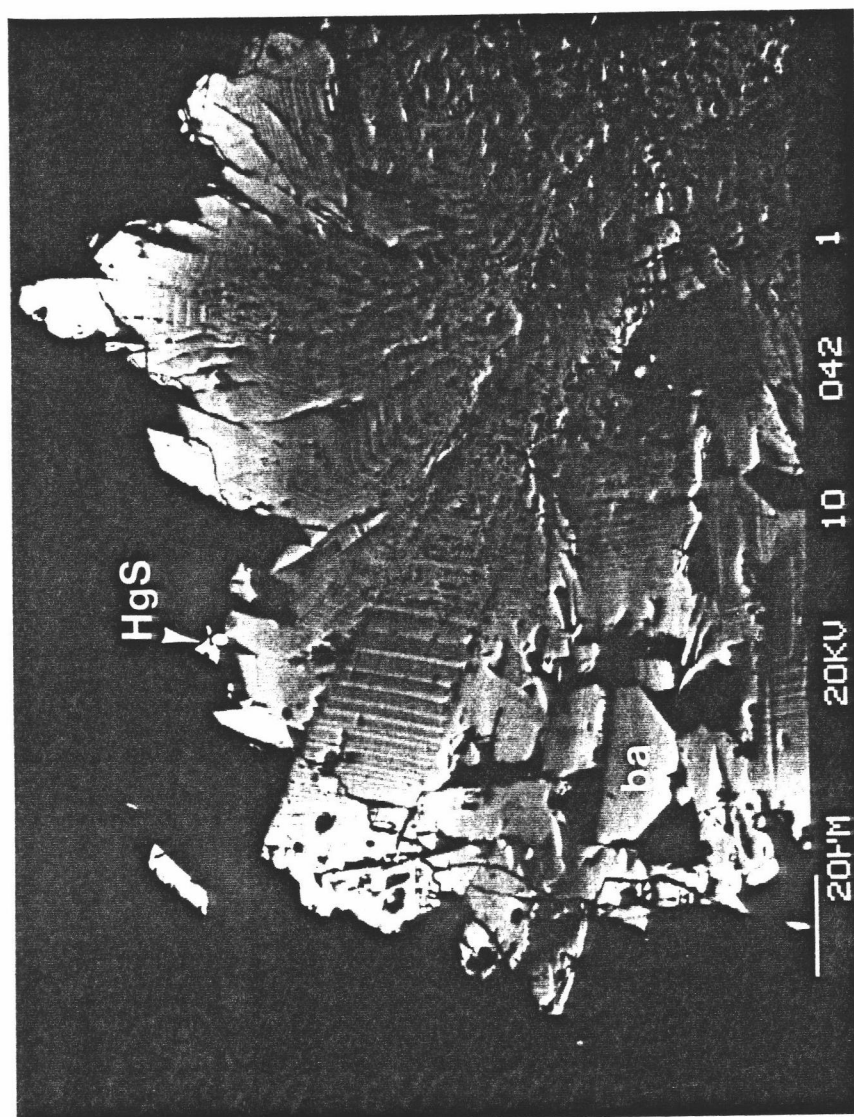


Fig. IV-5

Fig. IV-6. SEM backscattering image of fractured pyrrhotite crystal (po) showing oxidation to marcasite (mc). The corresponding SEM spectra for points 1, 2 and 3 show a decrease in the Fe/S ratio reflecting the oxidation of pyrrhotite (2) to marcasite (1). Spectra (3) represents near completion of weathering to FeOOH. Scale bar = 40  $\mu\text{m}$ .

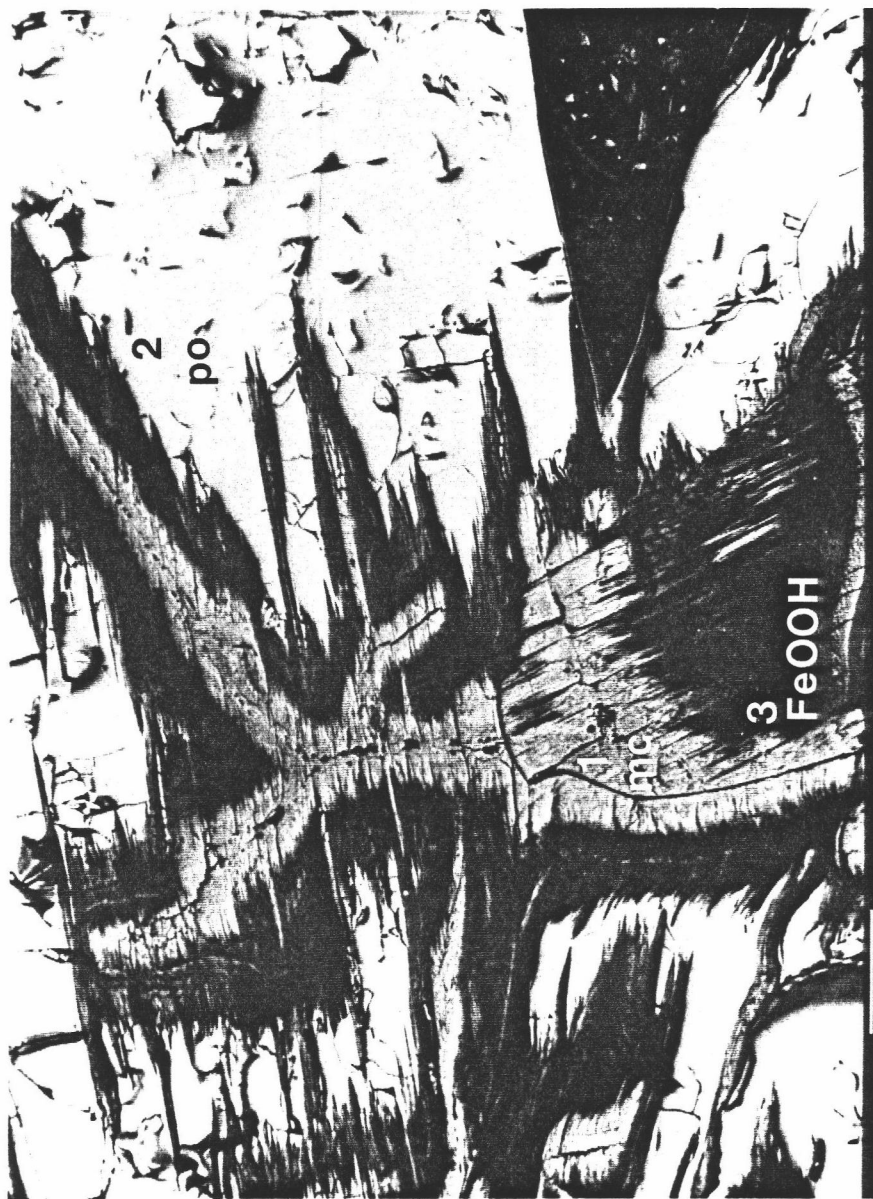


Fig. IV-6

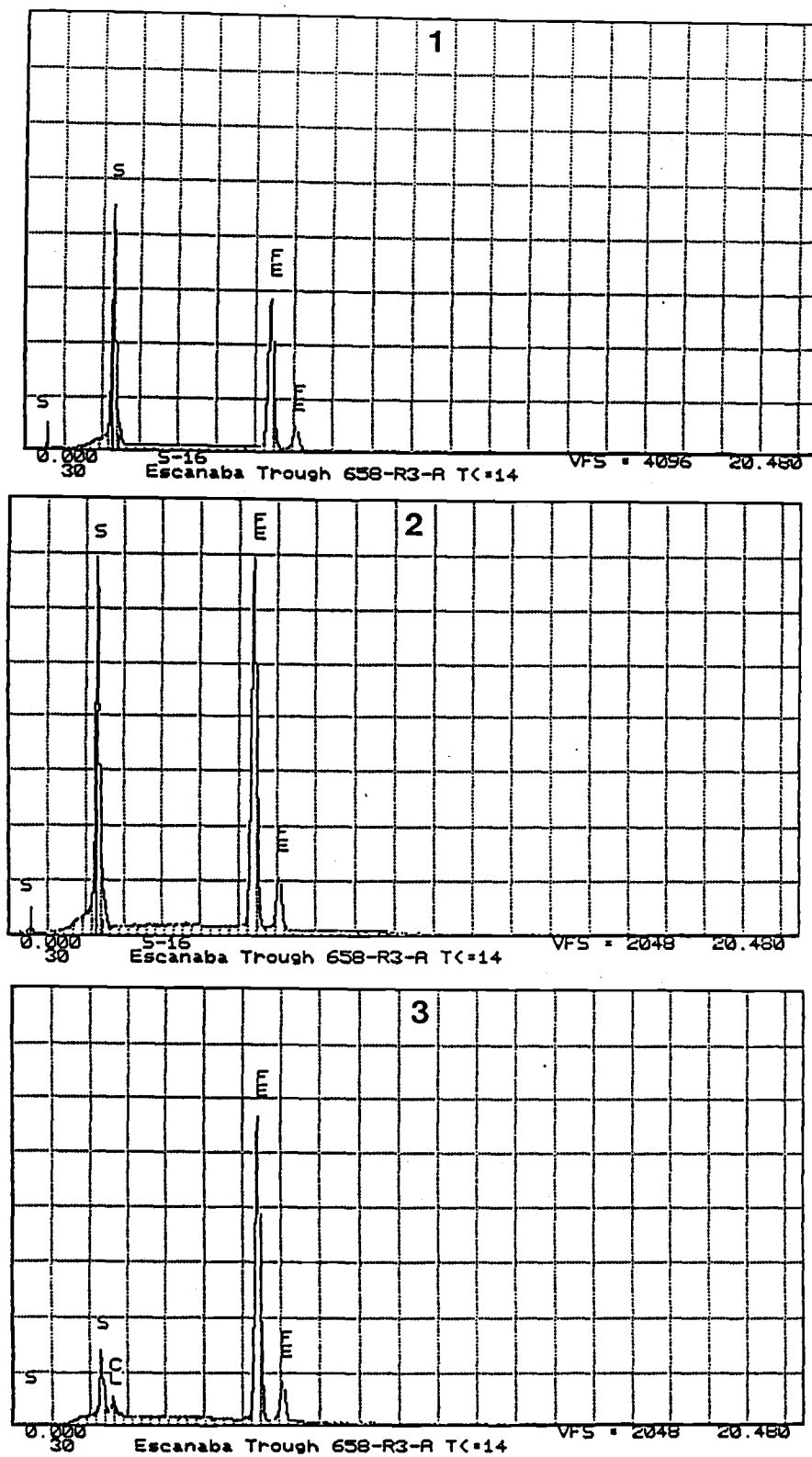


Fig. IV-6 (continued)

Fig. IV-7. SEM backscattering image of goethite and lepidocrocite ( $\text{FeOOH}$ ) from weathering of pyrrhotite (po). A distinct separation between Fe oxyhydroxides and pyrrhotite crystals indicates that precipitation is not simply from in situ alteration of pyrrhotite crystals. In this case, precipitation from cooler Fe oxyhydroxide saturated solutions is suggested.

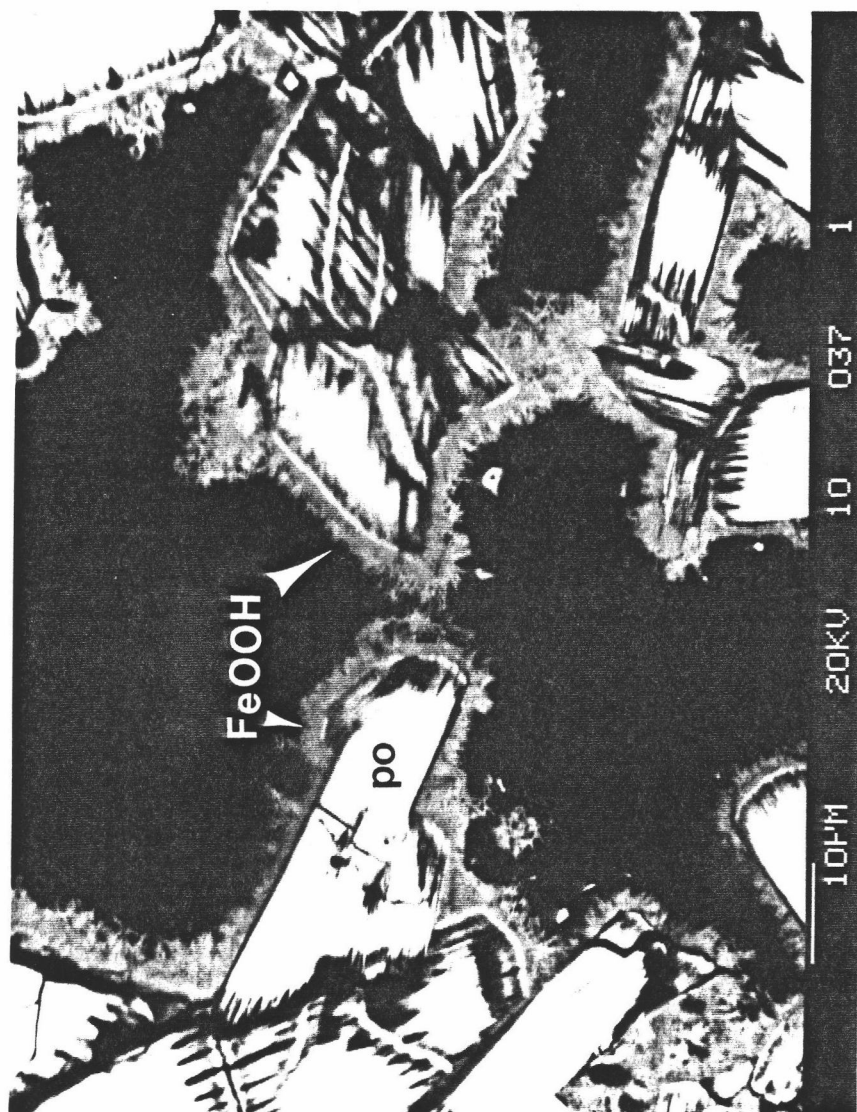


Fig. IV-7

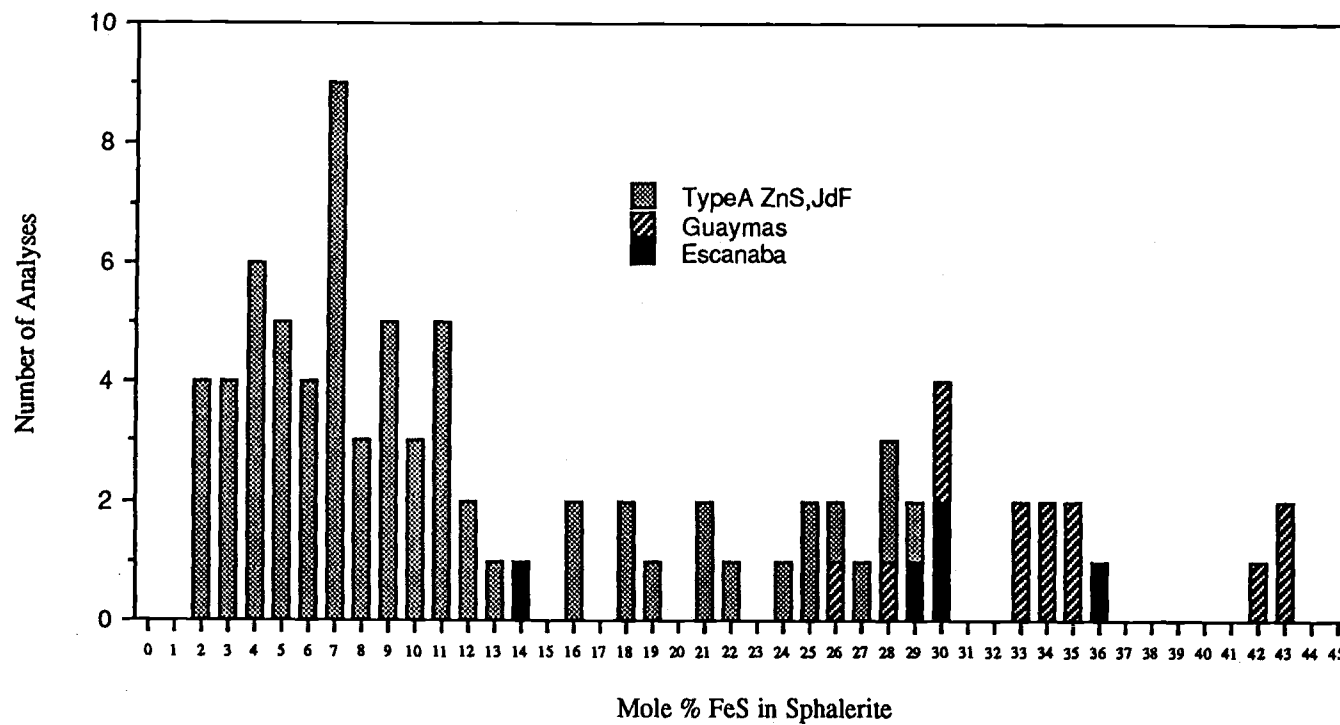


Fig. IV-8. Histogram of mole% FeS in sphalerite from the Escanaba Trough compared to Guaymas Basin (Koski et al., 1985), and Type A sphalerite from the southern Juan de Fuca Ridge (Koski et al., 1984).

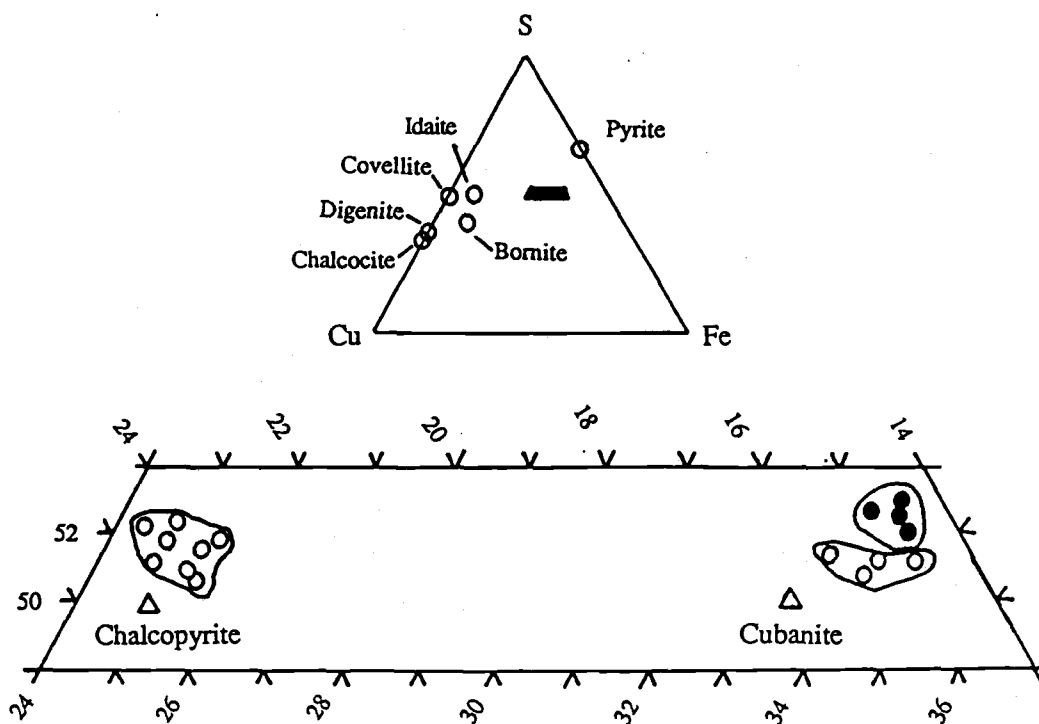


Fig. IV-9. Composition of cubanite from the Escanaba Trough (solid circles) compared to southern Juan de Fuca Ridge (open circles) (Koski et al., 1984). Labeled triangles are stoichiometric chalcopyrite and cubanite.



Fig. IV-10 Ternary diagram with apices Pb-Cu-Zn comparing the chemistry of Escanaba Trough sulfide deposits to other mid-ocean ridge sulfide deposits and deposits from the Troodos ophiolite, Cyprus. Numbers correspond to sample numbers of fresh Escanaba Trough samples in Table IV-3, M = Middle Valley (Davis et al., 1987), G = Guaymas Basin (Koski et al., 1985), C = Cyprus (Constantinou, 1972), O = Galapagos (Bischoff et al., 1983), ▲ = Juan de Fuca Ridge (Bischoff et al., 1983), △ = Juan de Fuca Ridge (Koski et al., 1984), ■ = 21°N, East Pacific Rise (Bischoff et al., 1983), □ = 21°N, East Pacific Rise (Zierenberg et al., 1984), ◻ = 21°N, East Pacific Rise (Hekinian et al., 1980).

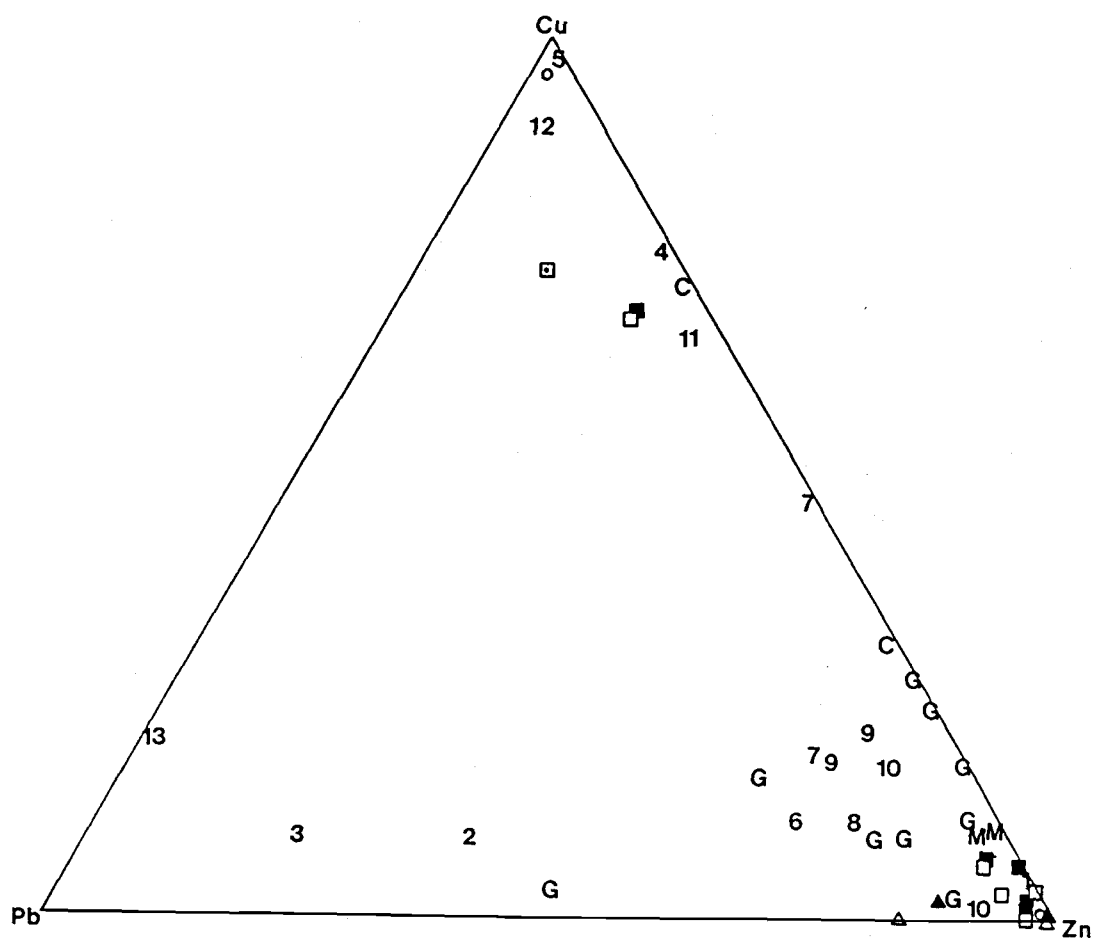


Fig. IV-10

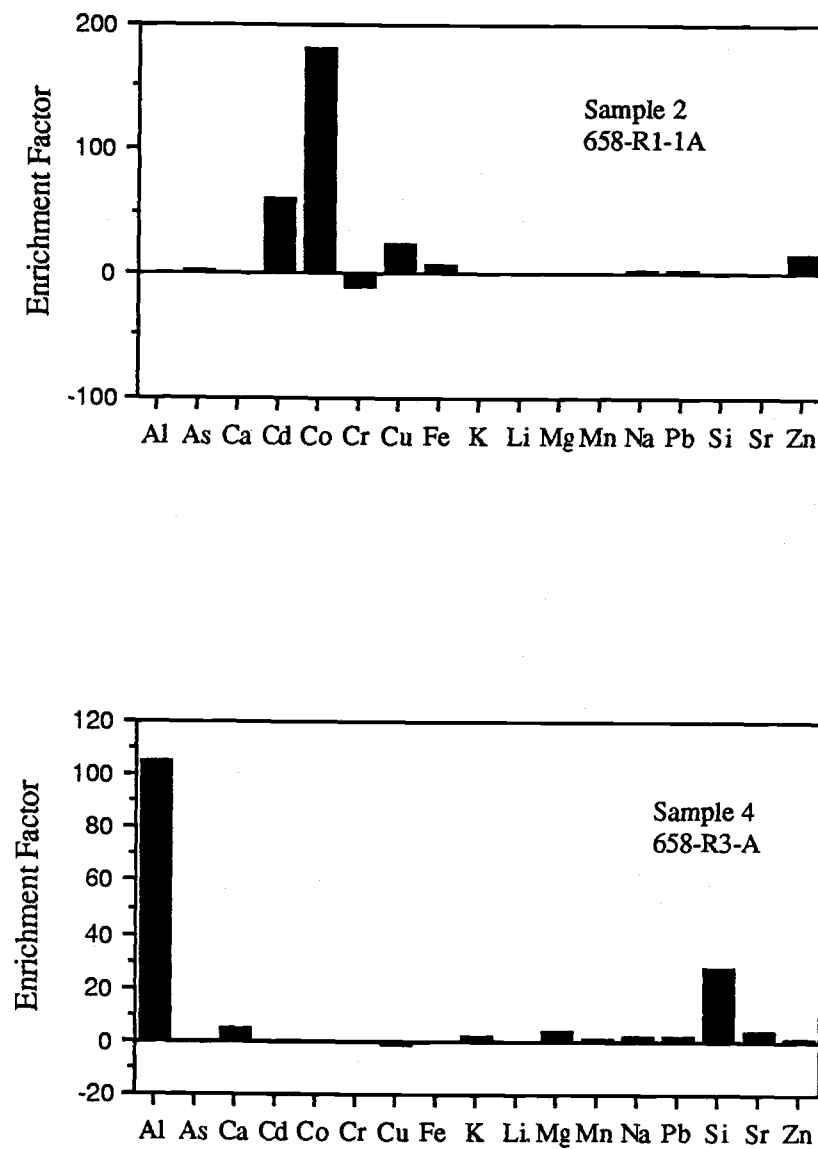


Fig. IV-11. Plots of enrichment factors versus selected elements calculated for chimney samples designated 2, 4, 6 and 11 in Table IV-3. Note vertical axes differ for each sample. See text for discussion.

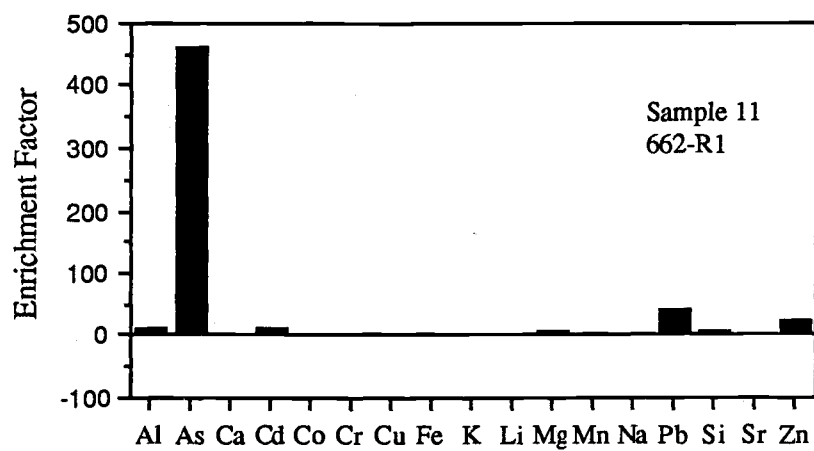
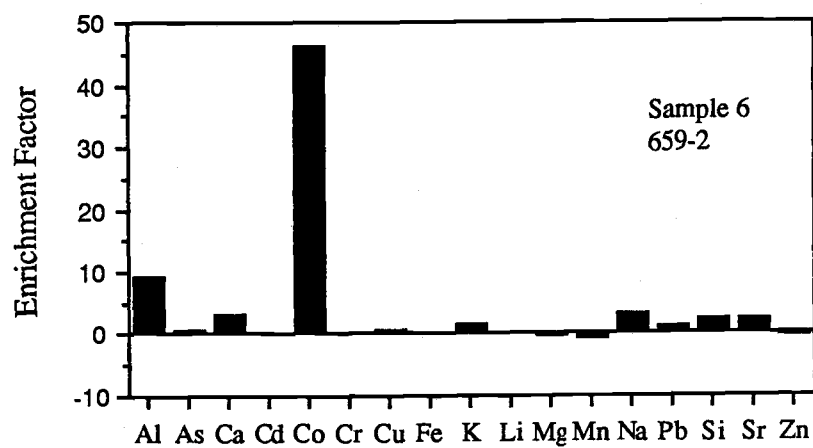


Fig. IV-11 (continued)

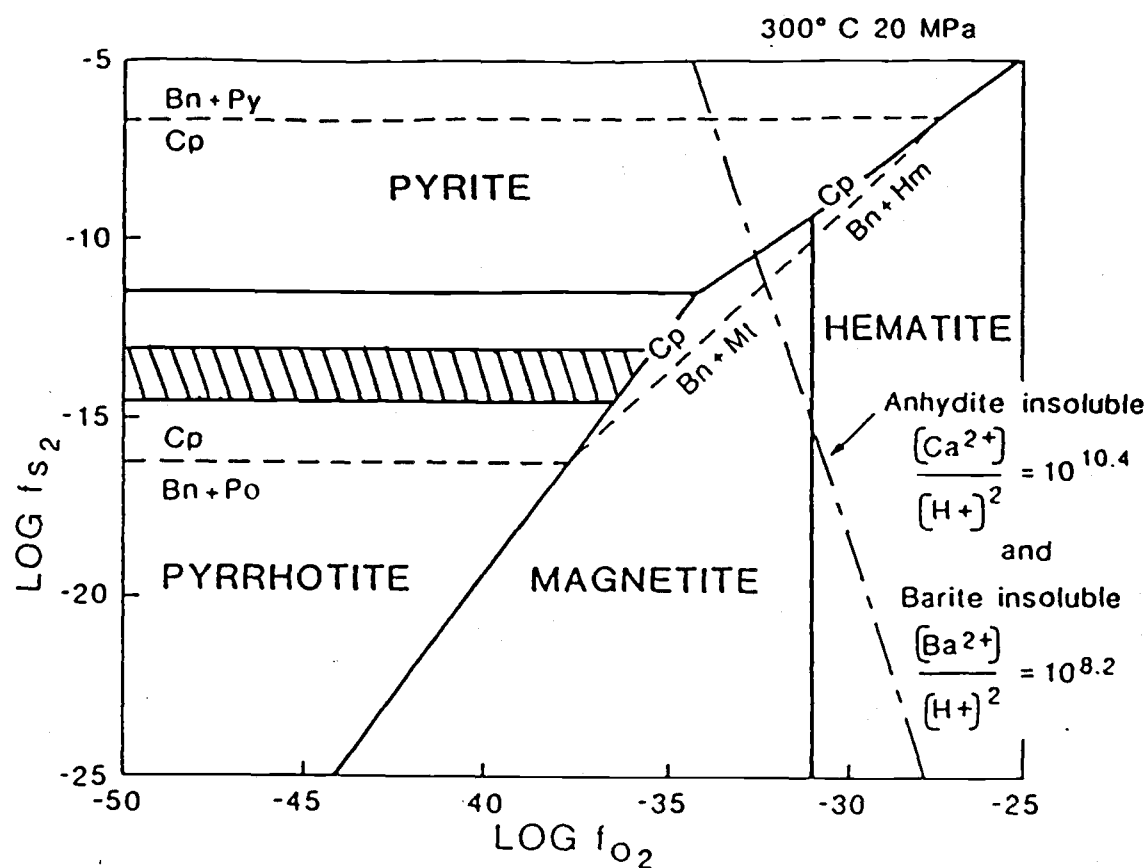


Fig. IV-12. Phase relations in the system Cu-Fe-S-O at 300°C and 20MPa from Koski et al., 1985 with approximate  $f_{S_2}$  for sphalerite with mole% FeS contents equal to those measured in Escanaba Trough sulfides (cross-hatched area).

## References

- Abbott, D. H., Morton, J.L. and Holmes, M.L. (1986) Heat flow measurements on a hydrothermally-active, slow spreading ridge: The Escanaba Trough. *Geophys. Res. Lett.* 13, 678-680.
- Albee, A.L. and Ray, L. (1970) Correction factors for electron probe microanalysis of silicates, oxides, carbonates, phosphates and sulfides. *Anal. Chem.* 42, 1408-1414.
- Alt, J.C., Lonsdale, P., Haymon, R., Muehlenbachs, K. (1987) Hydrothermal sulfide and oxide deposits on seamounts near 21°N, East Pacific Rise. *Geol. Soc. Am. Bull.* 98, 157-168.
- Atwater, T. and Mudie, J.D. (1973) Detailed near-bottom geophysical study of the Gorda Rise. *J. Geophys. Res.* 78, 8665-8686.
- Ballantyne, J.M. and Moore, J.N. (1988) Arsenic geochemistry in geothermal systems. *Geochim. Cosmochim. Acta.* 52, 475-483.
- Bence, A.E. and Albee, A.L. (1968) Empirical correction factors for electron microanalysis of silicates and oxides. *J. Geol.* 76, 382-403.
- Bischoff, J.L., Rosenbauer, R.J., Aruscavage, P.J., Baedeker, P.A. and Crock, J.G. (1983) Sea-floor massive sulfide deposits from 21°N, East Pacific Rise; Juan de Fuca Ridge; and Galapagos Rift: Bulk chemical composition and economic implications. *Econ. Geol.* 78, 1711-1720.
- Brett, R., Evans, H.T. Jr., Gibson, E.K. Jr., Hedenquist, J.W., Wandless, M.-V. and Sommer, M.A. (1987) Mineralogical studies of sulfide samples and volatile concentrations of basalt glasses from the southern Juan de Fuca Ridge. 92, 11,373-11,379.
- Bowers, T.S., Von Damm, K.L. and Edmond, J.M. (1985) Chemical evolution of ridge crest hot springs. *Geochim. Cosmochim. Acta.* 49, 2239-2252.
- Constantinou, G. (1973) Geology and geochemistry of Cyprus sulfide deposits. *Econ. Geol.* 68, 83-86.
- Corliss, J.B., Lyle, M., Dymond, J. and Crane, K. (1978) The chemistry of hydrothermal sediment mound deposits near the Galapagos Rift. *Earth. Planet. Sci. Lett.* 40, 12-24.
- Craig, H., Welhan, J.A., Kim, K., Poreda, R. and Lupton, J.E. (1980) Geochemical studies of the 21°N EPR hydrothermal fluids. *EOS Trans. AGU.* 61, 992.
- Craig, J.R. and Scott, S.D. (1974) Sulfide phase equilibria, in: *Min. Soc. Am. Short Course Notes: Sulfide Mineralogy*, P.H. Ribbe, ed. CS1-CS110.
- Davis, E. E., Goodfellow, W.D., Bornhold, B.D., Adshead, J., Blaise, B., Villinger, H. and Le Cheminant, G.M. (1987) Massive sulfides in a sedimented rift valley, northern Juan de Fuca Ridge. *Earth Planet. Sci. Lett.* 82, 49-61.

- Deer, W.A., Howie, R.A. and Zussman, J. (1966) An introduction to the rock-forming minerals. J. Wiley & Sons, 528p.
- Dymond, J. and Roth, S. (1986) Plumefall: a record of the settling particle flux on the Endeavor Ridge using moored sensors. EOS, 67, 1027.
- Edmond, J.M. (1980) Ridge crest hot springs: the story so far. EOS, Trans. AGU. 61, 129-131.
- Fukui, S. (1976) Laboratory techniques used for atomic absorption spectrophotometric analysis of geologic samples. Oregon State University Reference 76-10.
- Gieskes, J.M., Elderfield, H., Lawrence, J.R., Johnson, J., Meyers, B. and Campbell, A. (1982) Geochemistry of interstitial waters and sediments, Leg 64, Gulf of California. In Initial Reports of the Deep Sea Drilling Project. Vol. 64 Pt. 2 (eds. J.R. Curray, D.G. Moore et al.) pp. 675-694. U.S. Govt. Printing Office, Washington.
- Grinenko, V.A. (1962) Preparation of sulfur dioxide for isotopic analysis. Zeits. Neorgan. Khimii. 7, 2478-2483.
- Harder, H. (1976) Nontronite synthesis at low temperatures. Chem. Geol. 18, 169-180.
- Haymon, R. (1983) The growth history of hydrothermal black smoker chimneys. Nature 301, 695-698.
- Haymon, R. and Kastner, M. (1981) Hot spring deposits on the East Pacific Rise at 21°N: preliminary description of mineralogy and genesis. Earth Planet. Sci. Lett. 53, 363-381.
- Hekinian, R., Fevrier, M., Bischoff, J.L., Picot, P. and Shanks, W.C. (1980) Sulfide deposits from the East Pacific Rise near 21°N. Science 207, 1433-1444.
- Holland, H.D. and Malinin, S.D. (1979) The solubility and occurrence of non-ore minerals. In Geochemistry of Hydrothermal Ore Deposits, pp. 461-508, John Wiley, New York.
- Howard, K.J. and Fisk, M.R. (1986) Hydrothermal precipitates from basalts on the Gorda Ridge and the President Jackson Seamounts. Oregon Department of Geology and Mineral Industries, Open-File Report 0-86-18.
- Howard, K.J. and Fisk, M.R. (1988) Hydrothermal alumina-rich clays and boehmite on the Gorda Ridge. Geochim. Cosmochim. Acta. 52, 2269-2279.
- Humphries, S.E. and Thompson, G. (1978) Trace element mobility during hydrothermal alteration of oceanic basalts. Geochim. Cosmochim. Acta. 42, 127-136.
- Karlin, R. and Lyle, M. (1989) History of Holocene volcanic and hydrothermal activity in axial valley sediments on the Gorda Ridge. Marine Geology (in press).
- Kerridge, J.F., Haymon, R.M. and Kastner, M. (1983) Sulfur isotope systematics at the 21°N site, East Pacific Rise. Earth Planet. Sci. Lett. 66, 91-100.

- Klinkhammer, G. and Hudson, A. (1986) Dispersal patterns for hydrothermal plumes in the South Pacific using manganese as a tracer. *Earth Planet. Sci. Lett.* 79, 241-249.
- Koski, R.A., Clague, D.A. and Oudin, E. (1984) Mineralogy and chemistry of massive sulfide deposits from the Juan de Fuca Ridge. *Geol. Soc. Am. Bull.* 95, 930-945.
- Koski, R.A., Lonsdale, P.F., Shanks, W.C., Berndt, M.E. and Howe, S.S. (1985) Mineralogy and geochemistry of a sediment-hosted hydrothermal sulfide deposit from the southern trough of Guaymas Basin, Gulf of California. *J. Geophys. Res.* 90, 6695-6707.
- Koski, R.A., Shanks, W.C. III, Bohrsen, W.A. and Oscarson, R.L. (1988) The composition of massive sulfide deposits from the sediment-covered floor of Escanaba Trough, Gorda Ridge: implications for depositional processes. *Can. Min.* 26, 655-673.
- Krissen, S.A. and Scott, S.D. (1982) Phase relations involving pyrrhotite below 350°C. *Econ. Geol.* 77, 1739-1754.
- Kvenholden, K.A., Rapp, J.B., Hostettler, F., Morton, J.L., King, J.D. and Claypool, G.E. (1986) Petroleum associated with polymetallic sulfide on the Gorda Ridge. *Science* 234, 1231-1234.
- Lonsdale, P.F., Bischoff, J.L., Burns, V.M., Kastner, M. and Sweeney, R.E. (1980) A high-temperature hydrothermal deposit on the seabed at a Gulf of California spreading center. *Earth Planet. Sci. Lett.* 49, 8-20.
- Lyle, M., Dymond, J.R. and Heath, G.R. (1977) Copper-nickel enriched ferromanganese nodules and associated crusts from the Bauer Deep, northeast Nazca Plate. *Earth. Planet. Sci. Lett.* 35, 55-64.
- Metz, S., Trefrey, J.H. and Nelsen, T.A. (1988) History and geochemistry of a metalliferous sediment core from the Mid-Atlantic Ridge at 26°N. *Geochim. Cosmochim. Acta.* 52, 2369-2378.
- Moore, G.W. and Sharman, G.F. (1970) Summary of SCAN site 4: In McManus, D.A. et al., eds. Initial Reports DSDP v.5, U.S. Gov't Printing Office, Wa. 761-773.
- Morton, J.L., Holmes, M.L. and Koski, R.A. (1987) Volcanism and massive sulfide formation at a sedimented spreading center, Escanaba Trough, Gorda Ridge. *Geophys. Res. Lett.* 14, 769-772.
- Mottl, M.J. (1983) Hydrothermal processes at mid-ocean spreading centers: application of basalt-seawater experimental results. In: *Hydrothermal Processes at Mid-Ocean Spreading Centers* (eds. P.A. Rona, K. Bostrom, L. Laubier and E.L. Smith) pp. 199-224.
- Mottl, M.J. (1986) Chemical processes in submarine hydrothermal plumes near 21°N on the East Pacific Rise. *EOS* 67, 1027.
- Murowchick, J.B. and Barnes, H.L. (1986) Marcasite precipitation from hydrothermal solutions. *Geochim. Cosmochim. Acta.* 50, 2615-2629.



- Ohmoto, H. and Lasaga, A.C. (1982) Kinetics of reactions between aqueous sulfates and sulfides in hydrothermal systems. *Geochim. Cosmochim. Acta.* 46, 1727-1745.
- Ohmoto, H. and Rye, R.O. (1979) Isotopes of sulfur and carbon. In *Geochemistry of Hydrothermal Ore Deposits* (ed. H.L. Barnes) 2nd edn, pp. 509-567. Wiley.
- Oudin, E. (1983) Hydrothermal sulfide deposits of the East Pacific Rise (21°N) Part I: Descriptive mineralogy. *Mar. Min.* 4, 39-72.
- Oudin, E., Picot, P. and Pouit, G. (1981) Comparison of sulfide deposits from the East Pacific Rise and Cyprus. *Nature* 291, 404-407.
- Perkin-Elmer (1982) Analytical methods for atomic absorption spectrophotometry. Perkin-Elmer Corporation, Norwalk, CT.
- Ramdohr, P. (1969) *The Ore Minerals and Their Intergrowths*. Pergamon, Oxford.
- Riddihough, R.P. (1980) Gorda plate motions from magnetic anomaly analysis. *Earth Planet. Sci. Lett.* 51, 163-170.
- Rona, P.A., Klinkhammer, G., Nelsen, T.A., Trefry, J.H. and Elderfield, H. (1986) Black smokers, massive sulfides and vent biota at the Mid-Atlantic Ridge. *Nature* 321, 33-37.
- Sakai, H., Des Marais, D.J., Ueda, A. and Moore, J.G. (1984) Concentrations and isotope ratios of carbon, nitrogen and sulfur in ocean-floor basalts. *Geochim. Cosmochim. Acta.* 48, 2433-2441.
- Sakai, H., Gunnlaugsson, E., Tomasson, J. and Rouse, J.E. (1980) Sulfur isotope systematics in Icelandic geothermal systems and the influence of seawater circulation at Reykjanes. *Geochim. Cosmochim. Acta.* 44, 1223-1231.
- Scott, M.R., Scott, R.B., Morse, J.W., Betzer, P.R., Butler, L.W. and Rona, P.A. (1978) Metal-enriched sediments from the TAG hydrothermal field. *Nature* 276, 811-813.
- Scott, S.D. and Barnes, H.L. (1971) Sphalerite geothermometry and geobarometry. *Econ Geol.* 66, 653-669.
- Scott, S.D. and Barnes, H.L. (1972) Sphalerite-wurtzite equilibria and stoichiometry. *Geochim. Cosmochim. Acta.* 36, 1275-1295.
- Seyfried, W.E. Jr. and Janecky, D.R. (1986) Chloride depletions and enrichments in seafloor hydrothermal fluids: constraints from experimental basalt studies. *Geochim. Cosmochim. Acta.* 49, 2545-2560.
- Seyfried, W.E. Jr. and Mottl, M.J. (1982) Hydrothermal alteration of basalt by seawater under seawater-dominated conditions. *Geochim. Cosmochim. Acta.* 46, 985-1002.
- Shanks, W.C. III, Bischoff, J.L. and Rosenbauer, R.J. (1981) Seawater sulfate reduction and sulfur isotope fractionation in basaltic systems: interaction of seawater

- with fayalite and magnetite at 200° - 350°C. *Geochim. Cosmochim. Acta.* 45, 1977-1995.
- Shanks, W.C. III and Seyfried, W.E. Jr. (1987) Stable isotope studies of vent fluids and chimney minerals, southern Juan de Fuca Ridge: sodium metasomatism and seawater sulfate reduction. *J. Geophys. Res.* 92, 11,387-11,399.
- Sillitoe, R.H. and Clark, A.H. (1969) Copper and copper-iron sulfides as initial products of supergene oxidation, Copiapo mining district, northern Chile. *Am. Min.* 54, 1684-1710.
- Spiess, F.N., Macdonald, K.C., Atwater, T., Ballard, R., Carranza, A., Cordoba, D., Cox, C., Diaz Garcia, V.M., Francheteau, J., Guerrero, J., Hawkins, J., Haymon, R., Hessler, R., Juteau, T., Kastner, M., Larson, R., Luyendyk, B., Macdougall, J.D., Miller, S., Normark, W., Orcutt, J., Rangin, C. (1980) East Pacific Rise: Hot springs and geophysical experiments. *Science*, 207, 1421-1433.
- Styrt, M.M., Brackman, A.J., Holland, H.D., Clark, B.C., Pisutha-Arnand, V., Eldridge, C.S., and Ohmoto, H. (1981) The mineralogy and isotopic composition of sulfur in hydrothermal sulfide/sulfate deposits on the East Pacific Rise, 21°N latitude. *Earth Planet. Sci. Lett.* 53, 382-390.
- Tivey, M.K. and Delaney, J.R. (1986) Growth of large sulfide structures on the Endeavor segment of the Juan de Fuca Ridge. *Earth. Planet. Sci. Lett.* 77, 303-317.
- Thode, H.G., Monster, J. and Dunford, H.B. (1961) Sulfur isotope geochemistry. *Geochim. Cosmochim. Acta.* 25, 159-174.
- Turekian, K.K. and Wedepohl, K.H. (1961) Distribution of the elements in some major units of the earth's crust. *Geol. Soc. Am. Bull.* 72, 175-192.
- Vallier-Silver, J.N., Tera, F., Klein, J. and Middleton, R. (1987) Beryllium 10 in hydrothermal vent deposits from the East Pacific Ridges: Role of sediments in the hydrothermal processess. *J. Geophys. Res.* 92, 11,364-11,372.
- Varekamp, J.C. and Buseck, P.R. (1984) The speciation of mercury in hydrothermal systems with applications to ore deposition. *Geochim. Cosmochim. Acta.* 48, 177-185.
- Von Damm, K.L., Edmond, J.L., Grant, B., Measures, C.I., Walden, B. and Weiss, R.L. (1985a) Chemistry of submarine hydrothermal solutions at 21°N, East Pacific Rise. *Geochim. Cosmochim. Acta.* 44, 2197-2220.
- Von Damm, K.L., Edmond, J.M., Measures, C.I. and Grant, B. (1985b) Chemistry of submarine hydrothermal solutions at Guaymas Basin, Gulf of California. *Geochim. Cosmochim. Acta.* 49, 2221-2237.
- Von Damm, K.L., Grant, B. and Edmond, J.M. (1983) Preliminary report on the chemistry of hydrothermal solutions at 21°North, East Pacific Rise. In: *Hydrothermal Processes at Seafloor Spreading Centers* (eds. P.A. Rona, K. Bostrom, L. Laubier and E.L. Smith), pp. 369-389. Plenum Press.

- Wilde, P., Chase, T.E., Holmes, M.L., Normark, W.R., Tomas, J.A., McCulloch, D.S. and Kulm, L.D. (1979) Oceanographic data off northern California-southern Oregon, 40° to 43° North including the Gorda Deep Sea Fan. LBL Publ. 251, Lawrence Berkeley Lab, Berkeley, Calif.
- Zierenberg, R.A., Shanks, W.C. III and Bischoff, J.L. (1984) Massive sulfide deposits at 21°N, East Pacific Rise: Chemical composition, stable isotopes and phase equilibria. Geol. Soc. Am. Bull. 95, 922-929.
- Zierenberg, R.A. and Koski, R.A., Shanks, W.C. III and Rosenbauer, R.J. (1986) Form and composition of sediment-hosted sulfide-sulfate deposits, Escanaba Trough, southern Gorda Ridge (abs): EOS Transactions Am Geophys. Union 67, 1282.

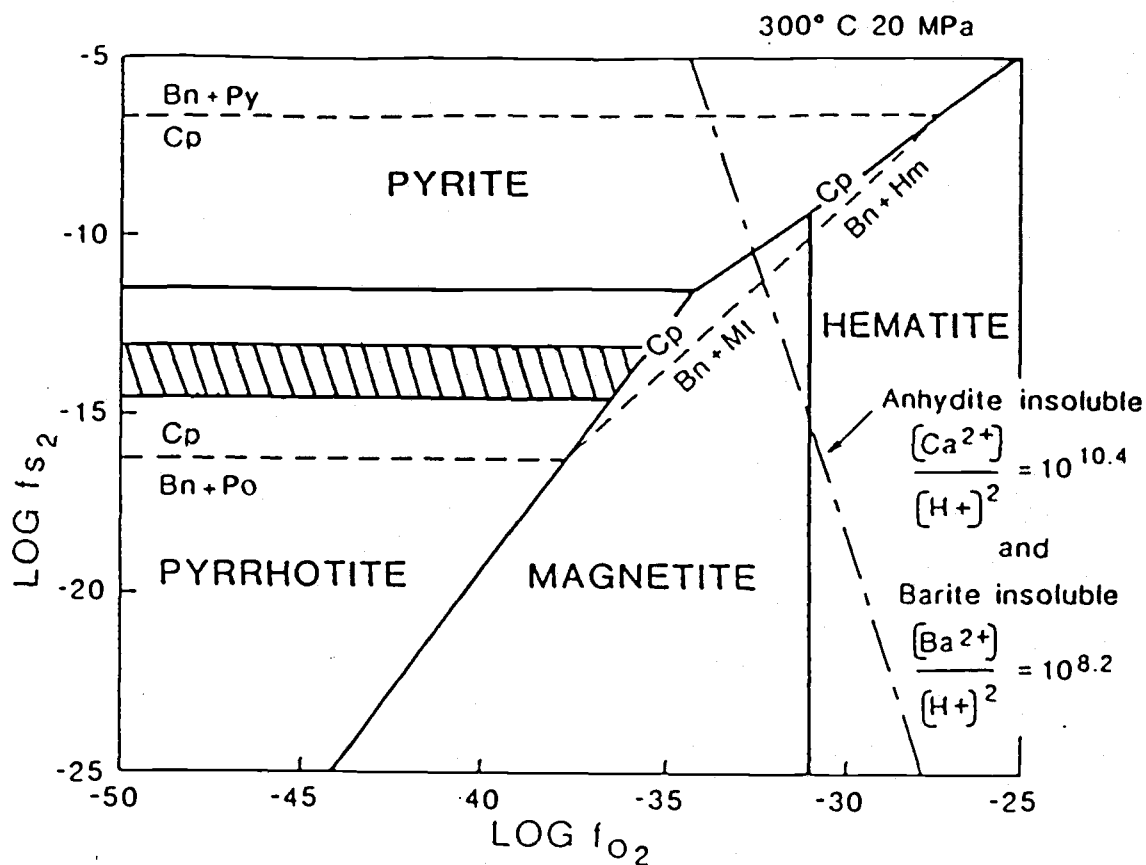


Fig. IV-12. Phase relations in the system Cu-Fe-S-O at 300°C and 20MPa from Koski et al., 1985 with approximate  $f_{S_2}$  for sphalerite with mole% FeS contents equal to those measured in Escanaba Trough sulfides (cross-hatched area).

## BIBLIOGRAPHY

- Abbott, D. H., Morton, J.L. and Holmes, M.L. (1986) Heat flow measurements on a hydrothermally-active, slow spreading ridge: The Escanaba Trough. *Geophys. Res. Lett.* 13, 678-680.
- Albee, A.L. and Ray, L. (1970) Correction factors for electron probe microanalysis of silicates, oxides, carbonates, phosphates and sulfides. *Anal. Chem.* 42, 1408-1414.
- Alt J.C. and Honnorez J. (1984) Alteration of the upper oceanic crust, DSDP site 417: mineralogy and chemistry. *Contrib. Min. Petrol.* 87, 149-169.
- Alt, J.C., Lonsdale, P., Haymon, R. and Muehlenbachs, K. (1987) Hydrothermal sulfide and oxide deposits on seamounts near 21°N, East Pacific Rise. *Geol. Soc. Am. Bull.* 98, 157-168.
- Alpin, A.C. and Cronan, D.S. (1985) Ferromanganese oxide deposits from the Central Pacific Ocean I. Encrustations from the Line Islands Archipelago. *Geochim. Cosmochim. Acta.* 49, 427-436.
- Arcyana, (1975) Transform fault and rift valley geology from bathyscaph and diving saucer. *Science* 190, 108-116.
- Atwater, T. and Mudie, J.D. (1973) Detailed near-bottom geophysical study of the Gorda Rise. *J. Geophys. Res.* 78, 8665-8686.
- Baker E.T., Massoth G.J., Collier R.W., Trefry J.H., Kadko D., Nelsen T.A., Rona P.A. and Lupton J.E. (1987) Evidence for high-temperature hydrothermal venting on the Gorda Ridge, Northeast Pacific Ocean. *Deep Sea Res.* 34, 1461-1476.
- Ballantyne, J.M. and Moore, J.N. (1988) Arsenic geochemistry in geothermal systems. *Geochim. Cosmochim. Acta.* 52, 475-483.
- Batiza, R. (1985) Qualitative assessment of polymetallic sulfide mineral deposits on seamounts. *Mar. Min.* 5, 181-191.
- Bass M.N. (1976) Secondary minerals in oceanic basalt, with special reference to Leg 34, Deep Sea Drilling Project. In Yeats, R.S., Hart, S.R., et al., 1976. Initial Report of the Deep Sea Drilling Project, Volume 34, Washington (U.S. Government Printing Office), pp. 393-432.
- Bence, A.E. and Albee, A.L. (1968) Empirical correction factors for electron microanalysis of silicates and oxides. *J. Geol.* 76, 382-403.
- Bischoff, J.L. (1980) Geothermal system at 21°N, East Pacific Rise: Physical limits on geothermal fluid and role of adiabatic expansion. *Science* 207, 1465-1469.
- Bischoff, J.L. and Dickson, F.W. (1975) Seawater-basalt interaction at 200°C and 500 bars: Implications for origin of sea-floor heavy metal deposits and regulation of seawater chemistry. *Earth Planet. Sci. Lett.* 25, 385-397.

- Bischoff, J.L., Piper, D.Z. and Leong, K. (1981) The alumino-silicate fraction of North Pacific manganese nodules. *Geochim. Cosmochim. Acta.* 45, 2047-2063.
- Bischoff, J.L., Rosenbauer, R.J., Aruscavage, P.J., Baedeker, P.A. and Crock, J.G. (1983) Sea-floor massive sulfide deposits from 21°N, East Pacific Rise; Juan de Fuca Ridge; and Galapagos Rifts: Bulk chemical composition and economic implications. *Econ. Geol.* 78, 1711-1720.
- Blain, C.F., and Andrews, R.L. (1977) Sulfide weathering and the evaluation of gossans in mineral exploration. *Minerals Sci. Engng.* 9, 119-150.
- Bonatti, E., Kraemer, T. and Rudell, H. (1972) Classification and genesis of submarine iron-manganese deposits, p.149-166. In: D.R. Horn (ed.) *Papers on a Conference about Ferromanganese Deposits on the Ocean Floor.* Washington, D.C., National Science Foundation.
- Bonatti, E., Simmons, E.C., Breger, D., Hamlyn, P.R. and Lawrence, J. (1983) Ultramafic rock/seawater interaction in the oceanic crust: Mg-silicate (sepiolite) deposit from the Indian Ocean floor. 62, 229-238.
- Bowers T.S., Jackson K.J. and Helgeson H.C. (1984) Equilibrium activity diagrams for coexisting minerals and aqueous solutions at pressures and temperatures to 5kb and 600°C. Springer-Verlag, 397 p.
- Bowers, T.S., Von Damm, K.L. and Edmond, J.M. (1985) Chemical evolution of ridge crest hot springs. *Geochim. Cosmochim. Acta.* 49, 2239-2252.
- Brett, R., Evans, H.T.Jr., Gibson, E.K. Jr., Hedenquist, J.W., Wandless, M.-V. and Sommer, M.A. (1987) Mineralogical studies of sulfide samples and volatile concentrations of basalt glasses from the southern Juan de Fuca Ridge. 92, 11,373-11,379.
- Brindley, G. W. and Brown, G. (1980) *Crystal Structures of Clay Minerals and their X-ray Identifications.* Spottiswoode Ballantyne Ltd.
- Brown G. and Brindley G.W. (1980) X-ray diffraction procedures for clay mineral identification. In: *Crystal structures of clay minerals and their X-ray identifications*, (eds. G.W. Brindley and G. Brown), Chap. 5, pp. 305-359. Spottiswoode Ballantyne Ltd.
- Browne P.R.L. (1978) Hydrothermal alteration in active geothermal fields, *Ann. Rev. Earth Planet Sci.*, 6, 229-250.
- Burns, R.G. (1976) The uptake of cobalt into ferromanganese nodules, soils and synthetic manganese (IV) oxides. *Geochim Cosmochim Acta.* 40, 95-102.
- Calvert, S.E. and Piper, D.Z. (1984) Geochemistry of ferromanganese nodules from DOMES Site A northern equatorial Pacific: multiple diagenetic sources in the deep sea. *Geochim. Cosmochim. Acta.* 48, 1913-1928.

- Calvert, S.E. and Price, N.B. (1977) Geochemical variation in ferromanganese nodules and associated sediments from the Pacific Ocean. *Mar. Chem.* 5, 43-74.
- Chave, K.E., Morgan, C.L. and Green, W.J. (1986) A geochemical comparison of manganese oxide deposits of the Hawaiian Archipelago and Deep Sea. *Applied Geochemistry* 1, 233-240.
- Clague, D.A., Friesen, W., Quinterio, P., Holmes, M., Morton, J., Bouse, R., Morgenson, L., and Davis, A. (1984) Preliminary geological, geophysical and biological data from the Gorda Ridge. U.S. Geol. Survey Open-File Report 84-364, 48p.
- Cole T.G. (1983) Oxygen isotope geothermometry and origin of smectites in the Atlantis II Deep, Red Sea. *Earth Planet Sci. Lett.* 66, 166-176.
- Collier, R.W., Holbrook, S. H. and Robbins, J.M. (1986) Studies of trace metals and active hydrothermal venting on the Gorda Ridge. Oregon Department of Geology and Mineral Industries, Open-File Report 0-86-13.
- Constantinou, G. (1973) Geology and geochemistry of Cyprus sulfide deposits. *Econ. Geol.* 68, 83-86.
- Corliss, J.B., Lyle, M., Dymond, J. and Crane, K. (1978) The chemistry of hydrothermal sediment mound deposits near the Galapagos Rift. *Earth. Planet. Sci. Lett.* 40, 12-24.
- Craig, H., Welhan, J.A., Kim, K. Poreda, R. and Lupton, J.E. (1980) Geochemical studies of the 21°N EPR hydrothermal fluids. *EOS Trans. AGU.* 61, 992.
- Craig, J.D., Andrews, J.E. and Meylan, M.A. (1982) Ferromanganese deposits in the Hawaiian Archipelago. *Mar. Geol.* 45, 127-157.
- Craig, J.R. and Scott, S.D. (1974) Sulfide phase equilibria, in: *Min. Soc. Am. Short Course Notes: Sulfide Mineralogy*, P.H. Ribbe, ed. CS1-CS110.
- Crane, K. and Ballard, R.D. (1981) Volcanics and structures of the FAMOUS-Narrowgate rift: Evidence for cyclic evolution: AMAR I. *J. Geophys. Res.* 86, 5112-5124.
- Cronan, D.S. (1977) Deep-sea nodules - distribution and geochemistry. In: G.P. Glasby (Ed.) *Marine Manganese Deposits*. Elsevier, Amsterdam, pp. 11-44.
- Czamanske, G.K. and Moore, J.G. (1977) Composition and phase chemistry of sulfide globules in basalt from the Mid-Atlantic Ridge rift valley near 37°N lat. *Geol. Soc. Am. Bull.* 88, 587-599.
- Davis, A. and Clague, D.A. (1988) Geochemistry, mineralogy and petrogenesis of basalt from the Gorda Ridge. *J. Geophys. Res.* 92, 10467-10483.

- Davis, E. E., Goodfellow, W.D., Bornhold, B.D., Adshead, J., Blaise, B., Villinger, H. and Le Cheminant, G.M. (1987) Massive sulfides in a sedimented rift valley, northern Juan de Fuca Ridge. *Earth Planet. Sci. Lett.* 82, 49-61.
- Deer, W.A., Howie, R.A. and Zussman, J. (1966) An introduction to the rock-forming minerals. J. Wiley & Sons, 528p.
- Delany J.M. and Helgeson H.C. (1978) Calculation of the thermodynamic consequences of dehydration in subducting oceanic crust to 100kb and >800°C. *Am. Jour. Sci.*, 278, 638-686.
- Dymond, J., Lyle, M., Finney, B., Piper, D.Z., Murphy, K., Conard, R. and Pisias, N. (1984) Ferromanganese nodules from MANOP Sites H, S, and R - control of mineralogical and chemical composition by multiple accretionary processes. *Geochim Cosmochim Acta*, 48, 931-949.
- Dymond, J. and Roth, S. (1986) Plumefall: a record of the settling particle flux on the Endeavor Ridge using moored sensors. *EOS*, 67, 1027.
- Edmond, J.M. (1980) Ridge crest hot springs: the story so far. *EOS, Trans. AGU*. 61, 129-131.
- Edmond, J.M., Measures, C.I., McDuff, R.E., Chan, L.H., Collier, R., Grant, B., Gordon, L.I. and Corliss, J. (1979) Ridge crest hydrothermal activity and the balances of the major and minor elements in the ocean: the Galapagos data. *Earth Planet. Sci. Lett.* 46, 1-18.
- Feely, R.A., Lewison, M., Massoth, G.J., Robert-Baldo, G., Lavelle, J.W., Byrne, R.H., Von Damm, K.L., Curl, H.C.Jr. (1987) Composition and dissolution of black smoker particulates from active vents on the Juan de Fuca Ridge. *J. Geophys. Res.* 92, 11347-11363.
- Fleet, A.J. (1983) Hydrothermal and hydrogenous ferro-manganese deposits: Do they form a continuum? The rare earth element evidence. In: *Hydrothermal Processes at Mid-Ocean Spreading Centers* (eds. P.A. Rona, K. Bostrom, L. Laubier and E.L. Smith) pp. 535-556.
- Fukui, S. (1976) Laboratory techniques used for atomic absorption spectrophotometric analysis of geologic samples. *Oregon State University Reference* 76-10.
- Gladney E.S. and Burns C.E. (1983) 1982 compilation of elemental concentrations in eleven United States Geological Survey rock standards. *Geostandards Newsletter*. 7, 3-17.
- Gieskes, J.M., Elderfield, H., Lawrence, J.R., Johnson, J., Meyers, B. and Campbell, A. (1982) Geochemistry of interstitial waters and sediments, Leg 64, Gulf of California. In *Initial Reports of the Deep Sea Drilling Project*. Vol. 64 Pt. 2 (eds. J.R. Curray, D.G. Moore et al.) pp. 675-694. U.S. Govt. Printing Office, Wasington.



- Gitlin, E. (1985) Sulfide remobilization during low temperature alteration of seafloor basalt. *Geochim Cosmochim Acta*. 49, 1567-1579.
- Goldschmidt V.M. (1968) *Geochemistry*. Oxford Clarendon Press, 730 p.
- Grinenko, V.A. (1962) Preparation of sulfur dioxide for isotopic analysis. *Zeits. Neorgan. Khimii*. 7, 2478-2483.
- Guilbert J.M. and Park C.F., Jr. (1986) *The Geology of Ore Deposits*. W.H. Freeman, 985 p.
- Hajash A. and Archer P. (1980) Experimental seawater/basalt interactions: effects of cooling. *Contrib. Mineral. Petrol.*, 75, 1-13.
- Hajash, A. and Chandler, G.W. (1981) An experimental investigation of high temperature interactions between seawater and rhyolite, andesite, basalt and peridotite. *Contrib. Min. Petrol.* 78, 240-254.
- Halbach, P., Hebisch, Udo, and Scherhag, C. (1981) Geochemical variations of ferromanganese nodules and crusts from different provinces of the Pacific Ocean and their genetic control. *Chem Geol.* 34, 3-17.
- Halbach, P. and Puteanus, D. (1984) The influence of the carbonate dissolution rate on the growth and composition of Co-rich ferromanganese crusts from Central Pacific seamount areas. *Earth Planet. Sci. Lett.* 68, 73-87.
- Harder, H. (1976) Nontronite synthesis at low temperatures. *Chem. Geol.* 18, 169-180.
- Hart, R.A. (1973) Geochemical and geophysical implications of the reaction between sea water and the oceanic crust. *Nature*, 243, 76-78.
- Haymon, R.M. (1983) Growth history of hydrothermal black smokers. *Nature* 301, 695-698.
- Haymon, R.M. and Kastner, M. (1981) Hot spring deposits on the East Pacific Rise at 21°N: preliminary description of mineralogy and genesis. *Earth Planet. Sci. Lett.* 53, 363-386.
- Haymon, R.M. and Kastner, M. (1986a) Caminite: A new magnesium-hydroxide-sulfate-hydrate mineral found in a submarine hydrothermal deposit, East Pacific Rise, 21°N. *Am. Min.* 71, 819-825.
- Haymon, R.M. and Kastner, M. (1986b) The formation of high temperature clay minerals from basalt alteration during hydrothermal discharge on the East Pacific Rise axis at 21°N. *Geochim Cosmochim Acta*, 50, 1933-1939.
- Hein, J.R., Manheim, F.T., Schwab, W.C. and Davis, A.S. (1988) Ferromanganese crusts from Necker Ridge, Horizon Guyot and S.P. Lee Guyot: Geological considerations. *Mar. Geol.* 78, 225-283.

- Hekinian R. (1982) Petrology of the ocean floor. Elsevier Scientific Publishing Co. 393p.
- Hekinian, R., Fevier, M., Bischoff, J.L., Picot, P., and Shanks, W.C. (1980) Sulfide deposits from the East Pacific Rise near 21°N. *Science* 207, 1433-1444.
- Hekinian, R. and Fouquet, Y. (1985) Volcanism and metallogenesis of axial and off-axial structures on the East Pacific Rise near 13°N. *Econ. Geol.* 80, 221-249.
- Hemley J.J., Montoya J.W., Marienko J.W. and Luce R.W. (1980) Equilibria in the system  $\text{Al}_2\text{O}_3\text{-SiO}_2\text{-H}_2\text{O}$  and some general implications for alteration processes. *Econ. Geol.* 75, 210-228.
- Herzig, P.M., Becker, K.P., Stoffers, P., Backer, H. and Blum, N. (1988) Hydrothermal silica chimney fields in the Galapagos Spreading Center at 86°W. *Earth Planet. Sci. Lett.* 89, 261-272.
- Hoffert, M. Perseil, A., Hékinian, R., Choukroume, P., Needham, H.D., Francheteau, J. and Le Pichon, X. (1977) Hydrothermal deposits samples by diving saucer in Transform Fault "A" near 37°N on the Mid-Atlantic Ridge, Famous area. *Oceanol. Acta.* 1, 73-86.
- Holland, H.D. and Malinin, S.D. (1979) The solubility and occurrence of non-ore minerals. In *Geochemistry of Hydrothermal Ore Deposits*, pp. 461-508, John Wiley, New York.
- Honnorez, J. (1980) The aging of the oceanic crust at low temperature. In: *The Sea* (ed. C. Emiliani) Vol. 7, Chap. 15 pp. 525-587. Wiley-Interscience.
- Howard, K.J. and Fisk, M.R. (1985) The effects of oxygen fugacity and alkali content on the formation of FeTi basalts. *EOS.* 67, 1283.
- Howard K.J. and Fisk, M.R. (1986) Hydrothermal precipitates from basalts on the Gorda Ridge and the President Jackson Seamounts. Oregon Department of Geology and Mineral Industries, Open-File Report 0-86-18.
- Howard, K.J. and Fisk, M.R. (1988) Hydrothermal alumina-rich clays and boehmite on the Gorda Ridge. *Geochim. Cosmochim. Acta.* 52, 2269-2279.
- Howard, K.J., Fisk, M.R. and Lyle, M. (1988) Weathered sulfide chimneys from the Escanaba Trough, Gorda Ridge. *EOS.* 69, 1484.
- Huang, P.Y. and Solomon, S.C. (1988) Centroid depths of mid-ocean ridge earthquakes: dependence on spreading rate. *J. Geophys. Res.* 93, 13445-13478.
- Humphries, S.E. and Thompson, G. (1978) Trace element mobility during hydrothermal alteration of oceanic basalts. *Geochim. Cosmochim. Acta.* 42, 127-136.
- Ingram-DePaolo, B.L. and Hein, J.R. (1988) Sr isotopes in hydrogenetic and hydrothermal Fe-Mn crusts. *EOS* 69, 1489.

- Janecky, D.R. and Seyfried, W.E. Jr. (1984) Formation of massive sulfide deposits on oceanic ridge crests: incremental reaction models for mixing between hydrothermal solutions and seawater. *Geochim. Cosmochim. Acta.* 48, 2723-2738.
- Jannash, H.W. (1983) Microbial processes at deep sea hydrothermal vents. In: *Hydrothermal Processes at Mid-Ocean Spreading Centers* (eds. P.A. Rona, K. Bostrom, L. Laubier and E.L. Smith) pp. 677-710.
- Karlin, R. and Lyle, M. (1989) History of Holocene volcanic and hydrothermal activity in axial valley sediments on the Gorda Ridge. *Marine Geology* (in press).
- Kennedy G.C. (1959) Phase relations in the system  $\text{Al}_2\text{O}_3\text{-H}_2\text{O}$  at high temperatures and pressures. *Am. Jour. Sci.* 257, 563-573.
- Kerridge, J.F., Haymon, R.M. and Kastner, M. (1983) Sulfur isotope systematics at the  $21^\circ\text{N}$  site, East Pacific Rise. *Earth Planet. Sci. Lett.* 66, 91-100.
- Kessman I. (1966) Zur hydrothermalen synthese von Brookit. *Zeitschrift fur anorganische und allgemeine Chemi.* 346, 30-43.
- Kimball, K.L. (1988) High-temperature hydrothermal alteration of ultramafic cumulates from the base of the Josephine Ophiolite, NW California. *J. Geophys. Res.* 93, 4675-4687.
- Klinkhammer, G. and Hudson, A. (1986) Dispersal patterns for hydrothermal plumes in the South Pacific using manganese as a tracer. *Earth Planet. Sci. Lett.* 79, 241-249.
- Koski, R.A., Clague, D.A. and Oudin, E. (1984) Mineralogy and chemistry of massive sulfide deposits from the Juan de Fuca Ridge. *Geol. Soc. Am. Bull.* 95, 930-945.
- Koski, R.A., Lonsdale, P.F., Shanks, W.C., Berndt, M.E. and Howe, S.S. (1985) Mineralogy and geochemistry of a sediment-hosted hydrothermal sulfide deposit from the southern trough of Guaymas Basin, Gulf of California. *J. Geophys. Res.* 90, 6695-6707.
- Koski, R.A., Shanks, W.C., III, Bohrsen, W.A. and Oscarson, R.L. (1988) The composition of sediment-hosted massive sulfide deposits from the Escanaba Trough, Gorda Ridge: Implications for fluid-sediment interaction and depositional processes. *Can. Min.* 26, 655-673.
- Krauskopf, K.B. (1957) Separation of manganese from iron in sedimentary processes. *Geochim. Cosmochim. Acta.* 12, 61-84.
- Krissen, S.A. and Scott, S.D. (1982) Phase relations involving pyrrhotite below  $350^\circ\text{C}$ . *Econ. Geol.* 77, 1739-1754.
- Kristmannsdottir H. (1977) Types of clay minerals in hydrothermally altered basaltic rocks, Reykjanes, Iceland. *Jökull.* 26, 30-39.

- Kvenholden, K.A., Rapp, J.B., Hostettler, F., Morton, J.L., King, J.D. and Claypool, G.E. (1986) Petroleum associated with polymetallic sulfide on the Gorda Ridge. *Science* 234, 1231-1234.
- Lister, C.R.B. (1983) The basic physics of water penetration into hot rock. In: *Hydrothermal Processes at Mid-Ocean Spreading Centers* (eds. P.A. Rona, K. Bostrom, L. Laubier and E.L. Smith) pp.141-168. Plenum Press.
- Lonsdale, P. (1977) Structural geomorphology of a fast-spreading rise crest, the East Pacific Rise near 3° 25'S. *Mar. Geophys. Res.* 3, 251-294.
- Lonsdale, P., Batiza, R. and Simkin, T. (1982) Metallogenesis at seamounts on the East Pacific Rise. *J. Mar. Technol. Soc.* 16, 54-61.
- Lonsdale, P.F., Bischoff, J.L., Burns, V.M., Kastner, M. and Sweeney, R.E. (1980) A high-temperature hydrothermal deposit on the seabed at a Gulf of California spreading center. *Earth Planet. Sci. Lett.* 49, 8-20.
- Loughnan, F.C. (1969) *Chemical weathering of the silicate minerals*. Elsevier, 154p.
- Lyle, M., Dymond, J. and Heath, G.R. (1977) Copper-nickel enriched ferromanganese nodules and associated crusts from the Bauer Basin, northwest Nazca plate. *Earth Planet. Sci. Lett.* 35, 55-64.
- Lyle, M. (1981) Formation and growth of ferromanganese oxides on the Nazca plate. In: *Geol Soc. Am. Mem.*
- Malahoff A., Embly R., Hammond S., Ryan W. and Crane K. (1982) Juan de Fuca and Gorda Ridge axial ridge morphology and tectonics from combined SEABEAM and SEA MARC data (abstr.). *EOS* 63,1147.
- Metz, S., Trefrey, J.H. and Nelsen, T.A. (1988) History and geochemistry of a metalliferous sediment core from the Mid-Atlantic Ridge at 26°N. *Geochim. Cosmochim. Acta.* 52, 2369-2378.
- Michard G., Albarede F., Michard A., Minster J.-F., Charlo J.-L. and Tan, N. (1984) Chemistry of solutions from the 13°N East Pacific Rise hydrothermal site. *Earth Planet Sci. Lett.* 67, 297-307.
- Moore, G.W. and Sharman, G.F. (1970) Summary of SCAN site 4: In McManus, D.A. et al., eds. *Initial Reports DSDP v.5*, U.S. Gov't Printing Office, Wa. 761-773.
- Morton, J.L., Holmes, M.L. and Koski, R.A. (1987) Volcanism and massive sulfide formation at a sedimented spreading center, Escanaba Trough, Gorda Ridge. *Geophys. Res. Lett.* 14, 769-772.
- Mottl, M.J. (1983) Hydrothermal processes at mid-ocean spreading centers: application of basalt-seawater experimental results. In: *Hydrothermal Processes at Mid-Ocean Spreading Centers* (eds. P.A. Rona, K. Bostrom, L. Laubier and E.L. Smith) pp. 199-224.

- Mottl, M.J. (1986) Chemical processes in submarine hydrothermal plumes near 21°N on the East Pacific Rise. *EOS* 67, 1027.
- Murowchick, J.B. and Barnes, H.L. (1986) Marcasite precipitation from hydrothermal solutions. *Geochim. Cosmochim. Acta.* 50, 2615-2629.
- Murnane, R. and Clague, D.A. (1983) Nontronite from a low-temperature hydrothermal system on the Juan de Fuca Ridge. *Earth Planet. Sci. Lett.* 65, 343-352.
- Northrup J., Menard H.W. and Duennebie F.K. (1968) Seismic and bathymetric evidence of a fracture zone on Gorda Ridge. *Science.* 161, 688-690.
- Norton, S.A. (1973) Laterite and bauxite formation. *Econ Geol.* 68, 353-361.
- Ohmoto, H. and Lasaga, A.C. (1982) Kinetics of reactions between aqueous sulfates and sulfides in hydrothermal systems. *Geochim. Cosmochim. Acta.* 46, 1727-1745.
- Ohmoto, H. and Rye, R.O. (1979) Isotopes of sulfur and carbon. In *Geochemistry of Hydrothermal Ore Deposits* (ed. H.L. Barnes) 2nd edn, pp. 509-567. Wiley.
- Oudin, E. (1983) Hydrothermal sulfide deposits of the East Pacific Rise (21°N) Part I: Descriptive mineralogy. *Mar. Min.* 4, 39-72.
- Oudin, E., Picot, P. and Poult, G. (1981) Comparison of sulfide deposits from the East Pacific Rise and Cyprus. *Nature* 291, 404-407.
- Perkin-Elmer (1982) Analytical methods for atomic absorption spectrophotometry. Perkin-Elmer Corporation, Norwalk, CT.
- Peterson C., Duncan R. and Scheidegger K. (1986) Sequence and longevity of basalt alteration at Deep Sea Drilling Project Site 597. In Leinen, M., Rea, D.K. et al., *Init Repts. DSDP, 92*: Washington (U.S. Govt. Printing Office), 505-515.
- Petersen, U. (1971) Laterite and bauxite formation. *Econ. Geol.* 66, 1070-1071.
- Rafal'skiy R.P. and Alekseyev V.A. (1986) Kinetics of reaction of silicates with aqueous solutions. *Geochemistry International.* 24, 68-77.
- Ramdohr, P. (1969) *The Ore Minerals and Their Intergrowths.* Pergamon, Oxford.
- Reeves, R.D. and Brooks, R.R. (1978) *Trace Element Analysis of Geologic Materials.* Wiley, New York. 421p.
- Riddihough, R.P. (1980) Gorda plate motions from magnetic anomaly analysis. *Earth Planet. Sci. Lett.* 51, 163-170.
- Riddihough R. (1984) Recent movements of the Juan de Fuca plate system. *J. Geophys. Res.* 89, 6980-6994.
- Robertson, A.H.F. and Boyle, J.F. (1983) Tectonic setting and origin of metalliferous sediments in the Mesozoic Tethys Ocean. In: *Hydrothermal Processes at Mid-Ocean*

- Spreading Centers (eds. P.A. Rona, K. Bostrom, L. Laubier and E.L. Smith) pp. 595-664.
- Rona P.A. and Clague D.A. (1986) Geologic setting of hydrothermal activity at the northern Gorda Ridge (abstr.), EOS 67, 1028.
- Rona, P.A. and Clague, D.A. (1989) Geologic control of hydrothermal discharge on the northern Gorda Ridge (in prep).
- Rona, P.A. and Gorda Ridge Technical Task Force Working Group B (1988) Hydrothermal activity on the Gorda Ridge. EOS 69, 1588.
- Rona, P.A., Klinkhammer, G., Nelsen, T.A., Trefrey, J.H. and Elderfield, H. (1986) Black smokers, massive sulfides and vent biota at the Mid-Atlantic Ridge. *Nature*, 321, 33-37.
- Rona, P.A., Thompson, G., Mottl, M.J., Karson, J.A., Jenkins, W.J., Graham, D., Mallette, M., Von Damm, K., and Edmond, J.M. (1984) Hydrothermal activity at the Trans-Atlantic Geotraverse Hydrothermal Field, Mid-Atlantic Ridge Crest at 26°N. *J. geophys. Res.* 89, 11365-11377.
- Rona, P.A., Widenfalk, L. and Bostrom, K. (1987) Serpentinized ultramafics and hydrothermal activity at the Mid-Atlantic Ridge crest near 15°N. *J. Geophys. Res.* 92, 1417-1427.
- Rosenbauer K.J. and Bischoff J.L. (1983) Uptake and transport of heavy metals by heated seawater: a summary of the experimental results. In: *Hydrothermal Processes at Seafloor Spreading Centers* (eds. P.A. Rona, K. Bostrom, L. Laubier and E.L. Smith), Plenum Press, 177-198. .
- Sakai, H., Des Marais, D.J., Ueda, A. and Moore, J.G. (1984) Concentrations and isotope ratios of carbon, nitrogen and sulfur in ocean-floor basalts. *Geochim. Cosmochim. Acta.* 48, 2433-2441.
- Sakai, H., Gunnlaugsson, E., Tomasson, J. and Rouse, J.E. (1980) Sulfur isotope systematics in Icelandic geothermal systems and the influence of seawater circulation at Reykjanes. *Geochim. Cosmochim. Acta.* 44, 1223-1231.
- Scheidegger, K.F. and Stakes, D.S. (1978) X-ray diffraction and chemical study of secondary minerals from DSDP Leg 51, Sites 417A and 417D. p. 1253-1263. In: T. Donnelly, J. Francheteau, W. Bryan, P. Robinson, M. Flower, M. Salisbury, et al., *Initial Reports of the Deep Sea Drilling Project*, v. 51,52,53, Part 2: Washington (U.S. Government Printing Office).
- Scott, S.D. and Barnes, H.L. (1971) Sphalerite geothermometry and geobarometry. *Econ Geol.* 66, 653-669.
- Scott, S.D. and Barnes, H.L. (1972) Sphalerite-wurtzite equilibria and stoichiometry. *Geochim. Cosmochim. Acta.* 36, 1275-1295.

- Scott, M.R., Scott, R.B., Morse, J.W., Betzer, P.R., Butler, L.W. and Rona, P.A. (1978) Metal enriched sediments from the TAG Hydrothermal Field. *Nature*. 276, 811-813.
- Seyfried W.E. Jr. and Bischoff J.L. (1981) Experimental seawater-basalt interaction at 300°C, 500 bars, chemical exchange, secondary mineral formation and implications for the transport of heavy metals. *Geochim. Cosmochim. Acta*. 45, 135-147.
- Seyfried, W.E. and Dibble, W.E. Jr. (1980) Seawater-peridotite interaction at 300°C and 500 bars: implications for the origin of oceanic serpentinites. *Geochim. Cosmochim. Acta* 44, 309-321.
- Seyfried, W.E. Jr., and Janecky, D.R. (1985) Heavy metal and sulfur transport during subcritical and supercritical hydrothermal alteration of basalt: Influence of fluid pressure and basalt composition and crystallinity. *Geochim. Cosmochim. Acta* 49, 2545-2560.
- Seyfried, W.E. Jr. and Janecky, D.R. (1986) Chloride depletions and enrichments in seafloor hydrothermal fluids: constraints from experimental basalt studies. *Geochim. Cosmochim. Acta*. 49, 2545-2560.
- Seyfried, W.E. Jr. and Mottl, M.J. (1982) Hydrothermal alteration of basalt by seawater under seawater-dominated conditions. *Geochim. Cosmochim. Acta*. 46, 985-1002.
- Shanks, W.C. III, Bischoff, J.L. and Rosenbauer, R.J. (1981) Seawater sulfate reduction and sulfur isotope fractionation in basaltic systems: interaction of seawater with fayalite and magnetite at 200° - 350°C. *Geochim. Cosmochim. Acta*. 45, 1977-1995.
- Shanks, W.C. III and Seyfried, W.E. Jr. (1987) Stable isotope studies of vent fluids and chimney minerals, southern Juan de Fuca Ridge: sodium metasomatism and seawater sulfate reduction. *J. Geophys. Res.* 92, 11,387-11,399.
- Shelley D., Smale D. and Tullock A.J. (1977) Boehmite in syenite from New Zealand. *Min Mag.* 41, 398-400.
- Sillitoe, R.H. and Clark, A.H. (1969) Copper and copper-iron sulfides as initial products of supergene oxidation, Copiapo mining district, northern Chile. *Am. Min.* 54, 1684-1710.
- Singer, A. and Stoffers, P. (1981) Hydrothermal vermiculite from the Atlantis II Deep, Red Sea. *Clays and Clay Min.* 29, 454-458.
- Sleep, N.H. (1983) Hydrothermal convection at ridge axes. In: *Hydrothermal Processes at Mid-Ocean Spreading Centers* (eds. P.A. Rona, K. Bostrom, L. Laubier and E.L. Smith) pp. 71-82.
- Solano, A.E. (1984) Crustal Structure and Seismicity of the Gorda Ridge. PhD thesis Oregon State Univ. Corvallis, OR. 185p.

- Spiess, F.N., Macdonald, K.C., Atwater, T., Ballard, R., Carranza, A., Cordoba, D., Cox, C., Diaz-Garcia, V., Francheteau, J., Guerrero, J., Hawkins, J., Haymon, R., Hessler, R., Juteau, T., Kastner, M., Larson, R., Luyendyk, B., Macdougall, J., Miller, S., Normark, W., Orcutt, J. and Rangin, C. (1980) East Pacific Rise: Hot springs and geophysical experiments. *Science*. 207, 1421-1433.
- Starkey, H.C., Blackmon, P.D. and Hauff, P.L. (1984) The routine mineralogical analysis of clay-bearing samples. U.S. Geol. Survey Bull. 1563. U.S. Government Printing Office, Washington.
- Stumm, W. and Morgan, J.J. (1981) *Aquatic Chemistry* 2nd ed. 780pp. J. Wiley and Sons, New York, N.Y.
- Styrt, M.M., Brackman, A.J., Holland, H.D., Clark, B.C., Pisutha-Arnand, V., Eldridge, C.S., and Ohmoto, H. (1981) The mineralogy and isotopic composition of sulfur in hydrothermal sulfide/sulfate deposits on the East Pacific Rise, 21°N latitude. *Earth Planet. Sci. Lett.* 53, 382-390.
- Sumi K. (1968) Hydrothermal rock alteration of the Matsukawa geothermal area northeast Japan. *Geol. Survey Japan. Report No. 225*, 42 p.
- Sumi K. and Takashima I. (1976) Absolute ages of the hydrothermal alteration halos and associated volcanic rocks in some Japanese geothermal fields. *Proc. 2nd U.N. Symp. Dev. Use Geotherm. Resour.* 1975, 1:625-34. San Francisco: United Nations, 844 p.
- Tettenhorst R. and Hofman D.A. (1980) Crystal chemistry of boehmite. *Clays. Clay Min.* 28, 373-380.
- Thode, H.G., Monster, J. and Dunford, H.B. (1961) Sulfur isotope geochemistry. *Geochim. Cosmochim. Acta.* 25, 159-174.
- Thompson, G. (1983) Basalt-seawater interaction. In: *Hydrothermal Processes at Mid-Ocean Spreading Centers* (eds. P.A. Rona, K. Bostrom, L. Laubier and E.L. Smith) pp. 225-278.
- Thompson, G., Mottl, M.J. and Rona, P.A. (1985) Morphology, mineralogy and chemistry of hydrothermal deposits from the TAG area, 26°N Mid-Atlantic Ridge. *Chem. Geol.* 49, 243-257.
- Tivey, M.K. and Delaney, J.R. (1986) Growth of large sulfide structures on the Endeavor segment of the Juan de Fuca Ridge. *Earth. Planet. Sci. Lett.* 77, 303-317.
- Tole M.P. (1987) Thermodynamic and kinetic aspects of formation of bauxites. *Chem. Geol.* 60, 95-100.
- Tomasson, J. and Kristmannsdottir, K. (1972) High temperature alteration minerals and thermal brines, Reykjanes, Iceland. *Contrib. Min. Petrol.* 36, 123-134.
- Toth, J.R. (1980) Deposition of submarine crusts rich in manganese and iron. *Geol. Soc. Am. Bull.* 91, 44-54.



- Turekian, K.K. and Wedepohl, K.H. (1961) Distribution of the elements in some major units of the earth's crust. *Geol. Soc. Am. Bull.* 72, 175-192.
- Valeton, I. (1972) *Bauxites*. Elsevier. 226pp.
- Vallier-Silver, J.N., Tera, F., Klein, J. and Middleton, R. (1987) Beryllium 10 in hydrothermal vent deposits from the East Pacific Ridges: Role of sediments in the hydrothermal processess. *J. Geophys. Res.* 92, 11,364-11,372.
- Varekamp, J.C. and Buseck, P.R. (1984) The speciation of mercury in hydrothermal systems with applications to ore deposition. *Geochim. Cosmochim. Acta.* 48, 177-185.
- Von Damm, K.L. and Bischoff, J.L. (1987) Chemistry of hydrothermal solutions from the southern Juan de Fuca Ridge. *J. Geophys. Res.* 92, 11334-11346.
- Von Damm, K.L., Edmonds, J.M., Grant, B., Measures, C.I., Walden, B. and Weiss, R.F. (1985a) Chemistry of submarine hydrothermal solutions at 21°N, East Pacific. *Geochim. Cosmochim. Acta.* 49, 2197-2220.
- Von Damm, K.L., Edmond, J.M., Measures, C.I. and Grant, B. (1985b) Chemistry of submarine hydrothermal solutions at Guaymas Basin, Gulf of California. *Geochim. Cosmochim. Acta.* 49, 2221-2237.
- Von Damm, K.L., Grant, B. and Edmond, J.M. (1983) Preliminary report on the chemistry of hydrothermal solutions at 21°North, East Pacific Rise. In: *Hydrothermal Processes at Seafloor Spreading Centers* (eds. P.A. Rona, K. Bostrom, L. Laubier and E.L. Smith), pp. 369-389. Plenum Press.
- Wakeham, S.E. (1977) Petrochemical patterns in young pillow basalts dredged from the Juan de Fuca and Gorda ridges, M.S. thesis, Oregon State Univ., Corvallis.
- Wilde, P., Chase, T.E., Holmes, M.L., Normark, W.R., Tomas, J.A., McCulloch, D.S., and Kulm, L.D. (1978) Oceanographic data off northern California - southern Oregon, 40° to 43° North including the Gorda Deep Sea Fan. LBL Publ. 251, Lawrence Berkeley Lab. Berkeley, Calif.
- Wilde, P., Chase, T.E., Holmes, M.L., Normark, W.R., Tomas, J.A., McCulloch, D.S., Carlson, P.R., Kulm, L.D. and Young, J.D. (1979) Oceanographic data off Oregon 43° to 46° North including Astoria Deep-Sea Fan. LBL Publ. 253, Lawrence Berkeley Lab, Berkeley, Calif.
- Williams, D. L., Green, K., van Andel, T-j H., Von Herzen, R.P., Dymond, J.R. and Crane, K. (1979) The hydrothermal mounds of the Galapagos Rift: Observations with DSRV Alvin and detailed heat flow studies. *J. Geophys. Res.* 84, 7467-7484.
- Wolska E. and Szajda W. (1980) Die bildung von kristallinem bohmit in gemeinsam gefallten AlFe(III)-Hyroxiden unter hydrothermalen bedingungen. *Monatshefte fur Chemie* 111, 1329-1334.

- Yang H.-Y. (1987) Stability of ilmenite and titanomagnetite in the presence of carbon dioxide - a thermodynamic evaluation. *Contrib. Mineral. Petrol.* 95, 202-206
- Zierenberg, R.A. and Koski, R.A., Shanks, W.C.III and Rosenbauer, R.J. (1986) Form and composition of sediment-hosted sulfide-sulfate deposits, Escanaba Trough, southern Gorda Ridge (abs): *EOS Transactions Am Geophys. Union* 67, 1282.
- Zierenberg, R.A., Shanks, W.C. III and Bischoff, J.L. (1984) Massive sulfide deposits at 21°N, East Pacific Rise: Chemical composition, stable isotopes and phase equilibria. *Geol. Soc. Am. Bull.* 95, 922-929.

## APPENDICES

**APPENDIX I**  
**Correlation Matrices**

Set I (a): Correlation matrix for Gorda Ridge axis and off axis samples and President Jackson Seamount samples.

	Ca	Cu	Fe	K	Mg	Mn	Na	Ni	Si	Ti	Zn	Depth	Age
Al	0.65	-0.25	-0.68	-0.50	0.16	-0.47	0.19	-0.42	0.21	0.77	-0.29	0.36	-0.57
Ca		-0.08	-0.47	-0.54	0.23	-0.31	0.29	-0.35	0.11	0.57	-0.23	0.40	-0.48
Cu			0.37	0.13	-0.11	0.32	0.20	0.39	-0.42	-0.20	0.14	-0.07	0.22
Fe				0.60	-0.32	0.28	0.07	0.28	-0.48	-0.59	0.04	-0.64	0.76
K					-0.36	0.26	0.02	0.32	-0.21	-0.54	0.17	-0.39	0.51
Mg						-0.28	-0.14	-0.30	0.04	0.31	-0.15	0.65	-0.45
Mn							0.25	0.96	-0.67	-0.37	0.94	-0.18	0.06
Na								0.17	-0.48	-0.07	0.18	-0.08	-0.20
Ni									-0.64	-0.32	0.91	-0.16	0.03
Si										0.16	-0.57	0.13	-0.05
Ti											-0.23	0.51	-0.62
Zn												0.02	-0.15
Depth													-0.80

Set I (b): Correlation matrix for Gorda Ridge axis and off axis samples.

	Ca	Cu	Fe	K	Mg	Mn	Na	Ni	Si	Ti	Zn	Depth	Age
Al	0.60	-0.57	-0.70	-0.66	-0.11	-0.58	-0.06	-0.55	0.52	0.77	-0.51	0.11	-0.11
Ca		-0.48	-0.37	-0.57	0.05	-0.38	0.17	-0.43	0.29	0.39	-0.36	0.11	-0.41
Cu			0.57	0.64	-0.13	0.78	0.34	0.77	-0.85	-0.64	0.78	-0.30	0.59
Fe				0.80	-0.04	0.30	0.37	0.33	-0.38	-0.53	0.22	-0.14	0.42
K					-0.39	0.51	0.39	0.53	-0.40	-0.60	0.43	-0.45	0.71
Mg						-0.32	-0.30	-0.36	0.07	0.11	-0.26	0.76	-0.59
Mn							0.26	0.97	-0.81	-0.62	0.98	-0.33	0.41
Na								0.16	-0.42	-0.46	0.17	-0.47	0.38
Ni									-0.73	-0.52	0.96	-0.41	0.50
Si										0.66	-0.81	0.12	-0.33
Ti											-0.52	0.11	-0.21
Zn												-0.27	0.38
Depth													-0.81

Set I (c): Correlation matrix for President Jackson Seamount samples.

	Ca	Cu	Fe	K	Mg	Mn	Na	Ni	Si	Ti	Zn	Depth	Age
Al	0.61	-0.10	-0.47	-0.10	0.50	-0.30	0.60	-0.21	-0.11	0.59	-0.04	0.24	-0.68
Ca		0.18	-0.45	-0.46	0.74	-0.05	0.48	-0.11	-0.13	0.76	0.10	0.57	-0.88
Cu			0.25	-0.09	0.13	0.48	0.34	0.65	-0.40	0.04	0.16	0.31	-0.03
Fe				0.26	-0.33	0.63	0.08	0.64	-0.72	-0.31	0.49	-0.41	0.62
K					0.03	-0.03	-0.22	0.19	-0.10	-0.28	0.13	0.10	0.32
Mg						-0.14	0.15	0.00	-0.08	0.51	0.15	0.60	-0.80
Mn							0.27	0.87	-0.78	0.25	0.82	-0.17	0.11
Na								0.25	-0.63	0.38	0.20	-0.10	-0.32
Ni									-0.77	0.05	0.78	0.00	0.08
Si										-0.30	-0.75	0.16	-0.01
Ti											0.41	0.44	-0.72
Zn												0.04	-0.19
Depth													-0.56

Set II (a): Correlation matrix for Gorda Ridge axis and off axis samples and President Jackson Seamount samples minus samples with undetermined elements.

	Ba	Ca	Co	Cu	Fe	K	Li	Mg	Mn	Na	Ni	Rb	Si	Sr	Ti	Zn	Depth	Age
Al	-0.27	0.83	-0.41	-0.21	-0.62	-0.38	-0.09	0.63	-0.42	0.24	-0.39	-0.12	0.09	-0.42	0.76	-0.24	0.46	-0.55
Ba		-0.35	0.10	-0.01	0.00	0.38	0.61	-0.30	0.68	0.28	0.66	0.14	-0.39	0.56	-0.12	0.64	0.10	-0.26
Ca			-0.19	0.00	-0.55	-0.53	-0.23	0.71	-0.32	0.26	-0.32	-0.42	-0.02	-0.23	0.77	-0.19	0.52	-0.57
Co				0.71	0.63	0.02	-0.11	-0.38	0.32	0.06	0.29	-0.19	-0.53	0.69	-0.10	0.03	-0.42	0.48
Cu					0.31	0.01	0.06	-0.07	0.27	0.20	0.35	-0.10	-0.40	0.26	-0.13	0.09	0.05	0.15
Fe						0.40	-0.19	-0.49	0.08	-0.04	0.10	0.39	-0.42	0.40	-0.47	-0.15	-0.62	0.71
K							0.26	-0.21	0.03	-0.15	0.10	0.75	-0.04	-0.05	-0.36	0.00	-0.08	0.33
Li								-0.06	0.75	0.14	0.78	0.11	-0.42	0.14	-0.19	0.86	0.17	-0.24
Mg									-0.27	0.13	-0.19	-0.21	0.02	-0.31	0.63	-0.12	0.60	-0.67
Mn										0.22	0.97	-0.27	-0.67	0.67	-0.22	0.94	0.04	-0.15
Na											0.22	0.00	-0.49	0.29	0.23	0.20	0.24	-0.50
Ni												-0.17	-0.69	0.59	-0.25	0.92	0.10	-0.18
Rb													0.10	-0.34	-0.42	-0.26	-0.27	0.36
Si														-0.69	-0.10	-0.56	0.02	0.10
Sr															0.03	0.44	-0.20	0.02
Ti																-0.14	0.48	-0.57
Zn																	0.21	-0.32
Depth																		-0.80



Set II (b): Correlation matrix for axis and off axis samples minus samples with undetermined elements.

	Ba	Ca	Co	Cu	Fe	K	Li	Mg	Mn	Na	Ni	Rb	Si	Sr	Ti	Zn	Depth	Age
Al	-0.81	0.95	-0.73	-0.72	-0.74	-0.87	-0.54	0.59	-0.70	-0.64	-0.71	-0.56	0.62	-0.84	0.85	-0.60	0.63	-0.66
Ba		-0.79	0.80	0.57	0.39	0.62	0.61	-0.90	0.79	0.51	0.75	0.30	-0.57	0.87	-0.76	0.71	-0.33	0.33
Ca			-0.66	-0.57	-0.69	-0.88	-0.49	0.60	-0.62	-0.49	-0.64	-0.58	0.47	-0.78	0.80	-0.51	0.64	-0.66
Co				0.61	0.33	0.37	0.58	-0.65	0.84	0.37	0.85	-0.01	-0.80	0.96	-0.70	0.75	-0.27	0.30
Cu					0.37	0.40	0.76	-0.35	0.81	0.30	0.83	0.08	-0.85	0.66	-0.76	0.79	-0.51	0.52
Fe						0.81	-0.09	-0.30	0.10	0.76	0.14	0.77	-0.19	0.51	-0.57	-0.03	-0.46	0.52
K							0.25	-0.42	0.33	0.63	0.34	0.87	-0.21	0.55	-0.68	0.23	-0.50	0.54
Li								-0.41	0.91	0.02	0.89	-0.13	-0.80	0.51	-0.55	0.95	-0.29	0.25
Mg									-0.59	-0.47	-0.53	-0.18	0.37	-0.70	0.62	-0.52	0.13	-0.11
Mn										0.17	0.99	-0.12	-0.90	0.80	-0.68	0.98	-0.36	0.35
Na											0.14	0.65	-0.20	0.47	-0.53	0.08	-0.26	0.32
Ni												-0.12	-0.93	0.81	-0.67	0.97	-0.42	0.41
Rb													0.21	0.19	-0.45	-0.22	-0.26	0.31
Si														-0.73	0.58	-0.90	0.30	-0.31
Sr															-0.78	0.68	-0.42	0.44
Ti																-0.58	0.47	-0.51
Zn																	-0.30	0.27
Depth																		-0.99

Set II (c): Correlation matrix for President Jackson Seamount samples.

	Ba	Ca	Co	Cu	Fe	K	Li	Mg	Mn	Na	Ni	Rb	Si	Sr	Ti	Zn	Depth	Age
Al	0.35	0.52	-0.22	-0.09	-0.36	0.10	0.62	0.38	-0.25	0.64	-0.13	0.54	-0.20	-0.18	0.49	-0.06	-0.04	-0.63
Ba		0.22	0.12	-0.10	-0.12	0.41	0.62	0.39	0.39	0.07	0.43	0.18	-0.30	0.39	0.63	0.68	0.22	-0.65
Ca			0.29	0.31	-0.15	-0.17	0.02	0.62	0.16	0.72	0.13	-0.06	-0.41	0.26	0.57	0.11	0.07	-0.73
Co				0.73	0.50	-0.28	-0.27	-0.02	0.90	0.36	0.75	-0.64	-0.68	0.82	0.47	0.55	0.05	-0.02
Cu					0.27	-0.11	-0.04	0.17	0.49	0.34	0.67	-0.25	-0.40	0.24	0.07	0.16	0.47	-0.07
Fe						0.04	-0.15	-0.10	0.62	0.10	0.62	-0.08	-0.73	0.47	-0.01	0.59	-0.09	0.44
K							0.63	0.37	-0.15	-0.25	0.09	0.65	-0.02	-0.29	0.03	0.17	0.71	-0.03
Li								0.39	-0.10	0.20	0.24	0.75	-0.17	-0.28	0.16	0.29	0.38	-0.47
Mg									-0.03	0.17	0.16	0.31	-0.20	-0.08	0.27	0.15	0.39	-0.72
Mn										0.27	0.86	-0.52	-0.78	0.91	0.49	0.85	-0.04	-0.06
Na											0.26	0.03	-0.64	0.27	0.47	0.20	-0.15	-0.44
Ni												-0.15	-0.76	0.61	0.27	0.81	0.26	-0.15
Rb													0.05	-0.64	-0.15	-0.12	0.35	-0.13
Si														-0.68	-0.53	-0.77	0.05	0.17
Sr															0.67	0.75	-0.25	-0.10
Ti																0.50	-0.01	-0.50
Zn																	0.01	-0.24
Depth																		-0.01

## APPENDIX II

1. Description of Escanaba Trough Sulfide Chimneys.
2. Selected X-Ray Diffractograms.
3. Description of SEM Results.

## Appendix II-1

## Description of Escanaba Trough massive sulfide deposits.

---



---

Sample: 658

Weight: 9g

Size: 3.5cm x 2.5cm x 1cm

## Description:

Massive sulfide weathered to grey clay speckled with quartz and pyrrhotite. Fe oxyhydroxides especially prominent on one side of sample indicate surface exposed to seawater. Sugary texture.

Color:<sup>1</sup> (2 subsamples)Mineralogy:<sup>2</sup>

- |   |   |   |
|---|---|---|
| 1 | Interior:<br>Massive sulfide weathered to very light grey (N8) clay with sugary texture and Fe oxyhydroxides. Speckled with black and yellow sulfide crystals and clear quartz. | mixed-layer clay<br>quartz<br>plagioclase<br>sphalerite?<br>pyrrhotite? |
| 2 | Exterior:<br>Thin coating, more Fe-stained  | mixed-layer clays<br>quartz<br>plagioclase<br>gypsum?                   |

---



---

Sample: 658-R1-1A

Weight: 46g

Size: 5.2cm x 4.0cm x 1.0cm

## Description:

Large pyrrhotite crystals (up to 1mm x 0.2mm) in blocky texture surrounded by Fe oxyhydroxides indicate chimney channelways. These change abruptly to finer grained pyrrhotite with spidery texture. Small blades of barite (0.2mm x 0.01mm) are dispersed throughout. Minor white material in surficial veins and cavities gave no XRD pattern and is tentatively identified as amorphous silica. Dark grey hexagonal plates suggest the presence of trace wurtzite, but could be surficially altered pyrrhotite.

Color: (2 subsamples)

Mineralogy:

- |   |  |  |
|---|--|--|
| 1 | Exterior: (altered)<br>blackish red (5R 2/2), dusky red (5R 3/4) to moderate reddish brown (10R 4/6), crusty material with large (0.5 mm) sulfides. White barite crystals in veins and cavities. | barite<br>pyrrhotite<br>sphalerite<br>chalcopyrite/iss |
|---|--|--|

- |   |  |  |
|---|--|--|
| 2 | Interior:<br>brownish black (5YR 2/1) to dark<br>grey (N3), with yellow hexagonal<br>pyrrhotite. | pyrrhotite<br>sphalerite<br>chalcopyrite/iss<br>barite<br>marcasite* |
|---|--|--|

Sample: 658-R2-B (Barite chimney)

Weight: 64g

Size: 10cm x 2.5cm x 1.5cm

**Description:**

Ivory colored barite blades with no apparent directional fabric average 0.2mm x 0.005mm in very open structure with interstitial amorphous Fe oxyhydroxides. The sample surface is coated with brown-black amorphous Mn-oxide. Bits of platy sulfides (pyrrhotite) are scattered throughout.

Color: (2 subsamples)

Mineralogy:

- |   |  |   |
|---|--|---|
| 1 | Exterior: (altered)<br>Greyish black (N2) coating of Mn<br>oxide with bits of dark yellowish<br>orange (10YR 6/6) Fe oxyhydrox-<br>ides. | amorphous Mn oxide<br>with trace barite,<br>goethite and<br>lepidocrosite |
| 2 | Interior:<br>Grey to yellowish grey (5Y 7/2)<br>porous barite.   | barite<br>cinnabar*   |

Sample: 658-R3-A (iron oxide from pyrrhotite clast)

Weight: 113g

Size: 10cm x 2cm x 2cm

**Description:**

Dominantly pyrrhotite with interstitial amorphous Fe oxyhydroxides and goethite. Very dense fine-grained massive region abruptly changes to 5mm wide more open cross-hatched, coarse pyrrhotite crystals (up to 1mm) representing chimney channelway. Minor surficial white granules are probably amorphous silica.

Color: (2 subsamples)

Mineralogy:

- |   |   |   |
|---|---|---|
| 1 | Exterior: (altered)<br>Moderate reddish orange (10R 6/6)<br>to moderate reddish brown (10R 4/6)<br>mixed with blackish red (5R 2/2)<br>or brownish black (5YR 2/1). | sphalerite<br>barite<br>hematite<br>goethite<br>amorphous silica? |
|---|---|---|

- 2 Interior:  
blackish red (5R 2/2) or brownish  
black (5YR 2/1).
- pyrrhotite  
barite  
sphalerite  
gypsum?  
chalcopyrite?  
cubanite\*  
Ni,Cu,Zn sulfide\*  
galena\*  
bismuth telluride\*

Sample: 658-R4-1A  
Weight: 64g  
Size: 7cm x 3cm x 2cm

Description:

Dense, surficially weathered massive pyrrhotite. Hexagonal plates of pyrrhotite line cavities and parallel lenses suggest either bedding planes or filled chimney channelways. In detail, coarser grained (0.4mm x 0.1mm) pyrrhotite is frequently pitted and fractured compared to finer grained (0.2mm x 0.05mm) pyrrhotite. Interstitial goethite is ubiquitous.

Color: (2 subsamples)

Mineralogy:

- |   |   |  |
|---|---|--|
| 1 | Interior:<br>brownish black (5YR 2/1)   | goethite<br>pyrrhotite<br>marcasite*<br>chalcopyrite<br>cubanite?<br>sulfur<br>lepidocrosite |
| 2 | Exterior: (altered)<br>greyish red purple (5RP 4/2) to<br>dusky blue (5PB 3/2) with stains of<br>moderate red (5R 4/6). | goethite<br>pyrrhotite<br>chalcopyrite<br>lepidocrosite<br>sulfur                            |

Sample: 659  
Weight: a) 0.8g                      Size: a) 2cm x 1.5cm x 2mm  
              b) 0.5g                      b) 2cm x 1cm x 3mm

Description/Color:

Light brown (5YR 5/6) fine-grained, non-porous, highly altered thin wafer. Exterior caked with amorphous Fe oxyhydroxide with resinous luster and scattered specks of black and yellow sulfides (< 0.1mm) surrounds core of solid black material.

Mineralogy: clays and amorphous material.

---

Sample: 659-2  
 Weight: 38g  
 Size: 5cm x 3cm x 1.5cm

Description:

Highly weathered massive sulfide. One side is weathered to powdery Fe oxyhydroxides. The other side is coated with bubbly, resinous Fe oxyhydroxide. White barite crystals are interspersed on the exterior. Pyrrhotite crystals are up to 2mm size in coarse-grained chimney channel-flow-zones. Cubic galena and hexagonal pyrrhotite crystals could be identified on one external surface.

Color: (3 subsamples)

Mineralogy:

- |   |  |  |
|---|--|--|
| 1 | Exterior: (altered)<br>Moderate brown (5YR 3/4) to dark yellowish brown (10YR 4/2), mottled with moderate reddish brown (10YR 4/6) | barite<br>pyrrhotite<br>galena   |
| 2 | Interior:<br>brownish black (5YR 2/1) to black (N1)  | pyrrhotite<br>sphalerite<br>barite<br>chalcopyrite<br>galena<br>cassiterite* |
| 3 | Exterior: (altered)<br>bubbly, resinous Fe oxyhydroxide<br>moderate red (5R 5/4) to pale reddish brown (10R 5/4)                   | pyrrhotite<br>sphalerite<br>chalcopyrite                                     |

---

Sample: 659-3  
 Weight: 23g  
 Size: 3.5cm x 2.5cm x 1.0cm

Description:

Layered interior with one section more massive, finer grained sphalerite-rich and one more porous section with larger pyrrhotite in interlocking texture. Small cavity on one exterior surface contains cubes of galena.

Color: (3 subsamples)

Mineralogy:

- |   |                                       |  |
|---|---------------------------------------|--|
| 1 | Interior:<br>brownish black (5YR 2/1) | pyrrhotite<br>sphalerite<br>chalcopyrite<br>cubanite<br>galena*<br>arsenopyrite* |
|---|---------------------------------------|--|

- |   |   |  |
|---|---|--|
| 2 | Exterior: (altered)<br>dusky yellowish brown (10YR 2/2) to<br>moderate yellowish brown (10YR 5/4)<br>with patches of (about 1mm <sup>2</sup> ) very light<br>grey (N8). | pyrrhotite<br>sphalerite<br>chalcopyrite<br>sulfur |
| 3 | Similar to 2 but more altered   | barite<br>sphalerite<br>chalcopyrite               |

Sample: 659-R1

Weight: 0.6g (aggregate)

Sizes: nine small fragments up to 1cm x 1mm.

Description:

Samples were separated by color.

Color: (2 subsamples)

Mineralogy:

- |   |  |                                  |
|---|--|----------------------------------|
| 1 | Dark yellowish orange (10YR 6/6)<br>Fe staining  | goethite<br>akaganéite?<br>clays |
| 2 | Dark brownish black (5YR 2/1) sulfide<br>rich with bits of Fe staining and light<br>grey (N7) to greyish orange (10YR 7/4)<br>tinted clay. | pyrrhotite<br>sphalerite<br>clay |

Sample: 659-R1-F

Weight: 32g

Size: 4.5cm x 4.0cm x 2.0cm

Description:

Granular, crystalline texture in brownish black sulfide rich region grading into a finer grained brown, dusky powdery region. Petroliferous odor. Surficially, dark yellowish brown (10YR 4/2) with occasional dark yellowish orange (10YR 6/6) Fe-stains.

Color: (4 subsamples)

Mineralogy:

- |   |   |  |
|---|---|--|
| 1 | Exterior: (altered)<br>Fe oxyhydroxide stains, bright orange<br>with bits of black sulfides.  | goethite<br>lepidocrocite                |
| 2 | Interior:<br>granular, brownish black (5YR 2/1)<br>sulfide rich speckled with yellow sulfides | pyrrhotite<br>sphalerite<br>chalcopyrite |



- |   |  |  |
|---|--|--|
| 3 | Exterior: (altered)<br>dusky yellowish brown (10YR 2/2)<br>coating, very thin and unavoidably<br>partially mixed with (2). | sphalerite<br>chalcopyrite<br>pyrrhotite<br>marcasite?<br>arsenopyrite<br>sulfur<br>akaganéite |
| 4 | Interior:<br>brownish black (5YR 2/1) beneath dusky<br>brown (3) above.  | sphalerite<br>chalcopyrite<br>sulfur<br>akaganéite   |

Sample: 661-R1

Weight: 1.6g

Size: 4cm x 2.5cm x 2mm

Description/Color: (2 subsamples)

Mineralogy:

- |   |   |  |
|---|---|--|
| 1 | About 1mm thick caked on light brown<br>(5YR 5/6) Fe stained.   | mixed-layer clay<br>(chlorite/smectite)<br>goethite<br>akaganéite<br>quartz<br>plagioclase |
| 2 | Dark yellowish orange (10YR 6/6)<br>and minor very pale orange<br>(10YR 8/2) with speckled sulfides<br>(yellow and black), core of shiny black<br>material. | mixed-layer clay<br>goethite<br>akaganéite<br>quartz<br>plagioclase                        |

Sample: 661-R1

Weight: a) 15g  
b) 8g

Size: a) 6cm x 3.5cm x 5mm  
b) 4cm x 3cm x 3mm

Description/Color: (4 subsamples)

Mineralogy:

- |   |  |   |
|---|--|---|
| 1 | Exterior: (altered)<br>moderate reddish brown (10YR 4/6)   | barite<br>goethite<br>sphalerite<br>mixed-layer clay<br>galena<br>pyrite? |
| 2 | Exterior: (altered)<br>sugary white material stained to greyish<br>orange (10YR 7/4) Fe oxyhydroxides. | barite<br>galena<br>amorphous silica                                      |

		cassiterite*
3	Interior: dark grey (N3) platy sulfides and rounded bubbly white material.	pyrite sphalerite barite (trace)
4	Interior: dark grey (N3).	sphalerite barite (trace)

---

Sample: 662  
 Weight: a) 15g                      Size: a) 6cm x 3.5cm x 5mm  
               b) 8g                        b) 4cm x 3cm x 3mm

Description/Color (4 subsamples)	Mineralogy:
1      Exterior (a): (altered) moderate reddish brown (10R 4/6)	barite goethite pyrite sphalerite clay galena
2      Exterior (b): (altered) sugary white material stained to greyish orange (10YR 7/4) Fe oxyhydroxides.	barite cassiterite galena amorphous silica
3      Interior (a): dark grey (N3) platy sulfides and rounded bubbly white material.	pyrite sphalerite barite (trace)
4      Interior (b): dark grey (N3).	sphalerite barite (trace)

---

Sample: 662-R1  
 Weight: 116g  
 Size: 7cm x 5.5cm x 3.5cm

Description/Color: (2 subsamples)	Mineralogy:
1      Exterior: (altered) Mostly greyish red (5R 4/2) with patches of blackish red (5R 2/2) and very dusky red (10YR 2/2) Fe stained, earthy, moist pasty region. Petroliferous odor. Specks of gold sulfides throughout.	sphalerite chalcopyrite lepidocrocite
2      Interior: Brownish black (5YR 2/1) with still lots of blackish red (5R 2/2) stains and glimmering	lepidocrocite pyrrhotite

hexagonal sulfides. Petroliferous odor.

chalcopyrite  
sulfur

---

**Sample: 663-R1****Weight: 21g (aggregate)****Size: Seven pieces ranging from 1cm<sup>3</sup> to 4cm x 2cm x 5mm****Description:**

Porous, massive sulfide weathered to red-brown Fe oxyhydroxide. Crusty Fe-stained exterior grades into softer mustard colored interior.

**Color: (4 subsamples)****Mineralogy:**

- |   |   |   |
|---|---|---|
| 1 | Exterior: (layer 1)<br>Crusty dark red (dried blood) outer surface.               | goethite<br>barite<br>akaganéite                        |
| 2 | Exterior: (layer 2)<br>mustard colored, softer, dark yellowish orange (10YR 6/6). | goethite<br>quartz<br>mixed-layer clay<br>plagioclase   |
| 3 | Interior (layer 3)<br>brownish black (5YR 2/1) sulfide rich.                      | unidentified 5.44Å<br>peak<br>marcasite<br>chalcopyrite |
| 4 | Exterior<br>dusky brown (5YR 2/2) and moderate brown (5YR 4/4) coating.           | gypsum<br>barite<br>goethite<br>sphalerite              |

---

**Sample: 663-R2****Weight: a) 12g**

b) 2g

c) 1g

**Size: a) 4cm x 3cm x 3cm**

b) 3cm x 1cm x 1.5cm

c) 2cm x 1.5cm x 5mm

**Description/Color: (4 subsamples)****Mineralogy:**

- |   |  |                                       |
|---|--|---------------------------------------|
| 1 | Exterior<br>white bubbly material found randomly on outer surface. | talc                                  |
| 2 | Exterior<br>crusty dark reddish brown (10R 3/4)                    | mixed-layer clay<br>amorphous silica? |

3	Exterior dark yellowish orange (10YR 6/6) (mustard colored, smooth, pasty texture)	goethite pyrite mixed-layer clay quartz plagioclase
4	Interior Most interior region, but still highly altered. Light brown (5YR 5/6) to brownish black (5YR 2/1) with tiny patches of light grey (N7) clay material.	mixed-layer clay

---

<sup>1</sup> Colors based on Rock Color Chart.

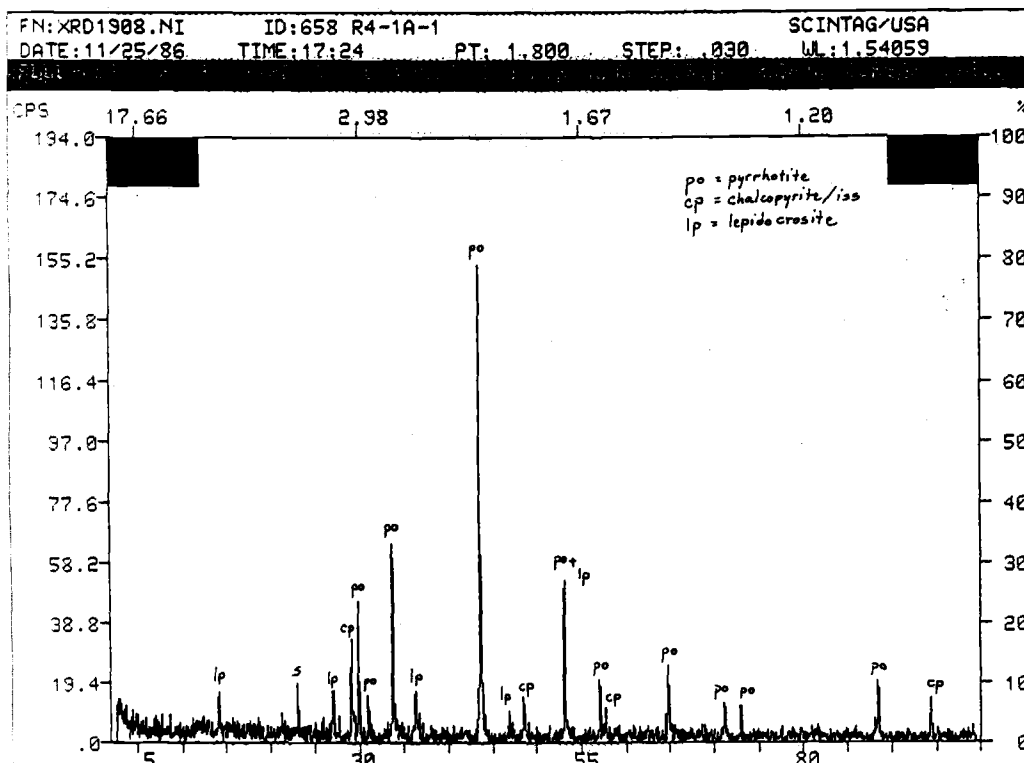
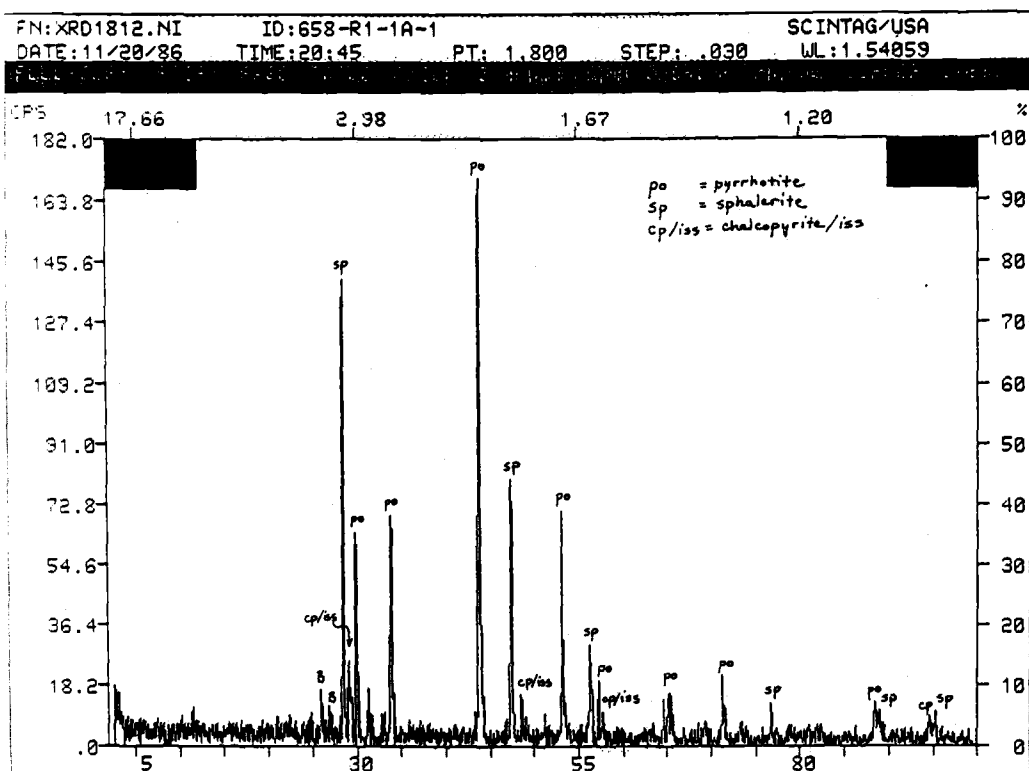
<sup>2</sup> Mineralogy in approximate order of abundance. Identifications made by megascopic examination, reflected and transmitted light microscopy, and XRD, unless otherwise noted. Amorphous Fe-oxyhydroxide is ubiquitous.

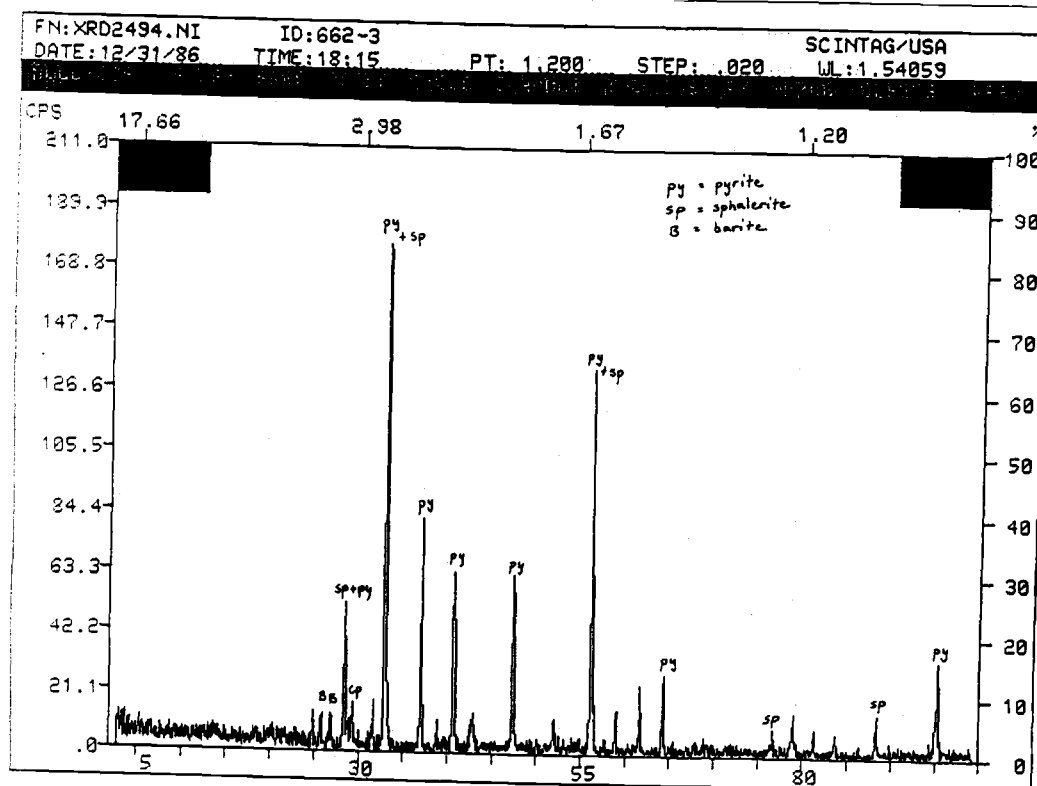
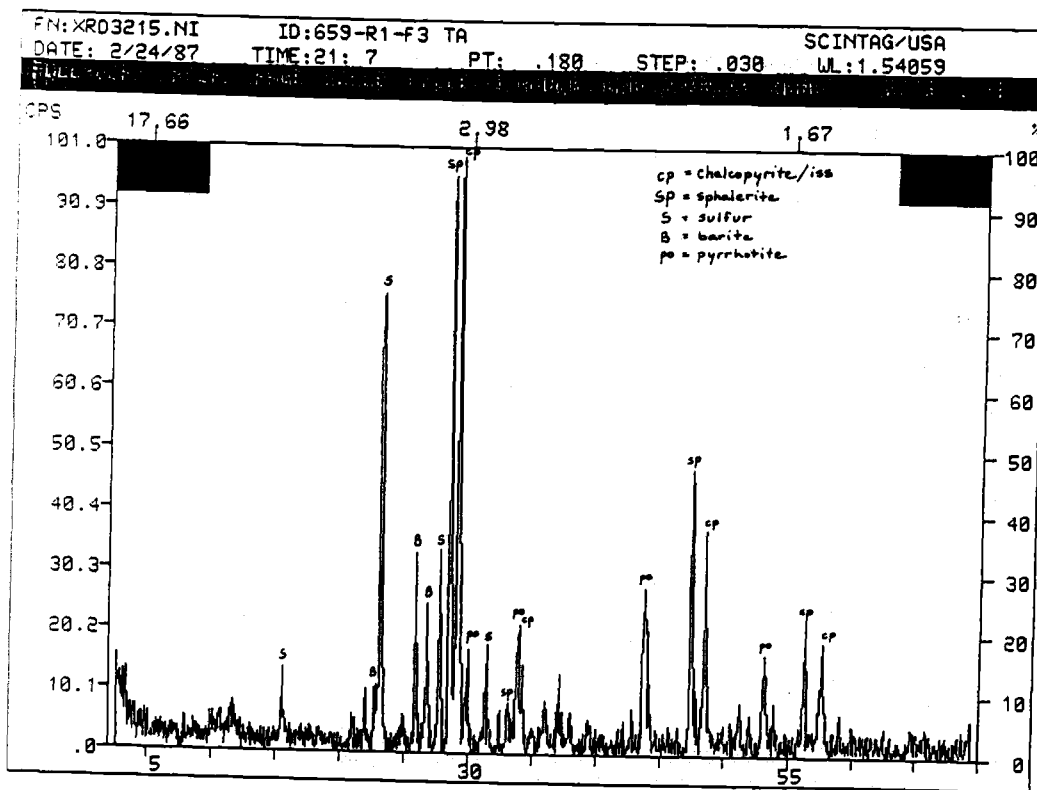
\* Identification by SEM.

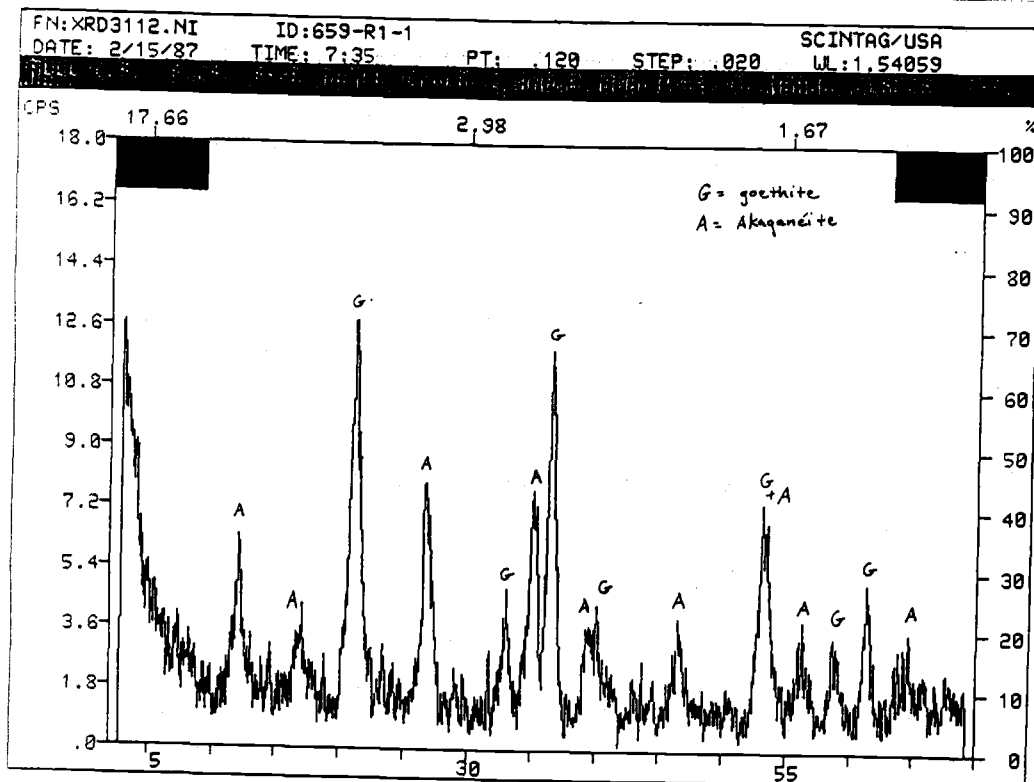
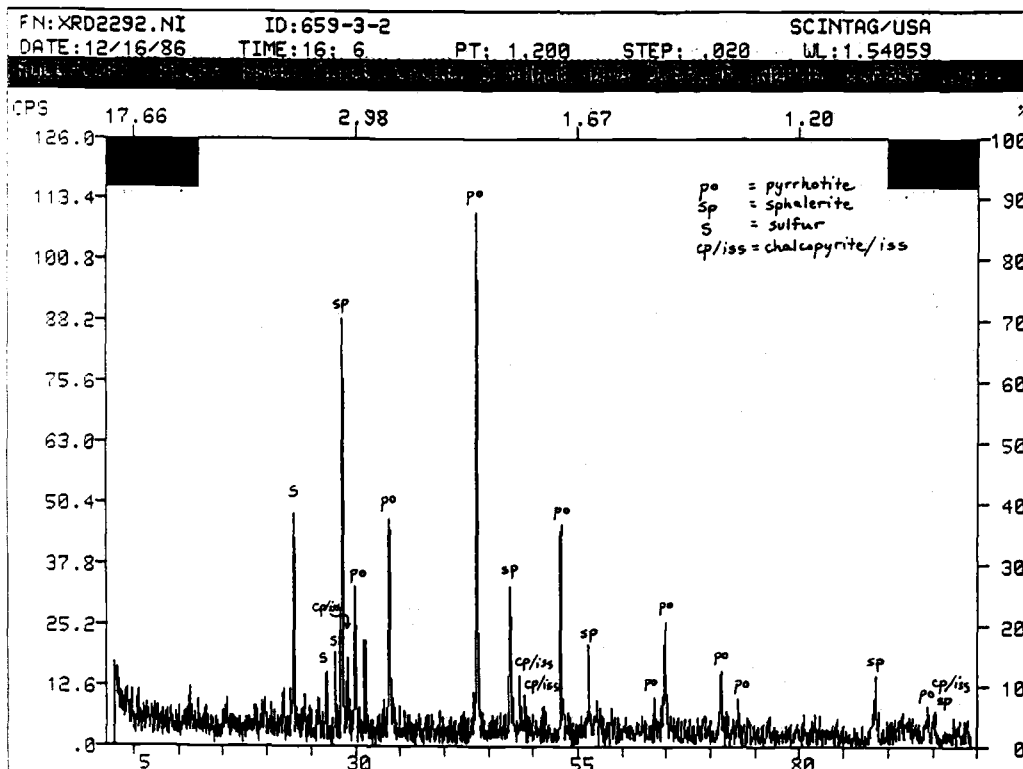
? implies tentative identification based on fewer than three diffraction peaks.

## Appendix II-2

## Selected X-Ray Diffractograms







## Appendix II-3

## Description of SEM results.

Dome B (Site 662)

The sample studied is predominantly porous pyrrhotite displaying marginal replacement by sphalerite. The sphalerite frequently contains inclusions of galena. A Sn-rich phase (cassiterite?) included in the pyrrhotite may contain minor FeS, but FeS is more likely contributed to the analysis by surrounding pyrrhotite. Abundant barite crystallized interstitially.

Dome D

## Site 658

Four chimney samples were selected for study from this site.

## (1) 658-R1-1A

This relatively Zn-rich sample contains mainly pyrrhotite altered to marcasite. Euhedral galena is frequently attached to inhomogenous sphalerite containing patches of isocubanite ( $\text{Cu Fe}_2\text{S}_3$ ). Unaltered sulfide grains are surrounded by goethite which is in turn surrounded by lepidocrosite crystals.

## (2) 658-R2-B (Barite chimney)

Radiating prisms of barite contain extremely fine scale compositional zoning and a nearby tiny crystal of cinnabar is still preserved. Compositional zoning is primarily from differential incorporation of Sr.

## (3) 658-R3-A

Pyrrhotite is being replaced by isocubanite and rare Cu,Zn,Ni sulfide. A tiny inclusion of bismuth telluride was also identified in pyrrhotite. Ragged margins of pyrrhotite crystals show the effects of the oxidation of  $\text{S}^{2-}$  to  $\text{S}^{1-}$  and reflects the replacement of pyrrhotite by marcasite. From interior to exterior, the Fe/S ratio decreases as a result of this oxidation reaction. An exterior rind of goethite and lepidocrosite surround the sulfide crystals.

## (4) 658-R4-1A

Highly fractured marcasite is rimmed by crystalline goethite and lepidocrosite. Separation between the sulfide and Fe oxyhydroxides suggest the latter precipitated from solution rather than resulted from in situ alteration of sulfides. The sample is highly porous.

## Site 659

Two chimney fragments were selected for study from this site.

## (1) 659-2

This sample displays the characteristic rimming of pyrrhotite grains by marcasite followed by Fe oxyhydroxides (goethite, lepidocrosite). Minor galena, barite and cassiterite (minor FeS probably contributed from surrounding pyrrhotite) were also observed.

## (2) 659-3

Cubanite replaced by Cu,Fe,Zn sulfide and sphalerite is intergrown with arsenopyrite. Arsenopyrite is suspected since significant sulfur was detected although loellingite has also been identified (Koski et al., 1987, Zierenberg and Koski, 1986).



### APPENDIX III

#### Experimental Study of the Formation of FeTi Basalts

## Introduction

Oceanic basalts that display significant enrichment of Fe and Ti above the average for mid-ocean ridge basalt (MORB) are called "FeTi" basalts. More specific definitions vary regionally. For example, at the Galapagos spreading center, Byerly et al., (1976) arbitrarily defined FeTi basalts as having greater than 12% total iron as FeO (FeO\*) and greater than 2.0% TiO<sub>2</sub> and on the Juan de Fuca Ridge (JdF), Vogt and Byerly (1976) chose 10% FeO\* and 1.5% TiO<sub>2</sub> as the lower limit for FeTi basalts. FeTi basalts are observed in a variety of tectonic settings in the ocean basins. Among these are fast-spreading ridges (Delaney et al., 1981), slow-spreading ridges (le Roex et al., 1982), fracture zones (Batiza et al., 1977) and aseismic ridges (Ludden et al., 1980), but FeTi basalts are most commonly associated with the tips of propagating rifts (Christie and Sinton, 1981, 1986, Delaney et al., 1981, Sinton et al., 1983). Byerly et al., (1976) observed FeTi basalts with up to 18.5 % FeO\* and 3.75 % TiO<sub>2</sub> near fracture zones along the Galapagos spreading center. Later, Hey (1977) proposed that these "fracture zones" were actually propagating rifts. Current hypotheses of FeTi basalt formation at propagating rift tips suggest that a balance between cooling rate and magma resupply rate to small, shallow level magma chambers isolated from the larger ridge crest system produce extensive fractional crystallization (Christie and Sinton, 1981, 1986, Delaney et al., 1981, Perfit et al., 1983).

FeTi basalts appear commonly in the unique tectonics of propagating rifts, but it may be that a characteristic chemistry of oceanic parental magmas in these regions are responsible for FeTi basalt formation. In MORBs, water content, oxygen fugacity ( $f_{O_2}$ ) and alkalis are typically low. These factors may encourage an extended Fe-enrichment trend and thus the formation of FeTi basalts prior to Si-enrichment by the suppression of iron-titanium oxide (FeTi oxide) crystallization during fractionation. This is supported by the observation that FeTi oxides are typically not an important fractionating phase in FeTi basalts. Usually, FeTi oxides are a minor, late fractionating phase occurring as quenched crystals in the glassy groundmass (Perfit et al., 1983, Perfit and Fornari, 1983, Batiza et al., 1977, Wakeham, 1978, le Roex et al., 1982). However, some problems with this hypothesis do exist. First, FeTi oxides are usually not a significant fractionating phase in most other submarine basalts as well. Further, FeTi basalts from the Ninetyeast Ridge contain FeTi oxides as a prominent phenocryst phase (Ludden et al., 1980). This implies that FeTi enrichment may continue beyond the initial onset of FeTi oxide crystallization. This possibility was suggested by Sato and Valenza (1980) in the Fe-

enriched zone of the Skaergaard intrusion. Second, some alkali-rich FeTi basalts, though rare, do occur (le Roex et al., 1982) and these are generally assumed to have higher water contents than the average MORB (Moore, 1970). Oxygen fugacities under which FeTi basalts crystallize are relatively uncertain. Calculation of  $f_{O_2}$  based on coexisting magnetite and ilmenite in Galapagos FeTi basalts showed that  $f_{O_2}$  was at about FMQ, but Sato and Valenza (1980) provide evidence that such Fe-enrichment may result from oxygen fugacities as much as two log units below FMQ. The experimental work described here was designed to more precisely define conditions which result in the formation of FeTi basalts. A description of current petrogenetic models of FeTi basalt formation and discussion of experimentally investigated parameters follows.

## Background and Objectives

### *Petrogenetic models*

Petrogenetic models developed for FeTi basalts generally propose low pressure cotectic crystallization of plagioclase, olivine and clinopyroxene close to a low-Ca pyroxene bearing reaction point (Grove and Baker, 1984). The most advanced degrees of crystallization are observed in the pigeonite bearing Galapagos lavas (Byerly et al., 1976), but the total range observed in Icelandic FeTi basalts can be explained by three phase cotectic crystallization without reaching low-Ca pyroxene saturation (Thy et al., 1988). Thy et al., (1980) have interpreted contrasting differentiation trends in Galapagos and Icelandic FeTi basalts as the result of differences in parental basalt chemistry.

Le Roex and Dick (1981) suggest that low magma supply rate relative to spreading rate is an important control on the production of Spiess Ridge FeTi basalts. Le Roex et al., (1982) propose that Spiess Ridge FeTi basalt is formed by extensive fractional crystallization as a new segment of the SW Indian Ridge breaks through the colder African plate during northward migration of the Bouvet triple junction. They cite enrichment of  $\text{Fe}_2\text{O}_3$  in quenched glass and enrichment of volatiles in addition to fractional crystallization models which relate two of the least evolved basalts dredged with two of the more evolved samples to support this hypothesis. In some cases, simple fractional crystallization models have not adequately explained observed FeTi basalt chemistry requiring some investigators to invoke variations in partial melting or source region heterogeneities to more precisely model their evolution (Christie and Sinton, 1986, Ludden et al., 1980). Since fractional crystallization alone may not account for FeTi basalt formation, alternatives should be examined. FeTi basalts are thought to form at shallow levels because of their high density.

### *Disequilibrium*

Melts that form in the upper mantle or lower crust may rise to the surface rapidly with little opportunity to achieve equilibrium (Fisk, 1984). The result is eruptive products exhibit disequilibrium effects. Evidence supporting this include inhomogenous glasses and zoned phenocrysts indicating that the entire crystal has not achieved equilibrium with the evolving melt. However, it is uncertain whether disequilibrium processes during magmatic evolution can account for large enough volumes of material to explain unusual compositions observed at mid-ocean ridges. Silver and Delany, (1983) propose that magma mixing has contributed to FeTi basalts formation on the Juan de Fuca Ridge. Others (Phillipotts, 1973, Roedder and Weiblen, 1971) have presented evidence that

immiscibility is important in producing both high iron and silica derivative magmas. Some believe that FeTi basalts may fractionate further to produce high silica extrusives (Byerly et al., 1976, Perfit et al., 1983). Alternatively, differences in volatile content may produce different fractionation trends from the same parent (Clague et al., 1981). The results of this study suggest that disequilibrium has some bearing on the formation of FeTi basalts and may need consideration as well when relating the formation of FeTi basalts and high silica extrusives.

#### *Investigated parameters*

The study described here was conducted primarily to determine the effects of (a) temperature, (b) oxygen fugacity ( $f_{O_2}$ ) and (c) composition (ie alkali content) on the formation of FeTi basalts. For this purpose, one-atmosphere melting experiments were conducted on two FeTi basalts, one "normal" FeTi basalt from JdF and one high alkali FeTi basalt from Spiess Ridge, under controlled temperature and oxygen fugacity. Table AI-1 compares the compositions of a normal MORB, the two FeTi basalts used in these experiments and the most FeTi enriched basalt from the Galapagos spreading center. The aim of these experiments was (a) to induce further Fe-enrichment in the experimental charges, bringing them closer to the Galapagos end member composition and hence provide evidence for conditions necessary for FeTi basalt formation and (b) to establish the oxygen fugacity at which FeTi oxides form. Charges were placed in a basalt capsule with a higher melting temperature to simulate conditions in a shallow magma chamber. Quenched charges were examined to determine if FeTi oxides had crystallized and glass was analyzed to determine if further FeTi enrichment had occurred. In the process, reactions involving olivine and disequilibrium effects on glass composition were examined as well. To better examine olivine-melt reactions, one experiment was conducted with an olivine nodule capsule.

Factors affecting FeTi enrichment of the melt or FeTi oxide formation investigated in this study are summarized below:

- (1) *Oxygen fugacity* - Increased oxygen fugacity increases the  $Fe^{3+}/Fe^{2+}$  ratio as represented by the reaction:  $2FeO + 1/2 O_2 = Fe_2O_3$ . Lower oxygen fugacity should suppress the formation of FeTi oxides and thus enhance the Fe-enrichment trend of the residual melt during fractionation.
- (2) *Temperature* - At higher temperatures, the  $Fe^{3+}/Fe^{2+}$  ratio of the melt decreases (Kennedy, 1948). As temperature decreases and crystals form,  $Fe^{3+}$  is concentrated in the melt by fractional crystallization processes. This should encourage crystallization of

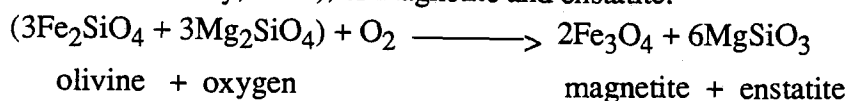
FeTi oxides. Eventually, with decreasing temperature, the residual melt should become depleted in iron and enriched in silica.

(3)*Alkali content* - At constant temperature and oxygen fugacity, the  $\text{Fe}^{3+}/\text{Fe}^{2+}$  ratio increases with increasing alkali content (Fudali, 1965) and is called the alkali-ferric iron effect (Carmichael and Nicholls, 1967). This should also encourage FeTi oxide formation which may be enhanced at higher temperatures (Paul and Lahiri, 1966).

(4)*Olivine reactions* - The reaction of olivine and liquid to produce low Ca-pyroxene and spinel during fractional crystallization was initially proposed by Bowen (1928) and has since been studied by several researchers (Kuno, 1950, Presnall, 1966, Grove and Baker, 1984). It can be confused with the FMQ buffer reaction involving the oxidation of olivine in which olivine and oxygen react to form magnetite and silica:



(Yoder and Tilley, 1962), or magnetite and enstatite:



(Muir, Tilley and Scoon, 1957).

Kuno (1950) illustrated the resorption of olivine to form magnetite in the center with a surrounding corona of hypersthene, but Muir, Tilley and Scoon (1957) reinterpreted this as the oxidation of olivine to form magnetite and enstatite. Grove and Baker (1984) suggest that a distinction between these two reactions may be made since the oxidation reaction should produce magnetite and enstatite coronas on olivine, but a reaction involving olivine and liquid should produce resorbed olivine with crystallization of low-Ca pyroxene occurring elsewhere in the melt.

## Sample Description

The two samples used for experimental charges include one quartz normative FeTi basalt from the Juan de Fuca Ridge (sample Y74-1-DR7-1 of Wakeham, 1978) and one olivine normative high-alkali FeTi basalt (AII 107 31-4) from the Spiess Ridge segment of the Southwest Indian Ridge (LeRoex et al., 1982) (see Table AIII-5 for bulk compositions and norms). The Juan de Fuca Ridge sample is unaltered and very fine-grained with <1% euhedral plagioclase phenocrysts (up to 0.5mm) and about 3% vesicles. The ground mass is about 50% devitrified glass and about 50% microphenocrysts of plagioclase laths (30%) and subhedral clinopyroxene (15%) and olivine (3%). The Spiess Ridge sample is highly vesicular (about 15% vesicles) and fine-grained, with minor ferric iron alteration in the ground mass (mainly around vesicles). The ground mass (55%) is devitrified glass. Phenocrysts (30%) of plagioclase (20%, up to 1mm) and clinopyroxene (10%, average 0.2 mm) often crystallize in about 1 mm size glomerocrysts. Elongate diamond-shaped olivine can be up to 0.5 mm, but is rare (<1%). Both samples contain FeTi oxides in the groundmass and mineral analyses from the Spiess Ridge sample show it to be a titanomagnetite (Table AIII-7). A brief description of the Spiess Ridge sample is also provided by LeRoex et al. (1982).

Capsules of Cascades Rim Rock (TRR) were used in all experiments except one for which an olivine nodule from Hawaii (HON) was used. The Rim Rock capsule is a medium-grained high-alumina basalt from the Cascades Range near Sisters, Oregon (Table AIII-5). It has about 10% olivine phenocrysts up to 1.0 mm that are frequently rimmed by iddingsite and FeTi oxides, and rare (<1%) plagioclase phenocrysts up to 0.7 mm. The ground mass (90%) contains plagioclase laths (70%) averaging 0.4 mm long, intergrown with clinopyroxene (20%) in 0.5 mm sized glomerocrysts. FeTi oxides (7%) and devitrified glass (3%) are dispersed throughout. The Hawaiian Olivine Nodule (HON) contains about 95% coarse-grained olivine (up to 5 mm) with a minor zone (5%) of fine-grained plagioclase, clinopyroxene and olivine intergrowths and abundant FeTi oxides.

Bulk composition of starting material (Table AIII-5) was determined by microprobe on glasses melted in the furnace. Table AIII-3 provides the temperature at which glass was made for measuring the starting compositions and compares liquidus temperatures calculated by Nielsen, (1988) and olivine and plagioclase geothermometry (Roeder and

Emslie, 1970, Langmuir, 1980). Pt wire loops from previous experiments were used to minimize Fe loss by Fe-Pt alloying (Donaldson, 1975).



## Experimental Design

Both experimental charges were ground by an  $\text{Al}_2\text{O}_3$  jaw crusher and disc pulverizer. The Juan de Fuca Ridge sample was additionally crushed in an  $\text{Al}_2\text{O}_3$  ball mill. Holes drilled approximately 5 mm deep in capsules of 1 cm diameter were filled with 50-80 mg of powdered basalt charge. The basalt crucible containing powdered basalt was then suspended from a platinum wire basket in the hot zone of the furnace. The platinum wires were not doped with iron since they were not in contact with the charge and it is unlikely that enough Fe would be lost through the crucible walls to effect its interaction with the charge.

All experiments were run at 1 atm pressure in Deltec vertical quench furnaces with  $\text{MoSi}_2$  heating elements. Oxygen fugacity was controlled by mixtures of  $\text{CO}_2$  and  $\text{H}_2$  gas passing through a manometer (Darken and Gurry, 1945). Oxygen fugacity was initially calibrated by the nickel-nickel oxide buffer, and over the temperature range of the experiments was accurate to within  $\pm 0.2$  log units (Huebner and Sato, 1970). Temperatures measured with Pt-Pt/10%Rh thermocouples calibrated against the melting point of gold are accurate to within  $\pm 5^\circ\text{C}$ .

Initially, the Rim Rock capsule was heated to  $1170^\circ\text{C}$  for about 2 hours to seal up holes in the surface against which the charge was placed. The HON capsule was too friable to drill and was heated to  $1400^\circ\text{C}$  to fuse the olivine grains together enough for drilling. A glassy margin was produced to simulate the newly formed crystal mush of the magma chamber walls (Wager, 1960) and to create a surface where reactions between the capsule partial melt and the charge could be examined. During heating of the crucibles, the oxygen fugacity was maintained at that of the anticipated experiment.

Experiments were performed at  $1150^\circ\text{C}$  and  $1125^\circ\text{C}$  ( $\pm 2^\circ\text{C}$ ) with oxygen fugacity held at  $10^{-11}$  to  $10^{-7}$  atm (Table AIII-2). This is about two log units above and below the FMQ buffer at these temperatures. In  $1150^\circ\text{C}$  experiments, furnace temperature was brought up to  $1150^\circ\text{C}$  and the charge and capsule were lowered into the hot zone. In  $1125^\circ\text{C}$  experiments, furnace temperature was initially brought up to  $1150^\circ\text{C}$  for about 2 hours to insure melting of the charge, then the temperature was lowered to  $1125^\circ\text{C}$  within 15 minutes (down-temperature runs). Experiments were conducted for about 12 hours, which should be sufficient time for oxidation ratio stabilization in basalts (Thornber et al, 1980), then quenched in distilled water. One experiment (SR6 OP41) was run for 24 hours to determine if time was a factor in the lack of crystallization of low-Ca pyroxene

(Dearing, 1984). Capsules were cut in half and ground into polished thin sections for microprobe analysis. Figure AIII-1 is a schematic drawing of the experimental design.

Microprobe analyses were performed on the University of Oregon ARL/EDX microprobe using 15 KV accelerating voltage and  $.15\mu\text{A}$  sample current and on line data reduction following the standard Bence and Albee (1968), Albee and Ray (1970) procedures.

## Results and Discussion

The run conditions of the experiments are listed in Table AIII-2 and Table AIII-4 contains modal analyses of quenched charges. Table AIII-7 contains microprobe analyses of olivine, Cr-spinel/magnetite and pyroxene.

### *Petrography*

In experiments run at 1150°C, crystallization of olivine and plagioclase in approximately equal proportions totaled about 11 to 16 % in Juan de Fuca charges and crystallization of plagioclase ranged from < 1 to 8 % in Spiess Ridge charges (Table AIII-5). The greatest percent crystallization in both charges reflects the crystallization of FeTi oxides. Otherwise, oxygen fugacity has little effect on percent crystallization and no influence over order of crystallizing phases, in agreement with other more extensive experiments conducted over a similar range of temperature and  $f_{O_2}$  (Dixon and Rutherford, 1979). FeTi oxides (opaque cubes of titanomagnetite) crystallized in the glass in both charges at  $\log f_{O_2} = -7$  atm, but abundance was significantly greater in the Spiess Ridge charge than in the Juan de Fuca charge (Table AIII-5). This may reflect both the higher alkali and higher  $TiO_2$  content of the Spiess Ridge charge compared to the Juan de Fuca Ridge charge. In both charges at  $\log f_{O_2} = -8$  and  $-9$  atm, FeTi oxides exist only as dusty inclusions in resorbing olivines reflecting the FMQ buffer reaction.

Opaque minerals are absent from both charges at lower oxygen fugacities except for FeTi 8 (OP33) and SR3 (OP35). These experiments, conducted at 1150°C and  $\log f_{O_2} = -11$ , crystallized opaque minerals as dusty inclusions in olivine and in FeTi 8 (OP33), tiny translucent cubes in the glass appeared again (Fig. AIII-2). These are presumably Cr-rich spinels and reflect the return of spinel stability at low oxygen fugacities (Hill and Roeder, 1974). The experiment using Spiess Ridge charge (SR3 OP35) probably did not crystallize Cr-spinel in the glass since Cr content was slightly less and pyroxene crystallization was slightly more than the comparable Juan de Fuca experiment (Table AIII-2, AIII-5). Similarly, an experiment conducted at 1125°C and  $\log f_{O_2} = -12$  atm (FeTi 14 OP48) probably did not crystallize any Cr-spinel because pyroxene crystallization robbed the melt of necessary Cr. Low-Ca pyroxene was not observed in any of the experiments and because olivine crystallization was observed in 1125°C runs, it can only be assumed that the stability field of low-Ca pyroxene is at a lower temperature for these compositions.

### *Compositional trends in glasses*

Major element-oxide variation diagrams from microprobe analyses of starting compositions and experimental glasses (Tables AIII-5, AIII-6) are shown in Fig. AIII-3a for Juan de Fuca Ridge charges and Fig. AIII-3b for Spiess Ridge charges. The fractional crystallization trend for the charge starting compositions was calculated according to the program TRACE.FOR (Nielsen, 1988). For Juan de Fuca Ridge starting composition, the model predicts an Fe-enrichment trend produced by cocrystallization of olivine, plagioclase and clinopyroxene followed by Fe-depletion and Si-enrichment at about 5 wt% MgO when spinel joins the liquidus. The Spiess Ridge fractionation trend is more similar to a calc-alkaline trend. Initially, plagioclase crystallization enriches the melt in FeO and MgO but this quickly reverses to Fe-depletion and Si-enrichment as olivine and pyroxene join the liquidus. Calculations were made at oxygen fugacities corresponding to FMQ, and both two log units above and below FMQ. The various analyses in Fig. AIII-3 suggest that most points can be explained by (1) fractional crystallization from different starting compositions (2) capsule assimilation (3) partial melting of the capsule, or (4) disequilibrium effects.

The major differences in composition between experimental glasses produced in the two charge materials relative to their starting compositions reflect

(1) differential fractional crystallization and (2) degree of capsule assimilation.

Juan de Fuca charges exhibit more extensive crystallization than Spiess Ridge charges and residual glasses plot at lower wt% MgO than the charge (< 6.42 wt%) implying olivine fractionation has been significant. In Juan de Fuca experiments at 1150°C, olivine and plagioclase cocrystallize and at 1125°C, clinopyroxene joins the liquidus. In general, 1150°C experimental glasses cluster near the charge starting composition (Fig. AIII-3a) suggesting that relatively little capsule assimilation has occurred. Exceptions are a few glasses slightly enriched in K<sub>2</sub>O. In 1150°C experiments, wt% K<sub>2</sub>O is between the starting composition and the capsule partial melts and in 1125°C experiments K<sub>2</sub>O follows the calculated fractional crystallization trend (Fig. AIII-3a). The enrichment is greater in the higher temperature experiments, implying K<sub>2</sub>O diffusion from the capsule into the charge (Watson, 1982).

In contrast, compositional trends in glasses from Spiess Ridge charges are dominantly controlled by plagioclase fractionation at 1150°C and cocrystallization of olivine, pyroxene and plagioclase at 1125°C superimposed upon a strong mixing relationship between the charge and capsule (Fig. AIII-3b). All Spiess Ridge glass analyses plot at wt% MgO between the charge and capsule compositions and departure of glass analyses

in the charge from this mixing relation at 1150°C reflect crystallization of plagioclase. Generally, enrichments in  $\text{FeO}^*$ , and  $\text{TiO}_2$  above the mixing line and depletions in  $\text{Al}_2\text{O}_3$  and  $\text{Na}_2\text{O}$  below the mixing line are consistent with plagioclase fractionation.

An apparent direct correlation between oxygen fugacity and wt% MgO has been noted in Spiess Ridge experiments at 1150 °C and in Juan de Fuca Ridge experiments at both 1150°C and 1125°C. The correlation is opposite to that predicted by the experiments of Roeder and Emslie (1970). Typically an inverse correlation should be observed since higher  $f_{\text{O}_2}$  should increase the  $\text{Fe}^{3+}$  in the melt forcing crystallizing olivines to more magnesian compositions and thus lowering the magnesium in the residual melt. Unfortunately, not enough olivines in the charge were analyzed to provide a definitive answer, but some explanation may be found by comparison of crystallization products in Table AIII-2. Since higher  $f_{\text{O}_2}$  results in the crystallization of FeTi oxides, those experiments produced residual liquids more enriched in MgO. This presumably overrides a lesser effect on olivine compositions. In FeTi 11 (OP42), ( $f_{\text{O}_2} = 10^{-11}$  atm) the crystallization of spinel may also maintain the residual melt at higher wt% MgO.

(3) Glass analyses taken within the capsule in Juan de Fuca Ridge experiments are partial melts of the Rim Rock capsule. The higher FeO,  $\text{TiO}_2$ ,  $\text{K}_2\text{O}$  and  $\text{Na}_2\text{O}$  relative to the capsule starting composition is consistent with this interpretation. Partial melts of Rim Rock in Spiess Ridge experiments are similar in composition, but tend to be slightly higher in  $\text{K}_2\text{O}$  and lower in CaO than those observed in Juan de Fuca Ridge experiments.

(4) Disequilibrium in the charge produced the greatest inhomogeneities in Juan de Fuca Ridge experimental glasses at 1125°C. This is in part because greater crystallization caused disequilibrium melt to become trapped and kept it from mixing. The greatest variability is in  $\text{Na}_2\text{O}$  and could reflect differential diffusion and volatilization. At  $f_{\text{O}_2} = 10^{-8}$  (FeTi 11 OP42), minor crystallization of FeTi oxides may reduce disequilibrium effects by increasing the number of network modifiers in the melt resulting in relatively homogenous glass compositions. This seems opposite to the expected reaction since diffusion is inversely proportional to viscosity and increasing network modifiers should decrease the viscosity and thus increase the rate of diffusion as well.

Generally, Spiess Ridge experimental glasses appear more homogenous than Juan de Fuca Ridge glasses. This observation is consistent with the above suggestion regarding network modifiers since Spiess Ridge glasses are higher in network formers (alkalies and aluminum). Alternatively, glasses analyzed are not representative of the entire range of compositions and disequilibrium melt compositions were simply not analyzed. A few deviant analyses from within the capsule are significantly lower in FeO (Fig. AIII-3b). It

is possible that these analyses represent disequilibrium effects in the capsule, but since both are from the base of the capsule, they may have experienced Fe loss to the Pt-wire basket. Another unusual glass composition was determined in SR8 OP55 (Table AIII-5, AIII-6). This analysis was taken very close to an olivine dusted with opaques. The high  $\text{Al}_2\text{O}_3$ , low FeO content and slightly high total (101.21%) implies the analysis may have been influenced by a plagioclase crystal. However, no plagioclase was observed in the vicinity and the alkali content is identical with other glass analyses in the charge. Whether it represents unusual disequilibrium effects of the dissolving olivine or analysis of overlapping minute feldspar and glass is difficult to reconcile.

A group of analyses (from FeTi 11, Fig. AIII-3a) plot on and slightly above the fractional crystallization trend on the plot of FeO vs MgO where a shift in the model differentiation trend towards Fe depletion marks the onset of spinel crystallization. These analyses exhibit Fe-enrichment at approximately constant silica. Two possible explanations for Fe-enrichment are: (1) although FeTi oxides crystallized in this experiment, they are very minor (< 1%) and may not have significantly detracted from the Fe-enrichment trend. Thus, it may be possible to continue Fe-enrichment beyond the initial onset of FeTi oxide crystallization as was demonstrated by Sato and Valenza (1980) for the Skaergaard intrusion. (2) Alternatively, at the apex of this trend of Fe-enriched glasses is an analysis (from FeTi 12) near an olivine in the Rim Rock capsule. Since the analyses from FeTi 11 are from the border between the charge and capsule, it may be that they represent a mixture between charge and Fe-rich partial melt from the surrounding capsule. If Fe has been contributed from the breakdown of olivine, these analyses should be lower in  $\text{SiO}_2$  than predicted by fractional crystallization as is in fact observed. Also, the  $\text{TiO}_2$  enrichment above the fractional crystallization trend is significant since the breakdown of FeTi-oxides in the capsule could be contributing to the observed Fe and Ti increases instead of or in addition to olivine dissolution. However, the high Fe analysis from FeTi 12 is not correspondingly higher in  $\text{TiO}_2$  than the other glass analyses implying olivine addition is more likely. The addition of partial melt from the capsule or wall rock provides a possible mechanism for departure from the fractional crystallization trend which could enrich the melt in Fe above the upper limit predicted by the model calculations and further implies that mixing between an Fe-rich partial melt of a tholeiitic basalt (Rim Rock) and fractionally crystallizing FeTi basalt could induce conditions necessary for further Fe-enrichment.

Experimental glasses from the charge run in the HON capsule (FeTi 15 OP54) exhibit significant disequilibrium effects. In this experiment, glass compositions generally

follow the Fe-enrichment, fractional crystallization trend, but a pair of analyses are notably iron poor and although not extremely Si-rich, they are significantly enriched in alkalis ( $\text{Na}_2\text{O} + \text{K}_2\text{O} > 4 \text{ wt } \%$ ). These two liquids, however, are also significantly enriched in  $\text{TiO}_2$ , the opposite of what the liquid should be if it were an immiscible phase (Naslund, 1983). Both experiments were conducted at  $1125^\circ\text{C}$  and  $\log f_{\text{O}_2} = -10$  atm, within the spinel gap of Hill and Roeder (1974). Because Fe-rich melts apparently were not produced from the breakdown of olivine in this experiment, based only on this result it can only be concluded that olivine reaction alone is not sufficient to produce FeTi basalt by a mixing process. In lieu of an alternative explanation, it may be that the Fe/Mg ratio of mixing material is more critical than simply the contribution of Fe. The HON capsule at Fo 89 (Fe/Mg=0.3) may simply be too Mg-rich to produce the required results. For comparison, the Fe/Mg ratio for the Rim Rock capsule =1.0.

Several experiments produce pairs of analyses enriched in iron or silica. One such pair is from Juan de Fuca Ridge experiment FeTi 12 (OP45) (Fig. AIII-3a). The Fe-rich analysis is from the border between the charge and the capsule and may result from mixing with the Fe-rich capsule partial melt. The Si-rich analysis closely follows the  $\text{SiO}_2$  vs MgO fractionation model. Though they have been conducted under conditions known to produce immiscibility in tholeiitic basalts (Philpotts, 1977, 1983), the liquids produced that do not match normal fractional crystallization trends also do not match all criteria for immiscible liquids (Naslund, 1983). Fig. AIII-4 shows that none of the unusual analyses plot as immiscible liquids. They probably represent disequilibrium melts produced by local crystallization or reaction between crystals and liquid (Fisk, 1984).

## Summary and Conclusions

Processes controlling the formation of FeTi basalts are primarily governed by fractional crystallization with oxygen fugacity probably at or below FMQ. Above FMQ FeTi oxides cocrystallized with plagioclase ( $\pm$  olivine). Although this did not seem to drastically reduce the FeO and TiO<sub>2</sub> content of the residual glass relative to experiments conducted at lower  $f_{O_2}$ , FeTi oxides are not usually observed as an early fractionating phase in natural FeTi basalts. Fe-enrichment above the fractional crystallization trend may occur by mixing with the Fe-rich partial melt of a tholeiitic basalt produced by the breakdown of olivine (or conceivably other Fe-rich minerals such as pyroxene and FeTi oxides). This may be even more significant in high alkali FeTi basalt where mixing with the tholeiitic basalt capsule reversed the predicted fractionation trend forcing compositions towards further Fe-enrichment. The increased mixing between charge and capsule may result from the higher alkali content reducing the melting point of the capsule.

Since reaction between the HON and the charge apparently did not serve to increase the resulting residual glass in Fe as did the Rim Rock tholeiitic basalt capsule, it suggests that the Fe/Mg ratio may be more critical than simply the Fe contribution from the dissolution of olivine. The Fe enrichment produced by the breakdown of the relatively Mg-rich olivine in the HON capsule may be swamped by the high Mg content of the liquid, but a more Fe-rich olivine in equilibrium with tholeiitic basalt is more likely to increase the Fe/Mg ratio of the melt. This result is consistent with current models for FeTi basalt formation which require shallow level fractionation. Under these conditions, a FeTi basalt would be reacting with the magma chamber walls in the upper crust with material closer to tholeiite in composition.

### *The effect of alkalis*

The effects of increased alkalis on the nucleation of FeTi oxides in Spiess Ridge charges was minor. Apparently there is not enough difference between the two charge compositions to overcome the dominant effects of temperature and oxygen fugacity. A minor effect was observed in experiments at  $\log f_{O_2} = -7$  atm in which many more FeTi oxides crystallized in Spiess Ridge experiments than in comparable Juan de Fuca experiments. Table AI-5 shows that there was not a significant difference between ferric/ferrous ratios between the two charges at comparable temperatures and oxygen fugacities. The Spiess Ridge starting composition is not only higher in alkali content but is also 0.5 wt% higher in TiO<sub>2</sub> than the Juan de Fuca Ridge starting composition which may also contribute to the FeTi oxide crystallization.



The effect of bulk composition on FeTi oxide crystallization may require additional consideration. For example, because CaO is lower in the Spiess Ridge charge, its absence as a network former may counterbalance the effect of the increased alkalies. CaO can act as a network modifier, but when coupled with Al as  $\text{CaAl}_2\text{O}_4$ , it behaves as a network former possibly reducing the difference in melt structure between the two charges (Bottinga and Weill, 1970).

#### *The effect of oxygen fugacity*

FeTi oxides crystallized in the glass at  $\log f_{\text{O}_2} = -7$  atm in both charges. At  $\log f_{\text{O}_2} = -8$  and  $-9$  atm, FeTi oxides appeared as dusty inclusions in olivine representing the FMQ buffer reaction. FeTi oxides disappeared entirely at  $\log f_{\text{O}_2} = -10$  atm, but reappeared at  $\log f_{\text{O}_2} = -11$  atm. The latter are presumably Cr-spinel. Cr content and/or pyroxene crystallization determined whether Cr-spinel would crystallize (Hill and Roeder, 1974). The  $f_{\text{O}_2}$  effect on olivine composition was not investigated, but an apparent direct correlation between  $f_{\text{O}_2}$  and MgO results from crystallization of FeTi oxides below and within the spinel gap of Hill and Roeder (1974) with a reversal to an inverse correlation once the stability field for Cr-spinel is reached. Because many FeTi basalts are produced without fractionating enough to precipitate low-Ca pyroxene, a reaction involving olivine oxidation to produce FeTi oxides or reactions to form Cr-spinel may be more important in determining FeTi enrichment in the residual melt.

#### *Disequilibrium*

Although Philpotts (1979) has shown that 60% crystallization of tholeiitic basalt can produce immiscible liquids, iron and silica rich glasses produced in these experiments are the result of disequilibrium processes produced by reaction between charge and capsule or reactions during crystallization in the charge. It is doubtful that disequilibrium processes can account for the observed occurrence of FeTi basalts and associated high-Si extrusives at mid-ocean ridges, but its role as a contributing factor still warrants further evaluation.

#### *Future Experiments*

The most critical experiments to be run at this stage are lower temperature experiments. Since the stability field of low-Ca pyroxene was never intersected, this reaction and its effect on FeTi basalt formation could not be evaluated. Biggar (1981) has shown that  $\text{Na}_2\text{O}$  gain stabilizes olivine rather than low-Ca pyroxene so the different compositions used in the experiments of this study may differentially shift the position of the reaction point. However, Thy et al., (1988) report that crystallization is too complete at the reaction point to microprobe the residual glass.

Lower temperature runs at various oxygen fugacities would also be useful to determine when FeTi oxides will crystallize in quench textures such as those observed in MORBs or if further Fe-enrichment can occur at higher oxygen fugacities that crystallize FeTi oxides as a major fractionating phase.

Additional experiments using capsules with different Fe/Mg ratios would also provide insight into the shift in fractionation trend of the high alkali FeTi basalt in response to assimilation of capsule material.

#### *Acknowledgements*

We would like to thank Anton le Roex for a sample of high-alkali FeTi basalt from Spiess Ridge and Ed Taylor for a sample of Cascades Rim Rock. Mike Shaffer and University of Oregon, Department of Geology provided microprobe time. Discussions with Scott Hughes and Roger Nielsen regarding fractional crystallization and Haraldur Audunsson regarding FeTi oxides were helpful and entertaining. Haraldur Audunsson is thanked for use of his computer program for recalculating FeTi oxide microprobe analyses and Roger Nielsen is also thanked for providing a copy of TRACE.FOR to work with prior to publication.

## References

- Albee A.L. and Ray, L. (1970) Correction factors for electron probe microanalysis of silicates, oxides, carbonates, phosphates and sulfides. *Anal. Chem.* 42, 1,408-1,414.
- Batiza, R., Rosendahl, B.R., and Fisher, R.L. (1977). Evolution of oceanic crust 3. Petrology and chemistry of basalts from the East Pacific Rise and the Siqueiros Transform Fault. *J. Geophys. Res.* 82, 265-276.
- Bence, A.E. and Albee, A.L. (1968) Empirical correction factors for electron microanalysis of silicates and oxides. *J. Geol.* 76, 382-403.
- Biggar, G.M. (1981) Melting experiments on ocelli and matrix samples from Proterozoic lavas in South Africa. *Bull. Min.* 104, 369-374.
- Bottinga, Y. and Weill, D.F. (1970) Densities of liquid silicate systems calculated from partial molar volumes of oxide components. *Am. J. Sci.* 269, 169-182.
- Bowen, N.L. (1928) The evolution of the igneous rocks. Princeton University Press, Princeton N.J. 332p.
- Bowen, N.L. (1937) Recent high-temperature research on silicates and its significance in igneous geology. *Am. J. Sci.* 33, 1-21.
- Byerly, G.R. (1980) The nature of differentiation trends in some volcanic rocks from the Galapagos spreading center. *J. Geophys. Res.* 85, 3,797-3,810.
- Byerly, G.R., Melson, W.G., and Vogt, P.R. (1976) Rhyodacites, andesites, ferrobasalts and ocean tholeiites from the Galapagos spreading center. *Earth Planet. Sci. Lett.*, 30, 215-221.
- Christie, D.M. and Sinton, J.M. (1981) Evolution of abyssal lavas along propagating segments of the Galapagos spreading center. *Earth Planet. Sci. Lett.* 56, 321-335.
- Christie, D.M. and Sinton, J.M. (1986) Major element constraints on melting, differentiation and mixing of magmas from the Galapagos 95.5°W propagating rift system. *Contrib. Min. Petrol.* 94, 274-288.
- Clague, D.A., Frey, F.A., Thompson, G., and Rindge, S. (1981) Minor and trace element geochemistry of volcanic rocks dredged from the Galapagos spreading center: role of crystal fractionation and mantle heterogeneity. *J. Geophys. Res.*, 86, 9,469-9,482.
- Clague, D.A. and Bunch, T.E. (1976) Formation of ferrobasalts at East Pacific Mid-ocean spreading centers. *J. Geophys. Res.* 81, 4,247-4,256.
- Carmichael, I.S.E. and Nicholls, J. (1967). Iron-titanium oxides and oxygen fugacities in volcanic rocks. *J. Geophys. Res.* 72, 4665-4687.
- Darken, L.S. and Gurry, R.W. (1945) The system iron-oxygen. I. The wustite field and related equilibria. *J. Amer. Chem. Soc.* 67, 1,398-1,412.

- Dearing, K. (1984). Crystallization of protopyroxene from natural samples. *Prog. in Experimental Pet.* 6, 125-128.
- Delaney, J.R., Johnson, H.P., Karsten, J.L. (1981). The Juan de Fuca Ridge -- hot spot -- propagating rift system: new tectonic, geochemical and magnetic data. *J. Geophys. Res.* 86, 11,747-11,750.
- Dixon, S. and Rutherford, M.J. (1979) Plagiogranites as late-stage immiscible liquids in ophiolite and mid-ocean ridge suites: an experimental study. *Earth Planet. Sci. Lett.* 45, 45-60.
- Donaldson, C.H., Williams, R.J. and Lofgren, G.E. (1975) A sample holding technique for study of crystal growth in silicate melts. *Am. Min.* 60, 324-326.
- Fisk, M.R. (1984) Depth and temperatures of mid-ocean ridge magma chambers and the composition of their source magmas. In: *Ophiolites and oceanic lithosphere* (eds. I.G. Gass, S.J. Lippard and A.W. Shelton).
- Fisk, M.R. and Ford, C.E. (1984) Melting of Mauritius Island intermediate series lava. *Prog. in Experimental Pet.* 6, 114-117.
- Fudali, R.F. (1965) Oxygen fugacities of basaltic and andesitic magmas. *Geochim. Cosmochim. Acta.* 29, 1,063-1,075.
- Grove, T.L. and Baker, M.B. (1984) Phase equilibrium controls on the tholeiitic versus calc-alkaline differentiation trends. *J. Geophys. Res.* 89, 3,253-3,274.
- Hey, R. (1977) A new class of pseudofaults and their bearing on plate tectonics: A propagating rift model. *Earth. Planet. Sci. Lett.* 37, 321-325.
- Hill, R. and Roeder, P. (1974) The crystallization of spinel from basaltic liquid as a function of oxygen fugacity. *J. Geol.* 82, 709-729.
- Huebner, J.S. and Sato, M. (1970) The oxygen fugacity-temperature relationships of manganese and nickel oxide buffers. *Am. Min.* 55, 934-952.
- Kennedy, G.C. (1948) Equilibrium between volatiles and iron oxides in igneous rocks. *Am. J. Sci.* 246, 529-549.
- Kilinc, A., Carmichael, I.S.E., Rivers, M.L., and Sack, R.O. (1983) The ferric-ferrous ratio of natural silicate liquids equilibrated in air. *Contrib. Min. Petrol.* 83, 136-140.
- Kuno, H. (1950) Petrology of Hakone Volcano and the adjacent areas, Japan. *Bull. Geol. Soc. Am.* 61, 957-1020.
- Langmuir, C.H. (1979) A major and trace element approach to the petrogenesis of basalts. PhD Thesis, State University of New York, at Stony Brook.
- Ludden, J.N., Thompson, G., Bryan, W.B., Frey, F.A. (1980). The origin of lavas from the Ninetyeast Ridge, eastern Indian Ocean: an evaluation of fractional crystallization models. *J. Geophys. Res.* 85, 4405-4420.

- Moore, J.G. (1970) Water content of basalt erupted on the ocean floor. *Contrib Min Petrol.* 28, 272-279.
- Muir, I.D., Tilley, C.E. and Scoon, J.H. (1957) Contributions to the petrology of Hawaiian basalts. 1. The picrite basalts of Kilauea. *Amer. J. Sci.* 255, 241-253.
- Naslund, H.R. (1983) The effect of oxygen fugacity on liquid immiscibility in iron-bearing silicate melts. 283, 1,034-1,059.
- Nielsen, R.L. (1988) TRACE.FOR: A program for the calculation of combined major and trace element liquid lines of descent for natural magmatic systems. *Computers in Geos.* (in press ?).
- Paul, A. and Lahiri, D. (1966) Manganous-manganic equilibrium in alkali borate glasses. *J. Am. Ceram. Soc.* 49, 565-567.
- Perfit, M.R. and Fornari, D.J. (1983). Geochemical studies of abyssal lavas recovered by DSRV Alvin from eastern Galapagos Rift, Inca Transform and Ecuador Rift 2. Phase chemistry and crystallization history. *J. Geophys. Res.* 88, 10,530-10,550.
- Perfit, M.R., Fornari, D.J., Malahoff, A. and Embly, R.W. (1983) Geochemical studies of abyssal lavas recovered by DSRV Alvin from eastern Galapagos Rift, Inca Transform, and Ecuador Rift, 3, Trace element abundances and petrogenesis. *J. Geophys. Res.* 88, 10,551-10,572.
- Philpotts, A.R. (1976) Silicate liquid immiscibility: its probable extent and petrogenetic significance. *Am. J. Sci.* 276, 1,147-1,177.
- Philpotts, A.R. (1979) Silicate liquid immiscibility in tholeiitic basalts. *J. Petrol.* 20, 99-118.
- Philpotts, A.R. and Doyle, C.D. (1983) Effect of magma oxidation state on the extent of silicate liquid immiscibility in a tholeiitic basalt. *Am. J. Sci.* 283, 967-986.
- Presnall, D.C. (1966) The join forsterite-diopside-iron oxide and its bearing on the crystallization of basaltic and ultramafic magmas. *Am. J. Sci.* 264, 753-809.
- Roedder, E. (1951) Low temperature liquid immiscibility in the system  $K_2O-FeO-SiO_2$ . *Am. Min.* 36, 282-286.
- Roedder, E. and Weiblen, P.W. (1971) Lunar petrology of silicate melt inclusions, Apollo 11 rocks. *Proc. 11th Lunar Sci. Conf.* v.1, 801-837.
- Roeder, P.L., and Emslie, R.F. (1970) Olivine-liquid equilibrium. *Contrib. Min. Petrol.* 29, 275-289.
- le Roex, A.P., and Dick, H.J.B. (1981) Petrography and geochemistry of basaltic rocks from the Conrad fracture zone on the America-Antarctica ridge. *Earth Planet. Sci. Lett.* 54, 117-138.
- le Roex, A.P., Dick, H.J.B., Reid, A.M. and Erlank, A.J. (1982) Ferrobasalts from the Spiess ridge segment of the southwest Indian ridge. *Earth Planet. Sci. Lett.* 60, 437-451.

- Sack, R.O., Carmichael, I.S.E., Rivers, M. and Ghiorso, M.S. (1980) Ferric-ferrous equilibria in natural silicate liquids at 1 bar. *Contrib. Min. Petrol.* 75, 369-376.
- Sato, M. and Valenza, M. (1980) Oxygen fugacities of the layered series of the Skaergaard intrusion, east Greenland. *Am. J. Sci.* 280-A, 134-158.
- Silver, L.A. and Delaney, J.R. (1983) Melting experiments on Juan de Fuca ridge basalts: implications for petrogenesis. *EOS* 64, 888.
- Sinton, J.M., Wilson, D.S., Christie, D.M., Hey, R.N. and Delaney, J.R. (1983) Petrological consequences of rift propagation on oceanic spreading centers. *Earth. Planet. Sci. Lett.* 62, 193-207.
- Thornber, C.R., Roeder, P.L. and Foster, J.R. (1980) The effect of composition on the ferric-ferrous ratio in basaltic liquids at atmospheric pressure. *Geochim. Cosmochim. Acta.* 44, 525-532.
- Thy, P., Lofgren, G., Jakobsson, S.P. (1988) Experimental phase equilibria of Fe-Ti rich basalts from the rift zones of Iceland: shifts in pseudo-invariant compositions and the evolution of mildly alkalic lavas. *Abstr., V.M. Goldschmidt Conference.* p.78.
- Vogt, P.R. and Byerly, G.R. (1976) Magnetic anomalies and basalt composition in the Juan de Fuca- Gorda Ridge areas. *Earth. Planet. Sci. Lett.* 33, 185-207.
- Wager, L.R. (1960) The major element variation of the layered series of the Skaergaard intrusion and a re-estimation of the average composition of the hidden layered series and of the successive residual magmas. *J. Pet.* 1, 364-398.
- Wakeham, S.E. (1978) Petrochemical patterns in young pillow basalts dredged from the Juan de Fuca and Gorda Ridges. M.S. Thesis, Oregon State University, p.95.
- Watson, E.B. (1982) Basalt contamination by continental crust: some experiments and models. *Contrib. Min. Petrol.* 80, 73-87.
- Yoder, H.S. and Tilley, C.E. (1962) Origin of basaltic magmas: An experimental study of natural and synthetic rock systems. *J. Pet.* 3, 342-532.

Table AIII-1: Comparison of compositions of normal MORB with FeTi basalts used in experiments and end member FeTi basalt from the Galapagos spreading center.

	Normal MORB <sup>+</sup>	JdF FeTi basalt	Spiess Ridge FeTi basalt	Galapagos FeTi basalt <sup>+</sup>
SiO <sub>2</sub>	50.75	51.09	50.91	49.23
TiO <sub>2</sub>	1.18	2.35	2.86	3.71
Al <sub>2</sub> O <sub>3</sub>	15.52	12.54	14.06	11.24
Cr <sub>2</sub> O <sub>3</sub>	-	0.04	0.05	-
FeO*	9.38	12.59	12.21	18.43
MnO	-	0.27	0.25	-
MgO	8.09	6.42	4.57	4.26
CaO	12.26	10.58	8.53	9.18
Na <sub>2</sub> O	2.24	2.68	4.00	2.52
K <sub>2</sub> O	0.11	0.33	0.83	0.19
P <sub>2</sub> O <sub>5</sub>	0.08	-	-	0.31
Total	99.61	98.89	98.27	99.07

<sup>+</sup> from Byerly et al., (1976).

Table AIII-2: Experimental run conditions and run products.

Experiment	Temperature°C	log $f_{O_2}$	Duration (hrs)	Phases	Symbol
FeTi 4 OP21	1150	-10	11.8	ol, pl	□
FeTi 8 OP28	1150	-7	12.8	ol, pl, mt	△
FeTi 9 OP33	1150	-8	12.6	ol, pl, mt	+
FeTi 8 OP33	1150	-11	12.1	ol, pl, sp (?)	x
FeTi 11 OP42	1125	-8	12.3	ol, pl, cpx, mt	●
FeTi 12 OP45	1125	-10	12.3	ol, pl, cpx	◆
FeTi 14 OP48	1125	-12	12.3	ol, pl, cpx	✱
FeTi 15 OP54	1125	-10	15.2	ol, pl, cpx	✱
FeTi 16 OP54	1125	-9	12.1	ol, pl, cpx	✱
SR1 OP29	1150	-7	12.0	ol, pl, mt	□
SR2 OP31	1150	-8	13.0	pl	+
SR3 OP35	1150	-11	12.0	ol, pl, cpx	△
SR6 OP41	1150	-8	24.0	ol, pl	◆
SR7 OP44	1125	-8	12.0	ol, pl, cpx, mt	◆
SR8 OP	1125	-9	12.0	ol, pl, cpx, mt	●

Phases: ol = olivine, pl = plagioclase, cpx = Ca-rich pyroxene, mt = magnetite, sp = Cr-spinel



Table AIII-3: Liquidus temperatures of experimental starting materials and calculated equilibrium olivine and plagioclase compositions.

Sample T°C	Juan de Fuca Ridge	Spiess Ridge	Rim Rock
Starting comp. <sup>1</sup>	1170	1180	1250
Model liq. <sup>2</sup>	1169	1142	1220
Olivine liq. <sup>3</sup>	1179	1129	1201
Plag. liq. <sup>4</sup>	1169	1151	1270
Calculated equilibrium olivine (Fo) <sup>5</sup>	78	72	84
Calculated equilibrium plagioclase (An) <sup>6</sup>	71	57	81

1 = temperature at which starting composition was determined.

2 = liquidus temperature of starting composition calculated by Nielsen (1988) fractional crystallization model.

3, 5 = calculated liquidus temperature and composition of olivine in equilibrium with starting composition using Roeder and Emslie (1970).

4, 6 = calculated liquidus temperature and composition of plagioclase in equilibrium with starting composition using Langmuir (1980).

Table AIII-4: Modal analyses<sup>(1)</sup> and maximum crystal sizes<sup>(2)</sup> of experiments.

Run	Crystals %	Olivine % (mm)	Cpx % (mm)	Plag % (mm)	FeTi oxides % (mm)	Point counts
FeTi 4 (OP 21)	11	5.5 (0.09)	—	5.5 (0.13)	—	109
FeTi 8 (OP 28)	18	3.4 (0.10)	—	13 (0.09)	1.5(0.015)	322
FeTi 8 (OP33)	16	7 (0.09)	(< 1% if any)	9 (0.09)	dust in ol	301
FeTi 9 (OP33)	14	6 (0.05)	—	8 (0.09)	dust in ol	297
FeTi 10 (OP39)		(0.04)	(0.05)	(0.09)	—	—
FeTi 11 (OP42)	43	8 (0.08)	18 (0.2)	16 (0.2)	< 1	221
FeTi 12 (OP45)	57	7 (0.09)	34 (0.09)	16 (0.18)	—	104
FeTi 14 (OP48)	51	7 (0.05)	17 (0.18)	28 (0.09)	—	361
FeTi 16 (OP54)	36	9 (0.08)	15 (0.3)	12 (0.2)	—	320
SR1 (OP29)	13	< 1 (0.05)	—	5 (0.18)	7 (0.02)	295
SR2 (OP31)	< 1	—	—	< 1 (0.18)	—	87
SR3 (OP35)	9	< 1 (0.18)	< 1 (0.18)	8 (0.27)	—	325
SR7 (OP44)	18	3 (0.18)	2.5 (0.09)	12.5 (0.45)	dust in ol	300
SR8 (OP55)	24	4 (0.14)	< 1 fuzz	19 (0.36)	dust in ol	181

- (1) Modal analyses were made using 0.07 mm spacing. Amount of charge material restricted the number of counts.  
(2) Number in ( ) is maximum size crystal observed in mm.

Table AIII-5: Microprobe analyses of starting compositions, average, and unusual compositions, and C.I.P.W. norms in experimental charges.

Charges			Capsules	
Juan de Fuca Ridge FeTi basalt		Spiess Ridge High alkali FeTi basalt	Cascades Rim Rock High alumina Tholeiitic basalt	Hawaiian Olivine Nodule (HON)
SiO <sub>2</sub>	51.09	50.91	49.68	SiO <sub>2</sub> 39.16
TiO <sub>2</sub>	2.35	2.86	0.92	FeO 13.66
Al <sub>2</sub> O <sub>3</sub>	12.54	14.06	18.04	MnO 0.18
Cr <sub>2</sub> O <sub>3</sub>	0.04	0.05	0.05	MgO 45.91
FeO	12.59	12.21	8.86	NiO 0.29
MnO	0.27	0.25	0.20	Total 99.20
MgO	6.42	4.57	8.33	
CaO	10.58	8.53	10.50	Fo 85
Na <sub>2</sub> O	2.68	4.00	2.51	
K <sub>2</sub> O	0.33	0.83	0.32	
Total	98.89	98.27	99.41	
Q	1.47	0.00	0.00	
or	1.97	4.99	1.90	
ab	22.94	34.46	21.38	
an	21.46	18.28	37.25	
di	26.18	20.83	12.43	
w	13.21	10.35	6.34	
e	6.48	4.09	3.52	
f	6.49	6.39	2.56	
hy	19.41	5.41	12.48	
e	9.69	2.11	7.22	
f	9.71	3.30	5.26	
ol	0.00	10.27	12.79	
fo		3.78	7.10	
fa		6.51	5.69	
mgt	2.05	0.20	0.01	
il	4.51	5.53	1.76	
Total	100.22	99.97	100.00	
#	4	5	6	4
alkalies <sup>+</sup>	3.01	4.83	2.83	--
Fe <sup>3+</sup> / Fe <sup>3+</sup> + Fe <sup>2+</sup>	0.40	0.35	0.44	-

\* Norms for starting compositions calculated using  $\text{Fe}_2\text{O}_3 = 0.1 \text{ FeO}$ . Norms and Mg# for experimental runs calculated after Fe was distributed among FeO and  $\text{Fe}_2\text{O}_3$  according to Sack et al., 1980 and Kilinc et al., 1983 using experimental temperature and  $\text{fo}_2$ . # = number of averaged analyses. + =  $\text{Na}_2\text{O} + \text{K}_2\text{O}$ , wt%

Table AIII-5 (con't)

Juan de Fuca Ridge 1150°C Runs				
	FeTi 4 OP21	FeTi 8 OP28	FeTi 9 OP33	FeTi 8 OP33
SiO <sub>2</sub>	50.26	50.33	50.31	52.88
TiO <sub>2</sub>	2.20	2.30	2.30	2.23
Al <sub>2</sub> O <sub>3</sub>	13.14	12.58	13.17	13.21
Cr <sub>2</sub> O <sub>3</sub>	0.04	0.04	0.05	0.05
FeO	12.48	12.65	12.82	11.20
MnO	0.26	0.26	0.27	0.29
MgO	5.89	6.38	6.34	4.92
CaO	10.64	10.30	10.46	8.21
Na <sub>2</sub> O	2.82	2.65	2.84	2.99
K <sub>2</sub> O	0.51	0.44	0.52	0.95
Total	98.24	97.93	99.08	96.93
Q	0.00	2.74	0.00	4.14
or	3.07	2.65	3.10	5.79
ab	24.28	22.83	24.21	26.10
an	22.07	21.51	21.82	20.45
di	26.34	25.01	25.15	18.02
w	13.21	12.74	12.72	9.01
e	5.97	7.01	6.43	3.87
f	7.16	5.26	5.99	5.15
hy	15.90	16.04	17.41	21.46
e	7.23	9.17	9.01	8.77
f	8.67	6.88	8.40	11.68
ol	2.81	0.00	0.65	0.00
fo	1.21		0.32	
fa	1.60		0.33	
mgt	1.30	4.77	3.26	0.67
ilm	4.25	4.45	4.40	4.37
Total	100.02	100.00	100.00	101.00
#	4	5	2	1
alkalies	3.33	3.09	3.36	3.94
Fe <sup>3+</sup> /				
Fe <sup>3+</sup> + Fe <sup>2+</sup>	0.33	0.13	0.08	0.02
(Mg/				
Mg+Fe <sup>2+</sup> )x100	47	54	51	45

Table AIII-5 (con't)

Juan de Fuca Ridge 1125°C Runs					
	FeTi 11 OP42	FeTi 12 OP45		FeTi 15 OP51	
SiO <sub>2</sub>	50.95	50.95	55.44	49.91	51.57
TiO <sub>2</sub>	3.18	3.58	3.22	3.36	4.19
Al <sub>2</sub> O <sub>3</sub>	11.66	11.95	12.61	11.68	12.39
Cr <sub>2</sub> O <sub>3</sub>	0.04	0.05	0.05	—	—
FeO	14.92	14.87	12.91	13.37	10.82
MnO	0.30	0.31	0.23	0.26	0.23
MgO	5.11	4.19	3.91	5.37	5.22
CaO	9.19	8.71	8.25	9.92	9.10
Na <sub>2</sub> O	2.96	2.88	2.86	3.00	3.24
K <sub>2</sub> O	0.45	0.55	0.59	0.47	0.79
Total	98.76	98.04	100.07	97.34	97.55
Q	3.93	4.04	10.11	0.78	3.49
or	2.69	3.31	3.48	2.85	4.78
ab	25.29	24.84	24.17	26.05	28.08
an	17.37	18.43	19.80	17.46	17.34
di	23.87	21.65	17.75	27.54	23.79
w	11.97	10.71	8.80	13.80	12.07
e	5.41	3.88	3.33	6.12	6.30
f	6.48	7.06	5.62	7.63	5.43
hy	16.34	19.06	17.17	17.09	13.06
e	7.44	6.76	6.39	7.61	7.01
f	8.90	12.30	10.78	9.49	6.04
ol	0.00	0.00	0.00	0.00	0.00
fo					
fa					
mgt	4.42	1.77	1.40	1.68	1.31
ilm	6.10	6.93	6.11	6.55	8.15
Total	100.01	100.03	99.99	100.00	100.00
#	6	1	1	5	2
alkalies	3.41	3.43	3.45	3.47	4.03
Fe <sup>3+</sup> / Fe <sup>3+</sup> + Fe <sup>2+</sup>	0.10	0.04	0.04	0.04	0.04
(Mg/ Mg+Fe <sup>2+</sup> )x100	43	38	37	44	48

Table AIII-5 (con't)

Spiess Ridge 1150°C Runs				
	SR1 OP29	SR2 OP31	SR3 OP35	SR6 OP41
SiO <sub>2</sub>	50.92	51.13	52.24	51.44
TiO <sub>2</sub>	2.54	2.81	2.38	2.10
Al <sub>2</sub> O <sub>3</sub>	13.29	13.05	13.43	13.47
Cr <sub>2</sub> O <sub>3</sub>	0.04	0.04	0.04	0.05
FeO	11.99	11.91	12.45	12.23
MnO	0.22	0.26	0.21	0.26
MgO	5.69	5.29	5.06	5.83
CaO	9.21	8.35	9.41	9.91
Na <sub>2</sub> O	3.17	2.54	3.27	3.13
K <sub>2</sub> O	0.82	0.79	0.86	0.60
Total	97.89	96.17	99.35	99.02
Q	1.99	5.53	0.00	0.65
or	4.94	4.86	5.11	3.58
ab	27.32	22.36	27.84	26.70
an	19.98	22.75	19.55	21.11
di	21.77	16.87	22.97	23.53
w	11.09	8.49	11.45	11.88
e	6.12	4.03	4.75	5.89
f	4.55	4.34	6.76	5.76
hy	14.49	20.09	18.97	17.29
e	8.31	9.67	7.83	8.75
f	6.18	10.42	11.14	8.55
ol	0.00	0.00	0.19	0.00
fo			0.07	
fa			0.11	
mgt	4.59	2.00	0.82	3.11
ilm	4.91	5.55	4.55	4.02
Total	99.99	100.01	100.00	99.99
#	3		2	3
alkalies	3.99	3.33	4.13	3.73
Fe <sup>3+</sup> /				
Fe <sup>3+</sup> + Fe <sup>2+</sup>	0.13	0.07	0.02	0.09
(Mg/				
Mg+Fe <sup>2+</sup> )x100	52	48	43	50

Table AIII-5 (con't)

Spiess Ridge 1125°C Runs			
	SR7 OP44	SR8 OP55	
SiO <sub>2</sub>	51.64	51.20	51.85
TiO <sub>2</sub>	2.79	2.91	2.77
Al <sub>2</sub> O <sub>3</sub>	12.94	13.02	18.93
Cr <sub>2</sub> O <sub>3</sub>	0.05	0.04	0.04
FeO	13.24	12.58	8.76
MnO	0.28	0.25	0.13
MgO	5.04	4.97	4.96
CaO	9.01	9.00	9.72
Na <sub>2</sub> O	3.34	3.45	3.22
K <sub>2</sub> O	0.77	0.83	0.83
Total	99.10	98.25	101.21
Q	2.05	1.50	0.97
or	4.58	4.98	4.84
ab	28.45	29.65	26.89
an	18.17	17.86	34.30
di	22.26	22.74	10.85
w	11.21	11.47	5.55
e	5.32	5.63	3.21
f	5.74	5.63	2.08
hy	15.20	13.87	14.80
e	7.32	6.94	8.98
f	7.89	6.93	5.82
ol	0.00	0.00	0.00
fo			
fa			
mgt	3.94	3.80	2.16
ilm	5.33	5.61	5.19
Total	99.98	100.01	100.00
#	5	6	1
alkalies	4.11	4.28	4.05
Fe <sup>3+</sup> /			
Fe <sup>3+</sup> + Fe <sup>2+</sup>	0.10	0.10	0.08
(Mg/			
Mg+Fe <sup>2+</sup> )x100	45	46	54

Table AIII-6: Microprobe analyses of glasses from experiments.

<u>Experimental Run</u>							
FeTi 4 OP21							
	(1)	(2)	(3)	(4)	(5)	(6)	(7)
SiO <sub>2</sub>	51.00	50.08	49.28	50.69	50.29	50.58	51.93
TiO <sub>2</sub>	2.16	2.24	2.21	2.18	1.80	1.86	1.85
Al <sub>2</sub> O <sub>3</sub>	13.33	13.09	13.20	12.94	13.23	13.29	13.31
Cr <sub>2</sub> O <sub>3</sub>	0.04	0.04	0.04	0.04	0.05	0.04	0.04
FeO*	12.47	12.58	12.64	12.23	12.16	11.49	11.05
MnO	0.25	0.26	0.25	0.26	0.30	0.33	0.25
MgO	5.92	5.97	5.92	5.76	5.95	6.14	5.96
CaO	10.78	10.08	10.78	10.91	10.51	10.39	10.16
Na <sub>2</sub> O	2.77	2.81	2.90	2.81	2.81	2.76	3.03
K <sub>2</sub> O	0.55	0.50	0.52	0.46	0.58	0.60	0.60
SUM	99.27	97.65	97.74	98.28	97.58	100.48	98.18
Location*	b	b	b	e	co	co	co
FeTi 8 OP28							
	(1)	(2)	(3)	(4)	(5)	(6)	(7)
SiO <sub>2</sub>	49.96	50.01	49.98	50.66	51.05	51.03	51.85
TiO <sub>2</sub>	2.39	2.34	2.23	2.29	2.23	2.06	1.99
Al <sub>2</sub> O <sub>3</sub>	12.70	12.58	12.58	12.55	12.51	12.89	13.02
Cr <sub>2</sub> O <sub>3</sub>	0.05	0.04	0.04	0.04	0.04	0.04	0.04
FeO*	12.83	12.82	13.02	12.30	12.27	12.21	11.94
MnO	0.26	0.30	0.29	0.22	0.23	0.26	0.24
MgO	6.43	6.40	6.29	6.16	6.63	6.25	6.30
CaO	10.31	10.06	10.43	10.35	10.35	9.65	9.38
Na <sub>2</sub> O	2.61	2.61	2.62	2.80	2.61	2.92	2.95
K <sub>2</sub> O	0.46	0.42	0.45	0.42	0.43	0.56	0.63
SUM	98.00	97.58	97.93	97.79	98.35	97.87	98.34
Location	e	m	e	b	b	co	co



Table AIII-6 (con't)

FeTi 9 OP33					FeTi 8 OP33		
	(1)	(2)	(3)	(4)	(1)	(2)	(3)
SiO <sub>2</sub>	50.42	50.73	49.89	50.59	52.88	51.61	50.82
TiO <sub>2</sub>	1.94	2.34	2.25	2.00	2.23	2.02	1.97
Al <sub>2</sub> O <sub>3</sub>	13.42	13.33	13.01	13.38	13.21	13.56	13.18
Cr <sub>2</sub> O <sub>3</sub>	0.05	0.05	0.05	0.05	0.05	0.05	0.05
FeO*	13.16	12.83	12.80	13.60	11.20	11.98	12.34
MnO	0.27	0.26	0.27	0.36	0.29	0.29	0.27
MgO	5.99	6.36	6.31	5.47	4.92	5.17	5.30
CaO	9.73	10.33	10.58	10.29	8.21	8.52	9.74
Na <sub>2</sub> O	2.91	2.81	2.86	2.83	2.99	3.12	2.91
K <sub>2</sub> O	0.68	0.54	0.50	0.60	0.95	0.78	0.68
SUM	98.57	99.58	98.52	99.17	96.93	97.10	97.26
Location	co	e	b	co	cb	co	co

FeTi 11 OP42							
	(1)	(2)	(3)	(4)	(5)	(6)	(7)
SiO <sub>2</sub>	52.49	50.57	51.06	49.99	50.88	51.97	50.73
TiO <sub>2</sub>	3.06	3.13	3.18	3.16	3.45	3.14	3.12
Al <sub>2</sub> O <sub>3</sub>	11.83	11.69	11.59	11.75	11.50	11.79	11.59
Cr <sub>2</sub> O <sub>3</sub>	0.04	0.04	0.04	0.04	0.04	0.04	0.04
FeO*	14.26	14.82	15.14	14.89	14.91	14.29	15.47
MnO	0.31	0.30	0.30	0.32	0.32	0.26	0.26
MgO	5.12	5.18	5.16	5.02	5.09	5.14	5.07
CaO	8.75	9.37	9.21	9.13	9.24	8.76	9.44
Na <sub>2</sub> O	3.13	3.03	2.89	2.81	3.02	3.19	2.86
K <sub>2</sub> O	0.48	0.42	0.48	0.45	0.43	0.48	0.45
SUM	99.47	98.55	99.05	97.56	98.88	99.06	99.03
Location	e	m	b	b	b	co	b

Table AIII-6 (con't)

FeTi 12 OP45				FeTi 15 OP51			
	(1)	(2)	(3)	(1)	(2)	(3)	(4)
SiO <sub>2</sub>	50.60	55.44	50.95	51.75	50.56	49.09	49.90
TiO <sub>2</sub>	3.20	3.22	3.58	4.02	3.32	3.41	3.40
Al <sub>2</sub> O <sub>3</sub>	12.07	12.61	11.95	12.79	11.86	11.93	11.76
Cr <sub>2</sub> O <sub>3</sub>	0.05	0.05	0.05	nd	nd	nd	nd
FeO*	16.08	12.91	14.87	10.61	13.68	13.28	13.71
MnO	0.28	0.23	0.31	0.19	0.25	0.23	0.28
MgO	4.89	3.91	4.19	5.22	5.38	5.28	5.34
CaO	9.65	8.25	8.71	9.09	10.13	10.04	9.83
Na <sub>2</sub> O	2.97	2.86	2.88	3.21	3.01	3.01	2.87
K <sub>2</sub> O	0.44	0.59	0.55	0.81	0.46	0.48	0.48
SUM	100.29	100.07	98.04	97.69	98.65	96.75	97.57
Location	co	e	b	b	b	b	b

FeTi 15 OP51			
SiO <sub>2</sub>	49.67	50.35	51.39
TiO <sub>2</sub>	3.32	3.36	4.36
Al <sub>2</sub> O <sub>3</sub>	11.23	11.61	11.98
Cr <sub>2</sub> O <sub>3</sub>	nd	nd	nd
FeO*	13.10	13.08	11.02
MnO	0.28	0.28	0.27
MgO	5.36	5.51	5.22
CaO	9.77	9.84	9.10
Na <sub>2</sub> O	3.05	3.07	3.27
K <sub>2</sub> O	0.49	0.45	0.77
SUM	96.27	97.55	97.38
Location	b	b	b

Table AIII-6 (con't)

SR 1 OP29							
	(1)	(2)	(3)	(4)	(5)	(6)	(7)
SiO <sub>2</sub>	50.12	52.03	50.60	52.67	52.62	51.94	52.47
TiO <sub>2</sub>	2.60	2.58	2.45	2.07	2.19	2.60	2.23
Al <sub>2</sub> O <sub>3</sub>	13.36	13.42	13.10	13.04	12.84	13.15	12.89
Cr <sub>2</sub> O <sub>3</sub>	0.04	0.04	0.04	0.05	0.04	0.04	0.04
FeO*	12.21	12.19	11.57	11.59	10.83	10.86	11.42
MnO	0.23	0.23	0.21	0.26	0.17	0.27	0.25
MgO	5.52	5.60	5.94	5.64	5.96	5.79	5.55
CaO	9.08	9.32	9.22	9.29	8.59	8.53	8.95
Na <sub>2</sub> O	3.22	3.18	3.12	3.06	3.29	3.20	2.93
K <sub>2</sub> O	0.85	0.80	0.80	0.80	0.82	0.80	0.79
SUM	97.23	99.39	97.05	98.47	97.35	97.18	97.52
Location	m	m	m	c	co	b	co

SR 3 OP35				SR 6 OP41			
	(1)	(2)	(3)	(4)	(1)	(2)	(3)
SiO <sub>2</sub>	51.46	53.01	54.86	56.51	52.13	50.87	51.32
TiO <sub>2</sub>	2.25	2.51	1.90	1.81	2.08	2.18	2.05
Al <sub>2</sub> O <sub>3</sub>	13.50	13.36	13.96	14.12	13.56	13.51	13.34
Cr <sub>2</sub> O <sub>3</sub>	0.04	0.04	0.04	0.05	0.04	0.04	0.07
FeO*	12.35	12.55	9.78	9.11	12.17	12.29	12.24
MnO	0.22	0.20	0.22	0.20	0.25	0.28	0.26
MgO	4.95	5.16	5.26	4.89	5.80	6.01	5.69
CaO	9.38	9.43	8.92	8.57	9.72	10.11	9.91
Na <sub>2</sub> O	3.41	3.13	3.53	3.41	3.10	3.25	3.05
K <sub>2</sub> O	0.89	0.83	0.87	0.87	0.60	0.62	0.59
SUM	98.45	100.22	99.34	99.54	99.45	99.16	98.52
Location	bo	b	cb	cb	b	bo	bo

Table AIII-6 (con't)

SR 7 OP44						
	(1)	(2)	(3)	(4)	(5)	(6)
SiO <sub>2</sub>	50.82	50.24	52.18	50.64	51.85	53.10
TiO <sub>2</sub>	3.09	2.50	2.65	2.74	2.89	2.83
Al <sub>2</sub> O <sub>3</sub>	12.92	12.97	12.89	12.88	13.02	12.91
Cr <sub>2</sub> O <sub>3</sub>	0.05	0.05	0.05	0.05	0.05	0.05
FeO*	12.93	13.36	13.52	14.09	13.02	13.38
MnO	0.29	0.29	0.29	0.31	0.31	0.22
MgO	5.10	5.02	4.91	5.75	5.00	5.15
CaO	9.15	9.04	9.03	9.24	8.89	8.92
Na <sub>2</sub> O	3.26	3.20	3.22	3.01	3.51	3.52
K <sub>2</sub> O	0.78	0.78	0.70	0.65	0.79	0.78
SUM	98.39	97.45	99.44	99.36	99.33	100.86
Location	e	b	bo	co	e	b

SR 8 OP44							
	(1)	(2)	(3)	(4)	(5)	(6)	(7)
SiO <sub>2</sub>	51.06	51.02	51.67	50.88	51.07	51.85	51.49
TiO <sub>2</sub>	2.90	3.00	2.90	2.88	3.00	2.77	2.79
Al <sub>2</sub> O <sub>3</sub>	13.31	12.92	13.15	13.04	12.77	18.93	12.94
Cr <sub>2</sub> O <sub>3</sub>	0.04	0.04	0.04	0.04	0.04	0.04	0.04
FeO*	12.68	12.02	12.18	12.81	12.76	8.76	13.01
MnO	0.24	0.26	0.22	0.27	0.25	0.13	0.24
MgO	5.10	4.75	4.81	5.12	5.03	4.96	5.01
CaO	9.10	9.01	8.99	8.96	8.97	9.72	8.97
Na <sub>2</sub> O	3.51	3.54	3.37	3.30	3.49	3.22	3.49
K <sub>2</sub> O	0.85	0.85	0.85	0.80	0.83	0.83	0.81
SUM	98.79	97.41	98.18	98.10	98.21	101.21	98.19
Location	bo	e	e	m	b	bo	b

\* see legend at bottom of Table AI-7.

nd = not determined

Table AIII-7: Microprobe analyses of olivine from experiments.

	Rim Rock Capsule					Spiess Ridge starting comp.			FeTi 4 OP21		
	(1)	(2)	(3)	(4)	(5)	(1)	(2)	(3)	(1)	(2)	(3)
SiO <sub>2</sub>	39.19	39.18	40.79	40.61	39.27	37.56	36.76	37.21	39.80	38.91	39.17
FeO	15.66	15.65	11.31	11.69	14.40	22.70	25.11	28.00	12.37	16.76	18.50
MnO	0.34	0.32	0.27	0.20	0.30	0.35	0.47	0.53	0.16	0.27	0.29
MgO	44.32	43.28	47.06	46.30	44.20	37.68	35.31	32.13	46.98	44.06	42.44
NiO	0.23	0.21	0.24	0.18	0.23	0.12	0.13	0.08	0.27	0.24	0.21
SUM	99.74	98.63	99.67	98.98	98.39	98.41	97.78	97.95	99.59	100.23	100.61
Fo	83	82.7	87.7	87.3	84.2	74.4	71.1	66.7	87	82	80
Cations based on 4 oxygens											
Si	.992	1.002	1.009	1.013	1.001	0.997	0.995	1.017	0.992	0.985	0.994
Fe	.331	0.334	0.234	0.234	0.306	0.503	0.568	0.640	0.258	0.354	0.392
Mn	.007	0.006	0.005	0.004	0.006	0.007	0.010	0.012	0.003	0.005	0.006
Mg	1.672	1.650	1.736	1.722	1.679	1.491	1.425	1.309	1.747	1.663	1.606
Ni	.004	0.004	0.004	0.003	0.004	0.002	0.002	0.001	0.005	0.004	0.004
SUM	3.008	2.998	2.990	2.987	2.999	3.003	3.004	2.982	3.007	3.015	3.005
Cp/Ch	-	-	-	-	-	-	-	-	Cp	Cp	Cp
C/R/M	C	C	C	C	R	M	M	M	C	R	R
N/R	-	-	-	-	-	-	-	-	R	R	R
w	-	-	-	-	-	-	-	-	-	-	-

Table AIII-7: Olivine analyses (con't.)

	FeTi 8 OP28		FeTi 11 OP42		FeTi 12 OP45				FeTi 15 OP54		
	(1)	(1)	(2)	(1)	(2)	(3)	(4)	(5)	(1)	(2)	(3)
SiO <sub>2</sub>	37.80	39.26	36.93	36.44	36.63	36.97	36.06	36.78	39.90	40.02	39.50
FeO	17.48	16.60	26.92	29.12	27.89	23.11	30.90	27.48	14.39	14.62	13.26
MnO	0.34	0.32	0.53	0.46	0.42	0.43	0.53	0.38	0.24	0.19	0.19
MgO	42.03	43.49	36.61	32.68	33.24	38.40	31.30	34.20	45.21	44.91	46.14
NiO	0.22	0.12	0.13	0.18	0.17	0.17	0.15	0.16	0.28	0.33	0.31
SUM	97.88	99.79	101.12	98.89	98.36	99.08	98.94	99.00	100.01	100.07	99.40
Fo	80.9	82	70.4	66.2	67.6	74.4	63.9	68.6	84.4	84.2	85.7

Cations based on 4 oxygens

Si	0.986	0.996	0.975	0.995	0.999	0.979	0.993	0.994	0.999	1.002	0.991
Fe	0.381	0.352	0.594	0.664	0.636	0.511	0.711	0.621	0.301	0.306	0.278
Mn	0.007	0.006	0.011	0.010	0.009	0.009	0.012	0.008	0.005	0.003	0.004
Mg	1.634	1.645	1.441	1.330	1.351	1.516	1.285	1.378	1.688	1.677	1.727
Ni	0.004	0.002	0.002	0.004	0.003	0.003	0.003	0.003	0.005	0.006	0.006
SUM	3.014	3.004	3.025	3.005	3.001	3.021	3.007	3.006	3.000	2.997	3.008

Cp/Ch	Cp	Cp	Cp	Cp	Cp	Cp	Ch	Ch	Cp	Cp	Cp
C/R/M	R	C	C	M	C	C	M	R	R	R	C
N/R	-	R	R	N	R	R	N	N	R	R	R
w		w	w			w					

Table AIII-7: Olivine analyses (con't.)

	FeTi 15 OP54		SR1 OP29		SR3 OP35		SR6 OP41		SR7 OP44		
	(4)	(5)	(1)	(2)	(1)	(1)	(2)	(3)	(4)	(1)	(2)
SiO <sub>2</sub>	40.67	41.29	36.42	38.70	39.85	37.81	38.06	37.82	38.59	38.27	38.01
FeO	11.79	9.68	20.55	22.89	13.46	20.94	20.44	19.63	21.18	21.06	22.36
MnO	0.17	0.17	0.31	0.32	0.26	0.41	0.37	0.34	0.38	0.53	0.43
MgO	46.93	49.09	40.43	39.67	44.61	39.16	39.95	40.32	37.57	39.85	39.22
NiO	0.31	0.31	0.16	0.22	0.27	0.09	0.15	0.11	0.11	0.21	0.13
SUM	99.86	100.54	97.87	101.81	98.44	98.41	98.96	98.21	97.83	99.92	100.15
Fo	87.3	89.6	77.5	75.2	84.2	76.5	77.3	78.2	75.9	76.6	75.4

Cations based on 4 oxygens

Si	1.007	1.005	0.966	0.991	1.009	0.995	0.993	0.991	1.020	0.992	0.989
Fe	0.244	0.197	0.456	0.490	0.285	0.460	0.446	0.430	0.468	0.456	0.486
Mn	0.003	0.003	0.006	0.006	0.005	0.009	0.008	0.007	0.008	0.011	0.009
Mg	1.732	1.782	1.600	1.515	1.684	1.537	1.554	1.576	1.480	1.541	1.522
Ni	0.006	0.006	0.003	0.004	0.005	0.002	0.003	0.002	0.002	0.004	0.002
SUM	2.993	2.994	3.033	3.009	2.990	3.005	3.006	3.008	2.980	3.007	3.011

Cp/Ch	Cp	Cp	Cp	Cp	Cp	Cp	Cp	Cp	Cp	Cp	Ch
C/R/M	C	R	R	R	C	C	C	M	C	C	M
N/R	-	-	R	R	-	R	R	R	-	R	N
w	-	-	w	w	-	w	w	w	-	w	-

Table AIII-7: Olivine analyses (con't.)

	SR7 OP44		SR8 OP55			
	(3)	(4)	(1)	(2)	(3)	(4)
SiO <sub>2</sub>	38.32	36.97	38.03	40.14	37.99	37.16
FeO	22.77	23.25	24.56	23.56	26.48	24.48
MnO	0.42	0.47	0.46	0.43	0.48	0.46
MgO	38.82	37.76	36.09	32.56	35.38	35.58
NiO	0.13	0.17	0.11	0.16	0.14	0.08
SUM	100.46	98.62	99.25	96.84	100.48	97.76
Fo	74.8	73.9	71.9	70.7	70	71.8

Cations based on 4 oxygens

Si	0.995	0.984	1.008	1.077	1.003	1.002
Fe	0.494	0.517	0.544	0.528	0.585	0.552
Mn	0.009	0.010	0.010	0.009	0.010	0.010
Mg	1.502	1.498	1.426	1.303	1.393	1.430
Ni	0.002	0.003	0.002	0.003	0.002	0.001
SUM	3.005	3.015	2.992	2.923	2.996	2.998

Cp/Ch	Cp	Cp	Ch	Ch	Ch	Ch
C/R/M	R	R	M	C	R	R
N/R	N	R	N	R	-	-
w	-	-	-	w	-	-

Cp/Ch = capsule/charge

C/R/M = core/rim/micro

N/R = new/resorbed

w/ox = with opaque inclusions



Table AIII-7: Microprobe analyses of clinopyroxene from experiments.

	Rim Rock		SR		FeTi 11 OP42		
	(1)	(2)	(1)	(2)	(1)	(2)	(3)
SiO <sub>2</sub>	50.84	51.37	49.66	48.88	49.89	50.59	49.96
TiO <sub>2</sub>	1.11	0.78	1.66	1.82	1.19	0.86	1.12
Al <sub>2</sub> O <sub>3</sub>	3.94	2.98	4.02	4.67	4.21	3.81	1.64
FeO	8.31	6.94	7.09	11.30	10.16	11.53	10.77
Fe <sub>2</sub> O <sub>3</sub>	0.57	0.95	3.49	0.00	1.00	0.32	1.16
MnO	0.26	0.25	0.25	0.28	0.28	0.29	0.30
MgO	14.29	14.86	14.35	12.92	14.45	14.40	15.31
CaO	20.39	21.05	20.34	19.69	18.06	17.51	18.51
Na <sub>2</sub> O	0.35	0.32	0.41	0.51	0.30	0.29	0.32
Cr <sub>2</sub> O <sub>3</sub>	0.54	0.15	0.04	0.08	0.12	0.20	0.10
SUM	100.60	99.65	101.31	100.15	99.66	99.80	99.19

cations based on 6 oxygens

Si	1.887	1.911	1.833	1.871	1.870	1.898	1.897
Ti	0.031	0.022	0.046	0.052	0.034	0.024	0.032
Al	0.172	0.131	0.175	0.211	0.186	0.168	0.073
Fe <sup>2+</sup>	0.258	0.216	0.219	0.362	0.319	0.362	0.342
Fe <sup>3+</sup>	0.016	0.027	0.097	0.000	0.028	0.009	0.033
Mn	0.008	0.008	0.008	0.009	0.009	0.009	0.010
Mg	0.791	0.824	0.789	0.641	0.807	0.805	0.866
Ca	0.811	0.839	0.804	0.807	0.725	0.704	0.753
Na	0.025	0.023	0.029	0.038	0.022	0.021	0.024
En	42.51	43.85	43.55	35.39	43.61	43.04	44.17
Fs	13.88	11.49	12.07	19.99	17.21	19.34	17.44
Wo	43.61	44.66	44.38	44.62	39.19	37.62	38.39

Table AIII-7: Pyroxene analyses (con't)

	FeTi 12 OP45	SR 6 OP41	SR 7 OP44	
	(1)	(1)	(1)	(2)
SiO <sub>2</sub>	51.22	50.44	52.42	54.28
TiO <sub>2</sub>	1.05	0.73	0.89	0.42
Al <sub>2</sub> O <sub>3</sub>	3.10	3.81	3.73	1.98
FeO	9.58	5.41	7.89	7.87
Fe <sub>2</sub> O <sub>3</sub>	1.10	2.35	0.00	0.21
MnO	0.34	0.21	0.27	0.26
MgO	16.84	15.30	15.67	17.35
CaO	16.39	20.76	20.29	19.75
Na <sub>2</sub> O	0.27	0.32	0.28	0.20
Cr <sub>2</sub> O <sub>3</sub>	0.13	0.55	0.41	0.31
SUM	100.02	99.88	101.85	102.63

cations based on 6 oxygens

Si	1.897	1.875	1.907	1.951
Ti	0.029	0.020	0.024	0.011
Al	0.135	0.167	0.160	0.084
Fe <sup>2+</sup>	0.297	0.168	0.240	0.237
Fe <sup>3+</sup>	0.031	0.066	0.000	0.006
Mn	0.011	0.007	0.008	0.008
Mg	0.930	0.848	0.849	0.929
Ca	0.651	0.827	0.791	0.761
Na	0.019	0.023	0.020	0.014
En	49.53	46.00	45.18	48.24
Fs	15.82	9.13	12.76	12.28
Wo	34.66	44.87	42.06	39.48

Table AIII-7: Microprobe analyses of spinels and magnetites.

	Rim Rock			FeTi 8 OP28			
	(1)	(2)	(3)	(1)	(2)	(3)	(4)
SiO <sub>2</sub>	0.08	0.07	0.08	0.93	0.24	4.16	4.14
TiO <sub>2</sub>	0.34	15.61	0.19	4.79	4.05	1.85	1.86
Al <sub>2</sub> O <sub>3</sub>	41.31	0.23	43.71	12.12	18.01	16.06	10.87
FeO	13.00	34.91	13.62	26.85	25.45	29.17	25.67
Fe <sub>2</sub> O <sub>3</sub>	6.75	37.07	5.63	12.99	9.58	8.52	25.61
MnO	0.19	0.81	0.15	0.36	0.34	0.40	0.41
MgO	16.82	5.26	16.57	7.32	7.60	8.02	8.23
Cr <sub>2</sub> O <sub>3</sub>	21.62	0.05	19.97	31.80	30.64	32.67	17.61
SUM	100.11	94.01	99.92	97.16	95.91	100.85	94.40
cations based on 4 oxygen							
Si	0.0022	0.0027	0.0022	0.0319	0.0081	0.1336	0.1451
Ti	0.0071	0.4530	0.0040	0.1236	0.1028	0.0447	0.0490
Al	1.3613	0.0105	1.4313	0.4903	0.7167	0.6080	0.4489
Fe <sup>2+</sup>	0.3039	1.1267	0.3164	0.7706	0.7187	0.7834	0.7520
Fe <sup>3+</sup>	0.1420	1.0765	0.1176	0.3354	0.2435	0.2058	0.6752
Mn	0.0045	0.0265	0.0035	0.0105	0.0097	0.0109	0.0122
Mg	0.7010	0.3026	0.6862	0.3745	0.3825	0.3840	0.4298
Cr	0.4779	0.0015	0.4387	0.8631	0.8179	0.8296	0.4870
Location*	c	c	c	c	c	c	c
Fe <sup>3+</sup> /Fe <sup>2+</sup>	0.467	0.955	0.372	0.435	0.339	0.263	0.898

Table AIII-7 spinel and magnetite analyses (con't)

	FeTi 8 OP28			FeTi 9 OP33		
	(5)	(6)	(7)	(1)	(2)	(3)
SiO <sub>2</sub>	0.21	0.21	0.47	0.21	0.29	0.45
TiO <sub>2</sub>	1.78	1.72	6.96	3.36	4.20	4.22
Al <sub>2</sub> O <sub>3</sub>	28.91	9.42	10.39	8.56	4.97	5.33
FeO	22.44	17.87	28.58	24.13	25.52	25.65
Fe <sub>2</sub> O <sub>3</sub>	14.10	33.71	19.49	35.21	56.27	54.27
MnO	0.25	0.47	0.41	0.39	0.35	0.35
MgO	9.77	10.62	7.11	7.31	6.32	6.09
Cr <sub>2</sub> O <sub>3</sub>	20.48	25.13	25.27	19.33	0.15	0.06
SUM	97.94	99.15	98.68	98.50	98.07	96.42
cations based on 4 oxygen						
Si	0.0066	0.0071	0.0161	0.0073	0.0105	0.0165
Ti	0.0419	0.0436	0.1796	0.0881	0.1144	0.1167
Al	1.0653	0.3742	0.4201	0.3519	0.2122	0.2309
Fe <sup>2+</sup>	0.5864	0.5037	0.8201	0.7039	0.7730	0.7885
Fe <sup>3+</sup>	0.3316	0.8548	0.5031	0.9240	1.5337	1.5011
Mn	0.0066	0.0134	0.0119	0.0115	0.0107	0.0109
Mg	0.4553	0.5335	0.3636	0.3801	0.3412	0.3337
Cr	0.5063	0.6697	0.6855	0.5331	0.0043	0.0017
Location	c	c	c	c	c	c
Fe <sup>3+</sup> /Fe <sup>2+</sup>	0.565	1.679	0.613	1.313	1.984	1.904

Table AIII-7 spinel and magnetite analyses (con't)

	FeTi 11 OP42		FeTi 12 OP45		SR 1 OP29	SR 2 OP31	
	(1)	(2)	(1)	(1)	(1)	(2)	(3)
SiO <sub>2</sub>	0.27	0.24	0.27	0.26	0.20	0.20	0.28
TiO <sub>2</sub>	9.76	8.97	9.51	5.22	3.96	5.01	4.32
Al <sub>2</sub> O <sub>3</sub>	3.88	3.84	3.91	4.90	6.36	6.37	5.74
FeO	32.81	31.97	32.72	26.21	24.40	25.79	25.71
Fe <sub>2</sub> O <sub>3</sub>	43.49	46.30	46.80	52.97	45.60	43.29	34.62
MnO	0.42	0.43	0.49	0.34	0.35	0.38	0.29
MgO	4.46	4.47	4.67	6.28	6.86	6.73	6.11
Cr <sub>2</sub> O <sub>3</sub>	0.05	0.28	0.05	0.96	9.27	9.97	18.69
SUM	95.14	96.50	98.42	97.14	97.00	97.74	95.76

cations based on 4 oxygen

Si	0.0102	0.0090	0.0098	0.0095	0.0072	0.0072	0.0102
Ti	0.2773	0.2519	0.2609	0.1434	0.1073	0.1348	0.1189
Al	0.1728	0.1690	0.1681	0.2109	0.2701	0.2686	0.2476
Fe <sup>2+</sup>	1.0487	0.9984	1.0017	0.8005	0.7354	0.7715	0.7869
Fe <sup>3+</sup>	1.2507	1.3010	1.2890	1.4556	1.2367	1.1655	0.9533
Mn	0.0134	0.0136	0.0151	0.0105	0.0107	0.0115	0.0090
Mg	0.2512	0.2488	0.2539	0.3419	0.3685	0.3589	0.3333
Cr	0.0015	0.0083	0.0014	0.0277	0.2641	0.2820	0.5408
Location	b	b	b	b	c	c	c
Fe <sup>3+</sup> /Fe <sup>2+</sup>	1.193	1.303	1.287	1.818	1.682	1.511	1.211

Table AIII-7 spinel and magnetite analyses (con't)

	SR 3 OP35		SR 7 OP44		SR 31-4 I
	(1)	(2)	(1)	(2)	(1)
SiO <sub>2</sub>	0.18	0.44	0.31	0.42	0.16
TiO <sub>2</sub>	14.17	10.54	7.47	6.98	20.78
Al <sub>2</sub> O <sub>3</sub>	8.62	13.72	4.32	5.66	2.96
FeO	35.24	39.78	30.85	27.49	43.96
Fe <sub>2</sub> O <sub>3</sub>	18.45	8.93	49.44	44.06	26.74
MnO	0.34	0.31	0.36	0.36	0.45
MgO	6.72	6.48	4.66	4.59	4.23
Cr <sub>2</sub> O <sub>3</sub>	15.39	19.08	0.12	0.05	0.13
SUM	99.11	99.28	97.53	89.61	99.41
Location	c	c	b	b	

cations based on 4 oxygen

Si	0.0062	0.0161	0.0114	0.0167	0.0059
Ti	0.3682	0.2898	0.2071	0.2081	0.5683
Al	0.3511	0.5912	0.1877	0.2645	0.1267
Fe <sup>2+</sup>	1.0183	0.9431	0.9512	0.9413	1.3369
Fe <sup>3+</sup>	0.4797	0.2456	1.3717	1.2846	0.7153
Mn	0.0100	0.0096	0.0112	0.0121	0.0138
Mg	0.3461	0.3531	0.2561	0.2712	0.2292
Cr	0.4205	0.5515	0.0035	0.0016	0.0039
Location	c	c	b	b	-
Fe <sup>3+</sup> /Fe <sup>2+</sup>	0.471	0.260	1.442	1.365	0.608

\* Location of analyses

c = Rim Rock capsule

b = charge-capsule boundary

e = edge of charge

m = middle of charge

o = near resorbed olivine




I = analysis from le Roex et al., 1982

### Figure Captions

Fig. AIII-1: (a) Drawing of experimental design showing drilled basalt capsule filled with powdered charge and cut in half along A-B after quenching. (b) Photomicrograph of an experiment in thin section.

Fig. AIII-2: Photomicrograph of border between experimental charge and capsule from experiment FeTi 8 (OP33) showing opaques in olivine and nearby unaffected olivines in equilibrium with the experimental run conditions. P = plagioclase, Ol = olivine. Ol + Ox = olivine dusted with opaque oxides. Magnification = 20X.

Fig. AIII-3: Major element-oxide variation plots from microprobe analyses of glasses in experiments. Symbols as in Table AIII-2. \*'s denote calculated crystal fractionation trends at  $f_{O_2} = \text{FMQ}$  (see text). Solid lines are constraints on calculated fractional crystallization trend based on error in microprobe analyses of initial charge composition. Dashed lines are fractional crystallization trends calculated at 2 log units above FMQ. Dash-dot lines are fractional crystallization trends calculated at 2 log units below FMQ. Solid triangle = Rim Rock capsule starting composition. Solid square = starting composition of charge. Open symbols = 1150°C. Filled symbols = 1125°C. Symbols with interior circles are analyses from capsule. (a) Juan de Fuca Ridge charge. (b) Spiess Ridge charge. A mixing line connects the Spiess Ridge charge and Rim Rock starting compositions to facilitate discussion in the text.

Fig. AIII-4: Enlarged part of silicate immiscibility ternary after Naslund (1983). Dotted line = two liquid phase field. Dashed lines are phase boundaries in the system leucite-fayalite-silica (Roedder, 1951); dot dashed lines are phase boundaries in the system nepheline-fayalite-silica (Bowen, 1937), open circles with tie lines are matrix-ocelli pairs from alkaline dikes and sills (Philpotts, 1976); solid circles with tie lines are immiscible lunar glasses (Roedder and Weiblen, 1971). Table AIII-5 contains analyses of plotted liquid pairs from experiments in this study.  = FeTi 12 OP45,  = FeTi 15 OP54,  = SR8 OP55.

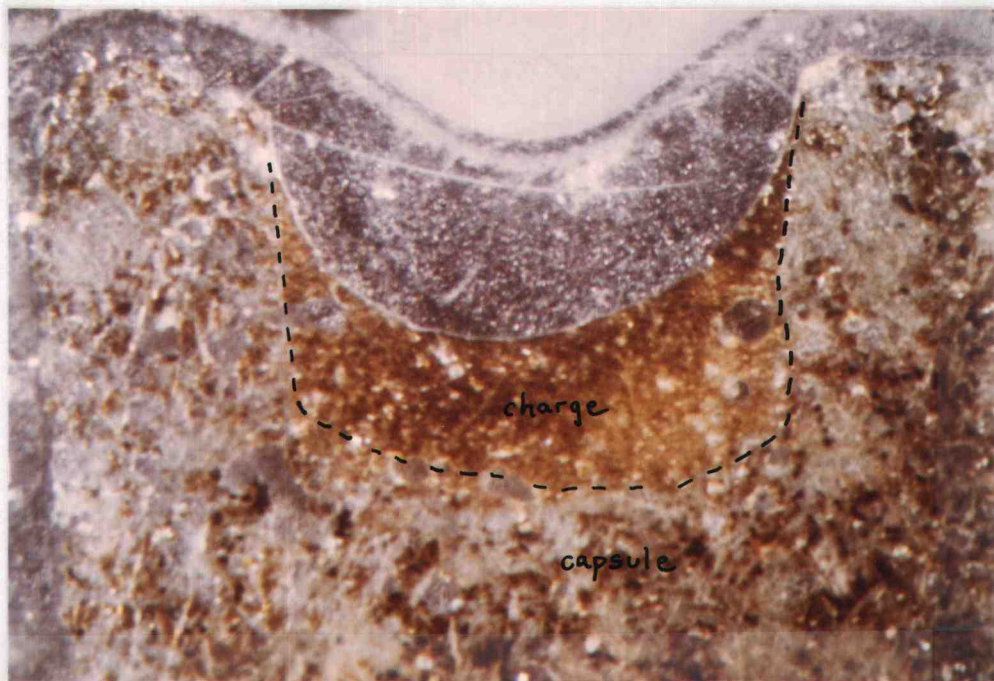
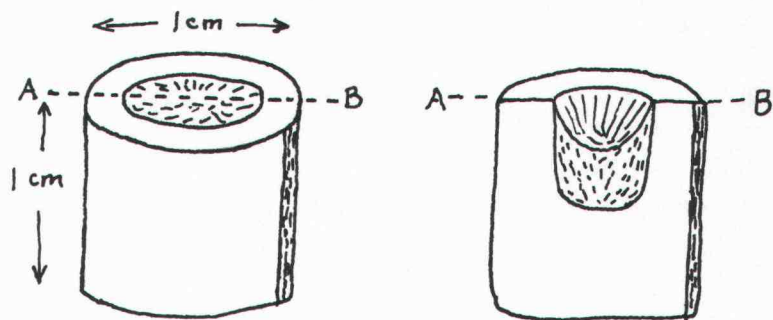


Fig.AIII-1



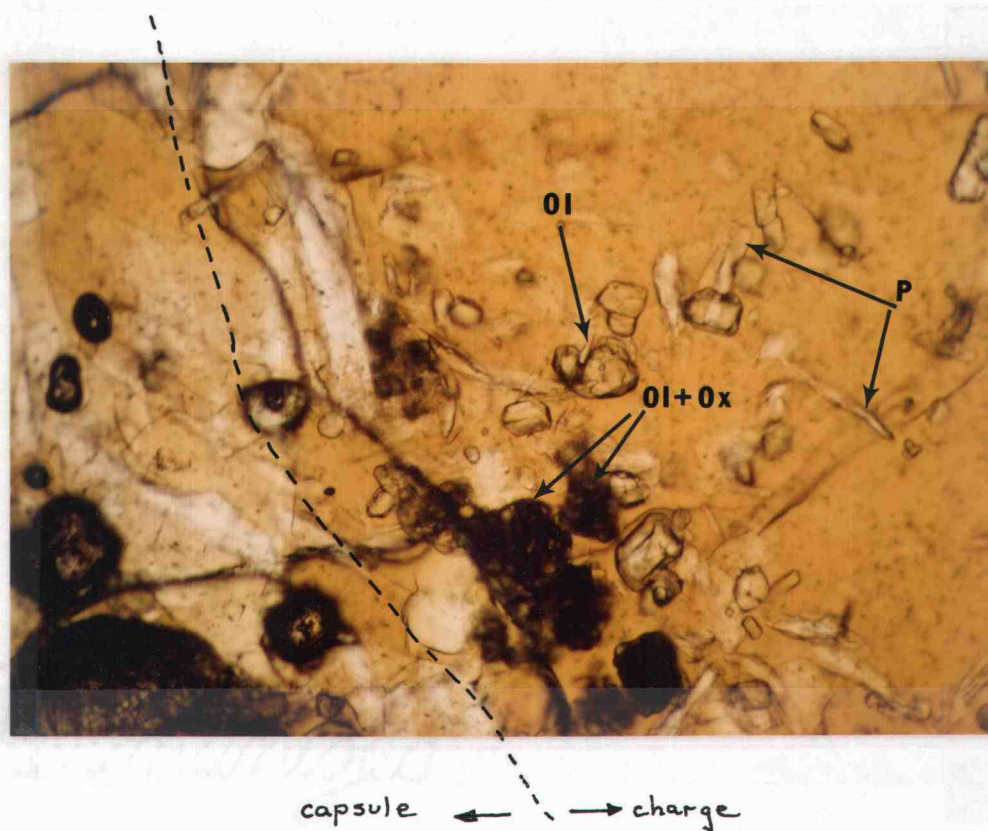


Fig. AIII-2

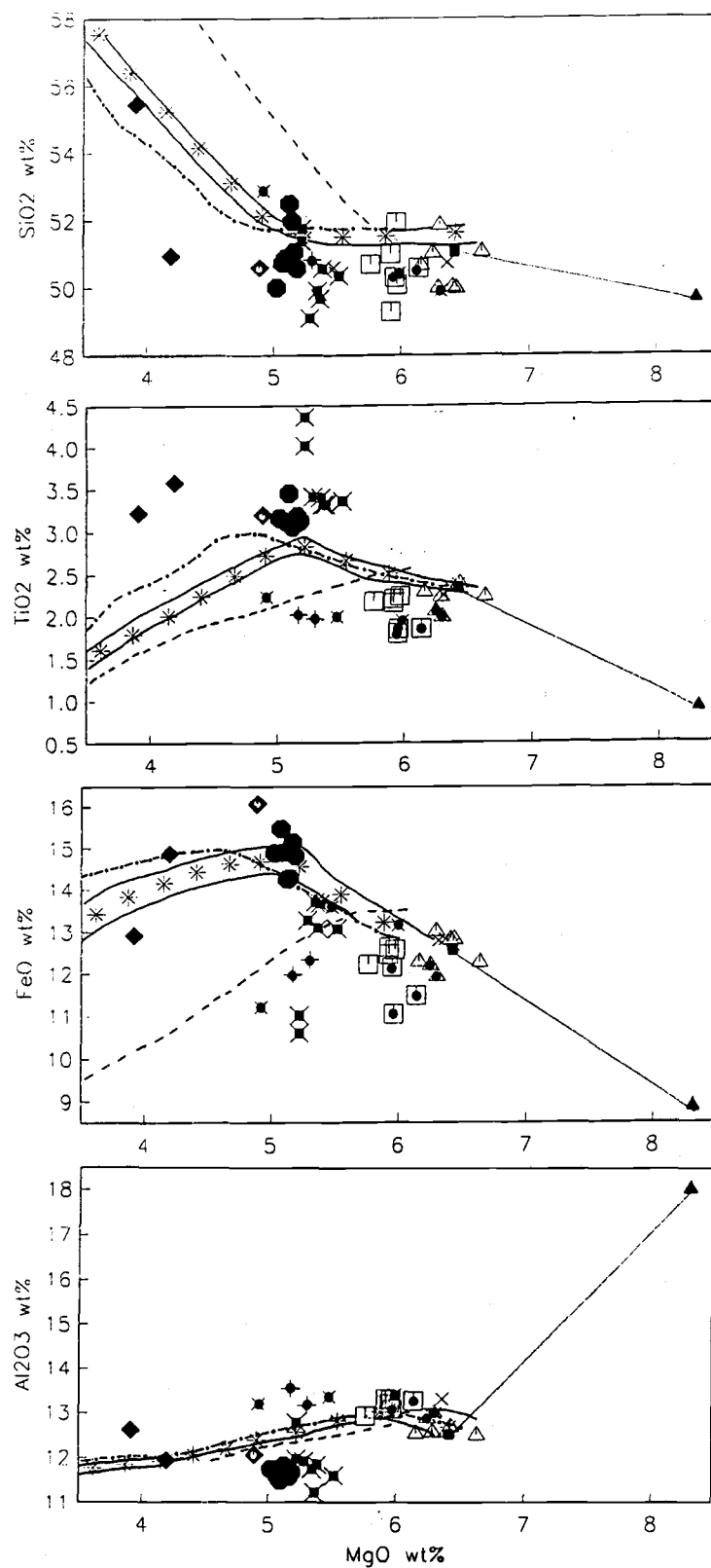


Fig. AIII-3a

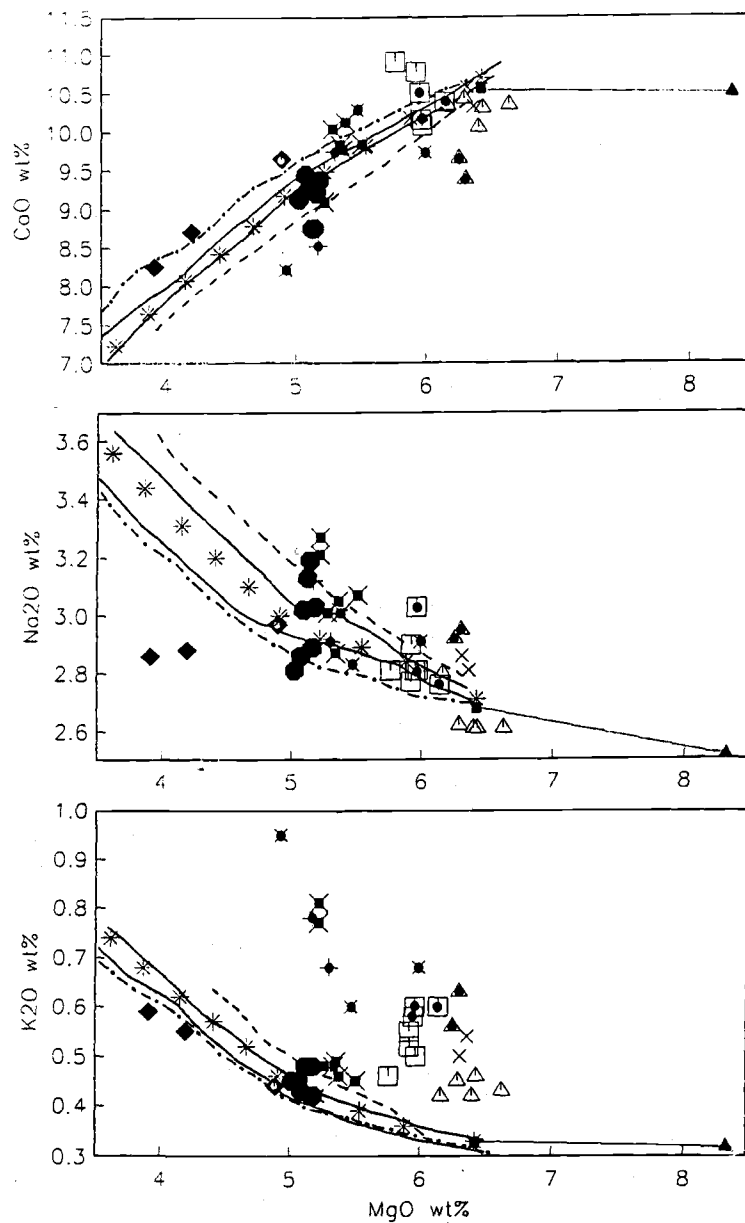


Fig. AIII-3a (continued)

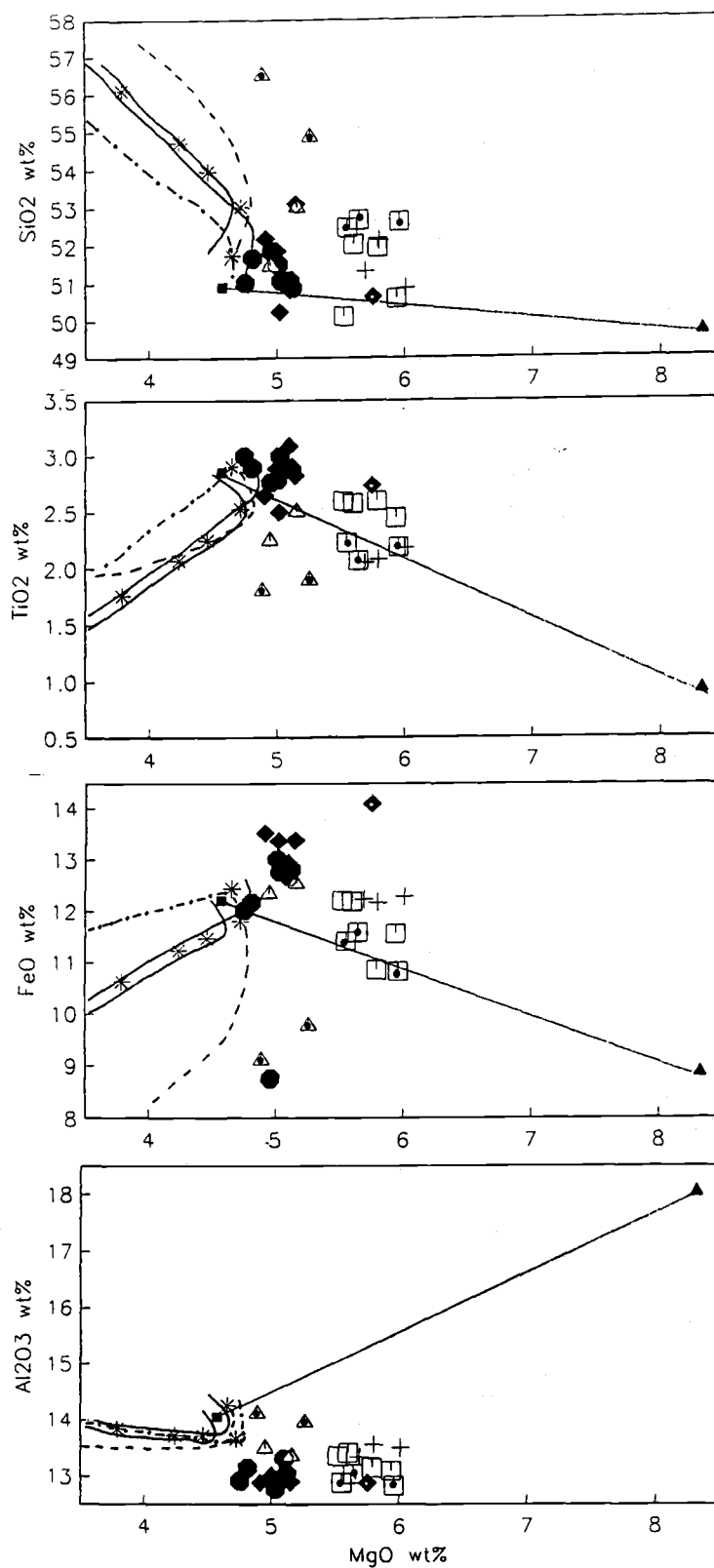


Fig. AIII-3b

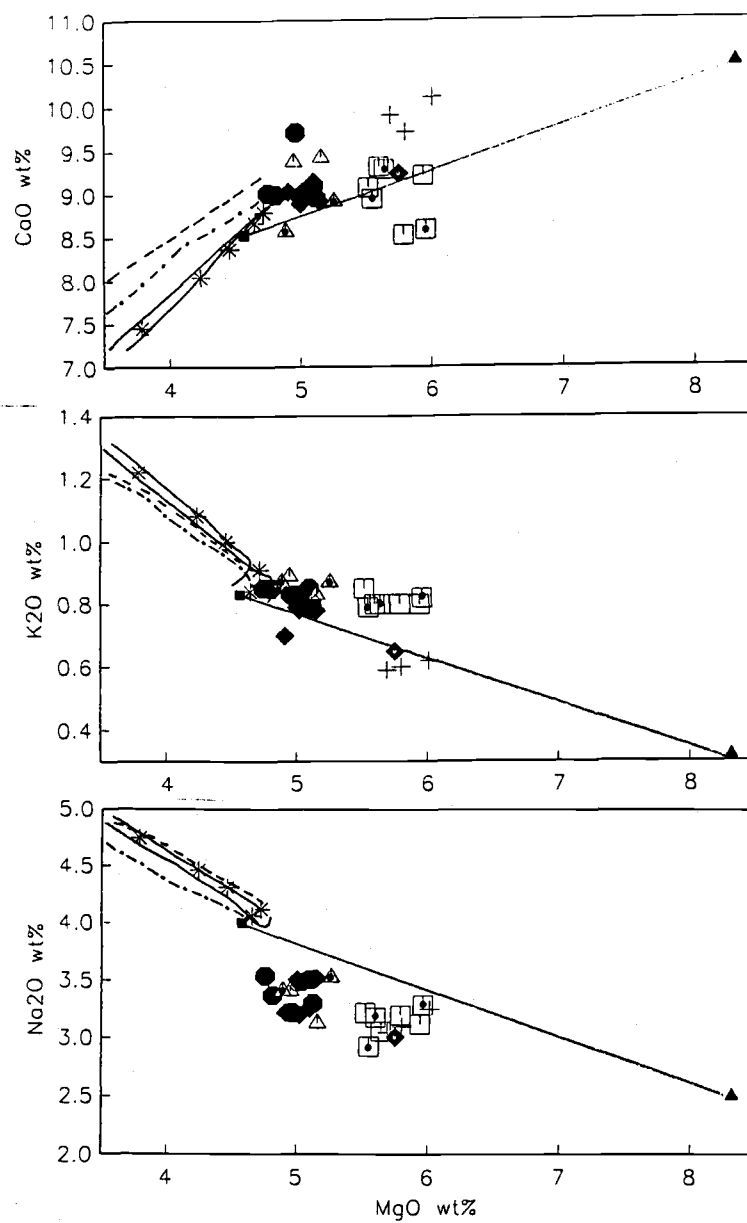


Fig. AIII-3b (continued)

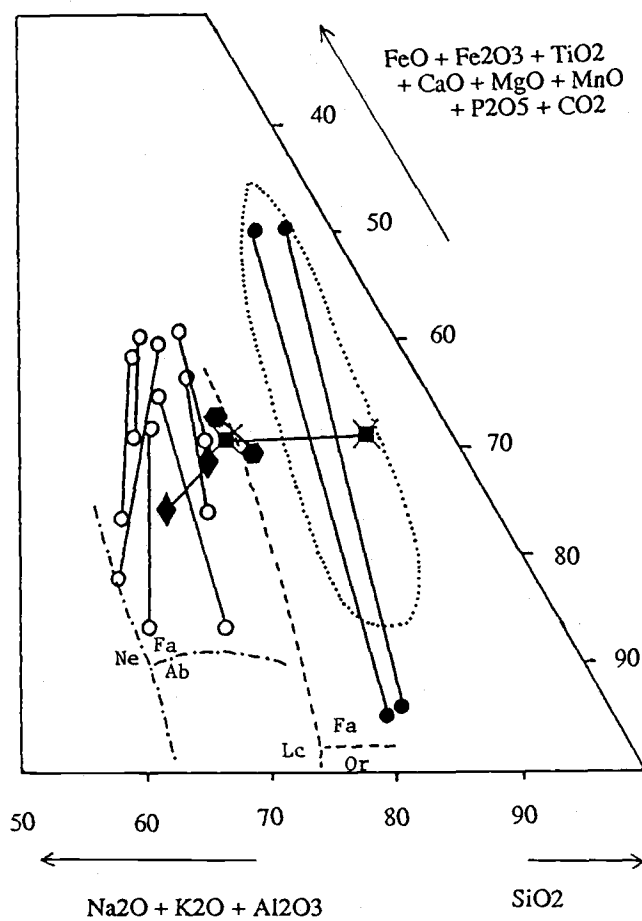


Fig. AIII-4